

Department of Geosciences, Geography
University of Fribourg (Switzerland)

Detection, mapping and monitoring of slope movements in the Alpine environment using DInSAR

THESIS

Presented to the Faculty of Science of the University of Fribourg (Switzerland) in
consideration for the award of the academic grade of *Doctor rerum naturalium*

by
Chloé Barboux

from
France

Thesis No: 1877

UNlprint

2014

Department of Geosciences, Geography
University of Fribourg (Switzerland)

Detection, mapping and monitoring of slope movements in the Alpine environment using DInSAR

THESIS

Presented to the Faculty of Science of the University of Fribourg (Switzerland) in
consideration for the award of the academic grade of *Doctor rerum naturalium*

by
Chloé Barboux

from
France

Thesis No: 1877

UNlprint

2014

Accepted by the Faculty of Science of the University of Fribourg (Switzerland) upon the recommendation of:

Prof. Claude Collet	University of Fribourg (CH)	Supervisor
Prof. Reynald Delaloye	University of Fribourg (CH)	Expert
Dr. Tazio Strozzi	Gamma Remote Sensing (CH)	Expert
Dr. Xavier Bodin	Savoie University (F)	Expert
Prof. Vincent Serneels	University of Fribourg (CH)	President of the jury

Fribourg, November 13th 2014

Thesis supervisor:

Prof. Claude Collet

Dean:

Prof. Fritz Müller

Table of contents

Abstract.....	5
Résumé	7
Acknowledgements	9
List of Abbreviations	11

1st Part: Introduction and generalities

1	Introduction	15
1.1	The Alpine environment	15
1.2	Alpine slope movements	15
1.3	Detection, mapping and monitoring of Alpine slope movements	19
1.3.1	Kinematic measurement techniques	19
1.3.2	The choice of DInSAR technique to detect, map and monitor Alpine landforms	22
1.3.3	Pilot study using DInSAR in the Western Swiss Alps and first issues.....	22
1.4	Objectives of the thesis	24
1.5	Outline of the thesis	26
2	Advances in the application of DInSAR for surveying mass wasting in the Alpine environment.....	29
2.1	Introduction	29
2.2	History of space-borne DInSAR	30
2.2.1	The origin of space-borne DInSAR	30
2.2.2	Space-borne DInSAR applications in mountain environments.....	30
2.3	Advances in the detection and mapping of Alpine moving landforms using DInSAR	31
2.3.1	Detecting Alpine slope movements in Austria	31
2.3.2	Alpine survey in Switzerland	32
2.4	Advances in the monitoring of Alpine moving landforms using DInSAR.....	36
2.4.1	Monitoring slope motion in Austria.....	36
2.4.2	Monitoring Alpine slopes in Switzerland	37
2.4.3	Some interesting results around the rest of the world.....	39
2.5	Synthesis of literature review	40
2.5.1	Suitability of DInSAR	40
2.5.2	Detection and mapping with DInSAR.....	41
2.5.3	Monitoring with DInSAR.....	41
2.6	Connection with thesis rationale	42
2.6.1	Suitability of DInSAR in the Alpine environment.....	42
2.6.2	Detection and mapping of Alpine moving landforms.....	42
2.6.3	Monitoring of Alpine moving landforms.....	43

2nd Part: Evaluation of DInSAR contribution to slope movement analysis in an Alpine environment

3	DInSAR for the observation of slope movements in the Alpine environment.....	47
3.1	Differential SAR Interferometry	47
3.1.1	SAR imaging system	47

3.1.2	SAR image.....	48
3.1.3	SAR Satellites	48
3.1.4	DInSAR processing	51
3.1.5	Interferometric products derived from DInSAR	52
3.2	Suitability of DInSAR in mountain areas.....	53
3.2.1	Generalities	53
3.2.2	Imaging geometry.....	53
3.2.3	DEM errors	54
3.2.4	Characteristics of the surface changes	55
3.2.5	Soil moisture.....	56
3.2.6	Snow.....	57
3.2.7	Vegetation.....	57
3.2.8	Atmosphere.....	58
3.3	Proof-of-concept study on the suitability of DInSAR data in surveying mountain slopes.....	61
3.3.1	Introduction and objectives	61
3.3.2	Layover and shadow mask	61
3.3.3	Index of the deformation rate measurability.....	63
3.3.4	Suitability of DInSAR data.....	65
3.3.5	Discussion.....	66
3.4	Conclusion.....	68
4	Towards semi-automated mapping of slope movements with DInSAR in the Alpine environment?.....	69
4.1	Introduction and background	69
4.1.1	Methodology of visual inventory for detecting mass wasting in the Swiss Alps.....	70
4.1.2	Objectives of an automated procedure	73
4.2	Statistical methods to classify DInSAR signal	76
4.2.1	Generation of textural image features	77
4.2.2	DInSAR signal classification from statistical methods.....	79
4.2.3	Performance.....	80
4.2.4	Conclusion	83
4.3	Mapping of the slope movements	83
4.3.1	Mapping of the DInSAR signal	83
4.3.2	Mapping of the slope movements.....	85
4.3.3	Performance.....	86
4.3.4	Recommendation	95
4.4	Discussion	95
4.4.1	Mapping of the slope stability or the slope movement?.....	96
4.4.2	Estimated time	96
4.4.3	External artifacts.....	97
4.4.4	Resolution.....	99
4.4.5	On the use of the ERS archives and current acquisitions.....	99
4.5	Conclusion.....	100
5	Challenges and solutions to monitor annual and seasonal displacement rates of Alpine rock glaciers and landslides using DInSAR.....	101
5.1	Introduction	101

5.2	Monitoring of Alpine landforms along a profile.....	102
5.2.1	Method of Alpine rock glacier monitoring along a profile.....	102
5.2.2	Performance.....	107
5.2.3	Discussion.....	112
5.2.4	Conclusion.....	114
5.3	Monitoring of rock glaciers using maps of DInSAR signal and maps of slope movements.....	114
5.3.1	Rock glacier behavior from automated mapping of DInSAR signal.....	114
5.3.2	Performance.....	119
5.3.3	Discussion.....	121
5.3.4	Conclusion.....	123
5.4	Overall conclusion.....	123

3rd Part: Applications using DInSAR technique for detecting, mapping and monitoring mass movements in the Western Swiss Alps

6	Suitability of DInSAR data for the research on mass wasting dynamics in the Western Swiss Alps.....	127
6.1	Potential of ERS DInSAR data for the detection of slope movements in the Western Swiss Alps.....	127
6.1.1	Detailed results observed in the Western Swiss Alps.....	127
6.1.2	Examples of detected Alpine landforms with ERS DInSAR data.....	130
6.1.3	Conclusion.....	132
6.2	Moving landforms monitored by DGPS in the Western Swiss Alps.....	133
6.2.1	Generalities.....	133
6.2.2	Characteristics of landforms.....	133
6.2.3	Direction of a landform's displacement at each DGPS position.....	135
6.2.4	Conclusion.....	136
6.3	Suitability of TSX DInSAR data in the Valais.....	137
6.3.1	Visibility.....	137
6.3.2	Maximum measurable deformation rate.....	139
6.3.3	Discussion.....	141
6.3.4	Conclusion.....	143
6.4	Conclusion.....	144
7	Mapping of slope movements in the Western Swiss Alps with DInSAR: pilot studies and promising applications.....	145
7.1	Update and upgrade of DInSAR polygon inventory.....	145
7.1.1	Study site and data processing.....	145
7.1.2	Visual update and upgrade of past inventoried DInSAR polygons.....	146
7.1.3	Automatic update of DInSAR polygon inventory.....	147
7.1.4	Performance.....	148
7.1.5	Discussion.....	150
7.1.6	Conclusion.....	152
7.2	Refining and assessing glacier outlines over debris-covered areas: A pilot study in the Upper Valais.....	154
7.2.1	Introduction.....	154
7.2.2	Detection of debris-covered glaciers using DInSAR and airborne photography.....	154

7.2.3	TSX DInSAR data processing and region study	155
7.2.4	Methodology for reassessing outlines from DInSAR data.....	156
7.2.5	Results observed in the Mischabel massif	161
7.2.6	Discussion.....	163
7.2.7	Conclusion	166
7.3	Conclusion.....	166
8	Example of DInSAR contribution for site specific analysis	167
8.1	Analyzing the pluri-decennial development of a rock glacier crisis using repeated DInSAR, terrestrial and airborne optical data.....	167
8.1.1	Introduction.....	167
8.1.2	The Grabengufer.....	168
8.1.3	Reconstruction of the destabilization.....	168
8.1.4	Conclusion	173
8.2	Detection of intra-seasonal variation and geomorphological processes	175
8.2.1	Gänder rock glacier.....	175
8.2.2	Jegi rock glacier.....	180
8.3	Discussion	184
8.3.1	DInSAR dataset	184
8.3.2	Spatio-temporal resolution of DInSAR data	184
8.3.3	Surveying Alpine landforms from DInSAR data	185
8.4	Conclusion.....	186
4th Part: Synthesis and Conclusion		
9	Conclusion and perspectives	189
9.1	General results and main contributions	189
9.2	Further improvements and future research	191
9.2.1	Suitability protocol.....	191
9.2.2	Algorithm for slope movement mapping.....	191
9.2.3	Requirements for the update and upgrade of past inventoried DInSAR polygons.....	192
9.2.4	Early warning system using continuous up-to-date DInSAR data	192
9.3	Perspective in Alpine geomorphology.....	193
9.3.1	Extension to other alpine regions.....	193
9.3.2	Processes understanding	194
9.4	Conclusion.....	194
Bibliography		195
Appendix 1		207
Curriculum Vitae.....		209

Abstract

Alpine environment areas are generally associated with high mountains located above tree line and are largely affected by slope movements. Instabilities include a wide variety of movements, ranging from the slow continuous displacement of entire slopes, where the main process is creep, to catastrophic landslides, where the mass slides fast down the valley. The origin, progress and effects of these mass movements are extremely variable. They are influenced by several factors, most significantly by the geological structure, the rock characteristics and the slope inclination. Water is also often involved in the initiation and the progress of these movements. As Alpine environments are potentially concerned by permafrost, it is expected that any change in the thermal state of the frozen soil may also play a key role in the observed processes affecting loose sediments (talus slopes, moraines, rock glaciers, landslides, etc.), as well as rock walls. Although Alpine slope movements concern mainly non-urban areas, potential natural hazards for people and infrastructures cannot be excluded. Consequently, the knowledge of the regional overview of slope instabilities and the understanding of the processes governing them is of prime interest.

The relatively new technique of Differential satellite Synthetic Aperture Radar Interferometry (DInSAR) has proven to be a useful tool for large-scale surveys of Alpine slope movements. It provides a regional overview of surface displacements at a mm to cm resolution over Alpine areas, where dense vegetation is no longer present. The use of ERS-1/2 DInSAR data in particular has been evaluated to estimate the magnitude and the spatial pattern of slope motion, and reveals the applicability of this remote sensing method for inventorying creeping landforms in the Alpine environment. DInSAR technique therefore looks very promising to provide accurate information and quantification of the deformation of moving landforms. Several studies have demonstrated the suitability of DInSAR for monitoring large width rock glacier displacements with a velocity of up to half a meter per year in the Alpine environment.

The main objective of this PhD thesis is to investigate the applicability of DInSAR technique to perform the detection, mapping and monitoring of terrain deformations in an Alpine environment. A methodological focus for this thesis is thus required to complete this objective successfully. A few applications are given in order to demonstrate the use of this technique to geomorphologists in the Alpine environment but are not meant to be exhaustive. The tests and applications are performed in the Alpine periglacial belt of the Western Swiss Alps whose topography, weather conditions, velocity and spatial scale of moving landforms challenge the limits of DInSAR technique. A pilot study was

performed in 2005, where DInSAR technique was used to compute several inventories of slope instabilities at a regional scale over the whole Swiss Alps. It appears that the area is largely affected by terrain changes where more than 2000 landforms, located in the Alpine periglacial belt, were visually detected on a large set of DInSAR data dating back to the nineties, with velocities ranging from a few centimeters to several meters per year. More recent data could be used to update these past inventories in order to detect changes in the activity rate of DInSAR detected landforms. In addition, the use of the new high technology of TerraSAR-X (TSX) should be explored and evaluated for Alpine research purposes.

These topics are investigated within the present dissertation. First, a standard protocol is proposed to determine the performance of DInSAR technique for the detection, mapping and monitoring of Alpine moving landforms over a delimited Alpine area. Then, different methods are developed to (automatically) detect, map and monitor Alpine moving landforms in this specific Alpine environment. Finally, the use of TSX DInSAR data is explored in various applications using the proposed methodologies over the region of interest. When possible, the results derived from qualitative or quantitative analysis of DInSAR data are compared to existing data, mainly from leveling and/or aerial images analysis.

As a result, DInSAR technique appears appropriate for a systematic detection and mapping of moving slopes in an Alpine environment. The extent of moving slopes are accurately detected and delimited from (automated) analysis of DInSAR data. Using TSX data, some specific cases of very active Alpine movement slopes (1-3.5 m/y) can be correctly monitored. However, the estimation of deformation rates remains generally approximate and cannot be precisely quantified in the case of rapid slope movements (≥ 1.5 m/year). Hence, the present study reveals that the DInSAR technique's accuracy is currently not sufficient for monitoring purposes. When trying to interpret specific processes involved in Alpine slope movements, DInSAR should first be used with a complementary technique such as leveling measurements, and second, it requires specific geomorphological knowledge and specific software skills in order to provide suitable DInSAR data. Together with industrial and manufacturing innovations, which are expected to increase the spatial and temporal resolution of the sensors in the upcoming years, the present work has the potential to open the doors for the monitoring of fast moving Alpine slopes, the precise mapping of velocity rate and the possibility to observe specific changes in the behavior of Alpine landforms.

Keywords: DInSAR, rock glacier, landslide, periglacial landforms, detection, mapping, monitoring, TerraSAR-X

Résumé

L'environnement alpin désigne l'ensemble du territoire montagnard commençant à la limite supérieure de la forêt jusqu'à l'étage nival, étage des neiges éternelles. Composé essentiellement d'étendues gazonnées semées d'îlots arbustifs et de roches nues ou débris rocheux, cette zone est potentiellement sujette à des mouvements de terrain de toute sorte, allant des déplacements lents et continus pouvant affecter l'ensemble d'une pente, aux glissements de terrain catastrophiques dont la masse chute rapidement vers la vallée. L'origine, le développement et les effets de ces instabilités sont diverses et variées. Différents facteurs y jouent un rôle plus ou moins prédominant dont les principaux sont la structure géologique du sol, les caractéristiques de la roche ou encore l'inclinaison de la pente ; l'eau y étant souvent reconnue comme agent d'activation. Enfin, cet environnement étant potentiellement concerné par le pergélisol, on peut aussi s'attendre à ce que la déformation (reptation) des matériaux gelés soit un mécanisme plus ou moins responsable des mouvements de terrain affectant les versants peu raides (éboulis, moraines, glaciers rocheux,...) tout comme les parois. Bien que la plupart de ces mouvements de terrain soient localisés dans des zones non-urbanisées, ils représentent parfois un réel danger pour l'Homme et les infrastructures. Il convient alors de procéder à une observation de ces instabilités à l'échelle régionale afin d'avoir une vue d'ensemble de la distribution, mais aussi à l'échelle locale afin de comprendre tout particulièrement les processus spécifiques les gouvernants.

La technique d'interférométrie différentielle par radar à synthèse d'ouverture satellitaire (traduction anglo-saxonne de « Differential satellite Synthetic Aperture Radar Interferometry » ou « DInSAR ») semble prometteuse pour l'obtention d'informations précises sur ces mouvements de terrain alpins. Cette technique permet d'avoir une vue d'ensemble des déplacements de surface de l'ordre du mm au cm en milieu alpin où la végétation y est souvent restreinte. Basées principalement sur l'utilisation des satellites ERS-1/2, plusieurs études ont démontré par le passé le fort potentiel cette technique pour estimer l'ampleur et l'étendue spatiale des instabilités de terrains alpins en termes de cartographie des mouvements de terrain, mais aussi pour l'estimation et catégorisation des vitesses de déplacements. Plusieurs études ont enfin montré la capacité de cette méthode pour l'observation précise de déformations de glacier rocheux dont les vitesses atteignaient le demi-mètre par an.

Le principal objectif de cette thèse de doctorat est d'évaluer la pertinence de l'utilisation de la technique DInSAR pour la détection, la cartographie ainsi que pour l'observation de mouvements de terrain en milieu alpin. De nombreux tests et applications sont réalisés au niveau de la ceinture périglaciaire des Alpes Suisses occidentales dont les caractéristiques topographiques et météorologiques ainsi que les mouvements observés en termes de dimension spatiale et vitesse en font un challenge de taille. En 2005, un inventaire précis des mouvements de terrain a été réalisé

dans cette région à partir de l'interprétation visuelle de données DInSAR datant des années nonante. Plus de 2000 formes de terrain ayant des vitesses de quelques centimètres à plusieurs mètres par an y ont été recensés. Il semblerait que les données les plus récentes peuvent être utiles pour mettre à jour ces anciens inventaires et détecter d'éventuels changements. Cette thèse s'attachera alors à évaluer particulièrement les performances des nouvelles données TerraSAR-X (TSX) pour l'observation de mouvements de terrain dans l'environnement alpin.

Le potentiel de la technique DInSAR est ainsi étudié en détail tout au long de cette dissertation. Dans un premier temps, un protocole standard est proposé afin d'évaluer les performances de la technique DInSAR pour la détection, la cartographie et l'observation de mouvements de terrain sur une région alpine quelconque. Différentes méthodes sont ensuite développées afin de détecter, de cartographier et observer (automatiquement) ces mouvements de terrains. Enfin, l'utilisation du nouveau satellite TSX est explorée en détail dans diverses applications utilisant les méthodes développées en amont appliquées à l'échelle des Alpes Valaisannes. Lorsque ceci est possible, les résultats sont comparés de manière quantitative ou qualitative avec des données existantes provenant principalement de relevés GPS sur le terrain et/ou d'analyses d'images aériennes.

En définitive, la technique DInSAR est évaluée en détail dans ce travail pour la détection, la cartographie et l'observation de mouvements de terrain en milieu alpin. Les résultats montrent la puissance de cette technique pour la détection et la délimitation des mouvements de terrain à large échelle. Cependant, la précision des mesures de déformations pour une étude en local reste assez faible. En effet, même si certains cas d'étude montrent la possibilité de suivre les mouvements de formes de terrain très actives (1-3.5 m/a), les déformations peuvent être approximativement estimées mais non précisément quantifiées la plupart du temps pour les mouvements rapides (≥ 1.5 m/an). Ainsi, ce travail montre que l'utilisation des données actuelles avec la technique DInSAR, ne semble pas suffisante pour l'observation précise des mouvements de terrain alpins. L'interprétation de processus spécifiques régissant les formes de terrain requière : 1) l'utilisation combinée de la technique DInSAR avec d'autres techniques comme par exemple des relevés sur le terrain, et 2) des connaissances approfondies en géomorphologie mais aussi spécifiques en traitement de données DInSAR. Avec les progrès des futurs capteurs embarqués sur satellite il est probable que les résolutions spatiale et surtout temporelle soient améliorées. Ainsi les possibilités s'en trouveront améliorées pour l'observation précise de mouvements de terrain, ainsi que pour la compréhension de processus gouvernant les mouvements de terrain en milieu alpin.

Mots-clés: interférométrie radar satellitaire, glacier rocheux, glissement de terrain, forme de terrain périglaciaire, détection, cartographie, observation, TerraSAR-X

Acknowledgements

To Reynald Delaloye and Claude Collet, for giving me the opportunity to integrate into the Geography Institute of the University of Fribourg. Claude, I really thank you for believing in me, for always supporting me and giving the help I needed to get back on track. I really appreciate your humor, your true motivation and energy. I wish you now a really happy retirement. Reynald, I am honored to have done my doctorate research with you; I appreciate your never ending encouragements, your serious involvement in my research and also your true sincerity. I also really appreciate sharing with you all these mountain trips, for science or just for rock, and I am now looking forward to the next ones.

To Tazio Strozzi from Gamma Remote Sensing SA (or simply from his beautiful remote canton of Tessin), for giving me his technical expertise and relevant feedback about DInSAR technique whenever it was needed, for his sincere involvement in my research and for his sympathy.

To Xavier Bodin from the Savoie University, for his deep reading of my thesis and for his precious contribution by bringing valuable and relevant feedback.

To Christophe Lambiel from the Institute of Earth Surface Dynamics (is it right?) of the University of Lausanne, for bringing his valuable inputs and relevant feedback into the field of geomorphology during my research and for his sincere kindness.

To Hugo Raetzo from the Office Federal for the Environment, for the collaboration in various projects, for providing some data, and for his curiosity about my research project.

To the (future) doctors Thomas Echelard and Jessica Papke, for sharing experience and interesting results about the use of DInSAR technique in Alpine environments, for our productive days of work together, for their sympathy and for the good times together in or outside work time.

To my friend Oriol Monserrat, met during my first conference in Bergen and then again and again, for the lot of fun drinking coffee at those never ending congress, for escaping science from time to time, and for his sincere sympathy and kindness. Looking forward to seeing you in España!

To my colleague Mauro Fischer, for his serious involvement in our short project together of debris-covered glacier mapping, for his scientific support and his sincere kindness.

To my friends and (past) colleagues Jonathan Dorthe, Damien Abbet and Sebastien Morard, for the spirit and frank camaraderie, for the good times together during field campaigns and the shared gastronomic events. Yummi yummi!

Last but not least, to my every other colleagues at The Geography Unit, PhD students, Post-PhD, MAs Profs and also all the staff, for their scientific, administrative or technical support as well as for keeping a friendly atmosphere in the Institute especially at the coffee break. A special thanks to Benno, Stephanie and Antoine for keeping a friendly atmosphere on the 2nd floor; to Valentine and Alexandre for discussions about everything except Science; and to Christine for the passionate discussions when we were returning home by train and for the ritual sushi!

To my Friends, for making my life full of good times and rich of experiences. Special thanks to my old friend Lélé, for encouraging me during all my life, for her happiness and her deep sincerity. To my good old friend Yann, for always sharing lots of fun even after all these years. To Quentin for rethinking the world together by a candle-side in small huts lost in the mountains. To JP&Helène, for inspiring me and for showing that everything is possible in the world as soon as you want it. To JC for always being there despite the distance. To the PeauPow Team, and especially to Aline&Pat, Géraud, Steph, Louis, Marc, Rem&Fi, Mad&Quentin and Fabien for sharing sportive experiences but also lots of good times outside the thesis.

To my Family, to Papa and Moon, for encouraging me to continue my post graduate education and providing me love and support. To my sisterssss and bro, for making family life so happy and so enjoyable. To Mariani's family, for welcoming me with open arms and for enjoying life simply. And to Mémé, who unfortunately could never see that I was not in Freiburg in Germany but in Fribourg in Switzerland, for always encouraging me in the life whatever the choice and whatever the direction, for making me what I am now.

To Benoit, for sharing the last 10 years of my life, and for many years to come, for always supporting and encouraging me, for taking care of me again with such of love. T'M my Doud'

And of course, to the other ho were not mentioned herein but somehow participated in the result of this thesis.

Finally, to various sources of data: TSX SAR data under proposals LAN411, LAN1145 and LAN2548 (© DLR); and DHM25, SwissAlti3D, Swissimages and Pixel Maps © Swisstopo.

List of Abbreviations

ASAR	Advanced Synthetic Aperture Radar
ASI	Italian Space Agency
ALOS	Advanced Land Observing Satellite
CSA	Canadian Space Agency
CSK	COnstellation of small Satellites for Mediterranean basin Observation
DEM	Digital Elevation Model
DInSAR	Differential InSAR
DGPS	Differential Global Positioning System
DLR	Deutsches Zentrum für Luft- und Raumfahrt
ESA	European Space Agency
ERS	European Remote Sensing
GIS	Geographic Information System
InSAR	SAR interferometry
JAXA	Japan Aerospace Exploration Agency
JERS	Japanese Earth Resource Satellite
LOS	Line Of Sight
PALSAR	Phased Array type L-band SAR
RMSE	Root Mean Square Error
SAR	Synthetic Aperture Radar
SLC	Single Look Complex
TSX	TerraSAR-X
TDX	Tandem-X

1st Part:

Introduction and generalities

The 1st Part introduces the topic of this thesis through two chapters. The first chapter introduces the context and generalities about slope movements occurring in the Alpine environment. Common techniques to perform kinematic measurements are presented, as well as the rational and motivations of the present research work. Finally the objectives and outline of the thesis are provided. The second chapter presents the state of the art in the field of DInSAR technique for surveying mountain landscapes, including a review of the technique according to the following approaches: 1) mapping the Alpine landform distribution and 2) understanding the Alpine landform processes.

1 Introduction

This introduction chapter aims to present the context of the thesis by first introducing generalities about the Alpine environment (Part 1.1) and about slope movements that occur there (Part 1.2). Next, Part 1.3 deals with the first issues related to the detection, mapping and monitoring of slope movement in the Alpine environment. It first presents common techniques used to observe and analyze Alpine landform kinematics. Second, it explains the choice of DInSAR technique. Third, it gives the rational and motivations of the present research work through the description of a past pilot study. Lastly, the objectives (Part 1.4) and outline (Part 1.5) of the thesis are detailed.

1.1 The Alpine environment

The Alpine environment refers to areas associated with high mountains located above the tree line and for botanists indicates native flora of alpine grasslands and tundra. Alpine vegetation grows close to the ground and consists mainly of alpine plants, which have adapted to the harsh effects of wind, cold temperatures, short growing seasons, dry conditions, and ultraviolet radiation. The area is typically covered by sparse grasses and alpine plants at lower elevations, and progressively becomes purely mineral at higher elevations before reaching the glaciated area.

In English, a lower case letter “a” is commonly used to properly designate this specific mountainous environment and an upper case “A” spatially restricts the definition to the Alps. Large parts of the area lying in the Alpine environment are potentially concerned by permafrost¹. The area situated between the tree line and the glacier zone corresponds to the belt, hereafter called the Alpine periglacial belt, where deep freeze/thaw cycles and sporadic to continuous permafrost conditions are likely to occur.

In the Swiss Alps, the lower limit of the discontinuous permafrost is estimated at an altitude around 2400 m a.s.l. in north-facing slopes and at 2700 m a.s.l. in southern exposures (Delaloye and Morand, 1997; Lambiel and Reynard, 2003). The Alpine periglacial belt is generally defined as the portion of the slope in between the tree line at 2000-2300 m and the glacier Equilibrium-Line Altitude (ELA) at 3000-3500 m.

1.2 Alpine slope movements

Mass movements are processes in which the solid material (stone or loose rock) is induced in downward motion mainly by gravity, and without the assistance of a transport medium. Alpine slope movements include a wide-range of types ranging from slow continuous displacement of entire

¹ Soil at or below 0°C for at least one year. Continuous permafrost is characterized by a continuous area affected by this thermal state and discontinuous permafrost when it isn't.

slopes, where the main process is creep, to catastrophic landslides, where the mass slides fast down valley. The origin, progress and effects of mass movements are extremely variable. They are influenced by several factors including the geological structure, the rock characteristics and the slope inclination. Water is often involved in the initiation and progress of the process. In the Alpine periglacial environment, it is expected that any change in the thermal state of permafrost (e.g. higher creep rates due to a warming of the permafrost) may also play a key role in the observed processes affecting loose sediments (talus slopes, moraines, rock glaciers, landslides, etc.) as well as rock walls. These changes may modify the transfer rate of loose material along Alpine slopes and can affect the frequency, the magnitude, as well as the type of related slope instabilities (Roer et al., 2005, 2008). In the Swiss Alpine environment for instance, various Alpine moving landforms can coexist in close proximity, constituting what is referred as an Alpine complex slope system (Figure 1.1). Examples of Alpine slope movements encountered in such specific regions are briefly described in the Table 1.1 and Figure 1.2 with some reference studies.

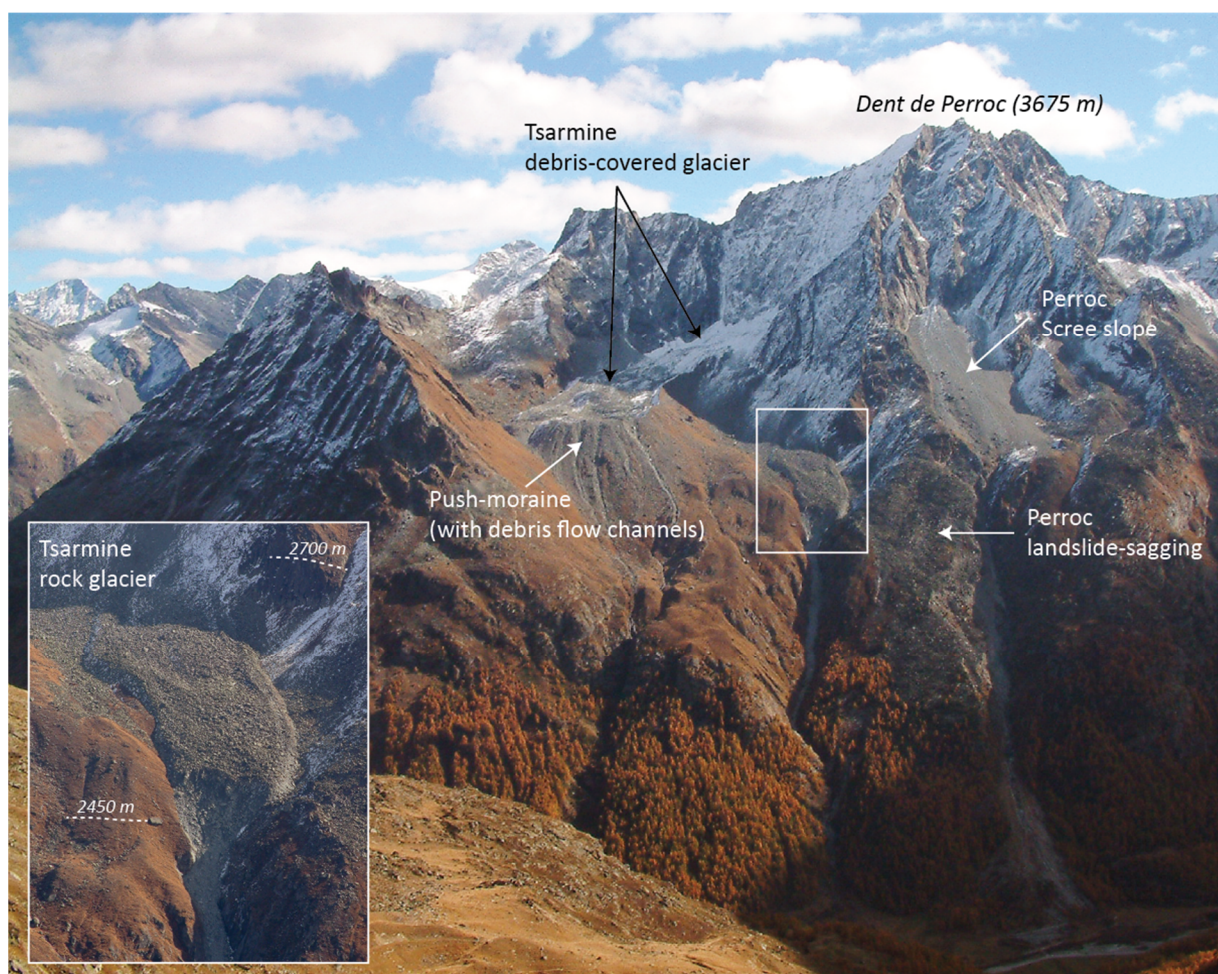


Figure 1.1: The periglacial belt is affected by different kinds of mass movements as illustrated by the orographic right side of the Arolla valley. Photo S. Morard 10/2005.

Alpine slope movement	Definition	Velocity	References
<i>Rock glacier</i> (Figure 1.2 a)	Lobate or tongue-shaped bodies of frozen debris separated from the surrounding terrain by a steep front and side slope. Perennially frozen loose material supersaturated with interstitial ice and ice lenses. From a few ten of meters up to several hundred of meters in width and up to a few kilometers in length.	. Destabilized (or surging): $\geq 2\text{ m/year}$. Active: several cm to m/year . Inactive: ~ 0 . Relict: no movement	Barsch, 1992; Delaloye et al., 2013; Giardino et al., 1987; Kääb, 2007; Lambiel et al., 2008; Roer et al., 2008
<i>Landslide</i> (Figure 1.2 b)	Downward movements of soil or rock masses on a sliding surface. Some landslides are large (up to several km^2) and may affect almost the entirety of a mountain slope.	some mm to several dm/year	Crozier, 2004; Lateltin et al., 2005
<i>Debris-covered glacier</i> (Figure 1.2 c,d)	Glacier tongues or cirque glaciers (or part of them) covered by material produced from surrounding areas. When retreating debris-covered glaciers may appear as dead-ice bodies no longer fed by a glacier.	cm/day	Bauder and Rüegg, 2009; Bosson and Lambiel, 2014
<i>Push-moraine</i> (Figure 1.2 f)	Topographic ridges transverse or parallel to the ice flow produced by proglacial deformation of frozen sediments, occurring at the glacier frontal and lateral margins, characterized by pure shear and compressional glacio-tectonics.	cm/year to cm/month	Delaloye, 2004; Haeberli, 1979; Lugon et al., 2004; Reynard et al., 2003
<i>Solifluction / gelifluction slopes</i> (Figure 1.2 e)	Includes all processes contributing to slow surficial periglacial mass wasting. Consists of soil creep associated with freezing (also called frost creep) and periodical water saturation. May occur on talus slopes of heavily weathered inclined regolith (or debris mantle). Tend to form characteristic surface features including lobes, terraces and sheets moving spatially and temporally heterogeneously on the slope.	mm to 0.5 cm/year	Harris, 2007; Matsuoka, 2004
<i>Rock fall</i> (Figure 1.2 g-i)	Generic term to describe free movement of material from steep slopes. - Pebble and block fall ($<100\text{m}^3$): characterized by a sudden detachment of individual components. - Rock fall ($>100\text{m}^3$): large volume of rock detached in mass. The mass disintegrates into individual boulders while falling. - Rock avalanche: large volume of rock (one to several million cubic meters) which detaches from a rock complex with high velocities and strong interactions between its components.	Sudden	Eberhardt et al., 2004; Ravelin et al., 2010
<i>Mud flow / debris flow</i>	Fast moving mixture of debris (pebbles, wood, soil, vegetation cover) and water originating on a steep slope or in sediment filled gullies.	Sudden (several m/second)	Bühler and Graf, 2013; Graf et al., 2013
<i>Subsidence/ uplift</i>	Downwards displacement of the Earth surface in response to geologic, water or man-induced causes. Uplift is the opposite phenomena resulting in an increase in elevation.	mm to cm/year	Strozzi et al., 2011; Zangerl et al., 2008

Table 1.1: Examples of Alpine slope movements encountered in the Swiss Alpine periglacial belt.

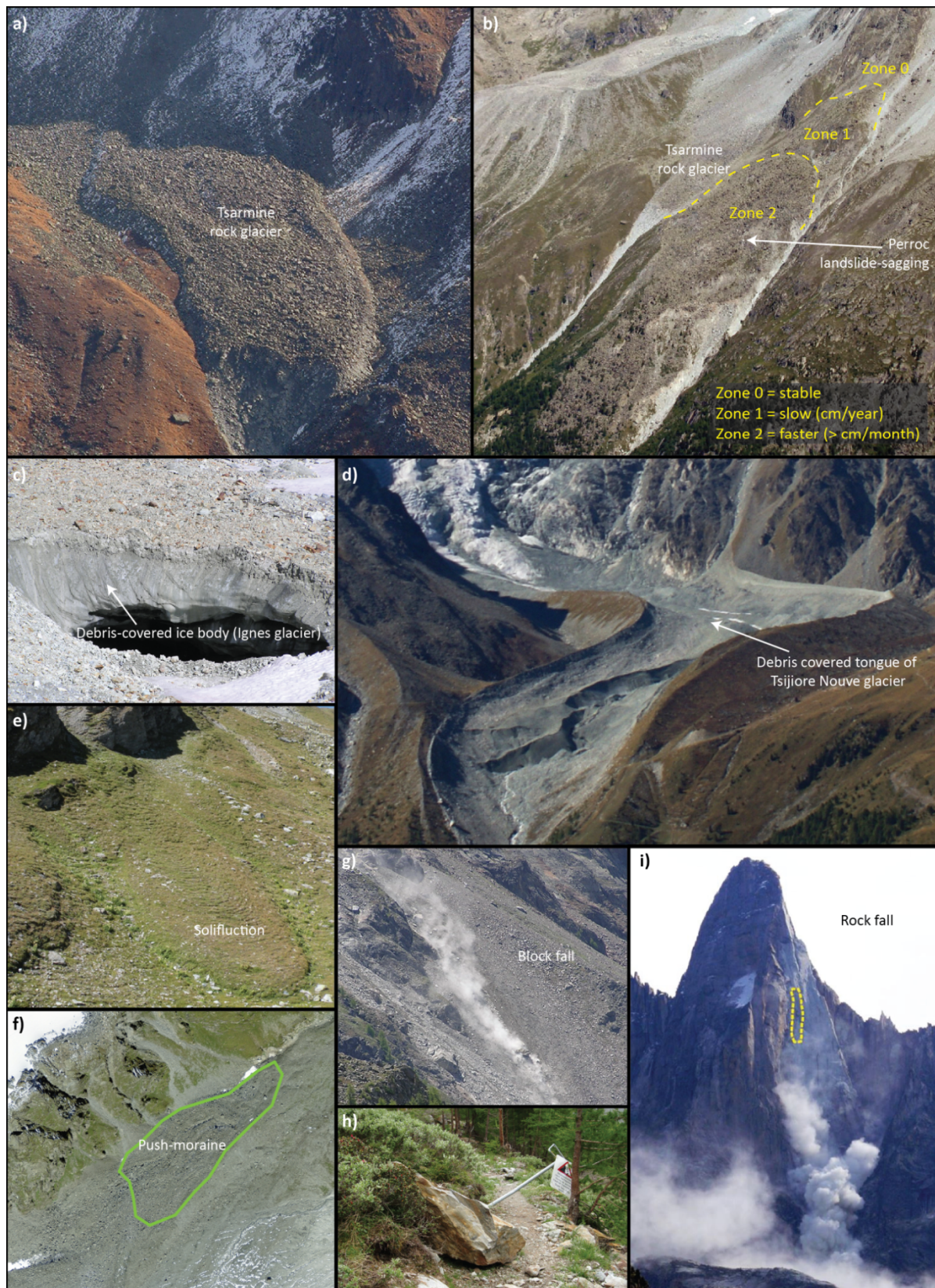


Figure 1.2: Examples of Alpine slope movements encountered in the Swiss Alpine periglacial belt. a) Tsarmine rock glacier. Arolla valley. Photo S. Morard 10/2005. b) Perroc landslide-sagging. Arolla valley. c) Lambiel 08/2005. c) Debris-covered ice body. Ignes glacier. Arolla valley. R. Delaloye 08/2004. d) Debris-covered tongue of Tsijiore Nouve glacier. Arolla valley. Photo C. Barboux 09/2011. e) Surface feature of solifluction. Meretschialp. S. Morard 08/2009. f) Orthoimages of the push-moraine of Ecoulaies. ©Swisstopo 2010. g) Block fall. Mattertal. R. Delaloye 06/2009. h) Block on a hiking trail. Mattertal. R. Delaloye 06/2009. i) Major rock fall on the west face of Les Drus. Mont-Blanc massif. L. Ravel 09/2011.

1.3 Detection, mapping and monitoring of Alpine slope movements

The changes in Alpine landforms surface geometry (along horizontal and vertical axes) are considered to give an insight into their ongoing processes. Consequently, the monitoring of the kinematics of an Alpine landform provides a basic understanding of its behavior over time. Moreover, in the context of climate change and in view of natural hazard risk management in mountain areas, especially in densely inhabited Alpine regions, there is a great need to investigate, to map and to monitor slope movements at both the local and the regional scale.

This leads us to formulate the two following important needs:

1) ***The detection and mapping*** providing an exact overview of the situation, in terms of location and activity rate of Alpine landforms over a specific region of interest, which would allow the evaluation of the distribution of moving slopes and the outlining of potentially dangerous landforms;

2) ***The monitoring*** giving an accurate observation of landform activity and specific velocity variations occurring from year to year and/or from season to season, in order to understand the processes involved in such Alpine landforms, and eventually to be able to warn about potentially dangerous activity.

1.3.1 Kinematic measurement techniques

In this section, the current techniques which are commonly used to observe Alpine landform kinematics are briefly presented (Table 1.2 and Figure 1.3). In-situ geodetic methods allow both the measurement of the surface displacements and the accurate location of measuring points. Remote sensing techniques refer to the acquisition of information by a distant device using multiple instruments (radar, lasers, cameras ...) at various wavelengths. The ground based remote sensing devices are distinguished from the air- and satellite-borne ones.

The characteristics of the presented techniques of kinematic measurements are synthesized according to the three different scales which are listed below (Table 1.2):

- The temporal scale, defined by the time interval in between measurements (or campaigns) and the availability of past data.
- The geometric scale, characterized by the geometric resolution (or sampling) of the measurement and its geometric span (or covered area).
- The thematic scale, expressed by the precision of the surface displacements measurement.

Technique	Definition	Temporal scale		Geometric scale		Thematic scale	References
		Time interval	Availability [year]	Resolution	Span	Precision	
In-situ geodetic methods	DGPS (Figure 1.3 a)	3 months - 1 year *	<1-10	Point network*	Local	cm	Berger et al., 2004; Krainer and Mostler, 2006; Lambiel and Delaloye, 2004; Noetzli, 2013; Perruchoud and Delaloye, 2007; Perruchoud, 2007
	Continuous GPS (Figure 1.3 b)	Continuous	<1-10	Unique point*	Local	cm	Baldi et al., 2008; Malet et al., 2002; Noetzli, 2013; Philippe and Grimm, 2009
Ground based remote sensing	Historical images (Figure 1.3 d)	Several years	10-100	m	Local to regional	m	Delaloye et al., 2013
	Webcam (Figure 1.3 e)	Continuous*	<1-10	dm-m*	Local to regional	cm	Delaloye et al., 2013
	Lidar (Light detection and ranging) (Figure 1.3 c)	1-2 months – 1 year*	<1	cm*	Local	cm	Abermann et al., 2010; Bühler and Graf, 2013
	Ground based InSAR (Figure 1.3 g)	Continuous*	<1-10	cm*	Local to regional	mm-cm	Werner et al., 2010
Air-/Satellite-borne remote sensing	Photogrammetry (Figure 1.3 f)	Several years	<1-100	dm	Regional	cm – m	Kääb, 2008; Kääb et al., 1997a, 1997b, 1998, 2003, 2005; Kaufmann, 1998; Kaufmann et al., 2007
	DInSAR (Differential Synthetic Aperture Radar Interferometry) (Figure 1.3 h)	1 day / 1 month 1 year / several years	<1 - 25	1-100 m	Regional	mm-cm	(Delacourt et al., 2004b; Delaloye et al., 2010b; Kenyi and Kaufmann, 2003; Lambiel et al., 2008; Nagler et al., 2001, 2002; Rignot et al., 2002; Rott et al., 1999b; Strozzi et al., 2009b, 2010a, 2004, 2005)

* User defined

Table 1.2: Some techniques of kinematic analysis commonly used in Alpine environments.

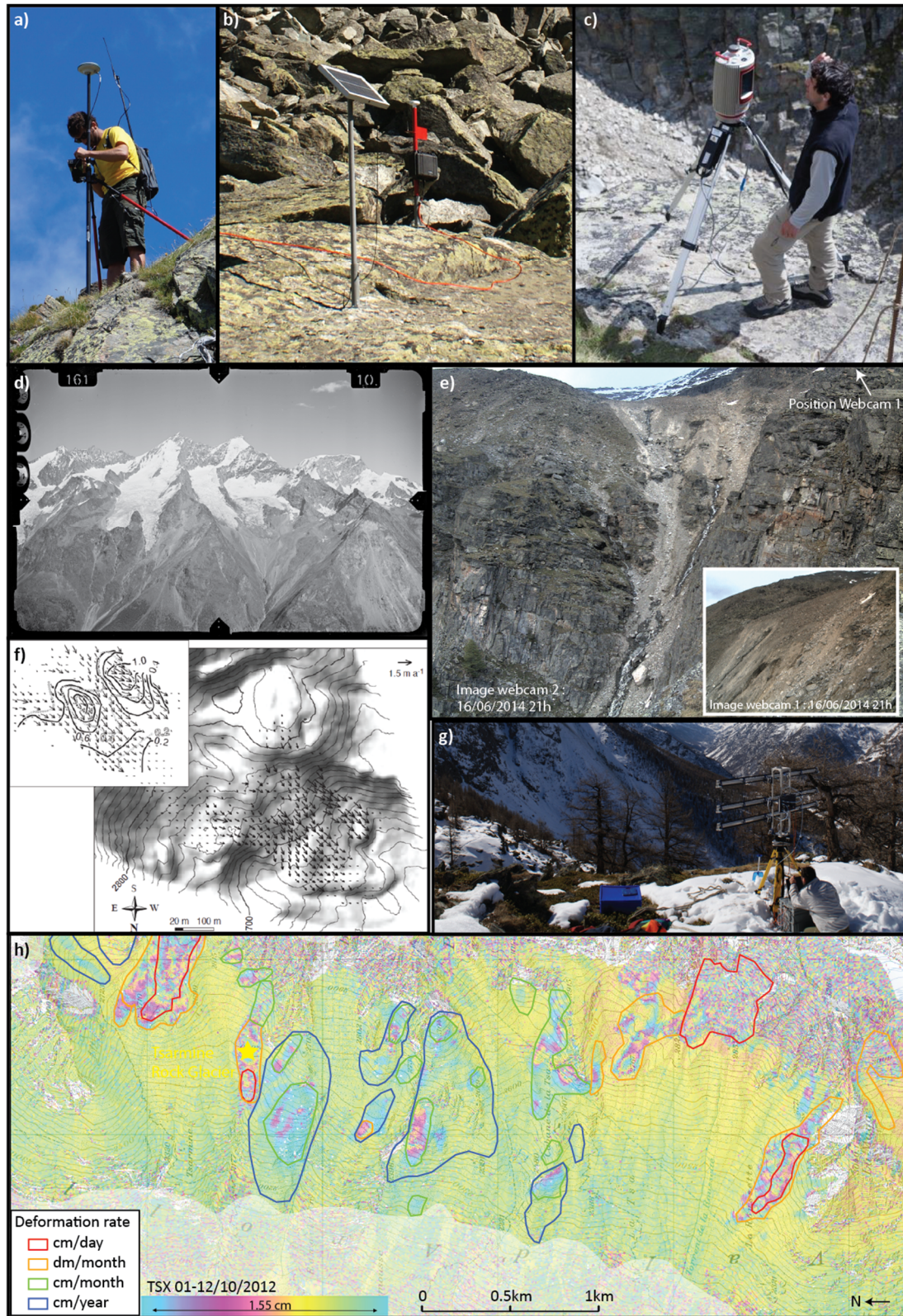


Figure 1.3: Current techniques of kinematics analysis commonly used in Alpine environments. a) Measure of marked points of interest using DGPS technique. C. Barbou 07/2013. b) GPS station installed on the Tsaarmine rock glacier. C. Barbou 09/2011. c) Lidar measurements. M. Bochud 06/2013. d) Historical photograph of the Mattertal valley. ©Swisstopo 1930. e) Images acquired by two webcams installed on the site of the Gugla rock glacier. © UniFR. f) Averaged horizontal surface velocities on the Becs-de-Bosson rock glacier measured using aerial photography from 1986, 1991 and 1999. From Käb (2005). g) Ground based InSAR measurements. C. Barbou 03/2011. h) DInSAR detected moving zones superimposed on the TSX interferogram from the 01-12/10/2012.

1.3.2 The choice of DInSAR technique to detect, map and monitor Alpine landforms

The improvement of in-situ geodetic techniques, in terms of precision and cost, offers new perspectives for the monitoring of Alpine landforms. Remote sensing techniques have seen important improvements these last years and, for some of them, their use is now well-established for the observation of Alpine moving landforms. Actually, it is quite complex to compare these techniques, as they provide complementary observations and offer the possibility to work at different temporal, spatial and thematic scales (Table 1.2).

The primary advantage of air- and satellite borne remote sensing techniques is that measurements can be performed in the absence of fieldwork, contrary to the ground base remote sensing and the in-situ geodetic methods. In addition, air- and satellite borne remote sensing methods are measuring over a wide area rather than providing only limited information like in-situ geodetic methods. Finally, air- and satellite borne remote sensing methods offering a large span and a high geometric resolution provide the possibility of both mapping and monitoring Alpine landforms, and so are especially interesting solutions to analyze the slope movements over mountainous regions which are often difficult to access.

While photogrammetry is probably the current best known method for quantifying the displacement of slope movements, it is subject to external artifacts such as snow, clouds or mission resources (cost, time, planning). This limits the use of this technique in mountainous regions which are particularly subject to difficult and disturbed weather conditions. The ability of the relatively new DInSAR technique to penetrate clouds and be operational at day and night, together with its ability to detect surface displacements at a subcentimetric resolution make it an attractive choice to observe slope movements in mountainous regions.

1.3.3 Pilot study using DInSAR in the Western Swiss Alps and first issues

The Western Swiss Alps extend east of the Mont-Blanc range, from the Bernese Oberland at the north through the Rhone Valley and the Penninic Alps to the Swiss-Italian frontier at the South (Figure 1.4). In 2005, several inventories of slope instabilities were compiled at a regional scale in this region using a large set of ERS-1/2 and JERS-1 DInSAR data dating back to the 1990s (Delaloye et al., 2005, 2008a). It appears that the area was largely affected by terrain changes, since more than 2000 landforms located in the Alpine periglacial belt were detected with a velocity ranging from a few centimeters to several meters per year. In particular, fast moving slopes (velocity ≥ 1.5 m/year) were detected thanks to the past ERS-1/2 sensors offering the unique possibility of 1 and 3 days repeat cycle (Delaloye et al., 2010b). The results of these inventories have been evaluated and verified on different selected sites with known phenomena. They have shown the efficiency of DInSAR technique

for inventorying creeping landforms in the mountain periglacial environment, and for estimating and categorizing their displacement velocities (Delaloye et al., 2007b; Lambiel et al., 2008).

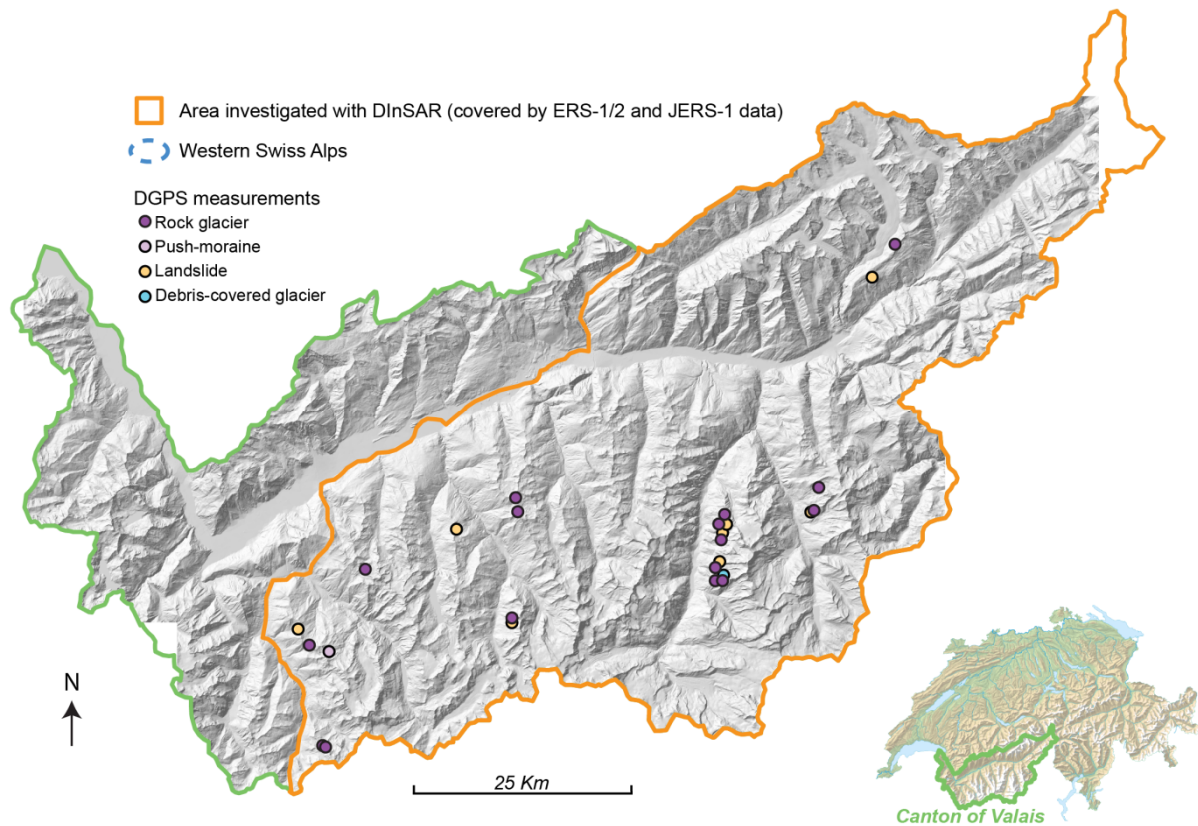


Figure 1.4: Location of the Western Swiss Alps and area investigated by systematic slope movement inventories based on ERS-1/2 and JERS-1 DInSAR data. Stars represent the twenty six study sites where DGPS measurements have been performed since at least 2006 and are a valued source of validation.

Among all the DInSAR detected landforms, twenty-six are currently monitored by DGPS campaigns in order to analyze and understand the processes governing them. In practice, however, it is not possible to perform such leveling campaigns to properly achieve knowledge about the processes involved in each moving slope of the entire region of interest due to the costs and human resources needed to perform the measurements.

The most recent DInSAR data could particularly be used to update the past inventories in order to detect potential changes in activity rate of DInSAR detected landforms. However, since the termination of ERS-1/2 tandem data which occurred more than a decade ago, it seems that no other DInSAR data permits the characterization of very active Alpine landforms. The relatively new high technology of TerraSAR-X (TSX) looks very promising to provide accurate information about rapid moving landforms, but its performance remains unclear. Thus far, the use of the new TSX data has not been explored and evaluated for Alpine research purposes. Hence, there is a great need to determine the scope of application of DInSAR technique, and especially the use of the new SAR sensors, for observing surface processes in Alpine terrain.

1.4 Objectives of the thesis

The technique of DInSAR and its relatively new application in Alpine terrains will be investigated in this PhD work. As previously formulated in the introduction of Part 1.3, two axes of research have to be investigated: 1) the detection and mapping of Alpine moving landform distribution and 2) the understanding of the processes governing Alpine moving landforms using Differential Synthetic Aperture Radar Interferometry (DInSAR). However, before the development of methodologies for the observation of Alpine moving landforms, the scope of application of DInSAR technique for the study of slope movements in a specific and restricted area must be defined. Thus, a primary axis of research related to the suitability of DInSAR technique has been added to the problematic in order to assess the use of DInSAR technique for the detection, mapping and monitoring of moving slopes in an Alpine environment. It should be no surprise then that a methodological focus for this thesis is required to complete the objectives successfully.

Tests, experiments and applications are performed in the Alpine periglacial belt of the Western Swiss Alps, whose topography, weather conditions, velocity and spatial scale of moving landforms challenge the limits of DInSAR technique. In addition, this study benefits from previous works and applications using DInSAR performed in this region, the data availability over this area, and its proximity to the University of Fribourg. These factors allow for an easier access to the field for onsite observations and make it the ideal place for the study.

This work aims more specifically to investigate these three main axes of research, by answering the following questions:

1) Suitability of DInSAR technique for the observation of Alpine moving slopes:

This first axis of research aims to investigate the possibilities and limitations of the use of DInSAR technique for the observation of slope movements in the Alpine environment. In particular, the objective is to outline the scope of application of DInSAR technique for this purpose according to the characteristics of the selected DInSAR data, of the study area and of the related observed slope movements. The following questions can be identified:

- a) To what extent can the DInSAR data be used to detect and map Alpine moving landforms at a regional scale (regional overview), and monitor them at a local scale (on the scale of a single landform)?
- b) How can we assess the potential of DInSAR data for determining the location, the distribution, the geometry as well as the displacement and deformation rates of Alpine landforms at a regional or local scale?

- c) Can we establish a systematic procedure for the assessment of the use of DInSAR data to survey a mountainous region?

2) *Detection and mapping of Alpine slope movements:*

The second axis of research aims to investigate the use of DInSAR technique for the detection and mapping of slope movements in the Alpine environment. The detection and mapping of movements aims to provide an exact overview of the situation, in terms of location and activity rate of Alpine landforms over a specific region of interest. This overview would allow for the evaluation of the distribution of moving slopes and the outlining of potentially dangerous landforms. The following questions have been identified from pilot studies and will be the guiding thread for the development of new methodologies:

- a) How to update the existing inventories of DInSAR detected slope movements by integrating the most recent data?
- b) How to detect the potential changes in the activity rate of past DInSAR detected landforms and new moving landforms?
- c) It is possible to automate these processes of Alpine slope movement's detection and mapping?

3) *Monitoring of Alpine slope movements:*

Finally, the third axis of research aims to explore the use of DInSAR technique for the monitoring of slope movements in the Alpine environment. The monitoring consists in giving an accurate observation of landform activity and specific velocity variations occurring from year to year and/or from season to season, in order to understand the processes involved in such Alpine landforms, and eventually to be able to warn about potentially dangerous activity. The following questions have been identified from past experiments and from the typical characteristics of moving landforms observed in Western Swiss Alps:

- a) What is the potential of DInSAR data, and in particular the high spatio-temporal resolution TSX interferograms, for monitoring very active Alpine moving landforms (1-3.5 m/y)?
- b) Could we use DInSAR data to detect and/or understand geomorphological processes governing the activity of Alpine landforms?
- c) To what extent could DInSAR data be used independently of field measurements to monitor Alpine landforms?

The outline of the thesis will be described in the next part (Part 1.5), providing an overview of these three main axes of investigation; the following chapter (Chapter 2) will offer an overview of past studies dealing with space-borne DInSAR for the observation of moving landforms in an Alpine context in order to understand and justify the rational of this thesis.

1.5 Outline of the thesis

The thesis is organized into nine chapters as illustrated in Figure 1.5. A more detailed diagram is given in Appendix 1.

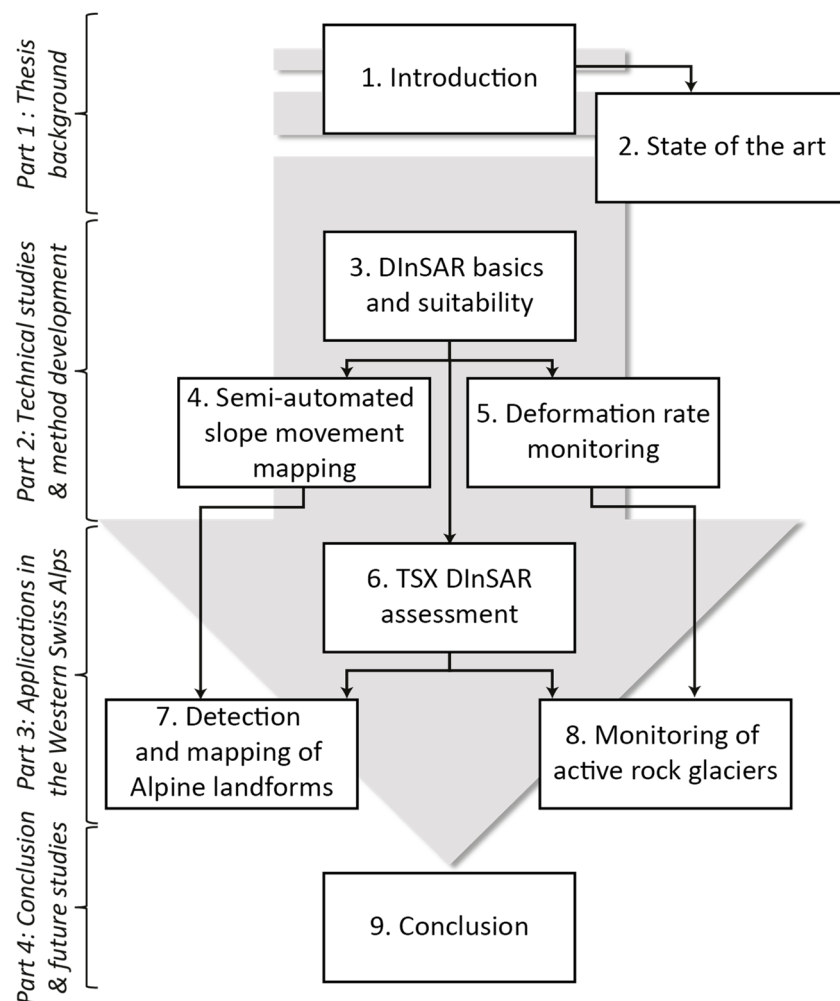


Figure 1.5: Detection, mapping and monitoring of Alpine moving landforms using DInSAR: outline of the thesis and chapters.

The **1st Part** introduces the topic of this thesis through two chapters.

Chapter 1 (current chapter) *introduces* the topic of this thesis, through the presentation of the Alpine environment, Alpine slope movements and common techniques behind the kinematics analysis used to detect, map and monitor these landforms. The *rational* and *motivations* behind the research work are explained together with the *objectives* and *outline of the thesis*.

Chapter 2 presents the *state of the art* in the field of DInSAR technique for surveying mountainous regions, including a *review of the technique* according to the following approach: 1) mapping the Alpine landform distribution and 2) understanding Alpine landform processes.

The **2nd part** is divided into three chapters and contains technical studies and methods developed in this thesis according to the three main axes of research.

Chapter 3 defines the *basics of DInSAR* and the behavior of DInSAR signals in mountains according to environmental and design parameters. Then, this chapter proposes a *procedure to evaluate the suitability of DInSAR technique* for slope motion mapping and monitoring in the Alpine environment.

Chapter 4 proposes an *automated method to map and assess the slope movements* in the Alpine environment from a selected dataset of TSX interferometric phase images. Validation of the procedure and evaluation of performances in a reduced region of interest are discussed.

Chapter 5 deals with the challenges and the solutions to *monitor annual and seasonal displacement rates of Alpine rock glaciers* using DInSAR. Specifically, the possibility to monitor annual and seasonal behavior of rapid rock glaciers (1.5-3 m/year) using the new high spatio-temporal resolution of TSX data is investigated. Three methods are proposed and discussed to show the potential of TSX DInSAR for observing Alpine rock glaciers.

The **3rd part** proposes applications of DInSAR technique, particularly using TSX DInSAR data that are limited to the specific Alpine environment of the Western Swiss Alps.

This part is divided into three chapters.

Chapter 6 proposes first the *assessment of the suitability of TSX DInSAR* data for the research on mass wasting dynamics using the methodology defined in Chapter 3 and is *limited to the specific area of the Western Swiss Alps*. The specific scope of application of TSX DInSAR technique is here determined for the study of slope movements in the selected area. Results on this specific region of interest are presented and discussed.

Then, the two following chapters offer a mixture of investigations performed in the Western Swiss Alps in order to demonstrate the use of DInSAR technique to geomorphologists for the mapping and monitoring of landforms in the Alpine environment.

Chapter 7 proposes the *mapping of slope movements in the Western Swiss Alps* with DInSAR: pilot studies and promising applications. Two applications are presented for the *mapping of Alpine slope movements* in order to illustrate the potential of slope movement maps proposed in Chapter 4. The first one proposes methods for the update and upgrade of past inventoried DInSAR polygons. The second one aims to *refine and assess glacier outlines* over debris-covered glaciated areas. Results are discussed in each respective application.

Chapter 8 proposes two applications for the *monitoring of Alpine rock glaciers*. The first one shows the possibility to analyze the *pluri-decennial development of a rock glacier* using DInSAR data combined with terrestrial and airborne optical data. The second one shows the potential of DInSAR data for the *detection of intra-seasonal variation* and *geomorphological processes* occurring on an Alpine rock glacier. A discussion is given about main results for the monitoring of Alpine moving landforms using DInSAR observed from applications.

Finally, the 4th Part is only composed of **Chapter 9** and provides a *general discussion* on the achievements of the thesis and the *perspectives* for future research.

2 Advances in the application of DInSAR for surveying mass wasting in the Alpine environment

The present chapter offers an overview of past studies dealing with space-borne DInSAR for detecting, mapping and monitoring moving landforms in an Alpine context. After a short introduction (Part 2.1), the following Part 2.2 introduces the history of DInSAR and the use of this technique for the specific Alpine environment. The two next Parts 2.3 and 2.4 describe in detail advances from the last fifteen years in the application of DInSAR technique, firstly for mapping and secondly for monitoring Alpine moving landforms. The potential of DInSAR for detecting and surveying processes in mountainous areas receives particular attention and is illustrated here through different examples of projects carried out by several groups of researchers around the world. Finally, a synthesis of main results is proposed (Part 2.5) allowing understanding of the rationale of this thesis (Part 2.6).

2.1 Introduction

Mountain geomorphology can be defined as “a regional component within geomorphology” (Barsch and Caine, 1984). It is concerned by the terrestrial surface processes and resultant landforms encountered in mountains. Geomorphologists are concerned with the morphology and composition of the land surface. They use this information to determine presently operating processes as well as their origin and their future changes.

In this research we are interested in the following approach: 1) the mapping of Alpine moving landform distribution and 2) understanding the processing governing the Alpine moving landforms using Differential Synthetic Aperture Radar Interferometry (DInSAR). As suggested by the literature, a third step could be added to this comprehensive approach, although it will not be investigated here, related to the prediction of potential hazard from these detected landforms in terms of rate or occurrence (Mantovani et al., 1996; Metternicht et al., 2005). In fact, monitoring the physiography of mountainous land is of great importance not only for the mountain itself, but also for adjacent lowlands. A significant number of contributions in geomorphology concern the identification of unstable landforms and sites with high probability of a catastrophic event (Rosenfeld, 2004). Many of the effects are predictable if proper information is available and goes through an appropriate evaluation (Mantovani et al., 1996). This means that mass movement inventory maps and understanding of Alpine landform processes derived from DInSAR analysis could both be used as preliminary tools for natural hazard management.

2.2 History of space-borne DInSAR

2.2.1 The origin of space-borne DInSAR

The first experiment of mapping small temporal variations due to deformations of the Earth's topography using DInSAR was performed by *Gabriel et al.* in 1989. It was assumed that DInSAR could serve to detect small temporal variations due to deformations of surface topography in the satellite line of sight (satellite-earth distance) on the order of a few centimeters or even less, which meant that the technique could provide accurate measurements of various geophysical phenomena. Since the launch of ERS1 in July 1991 by European Space Agency (ESA) a large set of available interferometric data has been archived. The use of DInSAR has rapidly been established for mapping different kinds of surface deformations and providing accurate kinematical data related to tectonic and volcanic activities, land subsidence, ice sheet and glacier movement, and landslides (Bamler and Hartl, 1998; Massonnet and Feigl, 1998; Rosen et al., 2000; Hanssen 2001). The technique of 2-pass DInSAR, which we use in this thesis, was first introduced by *Massonnet and Feigl (1998)*. The principle consists of interfering two SAR images from two separate flight tracks covering the same region, as well as removing the topography contribution introduced by parallax using a simulated topography phase generated from external Digital Elevation Model (DEM) (see Chapter 3 for further details). This technique is one of the most common methods in differential interferometry. The past decade has seen impressive improvements and DInSAR has become an accepted remote-sensing tool with diverse application in the Earth sciences (Smith, 2002). Since 2005, the concept of Persistent Scatterer Interferometry (PSI), a method derived from DInSAR, was introduced permitting an increase in the number of applications using SAR interferometry (Wegmüller et al., 2012). The main advantage of this new technique is the high accuracy in precisely monitoring slow moving landforms (on the order of some mm/year). However, as it is not suitable for fast moving landforms located in mountain areas (difficulty to find stable scatterers) and as it measures only point locations rather than over a broad area, it will not be investigated in this thesis.

2.2.2 Space-borne DInSAR applications in mountain environments

In the Alpine environment, the feasibility of DInSAR is discussed in many studies assessing the capability of DInSAR for analyzing slope movements (e.g. Delacourt et al. 2007; Strozzi et al. 2002, 2005) and offer a large number of requirements to select, analyze and interpret DInSAR correctly in this specific environment (e.g. Delaloye et al. 2007a, 2007b; Lambiel et al. 2008; Nagler et al. 2001, 2002; Strozzi et al. 2004). In particular, DInSAR provides data having extensive spatial coverage allowing regional overviews of phenomena which are difficult to obtain with classical geodetic techniques. However, significant difficulties are found when using this technique as a tool for

detecting and monitoring moving landforms in mountains, particularly related to the vegetation cover, the snow, the size of unstable slopes and their deformation rate, the atmosphere, as well as to the acquisition parameters like the incidence angle, the spatial resolution, the wavelength, and the acquisition time interval of sensors (Hanssen, 2005; Klees and Massonnet, 1999; Massonnet and Rabaute, 1993). Some clarification of technical aspects concerning basics and the suitability of DInSAR for surveying slope movement in the Alpine environment are proposed in Chapter 3.

2.3 Advances in the detection and mapping of Alpine moving landforms using DInSAR

The term *detection* is used here as a general term for mapping moving landforms using DInSAR products and includes two aspects: the *recognition* answering the question, “is it a moving landform?” and the *classification* giving information about the kind (or type) of moving landform (Mantovani et al., 1996). Two different combined approaches can be adopted for determining the characteristics of moving landforms. The first approach determines qualitative characteristics such as number, distribution, type and character of detected mass movements. The quantitative approach complements the initial analysis by giving information estimating dimensions such as length, width, thickness, local slope, motion, etc. (Metternicht et al., 2005). Since the end of the 1990s, numerous studies conducted by different research teams have shown the possibility of using space-borne DInSAR technique to detect moving landforms in Alpine environments. The main ones are reported here.

2.3.1 Detecting Alpine slope movements in Austria

Since 1999, scientists from the institute for Meteorology and Geophysics at the University of Innsbruck (Austria), namely Helmut Rott, followed by Thomas Nagler and associates have evaluated the potential of space-borne DInSAR for detecting slope movements in mountainous regions (Nagler et al., 2001, 2002; Rott and Nagler, 2003; Rott et al., 1999a, 1999b). Analyses were concentrated especially on mass movement related to rock glaciers, landslides and subsidence in various Alpine regions such as the Ötztal Alps (Austria), the Stubai Alps (Austria), as well as the Walliser Alps (Switzerland).

2.3.1.1 Statistical investigation of coherence and viewing geometry

The Austrian team first performed a statistical investigation of the interferometric coherence and viewing geometry of 30 ERS SAR images pairs covering the Ötztaler Alps in Tyrol (Rott et al., 1999b). They show that DInSAR motion analysis over annual time intervals is feasible on about 60 to 70% of the area above tree line using the two modes of ERS SAR data (Rott and Nagler, 2003; Rott et al.,

1999b). The main limitations in the Alpine environment are caused by decorrelation due to temporal changes of physical target properties (for instance melting snow or ice surfaces as well as vegetation) or due to motion at the sub-pixel scale (Rott and Nagler, 2003; Rott et al., 1999b). They also show that the SAR geometry is an important constraint. The geometric distortion affects the local spatial resolution and SAR is only sensitive to the motion component in the Line Of Sight (LOS). To deal with this last effect, they suggest looking back slope where the motion is directed in the LOS direction (Rott and Nagler, 2003; Rott et al., 1999a).

2.3.1.2 Use of DInSAR data to produce landslide maps

To produce landslide maps, Nagler et al. propose to detect landslide candidates by visually looking for phase distortions, which indicate possible mass displacements (Nagler et al., 2002). They also declare that this detection procedure requires at least two interferograms with a small perpendicular baseline. Actually, by cross-checking results from the selected interferograms, they can confirm together the good detection of a moving landform by excluding artifacts from filtering or atmospheric effects (Nagler et al., 2002). Even so, they suggest that a better quality of the mapping is obtained if a greater number of images are available. In fact, by increasing the number of DInSAR pairs there is a greater probability of obtaining good quality interferometric products, and it allows for reduction of the atmospheric effect propagation, as well as the production of interferograms with different periods to detect temporal variability of slow moving slopes (Rott and Nagler, 2003).

2.3.1.3 Results observed on slow slope movements and rock glaciers

Many landslides have been identified in small parts of the Austrian and Swiss Alps using ERS SAR images (Nagler et al., 2002). The detection was performed using mainly 1 year interferograms allowing mapping of only slow slope movements. Detected mass movements show surface velocities from a few mm up to a few cm/year and are mainly located above tree line where the surface is sparsely vegetated and where the coherence is preserved over long time intervals (Nagler et al., 2002). Because of the lack of vegetation, rock glacier surfaces are in principle well suited for interferometric analysis over long time intervals (Nagler et al., 2001). However, in particular zones of strong shear the signal may decorrelate within a short time interval if individual rocks within a SAR resolution element follow different trajectories. Consequently, the selection of the time interval for the SAR analysis depends on the coherence of the target and on the magnitude of velocity (Nagler et al., 2001).

2.3.2 Alpine survey in Switzerland

Since 2001, studies of mass movements' detection using DInSAR have been reported for the Swiss Alps, where two teams have been conducting different projects, although sometimes with

collaboration. The first one is made up of Tazio Strozzi and associates from Gamma Remote Sensing AG, Switzerland, and is mainly focused on the evaluation of the DInSAR potential. The second team brings Prof. Reynald Delaloye (University of Fribourg, CH), Prof. Christophe Lambiel (University of Lausanne, CH) and the Swiss Office Federal of Environment together from universities of Fribourg and Lausanne, Switzerland, and is much more interested in application aspects of the use of DInSAR to map Alpine moving landforms in the Swiss Alps.

2.3.2.1 *Interferograms selection for displacement detection*

Displacement detection is defined here as the process of determining the position extent, contour and approximate velocity of an unstable slope (Strozzi et al., 2002). For this purpose, it is suggested that phase unwrapping is not required. Moreover, phase noise is also an important tool to identify the position, extent and contour of rapid displacements (Strozzi et al., 2002). Early on, it was noted that the potential of short spatial baseline differential interferometry with adequate time intervals to map the motion of active landslides (Strozzi et al., 2001). Short spatial baselines are preferred because of the very strong influence of the topography on interferometric phase (Strozzi et al., 2002). A time interval is adequate if the displacement phase is between a significant fraction of a phase cycle and few phase cycles. Short intervals are used to detect fast deformations, while long ones for slow deformations (Strozzi et al., 2002). Pairs with different acquisition intervals have to be used to identify and quantify different deformation rates and multiple interferograms are suggested to allow cross-validation of the results (Strozzi et al., 2002).

2.3.2.2 *Promising tests in Matter Valley*

The first detection of unstable slopes was performed in the Matter Valley in Switzerland (Strozzi et al., 2002) and shows that ERS DInSAR data are suitable to quantify the degree of activity and the order of surface velocity of rock glaciers over large areas with the possibility to also detect very small movements of inactive and relict rock glaciers. Over these landforms, where dense vegetation is no longer present, high coherence is regularly observed during the snow free period between early summer and mid-autumn but large displacements may also cause decorrelation (Strozzi et al., 2009a). DInSAR is able to provide the speed for a large number of such landforms and might thus promote the understanding of the coupling between landscape climate and rock glacier activity (Strozzi et al., 2004). It is also suitable for detecting similar slope instabilities (Strozzi et al., 2002).

2.3.2.3 *Limiting factors in mountain environments*

The major limiting factors in mountainous terrain arise from decorrelation and the SAR image geometry, both leading to incomplete spatial coverage. There is a preferred slope direction where the technique is better suited for detection and monitoring, namely the slope facing away from the

SAR look vector (Strozzi et al., 2004). Moreover, in very rugged topography the geocoding introduces so many artifacts that the signal is sometimes no longer visible (Strozzi et al., 2004).

It was noticed that decorrelation occurs over snow covered areas (due to snow moisture, as well as different densities of the snow) and a lot of the region is affected by layover and shadow caused by rugged topography (Strozzi et al., 2004). Finally, they warn users that DInSAR interpretation is not conclusive, especially due to the incomplete spatial coverage, to the special SAR geometry, and to the fact that the observed motion is projected into the LOS direction (Wegmüller et al., 2012).

2.3.2.4 *Different sensors, different potentials*

Since the extinction of ERS1/2 tandem fifteen years ago, Strozzi et al. have started to compare the potential of each sensor for the detection of mass movement in the Alpine environment. It was reported that a regional survey of displacements using JERS interferograms of 44-132 days is more reliable for landslide maps compared to 35 days ERS interferograms which show more decorrelation (Strozzi et al., 2005). C-Band and L-Band DInSAR show relatively high coherence above tree line during the snow free period permitting detection and monitoring of unstable slopes (Strozzi et al., 2003). However, the coherence of C-band 35 days is very low due to temporal decorrelation occurring from changes in time of the scatterer characteristics in the vegetated areas, whereas L-band has the capability to complement the existing applications based on C-Band because of its capacity to penetrate canopy (Strozzi et al., 2005). Therefore, the large wavelength of L-Band is more appropriate than C-band 35 days for mapping rapid displacements (Strozzi et al., 2005).

More recent satellites such as ENVISAT, ALOS PALSAR as well as TerraSAR-X, permit the detection of more recent activity (Strozzi et al., 2008, 2009b, 2010a, 2012). Specifically, the team discussed the performance of TerraSAR-X in observing instabilities of relatively small size with a high spatial resolution (Strozzi et al., 2009b, 2012). It was concluded that since the termination of ERS1/2 tandem a decade ago there is no longer DInSAR data permitting the detection of slope movements up to several 5cm/day. The role of space-borne radar interferometry as an element in a warning system is thus for these cases limited (Strozzi et al., 2009a).

2.3.2.5 *First large inventory of mass movements in the Swiss Alps*

The first large inventory reported so far was performed by Delaloye et al. in 2005 (Delaloye et al., 2005, 2007a, 2007b, 2008a, 2008b, 2010b; Lambiel et al., 2008). They apply DInSAR techniques for assessing both the surface geometry and the activity of mass movements in the Western Swiss Alps. Detected mass movements are related to debris-covered (parts of) glaciers as well as to the creep of frozen debris (rock glaciers, push-moraines) or not (landslides, sagging) (Delaloye et al., 2005, 2008a). As the detection of surface motion does not provide information about the depth of the mass movement, the nature of the movement is sometimes difficult to interpret and requires additional

geomorphic field observations (Delaloye et al., 2007a). To prevent misinterpretations of the SAR interferograms, estimating the old and fresh snow condition on SAR image dates has proven to be a necessary first step (estimation of snow line, weather conditions... using daily reports). Moreover, they argue the need for reliable sets of interferograms, orthoimages and good knowledge of the local geomorphology to interpret correctly detected signals (Delaloye et al., 2007a).

The team proposes a typology of ERS InSAR signatures for different landforms with various rates of activity (Table 2.1) in order to aid in the interpretation of DInSAR data by people who are not familiarized with mountain periglacial geomorphology or with radar remote sensing techniques (Delaloye et al., 2007b).

Landform	Time interval			
	1 day (winter)	1 day (summer)	35-105 days (summer)	Year(s)
Glacier	c	d	d	d
Debris-covered glacier I	c	d	d	d
Debris-covered glacier II	-	d	d	d
Push-moraine	-	-	c/d	d
Active rock glacier				
<i>Surging</i>	c	c	d	d
<i>Very active</i>	-	(c)	d	d
<i>Active</i>	-	-	d	d
<i>Low active</i>	-	-	c	d
<i>Very low active (inactive)</i>	-	-	-	c
Landslide / sagging				
<i>Active</i>	-	-	c/d	d
<i>Low</i>	-	-	-	c
Gelifluction	-	(d)	d	d
Subsidence by drainage in bedrock	-	-	(c)	c

-: no signal; c: coherent signal; (c): possible coherent signal; d: decorrelated signal, (d): possible signal (decorrelated); c/d: coherent or decorrelated signal

Table 2.1: Potential of ERS InSAR for detecting slope movement from (Delaloye et al., 2007b)

They also propose a classification of rock glaciers according to their surface velocity (Table 2.2). DInSAR may constitute an interesting tool for the study of rock glacier dynamics in the context of general acceleration of these landforms (Lambiel et al., 2008).

Classical classification	ERS DInSAR signal	Estimated surface velocity	Velocity classification	Destabilization
Active	1 day	> 2 m/y	very high	very frequent
	(1 day)/35 days decorrelated	1-2 m/y	high	frequent
	35 days	0.2-1 m/y	medium	possible
	(35 days decorrelated)/1 year	0.03-0.2 m/y	low	rare
Inactive	(1 year)	up to a few cm/y	very low	No
Relict	No	-	-	No

Table 2.2: Classification of rock glaciers according to their surface velocities adapted from (Lambiel et al., 2008).

2.3.2.6 Results observed from large Alpine mass movements inventory

The large inventories of Alpine mass movements performed by Delaloye et al. in 2005 in the Swiss Alps shows the suitability of DInSAR technique for inventorying slope instabilities over Alpine areas where dense vegetation is no longer present, during the snow free period (between early summer and mid fall). The reliability of the inventory results (location and movement rate) was controlled by comparing with a rock glacier inventory, DGPS measurements and airborne photogrammetry. It shows that the quality of the inventory depends on the quality of the interferogram set (number of available scenes, variety of time interval...) (Delaloye et al., 2007a). The team also shows that the distinction of rapidly moving rock glacier is only possible on ERS 1-3 days interferograms. Using larger time intervals, these rapidly moving landforms are often lost in decorrelated areas (Delaloye et al., 2010b). They are aware of the subjectivity of the detection which is performed visually and might differ depending on the user (Delaloye et al., 2007a). As many others, they conclude that DInSAR technique is not favorable for analyzing steep rock walls and northern/southern oriented slopes which are not or partially illuminated.

2.4 Advances in the monitoring of Alpine moving landforms using DInSAR

Monitoring means the comparison of moving landform conditions such as areal extent, speed of movement, surface topography, soil humidity, etc. ... from different periods in order to assess the activity of a landform (Mantovani et al., 1996). In the Alpine environment, studies have focused on the interpretation and quantification of landform motion using DInSAR and have shown the potential of this technique to monitor landslides as well as rock glaciers. Main knowledge related to Alpine moving landform monitoring studies conducted by different research teams is reported in this section.

2.4.1 Monitoring slope motion in Austria

The team of Rott and Nagler has performed different tests to evaluate DInSAR potential for monitoring rock glaciers and slow slope deformation in an Alpine context. Another team brings Lado Kenyi and Viktor Kaufmann together from Institute of Digital Image Processing (Joanneum Research, Austria) who are involved in monitoring the Doesen rock glacier.

2.4.1.1 Monitoring slow slope motion

In Austria, studies are mainly focused on the analysis of slow slope deformation using DInSAR (Nagler et al., 2002; Rott and Nagler, 2003; Rott et al., 1999a). They show the potential of this technique for long term monitoring of mountain slopes. The advantage of DInSAR to provide continuous maps of

surface deformation is considerable compared to conventional techniques. The selection of the time interval for the DInSAR analysis depends on the coherence of the target and on the magnitude of velocity. Thus by combining interferometric analysis and field survey they suggest the potential determination of the process involved in the monitored slope.

2.4.1.2 *Monitoring rock glaciers*

Nagler et al. propose the derivation of motion fields on rock glaciers by unwrapping the interferometric phase. Moreover they suggest that the time intervals allow the detection of significant inter-annual variations. In this way, they show that the velocity of a rock glacier has significant temporal and spatial variability (Nagler et al., 2001).

Kenyi and Kaufmann estimate the deformation of Doesen rock glacier located in Austria using DInSAR data (Kenyi and Kaufmann, 2000, 2001, 2003). They perform quantitative validation of the results with annual geodetic measurements and multiyear photogrammetric investigations. However, comparisons are not adequate since the data are not taken during the same period and the measurements themselves are not directly comparable with each other (Kenyi and Kaufmann, 2003). As the deformation of a rock glacier is composed of a flow component and a component due to loss or gain of ice, the horizontal flow cannot be directly deduced from DInSAR measurements where the deformation is only known in the LOS. Moreover they warn about measurements which are subject to seasonal and annual variation: specific attention has to be paid during interpretation of one unique interferogram. To have the best result as possible, they also suggest looking for rock glaciers located in the back slope and having a flow direction parallel to the LOS.

2.4.2 Monitoring Alpine slopes in Switzerland

The team of Strozzi performs different tests to evaluate DInSAR potential for monitoring rock glaciers, landslides or subsidence; main results are reported here.

2.4.2.1 *Monitoring displacement field with DInSAR*

Monitoring is the process to quantitatively measure the displacement field of an identified landslide. For this purpose, phase unwrapping is required (Strozzi et al., 2004). Usually, as it is a difficult task that needs a cautious validation, only small and well defined areas are considered (Strozzi et al., 2004). According to the team, when the deformation geometry is complicated, even a combination of SAR data acquired in ascending and descending modes does not allow the resolution of the complete 3D displacement field without the use of additional information (Strozzi et al., 2001). For most of their studies they assume the creeping to be along the slope direction, thus the deformation known in the LOS from DInSAR technique is projected along the slope for comparison with displacement derived from other techniques.

The team of Strozzi provides comparisons between ERS DInSAR and photogrammetric measurements showing good agreement for several rock glaciers located in the Saas Valley, Switzerland (Strozzi et al., 2004). These comparisons show good results for large rock glaciers, many more difficulties for rapid displacements and advantages for detecting very small movements which were not seen with photogrammetry (Strozzi et al., 2004). Discrepancies were explained due to differences in time interval where displacements were compared (mean over 24 years for photogrammetry and time interval of the selected sensor). The information of the displacement field and in particular its temporal and spatial gradient is useful to select the most suitable SAR data with respect to time acquisition interval (Strozzi et al., 2004). Moreover, they show good quantitative results from JERS interferometry of a slow moving landslide Corvara (South Tyrol, Italy. Strozzi et al., 2005). They also compare results from different sensors (ERS, JERS, Envisat, Alos Palsar) with DGPS measurements on the Aletsch rock mass movement (Bernese Alps, Switzerland) and show good correspondence (Strozzi et al., 2007).

They conclude that rapid moving landforms are difficult to measure using DInSAR because they can deform the ground in excess to the phase gradient limit and commonly disturb the scattering surface destroying the interferometric correlation. In particular, high deformation rates of rapidly moving rock glaciers are too large to be analyzed correctly on C-Band and L-Band monthly interferograms (Strozzi et al., 2005).

2.4.2.2 *The combination with other data*

The team shows that scene topography and land use have an influence on the accuracy and robustness of monitoring. In areas of very rugged topography the successful application of SAR data is strongly reduced by the particular imaging geometry of the sensor. Consequently, they suggest combining DInSAR measurements with other data to understand processes. Combined use of DInSAR, DGPS, aerial photogrammetry and airborne photo interpretation represents an efficient remote sensing survey of Alpine displacements. Even if these types of analyses are still time consuming and restricted to specialists in the relevant disciplines, this combination allows for modeling the slide mechanisms involved in a particular mass movement (Strozzi et al., 2010a).

2.4.2.3 *Evaluation of sensor characteristics*

Once again, Strozzi et al. tried to evaluate the potential of each sensor for Alpine landform monitoring. In 2002, after the termination of ERS1/2 tandem, they denounced the temporal sampling and timeliness of current SAR sensors to be insufficient for direct use of the interferometric technique for real time monitoring required for slopes with high deformation rates (Strozzi et al., 2002). Some years after, they suggested that TSX, with short temporal sampling and high spatial resolution, is very well suited to analyze seasonal surface displacements in mountainous periglacial

areas, particularly to derive deformation information for more rapid displacement rates of some cm/year (Strozzi et al., 2009b, 2012).

2.4.3 Some interesting results around the rest of the world

Some interesting studies are reported here to illustrate other monitoring studies of rock glaciers or landslides in other parts of the globe. Specifically, the work of three teams is transcribed here. The first team is composed by Vern Singhroy and associates from the Canada Centre for Remote Sensing and focuses on landslides in Canada. Then the American team of Eric Rignot and associates from the Radar Science and Engineering, Jet Propulsion Laboratory (CA USA), evaluates surface motion of rock glaciers in Antarctica. Finally, the French team of Christophe Delacourt and associates from the Laboratoire de Sciences de la Terre UMR5570 and ENS Lyon perform some analysis on “La Valette” landslide located in the French Alps.

2.4.3.1 *Monitoring landslides in Canada*

In 2004, the team of Singhroy and Molch suggested that DInSAR techniques can be used to supplement field monitoring techniques on active landslides (Singhroy and Molch, 2004). They immediately showed the need for more frequent DInSAR observations to improve the quality of the results. Shorter acquisition intervals will enable measurements of fast motion. The second point put forward concerns DEM quality. The DEM resolution is very important for removing topography which sometimes masks deformation. The results are strongly affected by the choice of DEM especially for larger baselines.

2.4.3.2 *Rock glacier surface motion in the Beacon Valley, Antarctica*

Rignot et al. try to evaluate rock glacier surface motion in Beacon Valley, Antarctica (Rignot et al., 2002). They noticed that it is instructive to compare the pattern fringes on the rock glacier with micro-topography. The fringes are roughly parallel to some of the transverse ridges and lobes that are conspicuous on the rock glacier surfaces reflecting transverse as well as longitudinal gradients in surface velocity. They assume for this study the ice mass to be conserved because sublimation rates are insignificant ($\ll 1\text{m/y}$) relative to flow rates where they are resolvable by DInSAR, even if they recognize the fact that this assumption is questionable for rock glaciers where internal deformation reveals considerably more complex velocity profiles than in glaciers. Then they use Glen's flow law to derive surface displacement from DInSAR and DEM derived surface slopes to estimate surface velocity components, and thickness and flux of deforming ice.

2.4.3.3 *The case of la Valette landslide in French Alps*

In 2004, a study was conducted in the French Alps to monitor the activity of the landslide de la Valette (Delacourt et al., 2004a). They show the potential of 1 day motion monitoring using ERS1/2

tandem. They detect seasonal variation from a series of six interferograms which confirms the activity of the landslide all the year. They provide comparison between interferogram displacements and DGPS measurements projected along the LOS. A good correlation between the two methods of investigations is obtained. Consequently, despite severe limitation, they conclude that DInSAR may be a good mean to investigate landslide areas with displacement rates less than a few cm per day. They suggest that landslides should be favorably oriented along the line of sight; atmospheric artifacts should be detected and removed if possible. Certainly, the best is to associate DInSAR analysis with aerial photo interpretation and geomorphological analysis.

2.5 Synthesis of literature review

The main items retained from the literature review are listed in this part. They are classified into the three following subsections related to the three main axes of research on which this thesis focuses. Main results are also summarized in Table 2.3.

	<i>Detection & Mapping</i>	<i>Monitoring</i>
Requirements	<ul style="list-style-type: none"> - Look back slopes - Use short spatial baselines 	
	<ul style="list-style-type: none"> - Large set of data with various time intervals - Combination with external data 	<ul style="list-style-type: none"> - Large series of data to detect inter-annual variations - Both ascending and descending modes, assumptions about movement or combination with external data
++	<ul style="list-style-type: none"> - Provide continuous maps 	
	<ul style="list-style-type: none"> - Does not need phase unwrapping 	<ul style="list-style-type: none"> - New high spatio-temporal sensor probably well suited for monitoring fast movements
:	<ul style="list-style-type: none"> - Artifacts due to low quality of DEM 	
	<ul style="list-style-type: none"> - Interpretation not trivial 	<ul style="list-style-type: none"> - Need phase unwrapping - Extinction of ERS1-2 tandem - Movement only known in the LOS

Table 2.3: Synthesis of the main results observed from literature for the suitability and the use of DInSAR data for the detection, mapping and monitoring of moving slopes.

2.5.1 Suitability of DInSAR

- The DInSAR technique has the advantage to provide continuous maps of surface deformation compared to conventional techniques based on sampling.
- To deal with geometric distortions affecting the local spatial resolution and to be sensitive to the motion component in the LOS, most of studies suggest the use of DInSAR by looking back slope (slope facing away from the SAR look vector) where the motion is directed more or less in the LOS.

- In very rugged topography, the geocoding introduces many artifacts which appear to be due to the quality of the DEM used to produce the differential interferogram. The micro-topography can introduce additional fringes which are not related to movement. To deal with this effect, short spatial baselines are preferred because of the very strong influence of the topography on interferometric phase.
- Since the extinction of ERS1/2 tandem a decade ago there is no longer DInSAR data permitting the detection and monitoring of fast slope movements (cm/day).

2.5.2 Detection and mapping with DInSAR

- The detection of slope movement does not need phase unwrapping and is performed by looking for phase distortions. The phase noise is also an important tool to identify the position, extent and contour of rapid displacement. However, the rate of deformation cannot be quantified in this specific case.
- When producing landslide maps, there is a greater probability to obtain quality if a large number of interferograms is available allowing cross-validation of the results. Moreover pairs with different acquisition intervals have to be used to identify and quantify different deformation rates.
- The interpretation of DInSAR signal is not conclusive, especially due to incomplete spatial coverage, SAR geometry, motion in the LOS and atmospheric artifacts.
- Combination with other data, for instance aerial photogrammetry or airborne photo interpretation, is required to identify the typology of landform. However, it requires good knowledge in both DInSAR technique and geomorphology.

2.5.3 Monitoring with DInSAR

- The phase unwrapping is required to quantify landform deformation rates.
- Due to immediate decorrelation, rapid moving landforms (deformation rate of cm/day) cannot be monitored with the shortest time interval of current sensors.
- Studies suggest the use of a large series of interferograms in order to detect inter-annual or seasonal variation of landform deformation. The short temporal sampling and high resolution of new TerraSAR-X data is probably well suited to analyze seasonal displacement of more than some cm/year.
- The combined use of DInSAR with DGPS, aerial photogrammetry and airborne photo interpretation allows for modeling the slide mechanisms involved in a particular mass movement. However, these types of analyses are time consuming and are restricted to specialists in the relevant disciplines.

- To compute 3D motion derived from DInSAR, it is required to use either both ascending and descending modes of sensors when available or different kind of assumptions on the flow direction (Glen's law, along the slope direction, etc.).
- Comparisons of deformation derived from DInSAR with other in-situ data have to be performed cautiously according to time (time intervals, period of measurements) and direction of the movement (LOS direction, 3D ground, horizontal direction, etc.).

2.6 Connection with thesis rationale

In light of this literature review and of the most recent papers written in the last four years, the thesis rationale is set out in this part according to the three main axes of research.

2.6.1 Suitability of DInSAR in the Alpine environment

In the Alpine environment, the feasibility of DInSAR is discussed in many studies assessing the capability of DInSAR for analyzing slope movements in this specific environment. However, no one proposes a standard methodology to assess the use of DInSAR technique for the detection, mapping and monitoring of slope movements in a specific region of interest. After defining basics of DInSAR and the behavior of environmental and design parameters on DInSAR signal, Part 3.3 proposes a procedure to evaluate the suitability of DInSAR technique for slope motion detection, mapping and monitoring in an Alpine environment by estimating the areas in which layover and shadowing occur and by giving the measurability of a potential moving slope from one image acquired by a SAR sensor (Barboux et al., 2011). A similar approach has been developed at the same time by Plank et al. (2012) and goes further since they have developed a procedure using geographical information system (GIS) prior to the use of any existing radar image.

2.6.2 Detection and mapping of Alpine moving landforms

In the past few years, three other inventories have been found in the literature where rock glaciers are drawn up using DInSAR: in the French Alps (Echelard et al., 2013), in Sierra Nevada, California (Liu et al., 2013) and in Northern Iceland (Lilleøren et al., 2013). These three studies show the complementarity of an inventory created from aerial image analysis and the analysis of the activity states of the detected landforms based on DInSAR, providing together a more complete and valuable dataset. However, for each of these applications, the potential of DInSAR data has not been fully investigated (e.g. Echelard et al. only used descending mode, Liu et al. did not use ERS1/2 tandem) or partial use of data (e.g. Lilleøren et al. only used DInSAR on a subset of rock glaciers previously mapped from aerial imagery to validate their activity states).

The paper “Inventorying slope movements in Alpine environment” reports the work performed by Delaloye and Lambiel and gives specific keys to use and understand DInSAR signals in mountainous areas located above tree line, excluding glaciated areas (Barboux et al., 2014). It proposes a systematic procedure based on accurate visual interpretations of interferometric signals from a large DInSAR dataset to locate and estimate the displacement rate of moving zones. Moreover, it describes on the whole the results obtained in the Western Swiss Alps using this methodology, where about 2000 moving objects were detected above tree line using a large dataset of ERS and JERS interferograms dating from the 1990s.

In order to facilitate the update of this inventory as well as to make it free from the subjectivity of the operator, the main objective is now to automatically detect the slope motion in this Alpine context. Chapter 4 proposes a semi-automated method to map and assess the slope stability in the Alpine periglacial environment. Pilot studies are performed in Alpine context using this automated procedure to automatically update inventories (Chapter 7 Part 7.1, Barboux et al., 2013c) or for the detection of dead ice bodies (Chapter 7 Part 7.2, Fischer et al., 2014) using the new high spatio-temporal resolution of TerraSAR-X.

2.6.3 Monitoring of Alpine moving landforms

Previous studies show the high potential of DInSAR data to monitor active rock glaciers moving with a velocity rate lower than ~ 1.5 m/y, representing the simplest case of rock glacier monitoring. Larger movements are difficult to measure using current C- and L-bands monthly interferograms because they can deform the ground in excess to the phase gradient limit and commonly disturb the scattering surface, which destroys the interferometric correlation. These studies suggest that the short temporal sampling and high resolution of TerraSAR-X are well suited to analyze seasonal displacement over fast moving landforms (velocity ≥ 1.5 m/y). Since these studies, investigations have been performed to monitor seasonal and/or inter-annual variations of active rock glaciers using TerraSAR-X data (Barboux et al., 2011, 2012). They show the possibility to monitor some very active rock glaciers (1-3.5 m/y), when geometrical distortions do not hide them, with the shortest TerraSAR-X repeat pass of 11 days, especially using the mode facing the slope (i.e. ascending mode for west, descending mode for east oriented slopes). This thesis will focus specifically on the monitoring of very active rock glaciers located in our region of interest. Challenges of DInSAR and solutions for monitoring fast moving slopes in the Alpine environment are investigated in Chapter 5 (Barboux et al., 2012). A few examples of applications are given in Chapter 8 to illustrate the role of DInSAR in order to understand processes involved in the movement of specific landforms.

2nd Part:

Evaluation of DInSAR contribution to slope movement analysis in an Alpine environment

The 2nd part is divided into three chapters and contains technical studies and methods developed in this thesis. It first defines the basics of DInSAR technique and the behavior of DInSAR signal in mountains according to environmental and design parameters in order to evaluate the suitability of DInSAR technique for slope motion mapping and monitoring in the Alpine environment. Then it proposes an automated method to map and assess the slope movements in the Alpine environment from a selected dataset of TSX interferometric phase images. Finally it deals with the challenges and the solutions to monitor annual and seasonal displacement rates of Alpine rock glaciers using DInSAR.

3 DInSAR for the observation of slope movements in the Alpine environment

After defining basics of DInSAR (Part 3.1) and the behavior of DInSAR signal in mountains according to environmental and design parameters (Part 3.2), this chapter proposes a procedure to evaluate the suitability of this technique for slope motion mapping and monitoring in the Alpine environment by estimating the areas in which layover and shadowing will occur and by giving the ratio of measurability of movement of a potential moving slope from one image acquired by a SAR sensor (Part 3.3).

3.1 Differential SAR Interferometry

This section does not claim to fully explain the whole principles of DInSAR. Only basics concepts of SAR, InSAR and DInSAR are reported here. For further information please read Klees & Massonnet (1999) and Massonnet & Feigl (1998).

3.1.1 SAR imaging system

Synthetic Aperture Radar (SAR) is a microwave imaging system carried by a satellite having capabilities to penetrate cloud and to be operational day and night (Figure 3.1). An active sensor points to the ground's surface in a plane perpendicular to the orbit and emits a pulse (sinusoidal signal). At the surface of the Earth, the pulse is reflected by natural scatters or targets. The curvature of the Earth's surface is assumed to be flat and the incidence angle θ is defined between the nadir and the antenna direction, ranging from 20 to 50° in contemporary systems. The direction from the sensor to a scattered point on the ground's surface is called the Line Of Sight (LOS) or slant range. Current SAR satellites are polar orbiting and most of them are right side looking so the LOS is roughly east or west oriented. Two modes are defined, namely the ascending mode referring to a northward orbit and the descending mode to a southward orbit. The illuminated area on the ground is defined by the azimuth direction (along-track) and ground range direction (across-track). The sensor records on each position the measured distance in the LOS from the scatters. The repeat cycle is the minimum time in which a satellite comes back to image the same surface area.

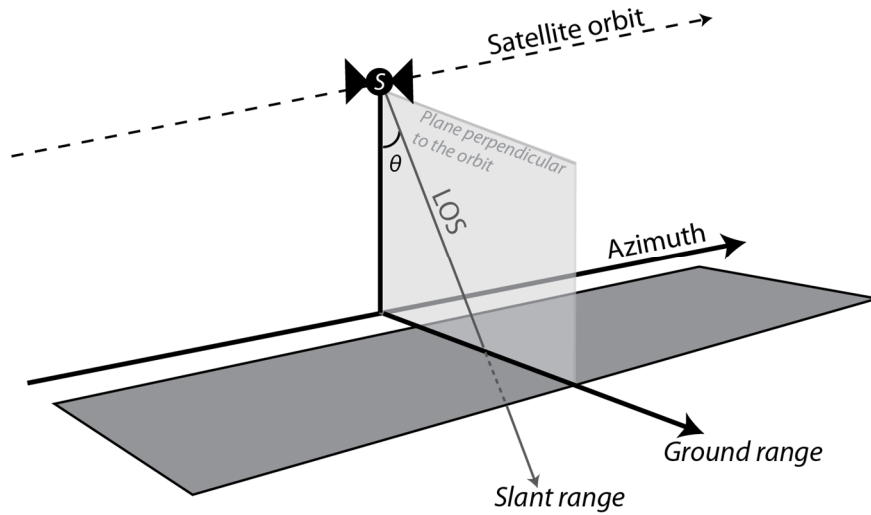


Figure 3.1: SAR system acquisition. Adapted from Ferretti et al. (2007)

3.1.2 SAR image

A SAR image is described by pixels associated with a defined area of the Earth's surface. The backscattered signal of the Earth's surface from a single microwave is measured by the sensor. The spatial resolution is defined as the minimum separation between measurements that the sensor is able to discriminate and determines the amount of speckle (scattering phenomenon which arises when the spatial resolution of the sensor is not sufficient to resolve individual scatters).

A SAR signal can be assimilated to a sinusoid (Figure 3.2). At each pixel of the SAR image, complex data is achieved containing both the phase Φ related to the propagation time of the wave, and the amplitude related to the intensity of the received signal. Φ can only take value between $[-\pi, \pi]$ and represents the phase shift between the transmitted and the received signal that covers the two way travel distance $2R$ to the targets.

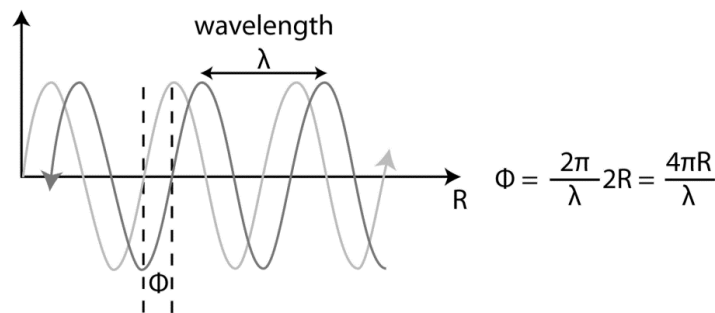


Figure 3.2: Phase shift Φ between the transmitted and received signal of a sinusoidal function covering the two-way travel distance $2R$. Adapted from Ferretti et al. (2007)

3.1.3 SAR Satellites

Several operational systems provide data that can be used for systematic monitoring of terrain deformations since ERS1 in 1991. Table 3.1 provides information about the most commonly proposed SAR systems that can be used for scientific purposes.

Satellite	TSX	CSK	ERS	Envisat	Radarsat1	Radarsat2	Alos	JERS
Date	from 2007	from 2007 ²	1:1991-2000 2:1995-2011	2002-2012	1995-2011	from 2007	2006-2011	1992-1998
Agency	DLR	ASI	ESA	ESA	CSA	CSA	JAXA	JAXA
Wavelength (cm)	3.1	3.1	5.6	5.6	5.6	5.6	23.6	23.6
Band	X	X	C	C	C	C	L	L
Incidence angle (°)	15-60	20-60	23	15-45	20-50	10-60	8-60	35
Range resolution (m) ¹	1-16	1-100	26	30-150	10-100	3-100	7-100	18
Azimuth resolution (m) ¹	1-16	1-3-100	28	30-150	9-100	3-100	7-100	18
Swath (km)	10-100	10-200	100	100-400	45-500	50-500	40-350	75
Repeat cycle (day)	11	1-4-8-16	(1-3)-35 ³	35	24	24	46	44
Polarization ⁴	S, D	S, D	VV	S1, D	HH	S, D, Q	S1, D, Q	HH

¹ The resolution in range and azimuth depends on the image acquisition mode. Common modes are the spotlight mode (extra precise), stripmap/standard mode and Wide/ScanSAR mode (extended).

² Constellation of small Satellites for Mediterranean basin Observation (1st and 2nd satellites launched in 2007, 3rd in 2008 and 4th in 2010)

³ 3 days with ERS-1 in 1991, 1day with tandem ERS-1/-2 from 1995

⁴ S = Single, S1 = Single one (HH or VV only), D = Dual, Q = Quad

Table 3.1: Radar characteristics of the most commonly used SAR systems from Barboux et al. (2014).

3.1.3.1 Characteristics of Acquisition

The most preferred polarizations are horizontal wave transmit and horizontal receive (HH) or vertical wave transmit and vertical receive (VV). The new generation of SAR satellite proposes also cross-polarization (HV or VH). However, the cross-polarization backscatter is generally lower since the cross-polarized return appears through multiple scattering. Most of the SAR satellites are able to operate in one polarization mode only at one time (Single), and this polarization mode can be selected for each acquisition. Some satellites use Dual mode where the images are polarized in dual combinations HH+HV or VV+VH. In the case of QuadPol (quadrature polarization), all four combinations HH, VV, HV, VH of the scene are created.

In modern satellites, several common image acquisition modes are used:

- *Stripmap/Standard mode* is a standard mode.
- *Wide/ScanSAR mode* has a similar principle to the Stripmap mode but the swath (width of an imaged scene in the range direction) is larger and the resolution is much coarser.
- *Ping-pong/Alternating polarization/Co-polar mode* is a special form of acquisition mode. After a short illumination to synthesize a radar image in the required range resolution, the instrument switches into a different polarization scanning mode and repeats the operation several times. The resolution is usually two times coarser than in Stripmap mode.
- *Spotlight mode* is an extra precise resolution (less than 1m in azimuth direction). All current X-band satellites and also Radarsat-2 are able to use the Spotlight mode.

As the radar response is sensitive to the geometry of reflecting objects, only acquisitions from the same direction and the same polarization angle can be used for SAR interferometry. In fact, even if satellites have almost a full global coverage, the areas that are acquired and archived often need to be ordered. Consequently, it is sometimes necessary to plan the required acquisitions in advance.

SAR acquisitions can be provided using different formats. The most common format is the Single Look Complex (SLC) where phase is preserved and a slant range image is generated from raw SAR data. The SLC is generated upon request and is intended for use in SAR quality assessment, calibration and interferometric applications.

3.1.3.2 Four main organizations

The four main organizations in satellite based SAR remote sensing are the European ESA, the Japanese JAXA, the German DLR and the Canadian CSA.

The ESA's C-band ERS satellites were really successful due to their large amount of continuous archived data. During 1995-1998 ERS-1 and ERS-2 shared the same orbit plane allowing a tandem mission with 1-day time delay. Both satellites exceeded their planned lifetime by far. ERS-1 expired in 2000 due to a hardware failure, and ERS-2 in 2011. The Advanced Synthetic Aperture Radar (ASAR) of ESA's Envisat provides observations of more polarities and extends observed swath dimensions.

JAXA satellites JERS-1 (Japanese Earth Resource Satellite-1) and ALOS (Advanced Land Observing Satellite) are unique L-band SAR sensors. Specifically, ALOS contains a Phased Array type L-band SAR (PALSAR) capable of Fine and ScanSAR mode acquisitions.

The Canadian CSA's C-band SAR satellites, Radarsat-1 and Radarsat-2, fly in an orbit with about fifty minutes separation and are designed to view any part of Canada within three days. These satellites possess various acquisition modes.

The German DLR's X-band's TerraSAR-X satellite is the first commercially available radar satellite that offers high resolution image products (about 1m resolution in Spotlight mode).

3.1.3.3 Constellation mission

Current satellites are designed to work in constellations. The Italian constellation of four X-band SAR satellites, known as Cosmo-SkyMed (CSK, Constellation of Small Satellites for Mediterranean basin Observation), is providing advantages of a short revisiting time allowing the monitoring of fast deformation rates. This mission mainly flies over the Mediterranean basin. The complete CSK constellation has been running since October 2010. While each satellite performs one Earth cycle in 16 days, within a regularly distributed constellation it is possible to achieve interferometrically combinable SAR acquisitions every 4 days. It is also possible to reconfigure the orbits for tandem

interferometry where two satellites reach the same position in 20 seconds or a tandem-like interferometry with a shortest time delay of 1-day (Covello et al., 2010).

The mission of TSX has been enhanced since June 2010 by a second satellite flying at a nominal distance of a few hundred meters. Both satellites together form a constellation called TanDEM-X (TDX) that will generate a global highly accurate DEM model (resolution of 12m, 2m relative height accuracy). The global DEM is planned to be completed in 2014. The satellites have the particularity to fly in a helix track and have a unique ability to achieve bistatic SAR images – one satellite transmits the radar signal, while both satellites receive its reflection.

A Canadian RADARSAT Constellation Mission is planned to be fully functional in 2015. This constellation will be composed of three new satellites with C-band SAR instruments with a 12-days repeat cycle and a spatial resolution up to 5 m. Korean Kompsat-5 and later on Kompsat-7 are also planned to work in a constellation. Project SMMS of China includes four SAR satellites operating in S-band. Finally, the ESA Sentinel-1 mission is a constellation of two C-band SAR satellites that will provide monitoring of sea ice, marine environments and land surface in terms of GMES project requirements. The first satellite was launched in 2012, the second will follow.

3.1.4 DInSAR processing

3.1.4.1 SAR Interferometry

SAR interferometry (InSAR) is a technique for extracting information about three-dimensional objects from complex radar signals. Repeat-pass interferometry involves phase measurements from successive satellite SAR images. The time between the two acquisitions, called the time interval, is a multiple of the repeat cycle. A pair of images taken from the same sensor is mixed or interfered to identify pixels corresponding to the same area on the ground surface. The two acquisitions, or passes, must have similar geometries in order to allow extraction of the relative phase difference. The interferometric baseline, also called spatial baseline or perpendicular baseline, is defined as the separation between the two repeated satellite orbits. Finally, for each pixel, the phase values are subtracted to produce the difference of phase image known as interferogram or interferometric phase (For further details please see Massonnet and Feigl, 1998).

3.1.4.2 Topography removal

When spatial baseline increases, the parallax introduces additional cycles to the interferogram related to surface topography. The altitude of ambiguity h_a is defined as the shift in altitude needed to produce one topographic fringe (Massonnet and Feigl, 1998) and is inversely proportional to the spatial baseline. If ground motion has not occurred, the value of interferometric phase can be converted to elevation. When motion occurs, topographic and displacement components have to be

separated by differential SAR interferometry (DInSAR). The 2-pass Differential interferometry is one of the most common methods in differential interferometry and uses an external DEM containing only topographic information in conjunction with the precise knowledge of the satellite orbits to estimate and compensate the topography in the final interferogram (Wegmüller and Strozzi, 1998).

3.1.5 Interferometric products derived from DInSAR

3.1.5.1 Interferometric phase

The interferometric phase, or interferogram, is ambiguous as it can only take values between $[-\pi, \pi]$ represented by a fringe in a full color cycle. The phase unwrapping is the integration of the phase differences between neighboring pixels which solves the ambiguity. Three different patterns can be observed on interferometric phase image: no change of the phase signal defined by a plain pattern; a smooth change of the phase signal characterized by a (partly) fringe pattern and a noisy phase signal expressed by a noise pattern (neighboring pixels with contrasted colors).

Fringe patterns can be related to the terrain deformations. Due to the two-way travel distance of the transmitted and received signals, a fringe is equivalent to a deformation in the LOS direction between an object imaged by the first and by the second SAR antenna of half a wavelength $\lambda/2$ (Massonnet and Feigl, 1998). The change of color in the resulting interferogram expresses the 3D ground deformation projected into the 1D LOS direction (Figure 3.3). As the deformation is only known in the direction of the line of sight, the vertical and horizontal components of the deformation cannot be distinguished.

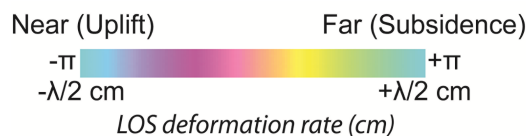


Figure 3.3: The difference in deformation rate between places having the same color is a multiple of $\lambda/2$. When the color turns from pink to yellow, the ground moves away from the satellite. When the color changes in the opposite direction, the ground moves closer to the satellite.

3.1.5.2 Interferometric coherence

The phase noise, also called decorrelation or coherence loss, is expressed on an interferogram by a noise pattern. The interferometric coherence can be estimated from the interferometric SAR pair by means of the local correlation (cross-correlation coefficient of the SAR image pair calculated over a small window) and gives the degree of coherence measuring the phase noise in the interferogram. The coherence values usually range from 0, where there is no useful information in the interferogram, to 1, where there is no noise in the interferogram. Interferometric correlation is affected by some change in surface conditions that makes the radar images incoherent to each other (see following Part 3.2).

3.2 Suitability of DInSAR in mountain areas

The feasibility of DInSAR for detecting and quantifying deformation is limited by the characteristics of the deformation and the terrain, the time interval and the baseline between the two acquisitions, the quality of the DEM and a number of other additional phase effects. This Part 3.2 is extracted and adapted from (Barboux et al., 2014).

3.2.1 Generalities

The suitability of DInSAR for application in the Alpine environment is discussed in many studies assessing the capability of DInSAR for analyzing slope movements (e.g. Delacourt et al. 2007; Strozzi et al. 2002, 2005) paying regard to the large number of requirements to select, analyze and interpret DInSAR correctly in this specific rough topographical context (e.g. Delaloye et al. 2007a, 2007b; Lambiel et al. 2008; Nagler et al. 2001, 2002; Strozzi et al. 2004). A successful use of DInSAR is dependent on a combination of design and environmental parameters (Hanssen, 2005). The main parameters include the imaging geometry, the radar wavelength, the spatial baseline, the temporal baseline, the atmosphere, the topography, the surface roughness (surface slope, geometry of the vegetation), the deformation characteristics (variation of surface height) as well as the surface materials (soil moisture, snow). Different combinations of these parameters may cause changes in the phase or may affect the interferogram by making the radar images locally or fully incoherent to each other. As seen in paragraph 3.1.5.2, the quality of the interferogram is given by the interferometric coherence. The coherence is lost when the scattering of the imaged surface changes during a time interval, causing the so-called temporal decorrelation. It can be related to a geometric change, as well as to a change in the dielectric properties of the surfaces or volumes imaged. While the effects related to system and geometry are well understood, the others are also important to characterize in order to avoid misinterpretation of DInSAR signals (Klees and Massonnet, 1999).

3.2.2 Imaging geometry

The applicability of the method depends on areas of missing information due to terrain topography and SAR imaging geometry (Figure 3.4). The foreshortening (a-d) is the effect of imaged terrain surface sloping towards the radar (A-D) appearing shortened: the signal is compressed and the ground resolution can be severely reduced. Layover (d-c) is an extreme form of foreshortening in which the top of a reflecting object, such as mountain, is closer to the radar (in slant range) than the lower parts of the object. It can affect a larger part of the ground, namely the portions (B-C) and (D-E), which are “passive layover”, whereas (C-D) corresponds to the “true layover”. The shadowing (f-h) indicates the portion of the ground (F-H) which is not illuminated by the radar and is located in the shade created by the obstacle (F-G). (F-H) can be identified as two separate effects: the “true

shadow" (F-G), where the slope is such that the radar does not see the surface (it looks at the surface from below) and the "passive shadow" (G-H), where there is an obstacle in the way of the LOS, so the surface cannot be mapped by the radar. In mountainous topography a lot of areas are affected by shadow and layover and cannot be analyzed. However, these areas are easily identified using standard SAR software.

As the LOS of current satellites is roughly east or west, this has an impact on which slopes are well-suited for analysis. Northern and southern facing slopes, where deformations are often directed in the plane perpendicular to the LOS, can be difficult to analyze. Back-facing slopes (D-I), defined as the western slope when viewing in descending mode and the eastern slope in ascending mode, are the most appropriate configurations (Rott and Nagler, 2003; Rott et al., 1999; Strozzi et al., 2004): the local spatial resolution is less affected by geometric distortions and deformations are more or less directed in the LOS. The away facing slopes (A-D) are the opposite and are therefore less favorable for DInSAR analysis.

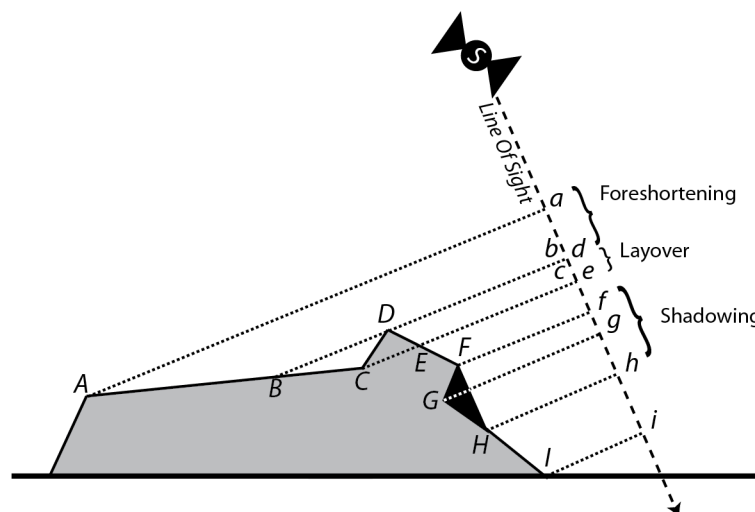


Figure 3.4: SAR acquisition geometry in the plane perpendicular to the orbit.

3.2.3 DEM errors

Spatial decorrelation is due to differences between the acquisition geometry of two SAR images involving difficulties to match them during the registering phase. A large spatial baseline between acquisitions may cause disparities between resulting SAR images, especially in complex mountainous regions.

As seen in Part 3.1.4.2, the effect of topography is dependent on the perpendicular baseline of the computed interferogram. Because 2-pass DInSAR uses a simulated topographic phase generated from an external digital elevation model (DEM) to eliminate the topographic contribution in the final interferogram (Wegmüller and Strozzi, 1998), the feasibility of DInSAR for detecting and quantifying

deformation is limited by the quality of this DEM in terms of resolution and vertical accuracy. If the DEM contains errors, the resulting interferogram will contain artificial fringes. As they appear in the same location in every interferogram using that DEM, the misinterpretation can be avoided with a large number of available interferograms (Massonnet and Feigl, 1998). To prevent artifacts, either an accurate DEM has to be used to remove the topography component correctly or image pairs with short spatial baselines should be chosen (Klees & Massonnet 1999, Walter and Busch, 2012).

		TSX ($\theta = 41^\circ$)	Envisat ($\theta = 23^\circ$)	ALOS ($\theta = 38^\circ$)
City	$\partial h < 20\text{m}$	100m	200m	700m
	$\partial h \geq 20\text{m}$	50m	100m	350m
Dumps and slopes	$\partial h < 5\text{m}$	200m	300m	1000m
	$\partial h < 10\text{m}$	100m	150m	500m
	$\partial h \geq 10\text{m}$	<50m	< 100m	<300m
Vegetation	$\partial h < 30\text{m}$	-	100m	250m

Table 3.2: Recommendations for maximum perpendicular baseline. From Walter et al. 2012

3.2.4 Characteristics of the surface changes

The phase difference provides only the LOS component of the 3D surface displacement vector. Thus, the change of color in the resulting interferogram expresses the ground deformation projected into the LOS direction and the resulting fringe is equivalent to a change in the LOS direction between an object imaged by the first and by the second SAR antenna of half a wavelength (Massonnet and Feigl, 1998). The direction of the change can be interpreted using the key in Figure 3.3. Positive phase value direction means that the radar beam has travelled further in the second acquisition and thus corresponds to a subsidence. In the opposite case, it will be interpreted as uplift. To decompose the measured motion into the vertical and horizontal components (i.e. easting and northing) it is necessary to combine ascending and descending views of the same motion. If only one acquisition mode is available, the vertical and horizontal components can be computed only if external information, such as GPS data, modelling or assumptions about the expected motion is available (Duro et al., 2013).

The rate of terrain movement which can be detected depends, among others, on the time interval and on the wavelength (Figure 3.5). The interferometric SAR signal will decorrelate when the displacement gradient between adjacent pixels is higher than half the wavelength during the selected time interval (Massonnet and Feigl, 1998). This means that the decorrelation occurrence is favored by the roughness of the surface and the displacement rate. The time interval over which the displacement is measured must be matched to the observed surface deformation (Rosen et al., 2000). Finally, the nature of the change within a pixel can introduce noise in the measuring phase difference (Klees and Massonnet, 1999). The information on the deformation is coherent only if the entire

surface within the pixel deforms homogeneously. Glaciers for instance can be well monitored, whereas rock glaciers, with a smaller and more disturbed surface due to the roughness of the terrain, decorrelate at a faster velocity rate. In the 1990s, the 3-days repeat cycle of ERS-1 and the 1-day ERS-1/2 tandem mission (C-band) offered a unique opportunity to observe changes over a very short interval of time.

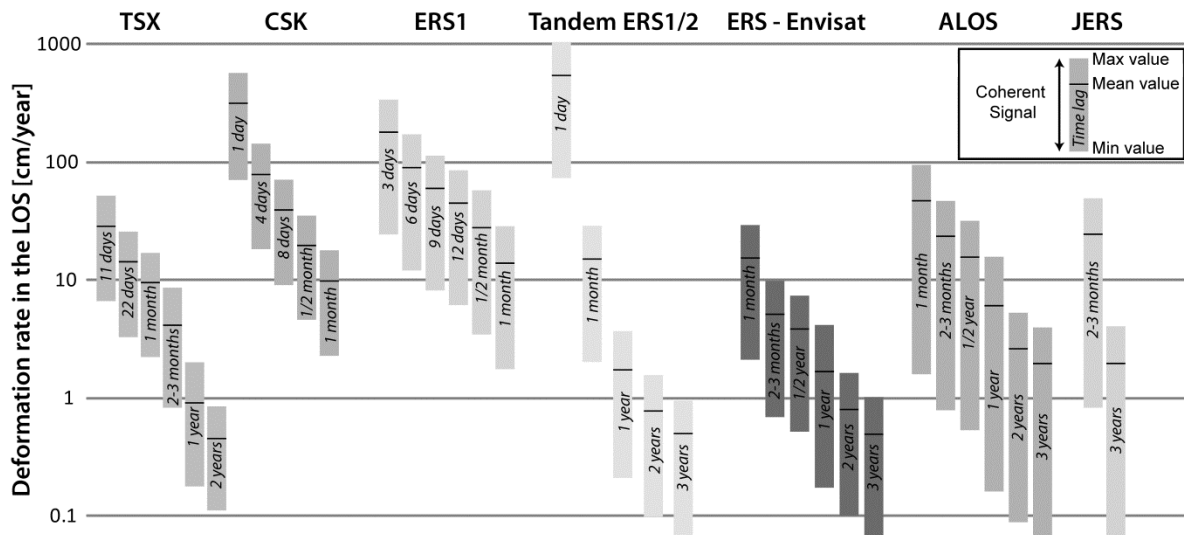


Figure 3.5: Deformation rate observed by SAR sensors for the most commonly used time lags. A bar defines the interval of deformation rate detected by a coherent signal or (partly) fringe pattern on the interferogram of the selected time lag. For a specific time lag: a movement higher than the maximal value of deformation rate will be decorrelated on the interferogram (noise pattern), a movement lower than the minimal value is not detectable (plain pattern). The line in each bar defines the mean value of observable deformation rate. From Barboux et al. (2014)

3.2.5 Soil moisture

After a rainfall, it could take several days for the soil to lose the moisture through evaporation. With clear nights especially, dew can be expected every morning for the next few days. It is established that the dielectric property of soils (namely the permittivity which is largely controlled by soil moisture), controls the penetration depth of microwaves (Ulaby et al., 1981). Thus the increase of moisture and the heterogeneity in soil moisture patterns due to rainfall for instance can contribute to a loss of coherence (Zhang et al., 2008). However, it is still difficult to define soil moisture variations as the only source of decorrelation. Indeed, several studies mention that a change in penetration depth (related to soil moisture variations) is not necessarily the cause of decorrelation and show that when surface roughness is not altered a change in soil moisture is often associated with a simple phase shift (Massonnet and Feigl, 1998; Nolan et al., 2003; Smith, 2002). In practice, we see that heavy rain events in the Alpine environment (when they occur up to 2 days before the acquisition) may partially decorrelate the signal. As almost all weather events such as fog, cloud, dew, frost etc... occur in the troposphere layer, the reason for this observed noise may also be explained by a tropospheric effect affecting the interferometric correlation (effects caused by atmosphere are

described further). Consequently, it is required to take weather conditions into consideration for DInSAR application.

3.2.6 Snow

In high mountains, the presence of snow and its temporal changes have significant influence on the coherence. In wintertime, using a one day time interval, the snow cover is kept cold and most of the illuminated area is well visible. Dry snow preserves stable scattering geometry allowing high degrees of coherence (Strozzi et al., 1999). Some pixels could remain noisy probably due to wet snow (fig. 3.6c). However, with a longer time interval, or when the snow surface is already melting, DInSAR interferograms are unusable due to the change of the scattering geometry (Strozzi et al., 1999). In fact, wet onset over the snow surface is commonly associated with a sharp decrease in radar backscatter intensity and wet snow cover dramatically reduces correlation (Smith, 2002; Strozzi et al., 1999).

In summertime, the snow-free period may strongly vary from year to year as well as from the location of the studied area, and may be delayed or advanced by several weeks (Delaloye et al., 2007a). Late-lying snow cover as well as avalanche cones also result in a typical decorrelated DInSAR-signal and may subsist during the whole summer season. Moreover, snowfall in summer and autumn may happen and does not preserve correlation (Smith, 2002).

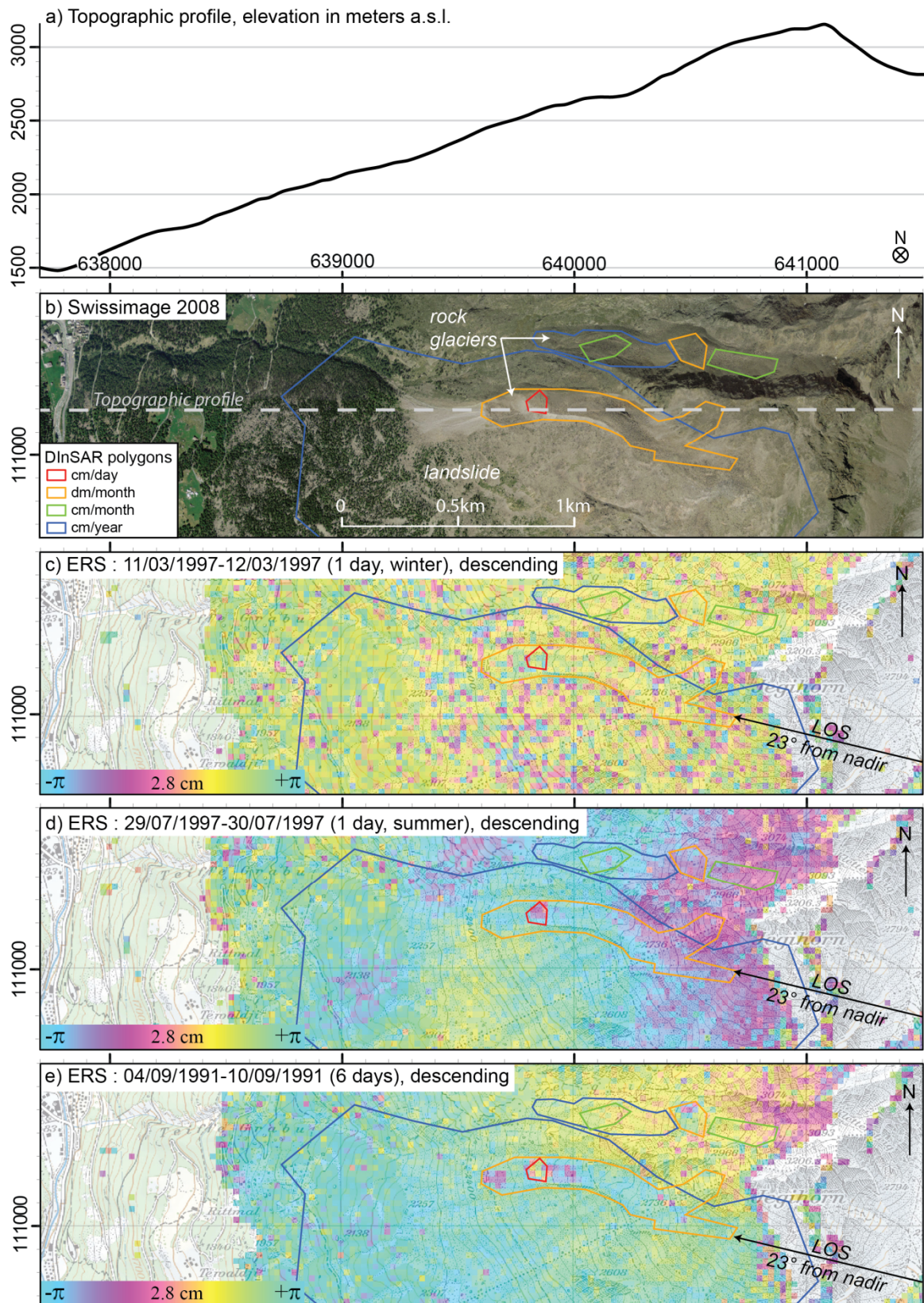
3.2.7 Vegetation

The vegetation canopy forms a complex and heterogeneous volume composed of leaves, stems, branches, and trunks, and disturbs the reflection of the radar wave (Figure 3.6). Temporal decorrelation is caused by the changes in the scatterer (growth or loss of foliage, wind motion) and/or changes in the dielectric constant in between the two satellite acquisitions (Balzter, 2001).

Forest canopies are usually modeled as a volume composed of random idealized identical objects (Jones and Vaughan, 2010). The wavelength λ of the sensor determines the penetration depth of the transmitted signal into the vegetation layer. Volume scattering is larger for shorter wavelengths whereas the penetration layer is deeper for longer wavelengths (Balzter, 2001; Jones and Vaughan, 2010). The L-Band wavelength is much larger than a typical tree leaf, thus certain vegetation types are transparent to the sensor and the signal penetrates through the upper vegetation layer and reflects from the soil surface (Balzter, 2001; Barrett et al., 2009; Jones and Vaughan, 2010). The short wavelength of the X-band sensor is mainly reflected at the top layer of the canopies (due to the presence of small objects, i.e. the tree leaves), disturbing the signal much more and causing a loss of coherence (Barrett et al., 2009). The behavior of the C-band is less predictable. As Alpine terrain is generally covered only by sparse grasses, it is especially suitable for DInSAR application.

3.2.8 Atmosphere

Atmospheric effects, producing systematic errors in surface displacements estimated from DInSAR, are assumed to be one of the main limiting factors for DInSAR (Klees and Massonnet, 1999). The different refraction index of the atmosphere disturbances causes pixel misregistration and artifacts in the phase difference (Tarayre and Massonnet, 1996; Zebker et al., 1997). In mountainous regions, a homogeneous tropospheric delay can affect the entire image creating a distinct color gradient visible from the bottom of the valley to the top (Figure 3.6d). As this delay is inversely dependent on the altitude of the terrain, it can be removed by adequate processing (Williams et al., 1998). Additional tropospheric turbulences, due to time and space variations of the vapor content, induce local heterogeneous atmospheric effects difficult to interpret (Tarayre and Massonnet, 1996). Variation in the upper part of the atmosphere, called the ionosphere, can also perturb the signal but less severely than the troposphere. Path delays can occur in the ionosphere due to the variations in the Total Electron Content influencing the whole scene rather homogeneously and by Travelling Ionospheric Disturbances sometimes causing local artifacts (Klees and Massonnet, 1999).



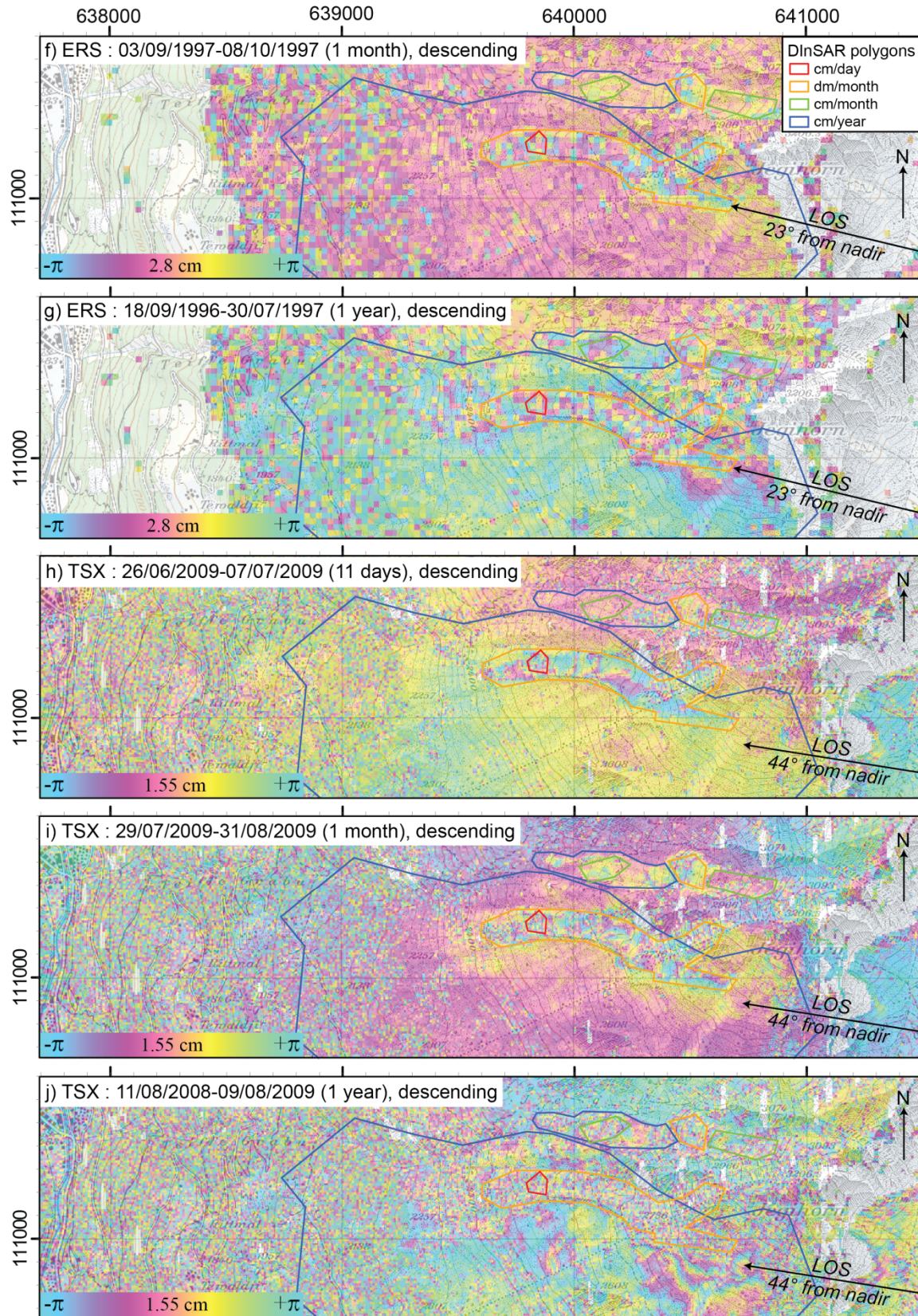


Figure 3.6: Saas Valley (Western Swiss Alps) a) Topographic profile, b) Orthoimage. Interferograms of the area using ERS c)-g) and TSX h)-j) data where layover and shadowing are masked (transparent). DInSAR detected moving zones are superimposed. From Barboux et al. (2014)

3.3 Proof-of-concept study on the suitability of DInSAR data in surveying mountain slopes

3.3.1 Introduction and objectives

In the Alpine environment, the feasibility of DInSAR is discussed in many studies assessing the capability of DInSAR for analyzing slope movements (e.g. Delacourt et al. 2007; Strozzi et al. 2002, 2005) and offer a large number of requirements to select, analyze and interpret DInSAR correctly in this specific environment (e.g. Delaloye et al. 2007a, 2007b; Lambiel et al. 2008; Nagler et al. 2001, 2002; Strozzi et al. 2004). However, no one proposes a methodology to assess the use of DInSAR based on the regional characteristics. This section suggests a standard procedure to evaluate the suitability of DInSAR for slope motion mapping and monitoring in a specific region by predicting the areas in which layover and shadowing will occur and by giving the ratio of measurability of movement of a potential moving slope from one image acquired by a SAR sensor (Barboux et al., 2011).

3.3.2 Layover and shadow mask

3.3.2.1 Definition

As DInSAR applications cannot be used in areas affected by layover and shadowing, it is very important to know whether the area of interest will be affected by these disturbances. The first step of the proof-of-concept study consists of excluding areas polluted by irreversible geometric distortions using one SAR image. A mask is created to locate invisible areas (shadows) and also reverse imaged areas (layover). Because acquisitions of scenes used for interferometry must have similar geometry, the mask of layover and shadow could be roughly estimated using only one SAR image.

3.3.2.2 Calculation

Most common DInSAR software is able to map layover and shadow areas using one SAR image. To create such a map, we use the *gc_map* procedure of Gamma software performing a geocoding lookup table based on DEM and SAR imaging geometry. This function is able to produce a layover and shadow mask *ls_map* in map projection (Figure 3.7).

3.3.2.3 Interpretation

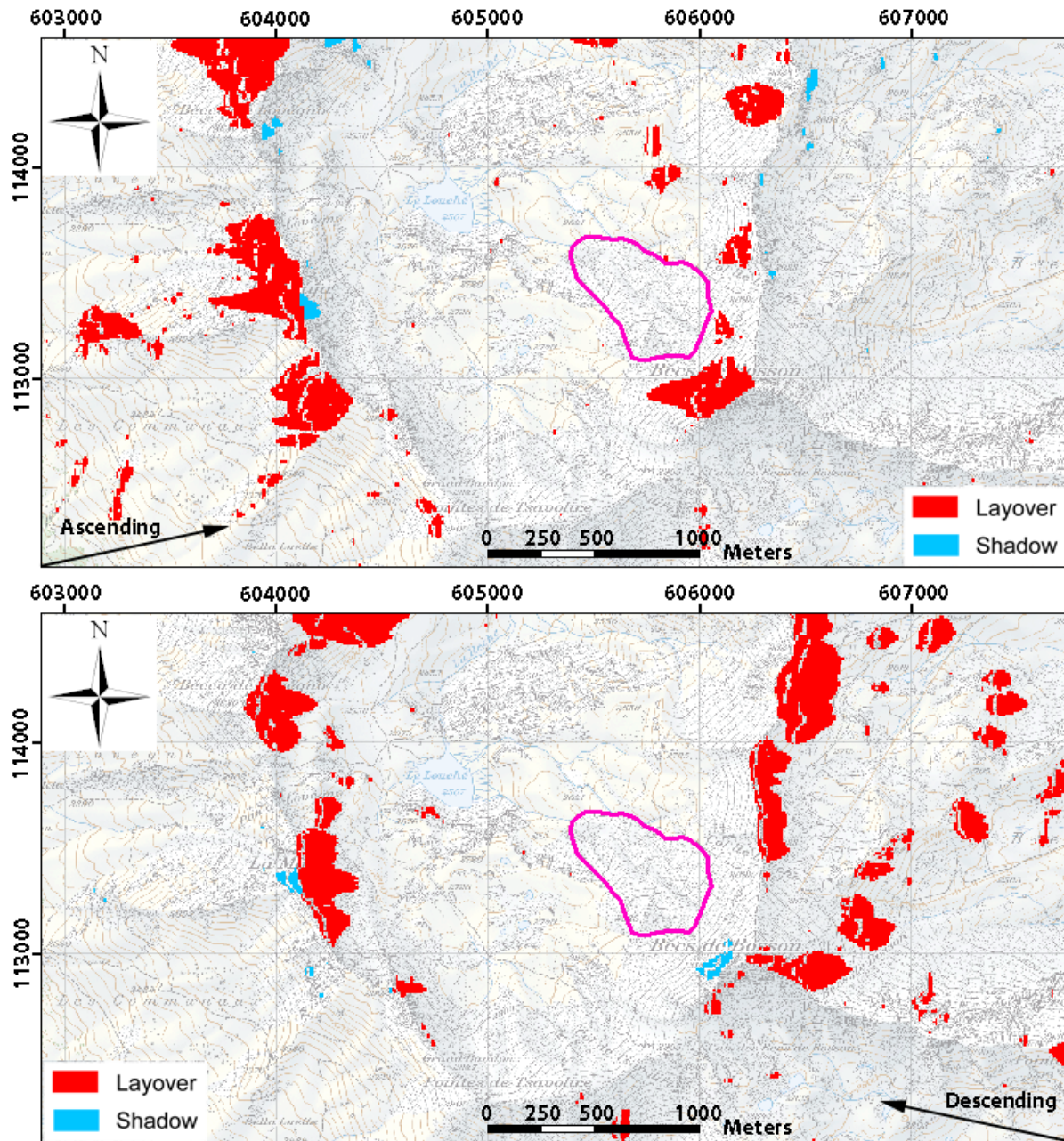


Figure 3.7: Examples of layover and shadow masks in a) ascending and b) descending mode (Vallon de Réchy). The pink polygon is the Becs-de-Bosson rock glacier, monitored by terrestrial surveying since 2001. Adapted from Barboux et al. (2011)

The result gives areas of layover and true layover in red, and shadow and true shadow in blue (Figure 3.7). The best is now to combine these results in order to produce a binary mask of visibility defined by: 1 where the area is visible and 0 where it is not (layover and shadow). It has to be taken into account that layover and shadow could have border effect propagation. Actually, because the signal is not correctly seen in these areas, noise appears in these places. By masking these areas, neighboring noise can still be present at their borders due to the fact that the view from two passes used for interferometry could actually slightly differ. It must be noted that the mask given in Figure

3.7 is the unprocessed output of the function “*gc_map*” of GAMMA software. Basic morphological operators (like erosion, dilatation or a combination of them) can also be applied to the layover and shadow mask image in order to partially reduce border effects and to improve the image segmentation.

3.3.3 Index of the deformation rate measurability

3.3.3.1 Definition of the index Md_{HS}

The second step of the proof-of-concept study consists of determining a quality index giving the ratio of the measurability of a potential moving slope Md_{HS} . The quality of the observation is evaluated here for the displacement on a unit area of the ground surface according to the topography and the look angle. It represents the ratio of total movement of a potential moving landform that can be detected from the satellite when using DInSAR technique. Because the satellite is only able to capture movements occurring in the LOS, Md_{HS} is almost equal to 1 if the motion direction is parallel to the satellite’s LOS or equal to 0 if the motion direction is perpendicular to the LOS. To compute this index, the potential slope movement is assumed to be in a particular direction in order to assess the measurability of this movement according to the orientation and inclination of the LOS. Using the simplest case is recommended, meaning that we assume that a slope movement is directed along the steepest gradient of the slope.

3.3.3.2 Calculation of Md_{HS}

Let:

- v_{HS} the displacement directed in the highest slope direction.
- v_{LOS} the projection of the displacement in the LOS direction.
- e_{LOS} the unit vector of the displacement in the LOS direction
- e_{HS} the unit vector in the highest slope direction

The scalar projection of the displacement v_{HS} in the direction of the unit vector e_{LOS} is defined by:

$$v_{LOS} = v_{HS} \cdot e_{LOS}$$

The index Md_{HS} is defined as the dot product between the unit vector in the maximum slope direction e_{HS} and the unit vector in the LOS direction e_{LOS} .

Thus:

$$\begin{aligned} Md_{HS} &= e_{LOS} \cdot e_{HS} \\ &= e_{LOS|x} \cdot e_{HS|x} + e_{LOS|y} \cdot e_{HS|y} + e_{LOS|z} \cdot e_{HS|z} \end{aligned}$$

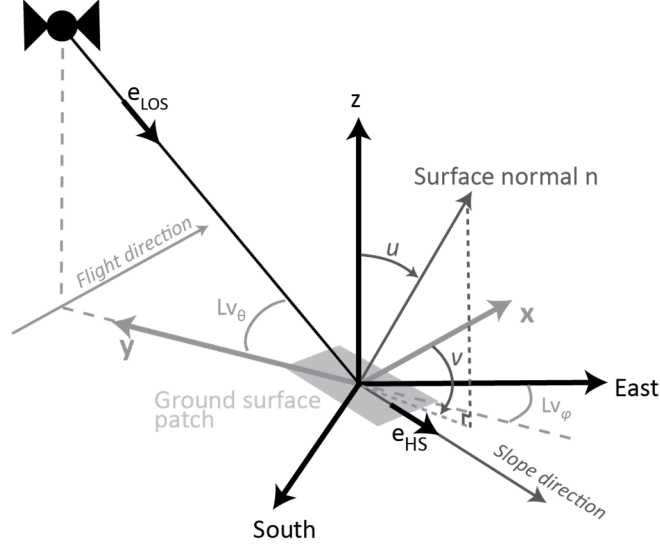


Figure 3.8: 3D geometry of SAR system when looking at a ground surface patch.

As defined in Figure 3.8, let:

- u the zenith angle of surface normal vector n (angle between z and n)
- v the orientation angle of n (between x and projection of n in xy plane)
- Lv_θ the SAR look-vector elevation angle (at each map pixel). $Lv_\theta: \pi/2 \rightarrow \text{up}, -\pi/2 \rightarrow \text{down}$.
- Lv_ϕ the SAR look-vector orientation angle at each map pixel $Lv_\phi: 0 \rightarrow \text{East}, \pi/2 \rightarrow \text{North}$.

Parameters u and v are given by the *gc_map* function of GAMMA software. Lv_θ and Lv_ϕ are computed from the *look_vector* function allowing the calculation of the SAR look-vector direction (pointing towards SAR) in map geometry.

Finally:

$$e_{LOS} = \begin{cases} \cos(Lv_\theta) \cos(Lv_\phi) \\ \cos(Lv_\theta) \sin(Lv_\phi) \\ \sin(Lv_\theta) \end{cases} \quad \text{and} \quad e_{HS} = \begin{cases} \cos(u) \cos(v - \pi/2 + Lv_\phi) \\ \cos(u) \sin(v - \pi/2 + Lv_\phi) \\ -\sin(u) \end{cases}$$

3.3.3.3 Interpretation of Md_{HS}

The surface deformations of the Becs-de-Bosson rock glacier (assumed in the highest slope angle direction) will be more reduced in ascending mode than in descending mode (Figure 3.9c-d). A substantial reduction could induce difficulties in interpreting velocities which are varying in a compressed range of values. Moreover, when the index Md_{HS} varies over the whole moving landform, the projection of the deformation also varies. Consequently, a spatially homogeneous deformation rate can produce a spatially heterogeneous DInSAR signal and therefore the signal has to be interpreted carefully. The reduction of deformation magnitude when projected in the LOS could however be very useful to monitor high deformation rates.

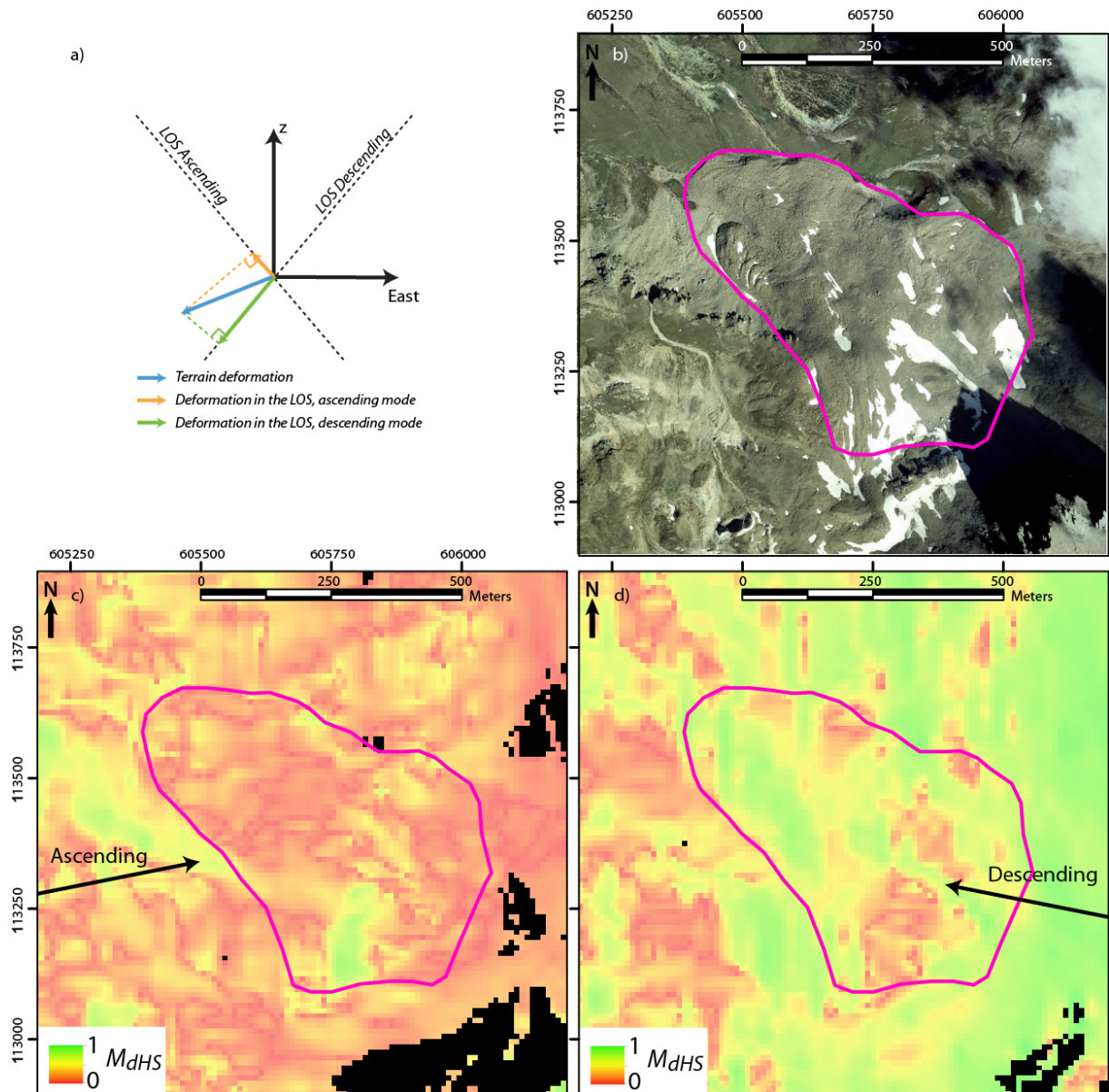


Figure 3.9: a) LOS deformation can differ from the real value of deformation. b) Orthoimage of the Becs-de-Bosson rock glacier, Vallon de Réchy (2005) and results of the visibility map compression in c) ascending and d) descending modes. Md_{HS} goes from red (highly compressed) to green (no compression). Layover and shadow is masked in black. Adapted from Barboux et al. 2011

3.3.4 Suitability of DInSAR data

Firstly, the suitability of DInSAR data for detecting and quantifying deformation has to be analyzed according to the different factors indicated in Part 3.2. The spatial resolution of the radar sensor, the SAR data availability, the quality of the available DEM, the land cover as well as the atmospheric disturbances, need to be considered when deciding whether to use DInSAR or not.

Then, the suitability of DInSAR for slope motion mapping and monitoring in a specific region can be assessed from the layover and shadow mask and from the index of measurability of deformation rate Md_{HS} . The layover and shadow mask shows the areas that cannot be analyzed. The percentage of visible area of the region of interest can therefore be derived from this mask. Then Md_{HS} can be

related to the maximum measurable deformation rate. In the LOS direction, the maximum measurable deformation rate $DMax_{LOS}$ is assumed to be one fringe per pixel per time difference between the two acquisitions forming the interferogram. For instance, using TerraSAR-X data with a wavelength of 3.1 cm and an 11-day orbital cycle, $DMax_{LOS}$ is equal to 0.51 m/year. If the deformation rate in the LOS exceeds this threshold the signal tend to be decorrelated and the moving slope could be detected but not be monitored. The maximum measurable deformation rate along the slope direction $DMax_{HS}$ can be computed as follow:

$$DMax_{HS} = \frac{DMax_{LOS}}{Md_{HS}}$$

This equation shows that the smaller Md_{HS} is, the larger the maximum measurable deformation rate along the slope direction will be.

Finally, this index can be used differently according to the objectives of the project: either to determine which deformation rates can be measured or detected on the region of interest or to assess if a defined moving slope (whose deformation rate is previously known) can be monitored using DInSAR.

3.3.5 Discussion

3.3.5.1 *Assumption of displacements directed along the slope direction*

The main limitation of this proof-of-concept study comes from the assumption that the displacement is directed along the highest slope direction, which is not verified for every slope movement encountered in the Alpine environment. Inevitably, the greater the difference between the actual displacement direction and the highest slope direction, the worse the assessment of maximum measurable deformation rate. This model is probably best suited for translational slides. The deformation of a rock glacier, for example, is composed of a flow component and a vertical component due to loss or gain of ice. Consequently, it would be useful to verify the assumption that deformation is directed along the slope direction before proceeding with this proof-of-concept study. If the assumption that displacements are directed in the highest slope direction is not verified, the proof-of-concept study is not recommended. In this case, the measurability of the deformation rate should be evaluated according to another hypothesis concerning the direction of the displacement.

In Chapter 6, Section 6.2.3, this assumption will be verified for the specific use of DInSAR in the detection and monitoring of Alpine landforms located in the periglacial environment of the Western Swiss Alps in order to see to what extent the direction of displacement can be considered in the highest slope direction. About 30 landforms composed of landslides, rock glaciers and push-moraines located in Valais will be analyzed and the direction of their displacements monitored by DGPS

measurements will be compared to the highest slope direction for 2 resolution levels: 25 meters using DHM25 (©Swisstopo 2010) and 2 meters using SwissAlti3D (©Swisstopo 2013).

Finally, it must be noted that the proposed proof-of-concept study is only used here to assess the potential of TSX DInSAR data for the observation of Alpine slope movements and to roughly estimate the maximum deformation rate that can be quantified in the study region. A methodological chapter (Chapter 5) will be specifically dedicated to the precise monitoring of Alpine landforms using TSX DInSAR data.

3.3.5.2 *Necessity of at least one SAR image*

The second main limitation of the proposed proof-of-concept study concerns the need for at least one available image acquired by a SAR sensor. Actually, Gamma software needs at least one SLC parameter file to compute *gc_map* and *look_vector* functions. Unfortunately, using the current version of the GAMMA software (version 2013), it is not possible to compute a rough estimation of layover and shadow, or to determine the looking vector parameters knowing only the basic flight direction parameters, namely the LOS direction. Yet it should be really useful to develop such an algorithm to help users performing a pre-survey analysis prior to the costly investment in a radar survey. While the rough estimation of Md_{HS} is easily computed using a classical environment for numerical computation (found in common toolbox of GIS software), the mask of layover and shadow is much more complex to perform; passive shadow and passive layover are especially complicated to determine. The present thesis does not investigate this issue as data was already acquired on the studied area to perform such an analysis directly with GAMMA software using one SAR acquisition. Moreover, a similar approach has been developed simultaneously by Plank et al. (2012) and goes further since it presents a geographical information system (on ArcGIS) procedure prior to the use of any existing radar image.

3.3.5.3 *Interpretation of the index of measurability of deformation rate*

The index of measurability of the deformation rate Md_{HS} gives the ratio of the measurability of a potential movement occurring on a slope. A small value of Md_{HS} means that the terrain deformation component is highly compressed in the LOS. Consequently, for a considered wavelength and a small value of Md_{HS} , a large deformation can be detected by a (partly) fringe pattern while a smaller one can be completely undiscernible (plain pattern). Thus, it is preferable not to directly associate the value of this index to the suitability of DInSAR for the mapping and the monitoring of moving slopes, but to estimate the maximum measurable deformation rate using this index, keeping in mind that the motion is assumed to be parallel to the surface.

The successful study of Plank et al. (2012) suggests that DInSAR can only be used for monitoring slow movements and does not take into account the expected maximum deformation measurable in the

LOS. They associate the percentage of measurability of movement to the quality of the observed deformation from green (100%, $Md_{HS} = 1$) to red (0%, $Md_{HS} = 0$). Thus, they do not explore the potential of high compression of deformation in the LOS for the monitoring of fast movements.

3.4 Conclusion

The automatic data storing and systematic acquisition of SAR data is ensured worldwide for most sensors and allows the use of DInSAR technique in other regions using data from the archive, although for very high resolution SAR satellites data storing is performed only on specific regions requested by the scientific community. However, accessibility of current data is not always possible. It is subject to costs sometimes too high for scientific purposes and to availability. TSX successive stripmaps are acquired by the same orbit, making the availability of two contiguous areas at the same time impossible. High quality DEM are not always available and the topography of the region might not be suitable for the application of DInSAR. This problem could maybe be solved with the upcoming global DEM from the Tandem-X mission. In any case, a study of feasibility has to be carried out to determine what analysis could be done in the region of interest with which kind of data.

4 Towards semi-automated mapping of slope movements with DInSAR in the Alpine environment?

This chapter proposes an automated method to map and assess slope movements in the Alpine environment from a selected dataset of TSX interferometric phase images. The first Part 4.1 introduces basic concepts of visual interpretation of DInSAR data performed a decade ago for inventorying Alpine slope movements in the Swiss Alps in order to conceive the development of an automated process. Then, the presentation is developed in two stages. First a process is presented to extract textural image features from the phase image and classify these features according to the three defined DInSAR signal patterns using different statistical methods (Part 4.2). Then a general approach is defined for the mapping of the DInSAR signal and the related mapping of the slope movements for a selected area (Part 4.3). Finally, a discussion and conclusion is proposed in Parts 4.4 and 4.5.

4.1 Introduction and background

In the framework of several projects carried out over the last decade (Delaloye et al., 2007a, 2007b, 2008, 2010; Lambiel et al., 2008), large inventories of Alpine slope movements have been performed in various regions of the Swiss Alps using 2-pass DInSAR and assess both the surface geometry and the activity of detected landforms. These slope movements may be related to glaciers and particularly to debris-covered (parts of) glaciers as well as to the creep of frozen debris (rock glaciers, push-moraines) or to landslides. The exploitation of DInSAR data and the set-up of an inventory have been carried out by visual interpretation on the basis of a large set of ERS interferograms with various time intervals (from 1 day to 3 years). To perform this inventory, a strict protocol was followed by several experts consisting of analyzing each selected interferogram to detect the outline of moving objects and estimate their deformation rate (Barboux et al., 2014).

Section 4.1.1 proposes a short review of the procedure of visual interpretation of DInSAR data performed a decade ago for inventorying Alpine slope movements in the Swiss Alps. This first section is offered to the reader in order to understand the main basis for the development of an automated process. Finally, objectives and motivation of an automated procedure will follow in Section 4.1.2.

4.1.1 Methodology of visual inventory for detecting mass wasting in the Swiss Alps

This section is extracted and adapted from Barboux et al. (2014). A short review about the procedure of visual interpretation of DInSAR data is proposed. It explains the data selection and processing, the methodology itself and the evaluation of the results. Finally, few words will be given on the inventory of slope movements performed in the Western Swiss Alps using this methodology.

4.1.1.1 Data selection and processing

To get a complete overview of slope movements in a given area and to prevent misinterpretation of detected mass wasting phenomena, it is essential to dispose of a large set of workable interferograms produced with various time intervals (e.g. daily, monthly and yearly) and a small spatial baseline. Several SAR sensors can be selected according to their availability and accessibility (Table 3.1). The major obstacle limiting the successful use of DInSAR in an Alpine environment is the presence of (wet) snow. Usable SAR scenes must be, as much as possible, snow free, which is usually between June and October in the Swiss Alps. SAR scenes with a daily time interval can also be used in the wintertime, when the snow is still cold.

After SAR image selection, DInSAR interferograms should be processed in a 2-pass approach applying standard processing steps (coregistration, interferogram generation, flat Earth removal, baseline correction, topographic phase estimation using external DEM, subtraction of the estimated topographic phase). In a mountainous region, the DEM used for topographic phase correction should have a minimum of 25m resolution and 3-5m height accuracy when working with ERS DInSAR data having a spatial baseline lower than 250m. With the same DEM quality and TSX data, the baseline has to be set lower (Tab. 3.2; Walter & Busch, 2012). The resulting interferometric products can be multi-looked in order to approximately obtain squared pixels. The process of multi-looking consists of averaging phase and coherence values at neighboring pixels comprised within a window of fixed size. An atmospheric phase model based on a linear regression of atmospheric phase with respect to the DEM can also be applied.

Finally, if no final spatial filtering is applied, phase noise and residual phase error terms must not be neglected when interpreting the interferogram. Estimating the occurrence of old or fresh snow and the weather conditions (rain event) at or up to two days before each SAR image date on the basis of available meteorological data has also proven to be a helpful step in evaluating the quality of an interferogram (Delaloye et al., 2007a).

4.1.1.2 Procedure for visual slope movement inventory

The methodology of a visual slope movement inventory aims a) to identify moving landforms over a large region, b) to spatially outline areas with an almost homogeneous deformation rate (hereafter

called DInSAR polygons), and c) to categorize the deformation rate of the detected DInSAR polygons by assessing qualitatively the DInSAR signals that can be observed on interferograms with different time intervals (Delaloye et al., 2007a). Detected moving landforms are indicated using polygons which are manually drawn. They describe an area where a given DInSAR signal is detected and do not necessarily fit the morphological outline of the landform.

The detection is performed by looking for a fringe pattern and/or noise on an interferogram, which means looking at a single pixel according to its neighbors. The minimal size of detectable targets is consequently limited by the spatial resolution of the interferogram as well as by the filtering applied to reduce noise. The estimation of the deformation rate is performed by comparing the phase signal inside and outside a detected polygon at different time intervals. The categorization of the deformation rate is then determined by combining observations from each interferogram (Figure 4.1). Depending on the sensor technology, several classes of deformation rates can be defined. These categories are related to the time intervals at which a moving feature is detected by either a coherent or decorrelated signal. For instance, four categories are well defined within ERS data (Delaloye et al., 2007a): “cm/day” refers to features detected on 1-day interferograms and decorrelated with larger time intervals, “dm/month” to features not detected on 1-day interferograms and decorrelated on 35-day interferograms, “cm/month” to features detected on 35-, 70- and 105-day interferograms and decorrelated for larger time intervals; and “cm/year” to features detected only on 1-, 2- or 3-year interferograms (Figure 3.5, Table 2.2).

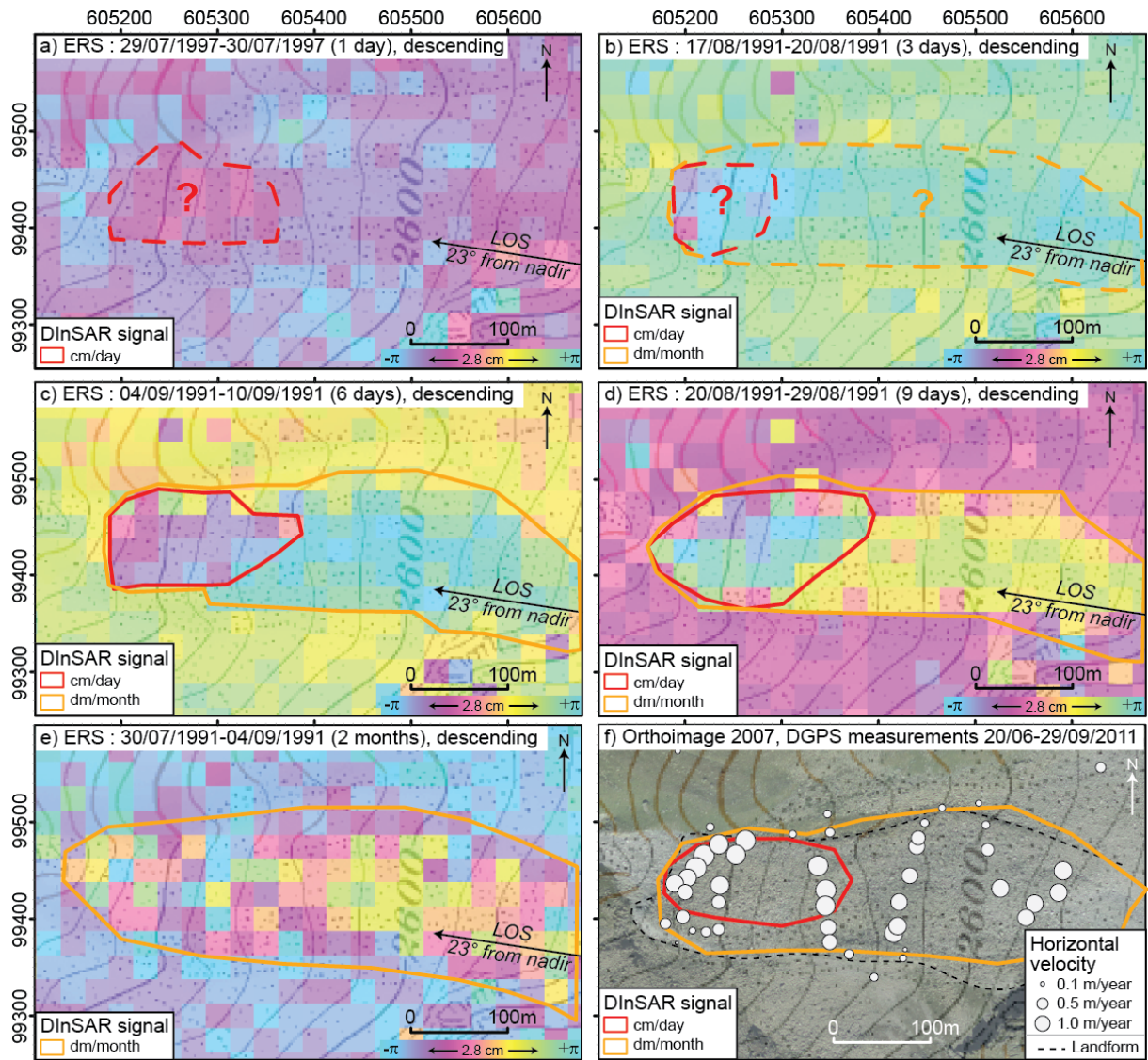


Figure 4.1: Detection of the Tarmine rock glacier using ERS data. A large set of valid combinations of interferograms with different time intervals is required to increase the confidence of detected polygons. DGPS are used only to validate the order of velocity rate detected by DInSAR interpretation. a) A small red signal could be detected on the 1-day interferogram. b) Using 3-day time interval, a signal could again be seen on the frontal part and around the whole landform. c) The frontal part is now well detected on the 6-day interferogram and a signal appears around the rock glacier. d) The frontal part becomes decorrelated on the 9-day interferogram. e) The entire rock glacier is decorrelated on the 2-month interferogram. f) Two DInSAR polygons have been drawn and classified in terms of the deformation rate as moving in the order of cm/day in red and of dm/month in orange. The outline of the landform and measured DGPS points from summer 2011 are indicated. From Barboux et al. 2014.

DInSAR polygons are described by their spatial outline, the category of deformation rate, the typology of the related landform and, when necessary, some remarks. In most cases the typology of the related landform (geomorphologic process) can be identified on satellite or airborne optical images or by field visits. As the confidence in a DInSAR polygon depends on the number of interferograms used for the detection and on the delimitation, which is subjective and obviously might differ depending on the user, an index of reliability indicating the quality of the detection is also advised.

4.1.1.3 Evaluation of the detected movements

When possible, inventoried DInSAR-detected movements must be compared with available field data. Pre-existing inventories of slope movement (landslide and/or rock glaciers), terrestrial geodetic survey data (DGPS, Total station, Lidar, etc.), as well as airborne photogrammetry data are, for instance, valued sources of validation. In the absence of terrestrial data, only the analysis of several interferograms and a good knowledge of the corresponding geomorphology allow the signal to be interpreted as a movement and not attributed to noise or atmospheric artifacts. In any case, the interpretation of the dataset by a second user is highly recommended in order to improve the overall quality of the inventory. Finally, the use of a reliability index is really important for any third user of the inventory to know how accurate the detected polygon is.

4.1.1.4 General results observed in the Western Swiss Alps

The methodology was applied at a regional scale on the periglacial belt of the Western Swiss Alps (~2650 km²), and was carried out over three months by at least two scientists using a large set of DInSAR data (Delaloye et al., 2007a, 2007b, 2008b, 2010b; Lambiel et al., 2008). Sixty-three interferograms from the European ERS-1/2 and Japanese JERS satellites were used for the period of 1993-2000, completed by some more recent acquisitions (2006-2007) from ENVISAT and ALOS PALSAR. A total of 1791 DInSAR polygons related to about 1500 landforms were detected, with velocities ranging from about one centimeter to several meters per year. DInSAR polygons were described by their location and geometry, the deformation rate according to four selected classes (cm/year, cm/month, dm/month and cm/day), the typology of the related landform and the reliability of the signal detection and interpretation.

4.1.2 Objectives of an automated procedure

4.1.2.1 Motivation of an automated approach

Thanks to this study, the potential of inventorying slope movements in a periglacial environment using DInSAR data is demonstrated. Since this time, several other studies have been reported on rock glacier inventories using DInSAR, like in the French Alps (Echelard et al., 2013), in the Sierra Nevada, California (Liu et al., 2013) as well as in Northern Iceland (Lilleøren et al., 2013). However, the potential of DInSAR has not always been fully investigated in terms of data selection (e.g. Echelard et al. only used descending mode, Liu et al. did not use ERS-1/2 tandem) or partial use of data (e.g. Lilleøren et al. only used DInSAR on a subset of rock glaciers previously mapped from aerial imagery to validate their state of activity).

Two main points have to be mentioned. First, we see the difficulties to work from a large quantity of data. The larger the dataset is, the longer time the detection takes. A great effort has to be deployed

to combine the results observed from a large dataset in order to produce a relevant synopsis of the detection of moving landforms in the region of interest. Secondly, it is clear that very experienced geomorphologists will produce the highest reliability map. Thus, it is important to give a useful key of interpretation for people who are not familiarized with the mountain periglacial geomorphology or with radar remote sensing techniques. Consequently, the motivation of an automated detection of slope movement is to deal with these two main aspects. This means 1) helping users to work with a large quantity of data and 2) support people in the detection and the interpretation of DInSAR signals.

4.1.2.2 Genesis of an automated approach

In practice, the detection of slope movements resides in the interpretation of the DInSAR signal and particularly in the distinction of three different patterns observed on the interferometric phase image: 1) no change defined by a plain pattern, 2) smooth change characterized by a (partly) fringe pattern and 3) decorrelated signal expressed by a noise pattern (Figure 4.2). This means that the interpretation of DInSAR data is performed by looking at the image texture of the interferometric phase image. Thus, the main goal of an automatic analysis is to map an interferogram into the three DInSAR signal classes related to the three defined patterns.

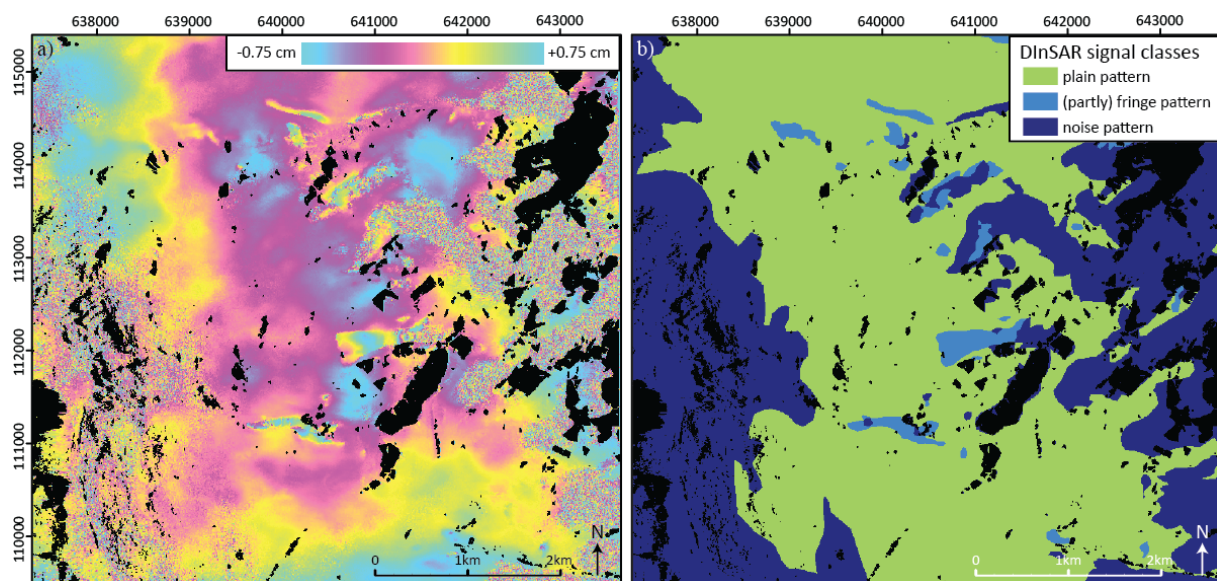


Figure 4.2: a) Interferometric phase image from 02-13/08/2012 and b) the respective manual interpretation of DInSAR signal. In black are the layover and shadow areas.

Large numbers of classification techniques have already been developed for different kinds of land cover classifications (Askne and Hagberg, 1993; Dammert et al., 1999; Engdahl and Hyypä, 2003; Wegmuller and Werner, 1995; Weydahl, 2001a, 2001b) or for change detection purposes (Preiss and Stacy, 2006; Wiesmann et al., 2001) using interferometric amplitude, coherence images and/or backscattering intensity. However, no work has thus far been produced to automatically map slope

movements from DInSAR scenes. Yet the large number of potential applications using these maps could largely compensate working efforts.

4.1.2.3 Studied region and TSX dataset

In this chapter, the chosen studied area is located on the east side of the Saas Valley. This portion of 37 km² (5.9x6.3km wide) was chosen as it is not too complex and is a representative example of landscapes encountered in the Western Swiss Alps with high slopes, rugged terrain and an altitude ranging from 1500m at the valley bottom (western part of the studied area) up to about 4000m at the top of the mountain (eastern part). Forty-four DInSAR polygons were visually inventoried in this west oriented slope using ERS and JERS images from the 1990s. This inventory is divided into signals from four different magnitude orders, namely the classes “cm/day”, “dm/month”, “cm/month” and “cm/year” defined above (Subsection 4.1.1.2). The inventory presents typical mass wasting processes encountered in the periglacial belt like landslide, sagging, rock glacier, debris-covered glacier, push moraine and creeping talus slope. This small region is suitable to test the performance of the presented algorithm as it does not show too complex of a slope system with very few superimposed moving landforms. Moreover, it is important to note that this region is relatively dry; the snow disappears quickly in spring and is rarely present in summer. This characteristic allows a larger number of valid interferograms.

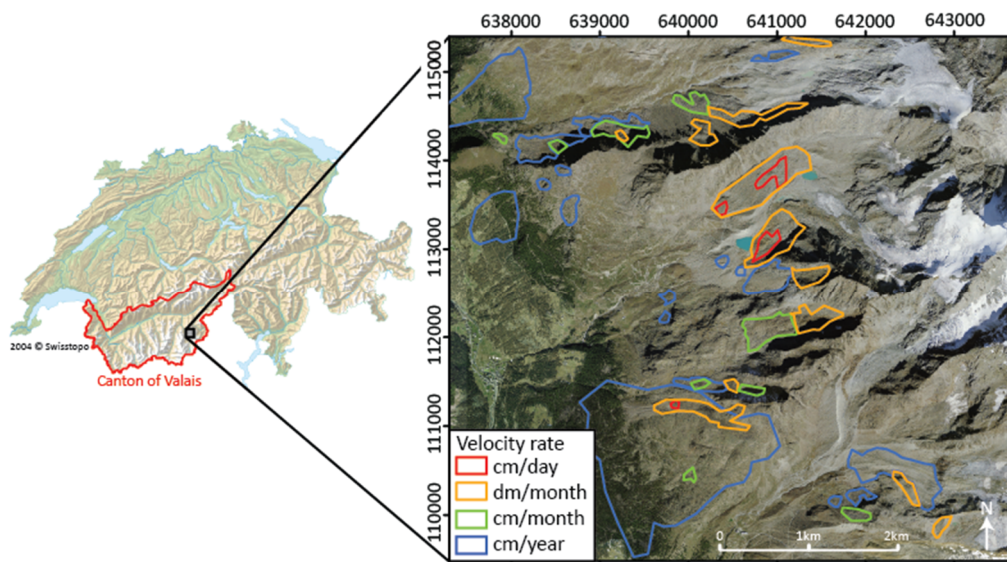


Figure 4.3 : Detected DInSAR polygons using ERS and JERS from the 1990s in the studied area.

Interferometric phase and coherence images were generated using TSX data scenes available from summers 2008 to 2012 with different time intervals in descending mode (Table 4.1). 140 interferograms were selected with a baseline lower than 250m.

Time intervals	Number of pairs
11 days	11
22 days	10
33 days	10
44 days	10
55 days	10
66 days	9
77 days	12
88 days	11
352d	12
363d	7
374d	8
638d	6
649d	5
660d	5
704d	6
715d	8
Total	140

Table 4.1: Number of selected interferograms from summers 2008 to 2012

The interferograms were produced using the commercial InSAR processing software “GAMMA”. Differential SAR interferograms were processed in the two-pass approach using a Digital Elevation Model (DEM) oversampled to 5 meters pixel spacing, the SwissAlti3D DEM (2011 © Swisstopo), having an estimated vertical accuracy of 1-3 meters for an original 2 meters pixel spacing. For heights up to 2000 meters the DEM is based on airborne laser scanning, while the higher areas are based on stereocorrelation from airborne images acquired from 2008 to 2011.

Standard processing steps were used: coregistration of the acquisitions, interferogram generation, flat Earth removal, baseline correction, estimation of the topographic phase using the DEM and subtraction of the estimated topographic correction from the interferogram. Note that the resulting interferometric products are multi-looked using a 5x5 window. Moreover, an adaptive filtering function based on local fringe spectrum (“adf” function of GAMMA software) was applied to each interferogram in order to reduce noise in the phase image and improve the quality for further classification in the algorithm. The function computes locally the interferogram power spectrum, designs a filter based on the power spectrum, filters the interferogram and estimates the phase noise coherence value for the filtered interferogram (Goldstein and Werner, 1998). According to software requirements, a small Fast Fourier Transform (FFT) of size of 32 was chosen for the filtering of rapidly changing phases associated with the topographic phase of rugged terrain. Outputs are the filtered phase and the phase noise coherence estimate (measured for the phase noise of the filtered interferogram) with a 5m posting.

4.2 Statistical methods to classify DInSAR signal

This part introduces a pixel-based classification applied to the interferometric phase image. The objective is to classify the DInSAR signal of the interferometric phase image using texture analysis

according to the three defined DInSAR signal classes: 1) **plain** pattern: no change detected on the phase signal, 2) **(partly) fringe** pattern: smooth change detected on the phase signal and 3) **noise** pattern: decorrelated signal (Figure 4.2). The textural image features are first extracted from an interferometric phase image using co-occurrence matrix. Then, features are normalized in order to consider them equally, and a standard Principal Components Analysis (PCA) is performed to reduce the dimensionality of the dataset. Finally, different statistical methods are presented to classify the reduced and transformed set of principal components as input features into one of the three classes.

4.2.1 Generation of textural image features

4.2.1.1 Features extraction

The texture is an important characteristic for the analysis of images. Image texture can be decomposed into 2 dimensions: the value of the specific pixel related to the local property, and the spatial organization of the neighboring pixels (Haralick, 1979). Due to the ambiguity of the phase values, the texture of the interferometric phase image is not concerned by the first dimension but only by the latter related to the spatial interrelationships between pixels.

To describe the textural properties of the neighborhood of a pixel we extract measures of local statistics based on two-dimensional (co-occurrence) histograms (Tuceryan and Jain, 1998) from an interferometric phase image. In this study, textural features are estimated in a square window of 17x17 pixels (~85x85m) related to the size of the landforms that have to be detected. The use of a gray-level co-occurrence matrix has proven to provide reasonable results in many studies to evaluate the texture (Haralick et al., 1973). This matrix analyzes pairs of adjacent pixels (four directions) in the phase image scaled to 8 levels of tone, and accumulates the total occurrence of each combination, producing an 8-by-8 output array. Each entry of a co-occurrence matrix is derived from the gray-level image as the expectation for the probability for two pixels having gray-value i and j and being d pixels separated in angle direction. We use a simple single co-occurrence matrix with angle directions of 0, 45, 90 and 135 degrees and a distance d of 1 pixel. The four standard following features are extracted: the contrast related to the amount of local variation present in the image, the correlation measuring the gray-tone linear-dependencies, the homogeneity measuring the uniformity and finally the energy measuring the local homogeneity.

4.2.1.2 Features normalization and features space reduction

To equally consider each feature dataset, it is important to normalize them. Two types of normalization are considered (Jain and Dubes, 1988). The linear normalization ranges features in between [-1 1]:

$$x' = \frac{2(x - \frac{\max + \min}{2})}{\max - \min}$$

and the standard value normalization produces features with a zero mean μ and a unit variance σ :

$$x' = \frac{x - \mu}{\sigma}$$

Linear normalization might be strongly influenced by an outlier, but will perfectly match the range of the data between the two most extreme values (Figure 4.4b). Standard value normalization, which is the chosen technique for the following operations, is based on the distribution of data. Therefore, if the number of data is sufficient, it is less influenced by outliers. However, looking Figure 4.4c, the data does not perfectly fall into the same range.

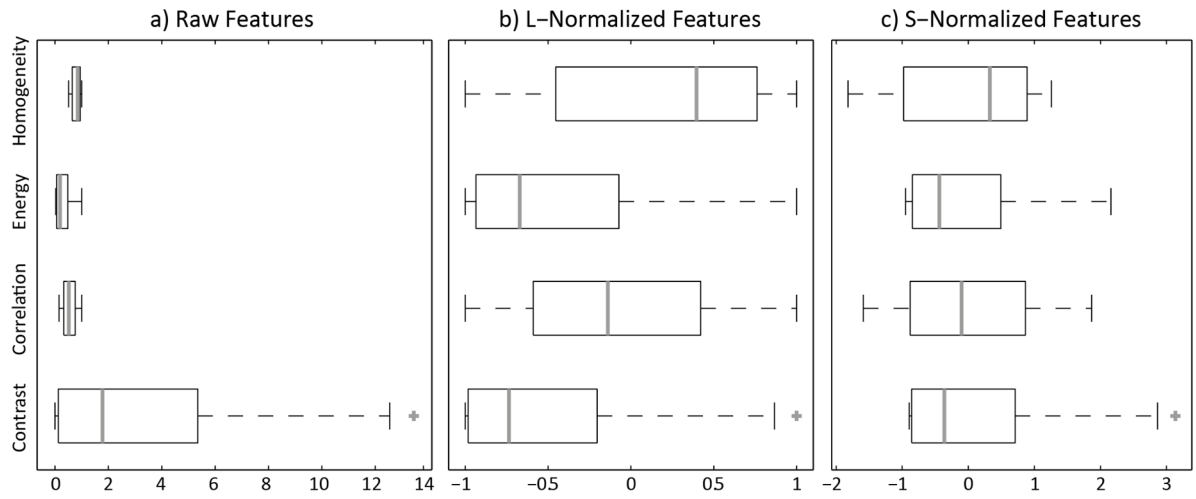


Figure 4.4: a) Raw features set, b) its normalization using linear and c) standard score method. The left and right of the box, the gray line and gray crosses show respectively the lower and upper quartiles, the median value and outliers.

A Principal Components Analysis (PCA) is then used to reduce the dimensionality of the dataset composed by these four textural features. The PCA is a procedure that transforms the dataset of possibly correlated variables into a set of linearly uncorrelated variables called principal components. Linear combinations of features can be found to best describe the variance of the samples. The dataset is projected into a new coordinate system such that the greatest variance by some projection of the data comes to lie on the first coordinate (first component), the second greatest variance on the second coordinate, and so on. As seen in Figure 4.5, the two first principal components explaining 90% of the variance can be kept as input features for further processing.

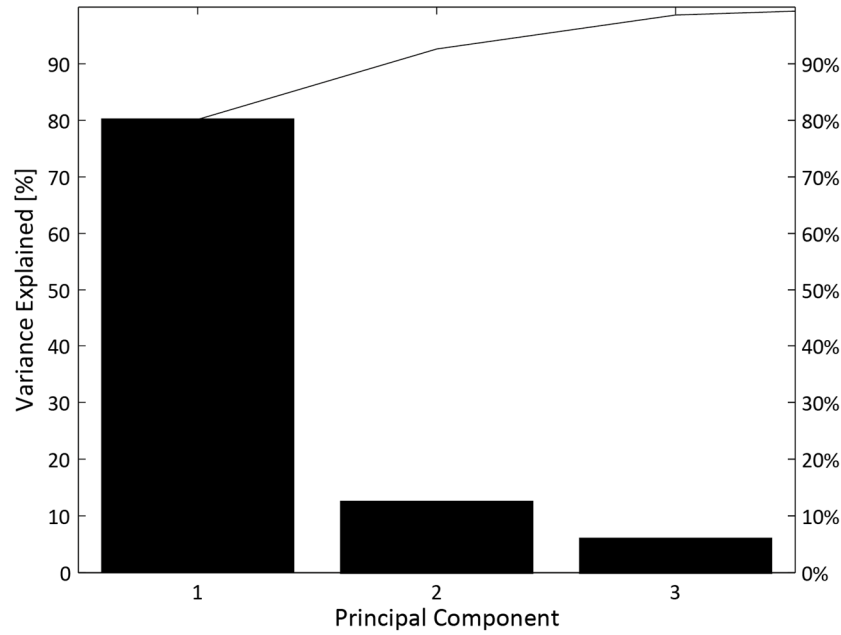


Figure 4.5: Variance explained versus number of principal components among the dataset of the four textural features.

4.2.2 DInSAR signal classification from statistical methods

This approach uses common statistical machine learning techniques on the reduced and transformed set of principal components as input features. Such methods are used in a wide range of classification problems in literature, and so they represent a good reference value for the near-optimal performance that could be reached with a specific training and testing dataset. The different statistical methods are presented to classify input features according to the three defined DInSAR signal classes.

4.2.2.1 Training and testing sets

All machine learning techniques require a certain amount of data to be used for training the classifier. In literature, it is common to split collected data with a certain percentage between training and a testing data. In our case, separate training and testing datasets were obtained using visual interpretation of the TSX interferogram from 02-13/08/2012 (Figure 4.2). A training dataset is constituted of 145 selected points from the phase image whose proportion is roughly equal in each class (46 plain pattern, 50 (partly) fringe pattern and 49 noise pattern). A testing dataset is a set of 132 selected points covering the entire studied area on a grid with regular spacing and taking into account the natural proportion of each class in the common studied surface.

4.2.2.2 Statistical methods

Different reference methods, including Linear Discriminant Analysis (LDA), K-nearest neighbor (KNN), Decision Tree (TREE) and Naive Bayes (NB) were used here. Such methods consist of classical data mining tools and consequently are not fully described for space consideration (see for further details

(Bishop, 2006)). LDA consists of defining linear borders in the space of features for each activity. KNN method consists of counting the majority number of training neighbors of a tested sample within a defined area. The decision tree consists of a simple yet powerful classification technique applying successive comparisons of single features to reach terminal states (called leafs). NB consists of assigning a new observation to the most probable class, assuming the features are conditionally independent given the class value.

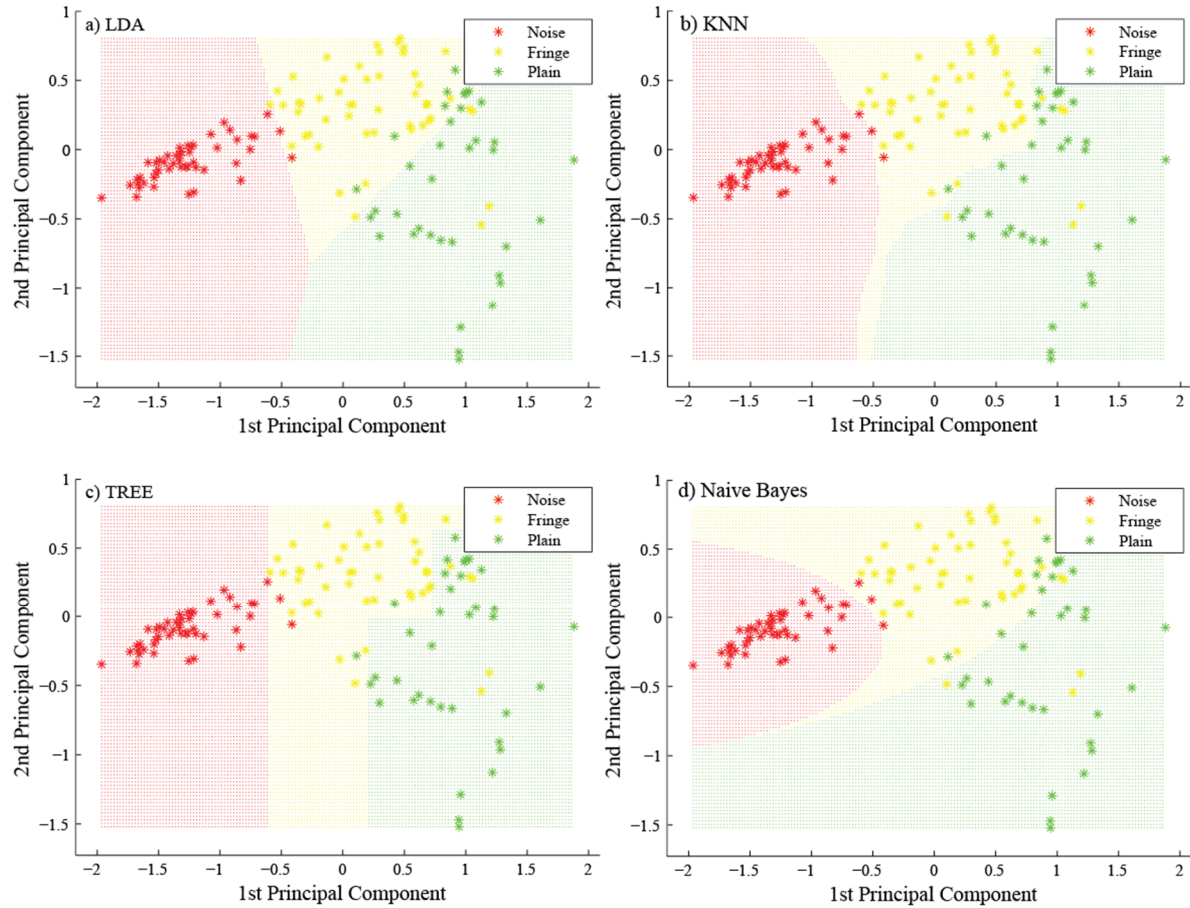


Figure 4.6: Illustration of DInSAR signal classification methods of a) Linear Discriminant Analysis, b) K-nearest neighbor ($K = 5$), c) full decision Tree, and d) Naive Bayes on a reduced set of 2 principal components.

4.2.3 Performance

To assess the performance of classifiers, the result of visual interpretation of DInSAR signal over the delimited studied region is taken as the reference. Tests are operated on the TSX interferogram from 02-13/08/2012 (Figure 4.2). To achieve a high level of accuracy, reference DInSAR signal mapping (Figure 4.2b) is developed by an experienced analyst, and describes in each position whether the pixel is in an area of plain pattern, in a (partly) fringe pattern or in a noise pattern.

The confusion matrix is established by counting the number of training and testing data assigned to each DInSAR signal class by the algorithm and comparing these with the reference class given by

visual interpretation (Conglaton and Green, 1998; Lillesand and Kieffer, 1994). The diagonal values of the confusion matrices represent agreement between map and ground, and off-diagonals represent different misclassifications. The overall accuracy A_o considers all off-diagonals together as classification failures and is computed in Table 4.2 from the confusion matrix.

$$A_o = \frac{\sum_{i=1}^3 x_{ii}}{n}$$

With x_{ii} number of observations in column and row i of the confusion matrix and n the total number of classifications.

The kappa index of agreement k is a useful measure of classification accuracy and has the advantage to take into account agreement occurring by chance; this is most important when working with few classes or if some classes cover a large proportion of the map (Cohen, 1960; Congalton, 1991; Conglaton and Green, 1998). This index is especially relevant in our case where the classes defined by plain and noise patterns are more likely to be encountered during field sampling than (partly) fringe pattern. For example, only 0.94 km² of the studied region is visually interpreted as (partly) fringe pattern, while 12.79 and 21.06 km² are respectively classified as noise and plain patterns in the reference visual mapping. k is calculated in Table 4.2 using the following formulas, only on the testing data as the training data set does not represent the natural probability of occurrence of each class:

$$\theta_1 = \frac{\sum_{i=1}^3 x_{ii}}{n} \quad \theta_2 = \frac{\sum_{i=1}^3 x_{i+} \cdot x_{+i}}{n^2} \quad k = \frac{\theta_1 - \theta_2}{1 - \theta_2}$$

With x_{i+} the marginal sum of row (mapped class) i and x_{+i} the marginal sum of column (reference class) i .

The first coefficient θ_1 is the overall accuracy A_o . The second coefficient θ_2 is the expected overall accuracy if there were chance agreement between reference and mapped data. A low value of kappa indicates that a large portion of the apparent classification could be due to chance agreement.

The sensitivity and specificity are good indexes to show the potential of binary test and are computed as follow:

$$\text{sensitivity} = \frac{\text{number of true positives}}{\text{number of true positives} + \text{number of false negatives}}$$

$$\text{specificity} = \frac{\text{number of true negatives}}{\text{number of true negatives} + \text{number of false positives}}$$

The confusion matrix is given in Table 4.2 for the classification of training and testing. Data are assigned to each DInSAR signal class by the algorithm and are compared with the reference class

given by visual interpretation. Sensitivity and specificity are computed for the identification of plain patterns.

LDA	Training Data					Testing Data				
		Noise	Fringe	Plain		Noise	Fringe	Plain		
	Noise	49	47	2	0	Noise	51	45	6	0
	Fringe	50	1	45	4	Fringe	5	0	3	2
	Plain	46	0	9	37	Plain	76	1	6	69
A0: 0.89 Sensitivity: 0.80 Specificity: 0.96 k: 0.83					A0: 0.89 Sensitivity: 0.91 Specificity: 0.96 k: 0.79					
KNN		Noise	Fringe	Plain		Noise	Fringe	Plain		
	Noise	49	46	3	0	Noise	51	43	7	1
	Fringe	50	0	43	7	Fringe	5	0	3	2
	Plain	46	0	4	42	Plain	76	1	5	70
	A0: 0.90 Sensitivity: 0.91 Specificity: 0.93 k: 0.86					A0: 0.88 Sensitivity: 0.92 Specificity: 0.95 k: 0.78				
TREE		Noise	Fringe	Plain		Noise	Fringe	Plain		
	Noise	49	47	2	0	Noise	51	43	8	0
	Fringe	50	0	45	5	Fringe	5	0	3	2
	Plain	46	0	2	44	Plain	76	1	5	70
	A0: 0.94 Sensitivity: 0.96 Specificity: 0.95 k: 0.91					A0: 0.88 Sensitivity: 0.92 Specificity: 0.96 k: 0.78				
Naive Bayes		Noise	Fringe	Plain		Noise	Fringe	Plain		
	Noise	49	46	3	0	Noise	51	40	9	2
	Fringe	50	0	45	5	Fringe	5	0	2	3
	Plain	46	0	12	34	Plain	76	1	4	71
	A0: 0.86 Sensitivity: 0.74 Specificity: 0.95 k: 0.79					A0: 0.86 Sensitivity: 0.93 Specificity: 0.91 k: 0.74				

Table 4.2: The confusion matrices summarize the performance of DInSAR signal classification for training and testing datasets according to the statistical methods (LDA, KNN, TREE and NB). Each column represents the instance in the predicted class (automated), while each row represents the instance in an actual class (reference).

We observe an excellent and comparable performance of all classification methods on training data with a maximal overall accuracy for TREE of 0.94. However, the test on training data is just indicative as the true validation is based on testing data. Regarding testing data, performance is also comparable regarding each classifier, even though Linear Discriminant Analysis provides the best classification accuracy (Ao 0.89, k 0.79) with a high sensitivity for identifying plain patterns reaching 0.91. Looking at each class separately, we see the difficulty of each model to classify correctly the small set of (partly) fringe pattern of testing data. These unfavorable results mainly come from the small size of (partly) fringe pattern set and cannot statistically represent the correct classification results for this pattern. However, this training set of DInSAR signal patterns reproduces the natural proportion of these three patterns encountered on a common interferometric phase image of the studied region.

4.2.4 Conclusion

The presented method extracts four textural image features at each pixel location from the interferometric phase image; namely the contrast, correlation, energy, and homogeneity derived from the gray-level co-occurrence matrix. It then classifies these features according to the three defined DInSAR signal classes: noise, (partly) fringe and plain patterns. By definition, this pixel-based method is really time consuming if applied on an entire interferometric phase image (TSX images are composed of about 70 million pixels at 5 meters pixel spacing).

The next part (Part 4.3) will present a comprehensive mapping of DInSAR signal on a specific region and the related mapping of slope movements. The idea is to reduce time consumption by identifying the plain pattern areas using a region growing algorithm. Firstly, several seed points evenly spaced on a grid are selected as plain pattern from one of these statistical models. Then, they are used as starting points in a region growing algorithm. As the classifier is used to identify plain pattern rather than (partly) fringe or noise patterns and the LDA statistical model provides the best classification accuracy with a high sensitivity of 0.91 to correctly identify plain pattern, it will be used for the further developments.

4.3 Mapping of the slope movements

The present part proposes a general approach allowing the mapping of the DInSAR signal from a selection of interferograms (Table 4.1). Then, by combining DInSAR signal maps from several interferometric phase images having the same time interval, the mapping of the related slope movements is deduced for this specific time interval.

4.3.1 Mapping of the DInSAR signal

Two models are developed for DInSAR signal mapping. The first model, model I, aims to reduce the time consumption involved in the pixel based classification presented in Part 4.2. To do this, a region growing algorithm is used in order to detect plain pattern areas from a set of selected seed points evenly spaced on a grid previously classified as plain pattern by the LDA model. The second model, model II, uses the LDA model to classify points evenly spaced on a high resolution grid into the three selected DInSAR signal classes and then interpolate result onto the whole area.

4.3.1.1 *Model I: Statistical classifiers applied to low grid resolution (≥ 100 meters)*

Each interferogram i is mapped according to the 3 defined DInSAR signal classes. The model I consists firstly of detecting noisy areas in the selected interferogram by thresholding the interferometric coherence (Figure 4.7b). Pixels with a coherence value below 0.8 are kept as noise. Then, the seed points are selected from the LDA model described in Part 4.2 as the points of plain pattern detected

from a set of points evenly spaced on a grid (Figure 4.7b). Finally, a standard region growing algorithm is applied to the interferometric phase image to segment the remaining areas into plain pattern or (partly) fringe areas (Figure 4.7c). Regions are segmented using 4-connected neighborhoods to grow from seed points and using the following region membership criterion:

$$\Delta\phi \leq \frac{\lambda}{2} RG_c$$

With $\Delta\phi$ the difference of phase values between two adjacent pixels and RG_c the region membership criterion.

The resulting map is thus classified into three defined DInSAR signal classes (Figure 4.7d).

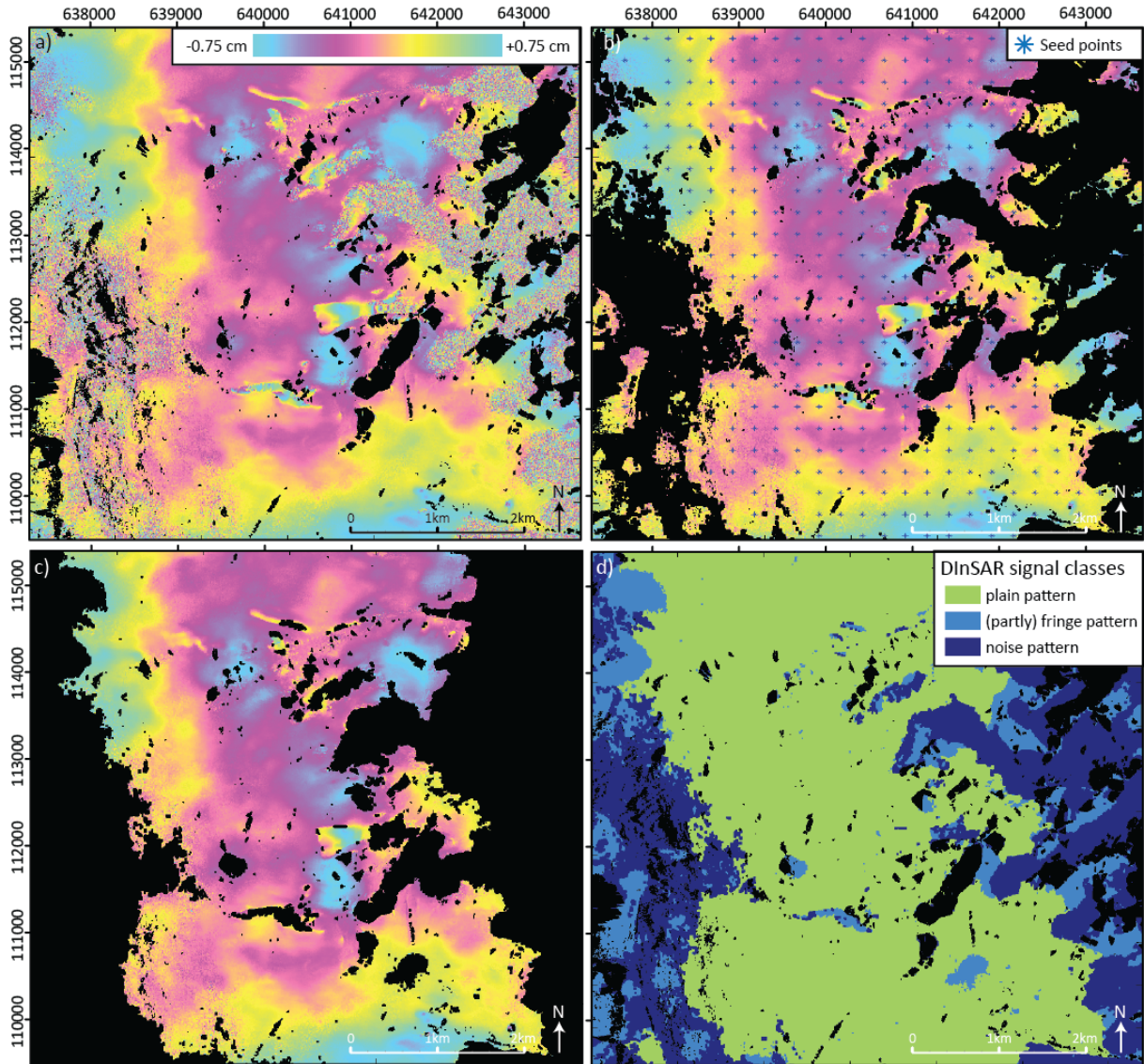


Figure 4.7: a) Original interferometric phase image from 02-13/08/2012. b) Selected seed point from a grid evenly spaced of 500m using LDA model. Noise pattern detected by threshold is in black. c) Plain pattern detected by region growing ($RG_c = 1/8$). Fringe and noise patterns are masked in black. d) Final classification. Layover and shadow are in black for the four figures.

4.3.1.2 Model II: Statistical classifiers applied to high grid resolution (< 100 meters)

The model II consists firstly of detecting noisy areas in the selected interferogram by thresholding the interferometric coherence. Pixels with a coherence value below 0.8 are assigned to noise. Then, the points evenly spaced on a grid are all classified into one of the three DInSAR classes using the LDA model. Finally, each remaining pixel of the interferometric phase image is mapped into one of the three DInSAR signal classes by using a standard nearest neighbor interpolation (Figure 4.8).

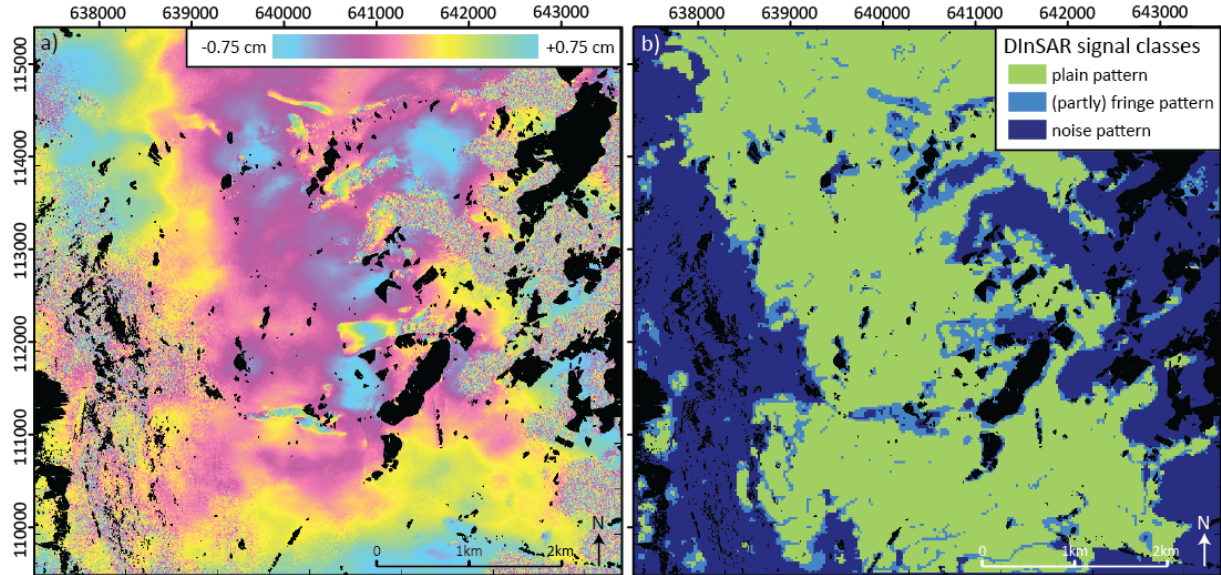


Figure 4.8: a) Original interferometric phase image from 02-13/08/2012. b) Final classification using model II for a grid resolution of 25 meters. Layover and shadow are in black for the two figures.

4.3.2 Mapping of the slope movements

The idea is to combine selected interferograms with the same time interval to determine the overall slope movements at this selected time interval. This combination is performed in order to produce a map assessing the occurrence of each DInSAR signal class and to prevent the presence of single artifacts. Thus, pixels are classified into the most represented DInSAR signal class in the set of selected interferograms. An extra class is added indicating when the algorithm is not able to clearly classify the pixel. An additional map is produced to give an index of reliability concerning the classification of each pixel. This map is created with the idea that the larger the number of images used for the classification and the more images used to classify the pixel in each specific class, the more reliable the classification is.

Then, an index of slope movements is deduced from the DInSAR signal. A moving slope is generally detected by a (partly) fringe or noise pattern surrounded by a plain pattern (Barboux et al., 2014). Assuming that the deformation rate of a detected moving slope is uniform in time, the relative DInSAR signal for this moving slope should be different according to the selected time interval. If the

time interval is too short, the moving slope does not show any signal (the deformation is too small in between the two selected dates). When the time interval is too large, the signal is decorrelated (the deformation rate is higher than half a wavelength during the two selected dates). In between, a (partly) fringe pattern is observed on the moving slope (Figure 3.5).

The classification can finally be transposed into the slope movement's index according to the 3 following classes: 1) plain pattern = no deformation rate, 2) (partly) fringe pattern = gentle deformation rate and 3) noise pattern = large deformation rate.

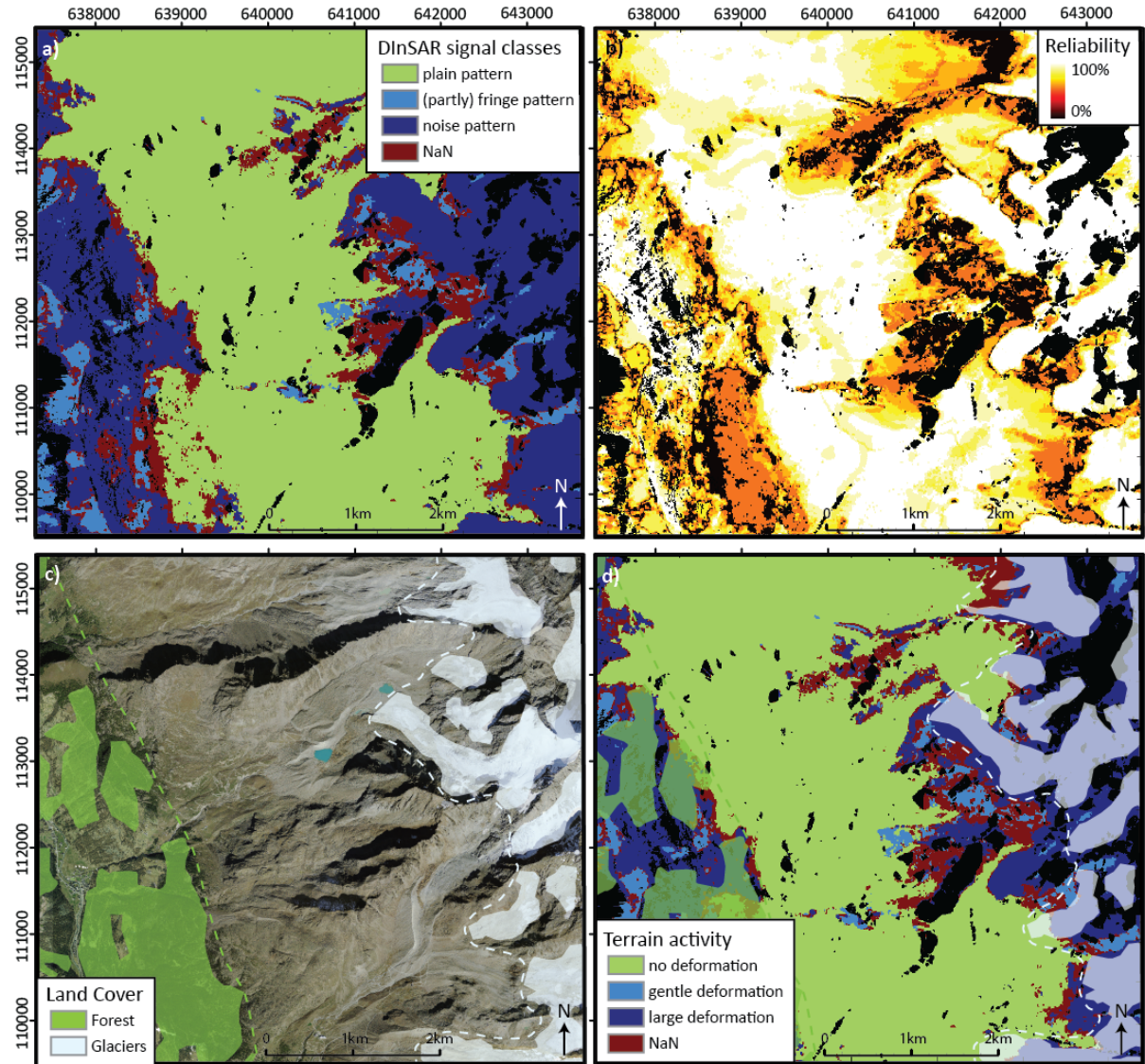


Figure 4.9: a) Result of the combined classification of DInSAR signal from 11 interferograms of 11 days' time interval and b) the corresponding reliability index (Grid: 500m, R_G : 1/8). c) Glaciers and forest are delimited from land cover Vector200 © Swisstopo 2010. d) Final mapping of the slope movement according to slope movements index.

4.3.3 Performance

4.3.3.1 Performance of the DInSAR signal mapping

The performance is evaluated on the DInSAR pair from the 02-13/08/2012 (Figure 4.2). The confusion matrix is computed to compare the performance of the automated DInSAR signal mapping

with the reference visual mapping (Figure 4.2b) according to the resolution of the grid used for the seed points generation ranging from 25, 50, 100, 250, 500 and 1000 m, and the region membership criterion RG_c ranging from $\frac{1}{4}$, $\frac{1}{8}$ and $\frac{1}{16}$ (Table 4.3). Model II is used for grids of 25 m and 50 m spacing.

				RGc 1/4			RGc 1/8			RGc 1/16		
Model I	Grid 1000		Total (km ²)	Noise	Fringe	Plain	Noise	Fringe	Plain	Noise	Fringe	Plain
		Noise	12.79	8.73	1.78	2.28	8.73	2.25	1.81	8.73	3.34	0.72
		Fringe	0.94	0.08	0.27	0.60	0.08	0.44	0.43	0.08	0.66	0.21
		Plain	21.06	0.05	0.50	20.50	0.05	3.02	17.98	0.05	7.16	13.84
				k: 0.69 Ao: 0.85			k: 0.60 Ao: 0.78			k: 0.48 Ao: 0.67		
	Grid 500		Total (km ²)	Noise	Fringe	Plain	Noise	Fringe	Plain	Noise	Fringe	Plain
		Noise	12.79	8.73	1.68	2.38	8.73	2.32	1.73	8.73	3.19	0.87
		Fringe	0.94	0.08	0.27	0.60	0.08	0.33	0.54	0.08	0.65	0.21
		Plain	21.06	0.05	0.49	20.52	0.05	1.55	19.45	0.05	4.65	16.36
				k: 0.69 Ao: 0.85			k: 0.69 Ao: 0.82			k: 0.56 Ao: 0.74		
	Grid 250		Total (km ²)	Noise	Fringe	Plain	Noise	Fringe	Plain	Noise	Fringe	Plain
		Noise	12.79	8.73	1.30	2.76	8.73	1.66	2.40	8.73	2.92	1.14
		Fringe	0.94	0.08	0.24	0.63	0.08	0.32	0.54	0.08	0.59	0.28
		Plain	21.06	0.05	0.29	20.72	0.05	0.55	20.45	0.05	1.96	19.05
				k: 0.70 Ao: 0.85			k: 0.69 Ao: 0.85			k: 0.66 Ao: 0.82		
	Grid 100		Total (km ²)	Noise	Fringe	Plain	Noise	Fringe	Plain	Noise	Fringe	Plain
		Noise	12.79	8.73	0.76	3.30	8.73	1.09	2.97	8.73	2.41	1.65
		Fringe	0.94	0.08	0.05	0.82	0.08	0.14	0.73	0.08	0.39	0.48
		Plain	21.06	0.05	0.15	20.86	0.05	0.28	20.73	0.05	0.96	20.05
				k: 0.69 Ao: 0.85			k: 0.69 Ao: 0.85			k: 0.69 Ao: 0.84		
Model II	Grid 50		Total (km ²)	Noise	Fringe	Plain						
		Noise	12.79	11.32	1.02	0.45						
		Fringe	0.94	0.22	0.50	0.22						
		Plain	21.06	1.43	2.15	17.47						
				k: 0.71 Ao: 0.84								
	Grid 25		Total (km ²)	Noise	Fringe	Plain						
		Noise	12.79	11.31	1.06	0.42						
		Fringe	0.94	0.19	0.55	0.20						
		Plain	21.06	1.20	2.15	17.71						
		k: 0.72 Ao: 0.85										

Table 4.3: The confusion matrices summarize the performance of the automated DInSAR signal mapping according to the couple of parameters (grid resolution; RG_c). Seed points are selected on the grid using LDA model. Performance is evaluated on the phase image from 02-13-2012 and is expressed in km². Each column represents the instance in the predicted class (automated), while each row represents the instance in an actual class (reference).

From Table 4.3, it seems that a lot of couples of parameters (*Grid Resolution*; RG_c) from model I have an overall accuracy reaching 0.85. Regarding plain pattern, more than 20.4 km² is correctly classified using these couples (Model I, Ao = 0.85). Actually, the smaller the grid resolution and the larger the value of RG_c , the better the model I correctly classifies the pixel as plain pattern. Regarding (partly) fringe pattern, the opposite behavior is observed: it seems that the larger the grid resolution and the smaller the value of RG_c , the better (partly) fringe pattern is correctly classified. In this case, the algorithm is able to detect very subtle changes in the DInSAR signal. The couple of parameters (*Grid Resolution*; RG_c) = (1000m; 1/16) is the best for detecting (partly) fringe pattern where 0.66 km² are correctly classified. Regarding noise pattern, 8.73 km² are correctly classified regardless of which

couple of parameters are used (*Grid Resolution; RGc*). By definition of the model I, noise pattern is determined by thresholding the coherence image. The remaining area can only be classified as either plain or (partly) fringe patterns. Consequently, the noise pattern area is always the same using the model I whatever the couple of parameters (*Grid Resolution; RGc*).

Regarding the performance of model II, the overall accuracy also reaches 0.85 for a grid resolution of 25 meters. In this case, the kappa value reaches 0.72 indicating that a large portion of the apparent classification could be due to a substantial agreement. The (partly) fringe and noise patterns are generally more frequently correctly classified with model II than with model I. Except when using a region growing criteria equal to 1/16 and a grid resolution larger than 250 m, which better classify (partly) fringe pattern.

4.3.3.2 Performance of the slope movement mapping

Two tests are performed in order to assess the performance of the slope movement mapping. The first one uses DGPS field measurements to assess the slope movement mapping according to time interval. The second test evaluates if the deformation class attributed by automated slope movement mapping follows the correct order when increasing the time interval; that is from 1) no deformation, 2) gentle deformation to 3) large deformation.

a. Comparison of the slope movement mapping with DGPS measurements

To compute the reference of a slope movement's classification using DGPS measurements, we have to go back to Section 3.2.4. As explained there, the observed pattern on the DInSAR signal phase is related to the displacement gradient between adjacent pixels. By definition, the displacement gradient for the time interval Δt is the basic measure of the deformation rate, and quantifies the relative displacement of two material particles at positions i and $i+1$. In our case, this means the relative displacement between the material particles contained in the area i of one pixel resolution and the material contained in the adjacent area $i+1$ of one pixel resolution.

$$Deformation\ n = displacement_{t_{i+1}} - displacement_{t_i}$$

Consequently, the interferometric SAR signal will decorrelate when the deformation rate or displacement gradient between adjacent pixels is higher than half the wavelength during the selected time interval.

Moreover, as seen in Section 3.2.4, the nature of the change within a pixel can introduce noise in the measuring phase difference (Klees and Massonnet, 1999). The information on the deformation is coherent only if the entire surface within the pixel deforms homogeneously. Glaciers for instance can be well monitored, whereas rock glaciers, which have a smaller and more disturbed surface due to the roughness of the terrain, decorrelate at a faster velocity rate. However, there is no typical

velocity rate that is known at which the DInSAR signal decorrelates on rock glaciers, and this threshold has to be deduced from experience. This rate depends, among other things, on the nature of the change and the roughness of the deformed surface.

In the area of investigation, two landforms are seasonally surveyed by DGPS campaigns. The Jegi and Gruben rock glaciers contain 137 points which are measured showing a velocity up to 3 m/year. In order to assess the automated slope movement mapping, the deformation rate of each of these points derived from two DGPS campaigns performed on 08.07.2013 and 07.10.2013 has to be compared with the 16 maps of slope movements defined for each time interval Δt (from 11 to 715 days).

The reference classification of the deformation rate is performed at each DGPS position using the component of the displacement projected in the LOS direction during the considered time interval Δt . Then, as the displacement gradient can only be derived from the interpolation of sampling DGPS measurements, the LOS displacement is interpolated using the standard IDW method (Inverse Distance Weighted). The method estimates cell values by averaging the values of sample data points in the neighborhood of each processing cell. The closer a point is to the center of the cell being estimated, the more influence, or weight, it has in the averaging process. Then, the LOS deformation is computed as the basic measurement of the displacement gradient for the considered time interval Δt .

Finally, each DGPS position is classified in one of the three deformation classes according to the following rule:

- Class “no deformation” (NDef): a velocity rate lower than $\frac{\lambda}{16} \times \Delta t$ (we consider that a change in the phase image lower than an eighth of the fringe is not visible).
- Class “large deformation” (LDef) : a LOS deformation higher than $\frac{\lambda}{2} \times \Delta t$ and a velocity rate higher than the typical velocity rate at which decorrelation is observed on the selected rock glacier (typically a velocity rate higher than 2λ for the Jegi rock glacier and a velocity rate higher than λ for the Gruben rock glacier were experienced)
- Class “gentle deformation” (GDef): in between

The performance is given for a time interval of 11 days in Table 4.4. The NaN class is used when the algorithm was not able to determine the right class.

				RGc 1/4				RGc 1/8				RGc 1/16			
Model I	Grid 1000			Noise	Fringe	Plain	NaN	Noise	Fringe	Plain	NaN	Noise	Fringe	Plain	NaN
		Noise	14	8	0	6	2	8	0	5	3	8	5	0	3
		Fringe	85	13	0	72	0	13	10	39	23	13	50	10	12
		Plain	36	0	0	36	0	0	0	34	2	0	3	32	1
				k: 0.11 Ao: 0.32				k: 0.21 Ao: 0.38				k: 0.66 Ao: 0.66			
	Grid 500			Noise	Fringe	Plain	NaN	Noise	Fringe	Plain	NaN	Noise	Fringe	Plain	NaN
		Noise	14	8	0	6	2	8	0	5	3	8	2	1	5
		Fringe	85	13	0	72	0	13	6	44	22	13	31	20	21
		Plain	36	0	0	36	0	0	0	35	1	0	1	32	3
				k: 0.11 Ao: 0.32				k: 0.19 Ao: 0.36				k: 0.34 Ao: 0.52			
	Grid 250			Noise	Fringe	Plain	NaN	Noise	Fringe	Plain	NaN	Noise	Fringe	Plain	NaN
		Noise	14	8	0	6	2	8	0	6	2	8	1	2	5
		Fringe	84	13	0	71	1	13	6	46	20	13	31	22	19
		Plain	36	0	0	36	0	0	0	35	1	0	1	34	1
				k: 0.11 Ao: 0.32				k: 0.18 Ao: 0.36				k: 0.35 Ao: 0.53			
	Grid 100			Noise	Fringe	Plain	NaN	Noise	Fringe	Plain	NaN	Noise	Fringe	Plain	NaN
		Noise	14	8	0	6	2	8	0	6	2	8	1	2	5
		Fringe	84	13	0	71	1	13	5	47	20	13	24	24	24
		Plain	36	0	0	36	0	0	0	35	1	0	0	34	2
				k: 0.11 Ao: 0.32				k: 0.18 Ao: 0.35				k: 0.31 Ao: 0.48			
Model II	Grid 50			Noise	Fringe	Plain	NaN								
		Noise	16	11	5	0	0								
		Fringe	75	21	39	15	10								
		Plain	35	2	6	27	1								
				k: 0.34 Ao: 0.56											
	Grid 25			Noise	Fringe	Plain	NaN								
		Noise	16	12	4	0	0								
		Fringe	75	22	47	6	10								
		Plain	35	1	4	30	1								
			k: 0.46 Ao: 0.65												

Table 4.4: The confusion matrices summarize the performance of the automated slope movement mapping according to the couple of parameters (RGc; grid resolution) for a selected set of DGPS positions. Here, performance is evaluated for a time interval of 11 days. Each column represents the instance in the predicted class (automated), while each row represents the instance in an actual class (reference).

From Table 4.4, it seems that the larger the grid resolution and the smaller the value of RGc, the better DGPS positions are correctly classified by the automated mapping using model I. The overall accuracy reaches 0.66 for couple of parameters (Grid Resolution; RGc) = (1000m; 1/16). As already seen in Part 4.3.3.1, this couple of parameters allows a better detection of (partly) fringe pattern. Actually, at the time interval of 11 days, the rate of these observed slope movements is mainly related to a (partly) fringe pattern. Thus, it also explains why the performance of the slope movement mapping given by the value of overall accuracy for each other couple of parameters (Grid Resolution; RGc) of the model I is low.

Again, the classification using Model II is quite good, especially for a grid resolution of 25 meters where the overall accuracy reaches 0.65.

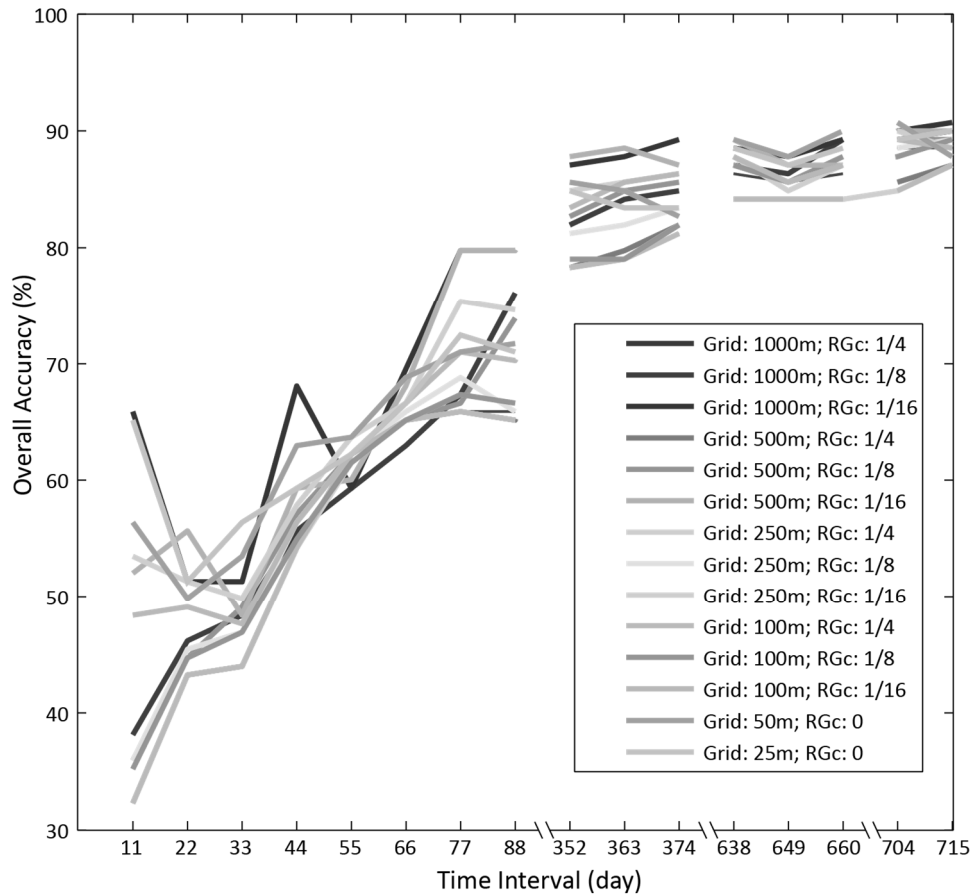


Figure 4.10: Evolution of the overall accuracy of the automated slope movements mapping for the selected pairs of parameters (Grid resolution; RGc) according to time interval.

Figure 4.10 shows the evolution of the overall accuracy for each selected couple of parameters (*Grid Resolution*; *RGc*) according to the time interval Δt . When Δt increases, the overall accuracy increases. Actually, the DGPS positions show larger deformation when Δt increases, and the DInSAR signal is decorrelated. As already seen in Section 4.3.3.1, the two models I and II are quite effective in classifying noise pattern.

The next figure (Figure 4.11) illustrates the correspondence between automated slope movement mapping and reference mapping observed at each DGPS position using model II and a grid resolution of 25 meters for a time interval of 11 days on the Jegi rock glacier.

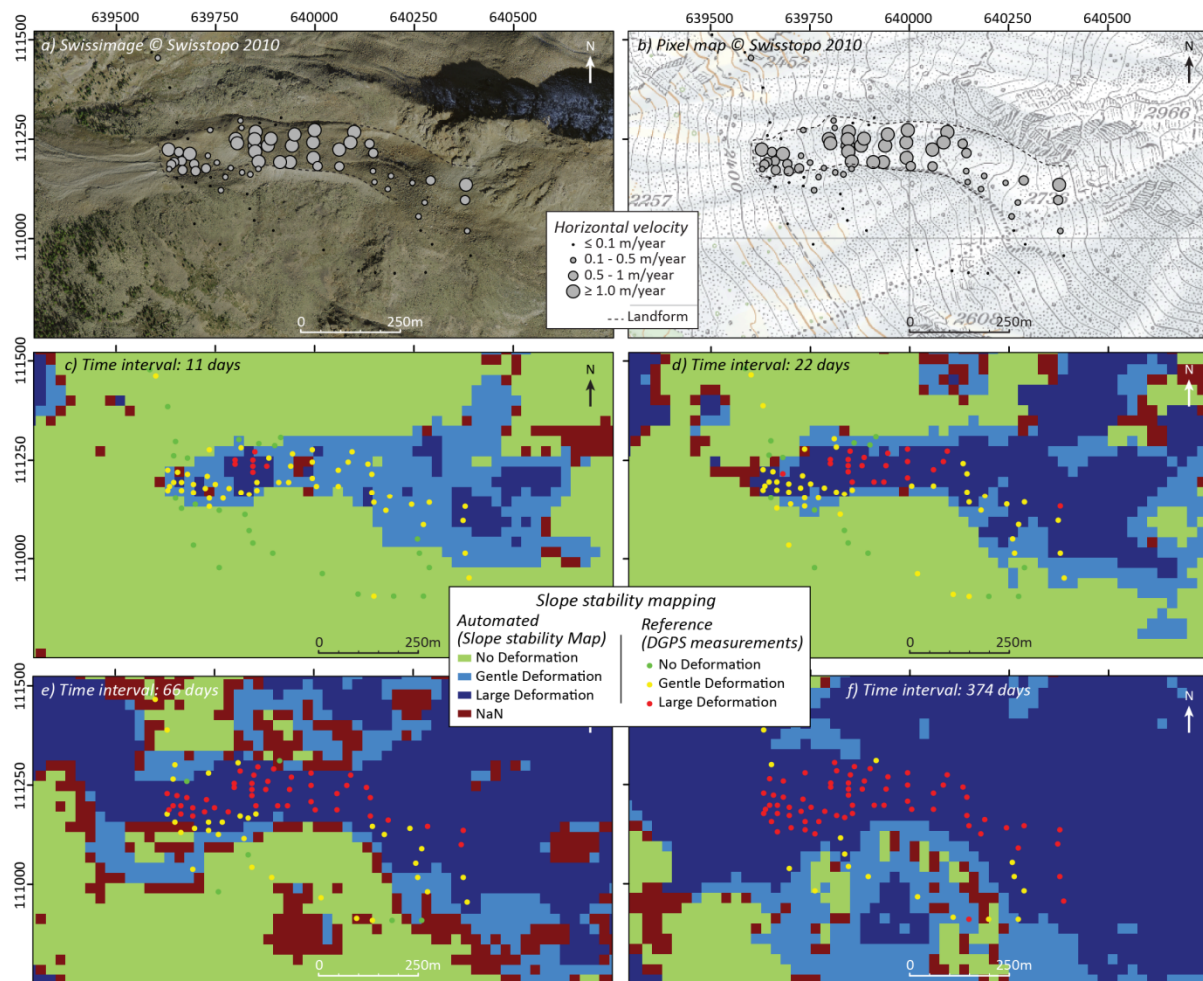


Figure 4.11: Jégi rock glacier and DGPS measurements derived from two DGPS campaigns performed on 08.07.2013 and 07.10.2013 on a) the Swissimage and b) the pixel map © Swisstopo 2010. Evolution of the automated slope movements mapping (Model II, 25 meters) and reference classification of DGPS points according to time interval: c) 11 days, d) 22 days, e) 66 days and f) 374 days.

b. Slope movement mapping according to time interval

By definition, when increasing the time interval Δt , the deformation detected on the interferogram is larger. Thus, the proposition is: the order of classification in terms of slope movement has to be respected when increasing the time interval, from no deformation, gentle deformation and large deformation. To perform this test, the evolution of a pixel's classification given by the automated slope movement mapping is evaluated according to the time interval. Each of the 16 slope movement maps (from 11 to 715 days) are successively compared to verify if the classification is developing correctly according to the proposition stated above.

Figure 4.12 shows the result for model II using a grid resolution of 25 meters. In Figure 4.12a, the pixels verifying the proposition are displayed in white. In this example, 53.35% of the area not masked by layover or shadow verifies the proposition stated above (Table 4.5). Figure 4.12b shows the number of times that the pixel verifies the stated proposition. 60.97% of the area not masked by

layover or shadow verifies the stated proposition at least 14 times, which means that the proposition is not verified for only two successive DInSAR signal maps (Table 4.5). We immediately see that the evolution of the classification is largely verified in vegetated and glaciated areas (white pixels over these areas) due to the fact that these areas are mainly classified as noise pattern regardless of the selected time interval. In the remaining area, the proposition seems to be verified (white pixels) for slope movements having a velocity rate of cm/day, dm/month or cm/month. These results reinforce what we have already seen before: the model II with a grid resolution of 25 meters is suited to correctly detect noise and (partly) fringe pattern. However, these results also have to be interpreted carefully as the DInSAR slope movements were detected from data dating back to the 1990s. The poor verification over the slowest DInSAR polygons ("cm/year") symbolized by black pixels can be explained by the high sensitivity of TSX to detecting small variations related here to the superficial surface deformation rather than the slope movement itself.

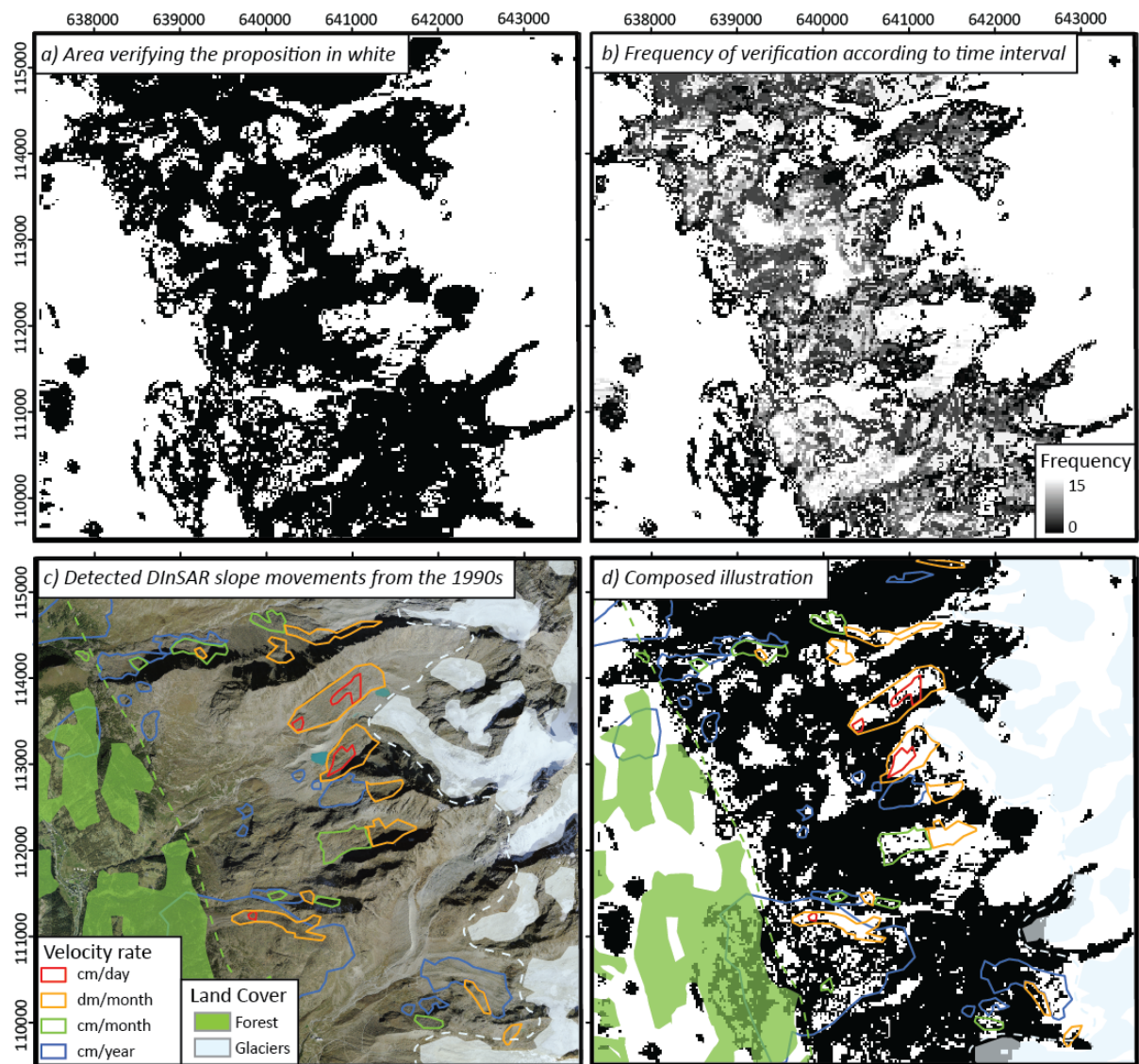


Figure 4.12: Verification of the proposition that a pixel follows a right order of slope movement's classification when increasing the time interval (Model II, grid resolution of 25 meters). a) Area verifying the stated proposition. b) Number of times that the pixel verifies the stated proposition. c) Detected DInSAR slope movements from data dating from the 1990s. Glaciated and vegetated areas are delimited from land cover Vector200 © swisstopo 2010. d) Superposition of DInSAR polygons, land cover and figure a.

The evolution of pixel classification according to time interval is summarized in Table 4.5 for model I and II. From these numbers, we see that the best performance is reached by the model I using the couple of parameters (*Grid Resolution; RGc*) = (100m, 1/4). This is explained by the fact that this selection of parameters allows an accurate detection of plain pattern (see Part 4.3.3.1). Noise pattern due to glaciers and vegetation represents a large area of the studied region and is generally correctly classified whatever the model. Differences in performance come mainly from (partly) fringe pattern, which represents generally small areas of the studied region. Consequently, the models which are able to correctly classify this pattern cannot be distinguished in this test.

	Grid resolution (m)	Verification ¹	RGc 1/4	RGc 1/8	RGc 1/16
Model I	1000	100%	57.32	41.86	42.01
		90%	71.88	48.93	51.20
	500	100%	58.71	48.40	41.44
		90%	72.65	56.90	48.80
	250	100%	60.51	54.07	43.84
		90%	74.96	64.53	50.60
	100	100%	62.02	56.82	46.85
		90%	77.71	68.83	53.91
Model II	50	100%	53.96		
		90%	61.53		
	25	100%	53.35		
		90%	60.97		

¹Verification: - 100 %: the pixel verifies the proposition for each successive Δt ,
- 90%: the pixel verifies the proposition in 90% of the cases.

Table 4.5: Percentage of the area verifying the stated proposition of the evolution of classification according to time interval.

4.3.4 Recommendation

The present part proposes a comprehensive approach for the mapping of DInSAR signals and the related mapping of slope movement. We immediately see that the performance of model I is influenced by the objectives and that the choice of the couple of parameters is totally dependent from the DInSAR signal we want to detect. The couple (*Grid Resolution; RGc*) = (100m; 1/4) is best suited for plain pattern detection related to areas without deformation whereas the couple (*Grid Resolution; RGc*) = (1000m; 1/16) is much more efficient for the detection of (partly) fringe pattern related to areas with gentle deformation. Consequently, the use of $RGc = 1/8$ with a grid resolution of 500 or 250 meters would be a good compromise.

Moreover, it seems that the efforts deployed to reduce time consumption from a pixel based approach were unrewarded based on the results using model I. The tests performed with model II are much more encouraging as it seems that a grid resolution of 25 meters is well suited for the DInSAR signal and slope movement mapping whatever the class of pattern. To conclude, the use of the model II with a grid resolution of 25 meters is thus recommended in order to produce more accurate maps of slope movements.

4.4 Discussion

The motivation of an automated detection of slope movements is to deal with the two following aspects: 1) helping users to work with a large quantity of data and 2) support analysts in the detection and the interpretation of DInSAR signal. The strength of the presented automated mapping is to propose a simple procedure in order to reach these targets. However, the accuracy and precision of the proposed model can be discussed according to several points of view.

4.4.1 Mapping of the slope stability or the slope movement?

When observing an interferometric phase image at a specific time interval, no change in the signal (plain pattern) implies that there is no movement detected, and that the slope can be considered stable in between the two selected dates. The strength of the DInSAR mapping using model I is used to propose a procedure based on a simple region growing algorithm allowing the growth of plain patterns from a set of selected stable seed points. To be detected as an area of plain pattern, at least one seed point is needed in the considered area. Consequently, a high grid resolution is needed when selecting seed points to detect plain patterns accurately. Using model II, the areas of plain pattern are detected on a pixel basis approach. Performance is quite good to determine this pattern; however, it is lower than with some couples of parameters (*Grid Resolution; RGc*) using model I.

With the two models, remaining areas imaged by (partly) fringe or noise patterns can be related to potential deformations or to external factors disturbing the signal (wet snow, vegetation, atmosphere, etc.). In any case, further investigations are needed to accurately identify the cause of these remaining patterns. Consequently, the proposed semi-automated slope movement mapping aims mainly to indicate areas without deformation to a user with high accuracy. Identified areas of gentle or large deformations have, by definition, to be taken into account carefully to determine if they are really related to slope movements.

The slope movement mapping is performed by combining DInSAR signal maps derived from each selected DInSAR pair for a selected time interval (Section 4.3.2). Each portion of the region of interest is classified into the most represented DInSAR signal pattern observed in the set of selected interferograms and is converted in terms of deformation. Consequently, the overall slope movements at this selected time interval are given by this procedure. For instance, when observing a specific moving slope showing seasonal variations in the selected set of DInSAR pairs at a time interval of 11 days, only the general behavior of this landform will be identified in the final slope movement map. This combination is performed in order to produce accurate maps of slope movements free from external artifacts due to atmosphere, snow, etc. However, exceptional variations in the velocity rate of a landform observed during one single interferogram will be smoothed by this process and cannot be detected.

4.4.2 Estimated time

When using model I, an area without deformation needs at least one seed point in the considered area in order to be correctly classified. Otherwise the area cannot be detected and will be mapped as (partly) fringe pattern. Consequently: a) a large number of seed points are required to correctly map the entire region of interest. This means the resolution of the grid used to detect seed points has to

be high enough; and b) the selection of seed points has to be as reliable as possible. A high sensitivity could assess the correct detection of a plain pattern.

While the sensitivity of the plain pattern classification is quite good regardless of the selected classifier model (Section 4.2.3), the choice of the couple of parameters (*Grid Resolution*; RG_c) is critical in terms of time consumption. The smaller the RG_c is, the faster the algorithm stops as it detects very subtle changes in DInSAR signal. And the smaller the grid resolution is, the longer the detection of seed points is, as the classification has to be performed on a larger number of points.

Moreover, it seems really difficult to choose the right couple of parameters (*Grid Resolution*; RG_c) when looking for performance to classify each class of DInSAR signal or slope movement separately using model I. In Section 4.3.4, the use of $RG_c = 1/8$ with a grid resolution of 500 or 250 meters of seed points is suggested as a good compromise. However, performance of model II is encouraging as it seems that a grid resolution of 25 meters is well suited for the DInSAR signal and slope movement mapping whatever the class. By measuring elapsed time used to compute slope movement maps derived from each model, it seems that the model II with a grid resolution of 25 meters takes roughly the same estimated time as the model I with $RG_c = 1/8$ with a grid resolution of 500 or 250 meters. Consequently, efforts deployed to reduce time consumption of a pixel based approach are ineffective, based on experiments using model I. Therefore, the use of model II with a grid resolution of 25 meters, showing good accuracy and precision for each slope movement's class, is recommended.

In order to be really accurate in classifying each class, a solution would consist of developing a mixed approach to detect each class separately from different couples of parameters (*Grid Resolution*; RG_c) and to combine the results. But this would be also extremely time consuming.

In any case, tests were performed on a small region of interest (5.9x6.3km wide = 1180x1260 pixels) using Matlab codes. To increase efficiency in future experiments, the algorithm should be coded in another language.

4.4.3 External artifacts

A local smooth change of the signal phase characterized by a (partly) fringe pattern may indicate a change in the surface geometry that can be quantified. However, it could also be due to external artifacts. In mountainous regions, a homogeneous tropospheric delay can affect the interferometric phase creating a distinct color gradient visible from the bottom of the valley to the top. This delay is inversely dependent on the altitude of the terrain and affects the entire image (Williams et al., 1998), however, it cannot be interpreted as a movement. In this study, no atmospheric phase model was applied on interferograms to compensate for this tropospheric delay. Unfortunately, a too small value of RG_c may involve the detection of this atmospheric artifact when mapping the DInSAR signal on each interferogram (Figure 4.13). Additional single tropospheric turbulences, due to the time and

space variations of the vapor content, induce local heterogeneous atmospheric effects (Tarayre and Massonnet, 1996). These local heterogeneous effects appear as single artifacts on interferograms and can also be detected during DInSAR signal mapping.

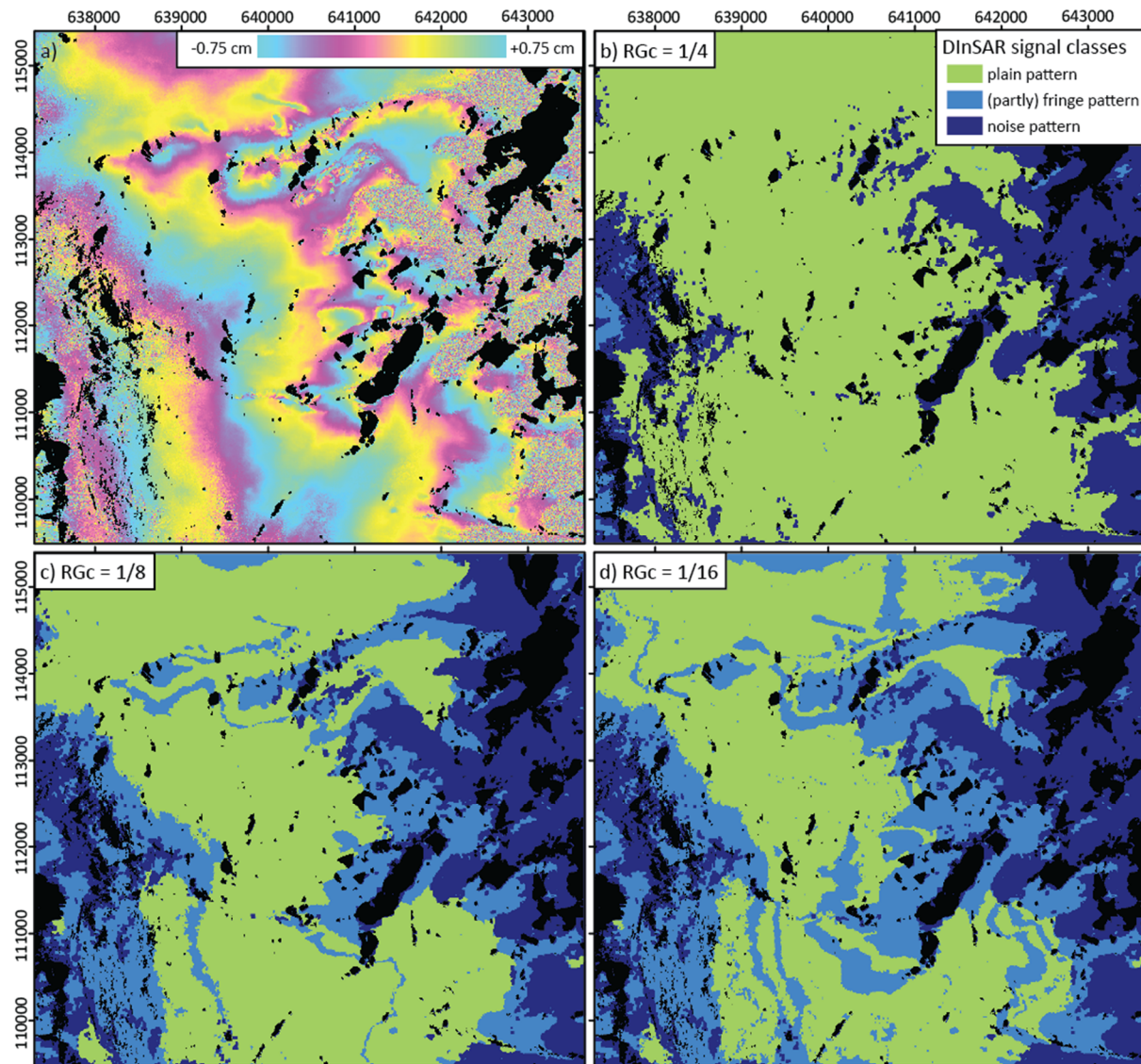


Figure 4.13: Atmospheric effect affecting the resulting DInSAR signal classification according to the parameter RG_c . a) Original interferometric phase image from 25/07-05/08/2011. Resulting DInSAR signal classification using a grid of seed points evenly spaced of 500m, LDA model and a) $RG_c = 1/4$, b) $RG_c = 1/8$ and $RG_c = 1/16$. Layover and shadow are in black.

The noise in the interferometric phase image can be due to a high deformation rate. However, in mountainous areas, the temporal decorrelation due to the change of the scattering geometry from wet snow (Strozzi et al., 1999) or vegetation (Balzter, 2001) and/or due to the change in the dielectric constant of the ground between the two satellite acquisitions (Richards, 2009) can also cause noise in the resulting phase image. Whereas the noise due to exceptional snowfall affects generally few pairs of phase images, the noise induced by vegetation is always present in the same location in the image.

When mapping slope movements, maps of DInSAR signal derived from several phase images having the same time interval are combined together. Pixels are classified into the most represented DInSAR signal class in the set of selected interferograms. Thus, the combination of DInSAR signal maps from several interferograms having the same time interval is a necessary and sufficient procedure to prevent from single external artifacts.

4.4.4 Resolution

The 5 meters sampling of TSX interferograms used in this study is adequate to detect small targets. However, it has to be noted that the coherence and phase values are multi-looked using a 5x5 window during interferogram processing, which means that several interferometric cells are used to determine a single multi-looked interferometric cell. This averaging procedure is applied in order to obtain a less noisy interferogram with squared pixels, though the price is paid in lower resolution. Moreover, an adaptive filtering function based on a local fringe spectrum (“adf” function of GAMMA software) is applied in order to reduce noise in the phase image and improve the quality for further classification algorithms. From the final interferograms, it was experienced that (partly) fringe and noise patterns with a length and a width smaller than about sixty meters (i.e. smaller than 12x12 pixels) were unfortunately eliminated, however, this choice of parameters shows a correct reduction of noise and residue in the resulting filtered images. Finally, textural features are estimated in a squared window of size 17x17 pixels (Part 4.2). This means that the texture is evaluated around the considered pixel within a radius of forty meters (8 pixels).

These values have been chosen according to the analysis of moving landforms observed in our region of interest. Rock glaciers, landslides, push moraines and other moving processes are often larger than eighty meters. The parameters should be adapted according to the size of observed landforms in the specific region of interest.

4.4.5 On the use of the ERS archives and current acquisitions

The compatibility between different sensors has also to be considered. The outline of the slope movement can differ mainly due to different ground resolution, incidence angle or acquisition mode. In comparison to ERS, recent very high-resolution X-Band sensors such as TerraSAR-X (TSX) and COSMO-SkyMed (CSK) permit a more precise spatial detection and delimitation of moving slopes. Moreover, with a repeated cycle of 11-days or 1-day respectively, subtle changes in the deformation rate of moving slopes can be detected on interferograms.

By improving the spatio-temporal resolution of detection, the spatio-temporal variability of the moving slope’s geometry increases too. Thus, the comparison of the mapping of slope movements

derived from different sensor technologies may be a difficult task and will have to be performed carefully.

4.5 Conclusion

This chapter proposes an automated method to map and assess the slope movements in the Alpine environment from TSX interferometric phase images. This protocol was developed on the basis of past studies using visual interpretation of DInSAR data for inventorying the Alpine slope movements in the Swiss Alps. Like the eyes of the expert, the process is based on the classification of the phase image texture in order to detect changes in the phase image related to surface deformation. Different models were developed and performance was evaluated according to visual interpretation established by expert, DGPS measurements as well as a proposition regarding DInSAR signal evolution. Finally, a standard procedure was recommended to accurately map slope movements.

The methods propose to identify areas without deformation, with gentle deformation and large deformation by the analysis of DInSAR signal previously mapped on a selected set of interferometric phase images. From the analysis of performance, the use of model II with a grid resolution of 25 meters, showing good accuracy and precision level for each type of slope movement, is recommended. By definition, the proposed mapping aims to indicate areas without deformation to a user with a high accuracy. Identified areas of gentle or large deformations have to be taken carefully into account to determine if they are really related to slope movement or external artifacts (like glacier or vegetation influences, for instance). In any case, further investigations are needed to accurately identify the cause of these remaining patterns.

Consequently, the combined use of the slope movement map with expert visual interpretations is absolutely recommended in order to produce a much more reliable analysis of slope movements in the region of interest, less subjective and quicker. Actually, this kind of slope movement map may support experts in the development of accurate slope movement inventories free from the subjectivity of the operator by using it as a useful tool for visual interpretation of DInSAR data, especially when using a large SAR dataset.

Different applications using slope movement maps can be suggested such as a) the development of new inventories, b) the update of past inventories, but also c) the detection of new moving areas. Chapter 7 will propose some of these applications.

5 Challenges and solutions to monitor annual and seasonal displacement rates of Alpine rock glaciers and landslides using DInSAR

In this chapter, the challenge is to monitor annual and seasonal behavior of rapid rock glaciers (1.5-3 m/year) using the new high spatio-temporal resolution of TSX data. Three methods are proposed in order to show the potential of TSX DInSAR for observing Alpine rock glaciers. The first one consists in a study of the interferometric coherence and phase images on a profile defined along a landform (Part 5.2). The two following methods (Part 5.3) consider the DInSAR signal observed on the whole studied landform using methodologies presented in Chapter 4 to roughly estimate its annual velocity rate (Section 5.3.1.1) and to detect potential seasonal changes in its behavior (Section 5.3.1.2). A final Part 5.4 presents the overall conclusion of this chapter.

5.1 Introduction

As previously discussed in Chapter 2, many studies have focused on the analysis of slope deformation using DInSAR and show the potential of this technique for long term monitoring of mountain slopes. The main advantage of DInSAR to provide continuous maps of surface deformation is considerable compared to conventional sampling techniques. Theoretically, the derivation of motion fields is performed easily by unwrapping the interferometric phase and computing the related motion in the LOS direction. With some assumptions about the direction of the movement, the displacements can moreover be projected in the real direction of the movement (Strozzi et al., 2004).

Due to the lack of vegetation, Alpine rock glacier surfaces are in principle well suited for interferometric analysis. However, in particular zones of strong shear the signal may decorrelate within a short time if individual rocks within a SAR resolution element follow different trajectories (Nagler et al., 2001, 2002). Moreover, these Alpine landforms, often located in complex mountain topography, are subject to severe shadow and/or layover effects. Finally, the complex movements of Alpine rock glaciers, showing significant spatio-temporal variability, may affect the complete distribution of their surface deformation derived from DInSAR data using conventional unwrapping processes (Nagler et al., 2002; Rott et al., 1999a). Rock glaciers generally display strong inter-annual and seasonal velocity variations, with maximal values often reached in late summer or autumn (e.g. Delaloye et al., 2010a; Noetzli, 2013; Perruchoud and Delaloye, 2007; Wirz et al., 2014). Some rock glaciers could for instance show a single peak in acceleration of the deformation rate at the end of spring or early summer (Wirz et al., 2014). Consequently, depending on what time an interferogram is available, the DInSAR-detected deformation rate may slightly differ from the average annual

deformation rate. This also means that DInSAR may be used to monitor the kinematics of these specific landforms, defined as the quantification of their movement in terms of velocity and acceleration.

As seen in recent studies (Barboux et al., 2011, 2012; Papke et al., 2012), the higher spatio-temporal resolution of TerraSAR-X (TSX) makes the localization of structures like rock glaciers much more recognizable and the identification of their displacements more accurate. Moreover a complete set of repeated acquisitions of TSX data in summer may allow the detection of seasonal variations (Barboux et al. 2012). In this chapter, the analysis focuses on the monitoring of rapid rock glaciers (1.5-3 m/year) using the new high spatio-temporal resolution of TSX data. DInSAR analysis appears to be unsuited for higher deformation rates, which are most of the time associated with a noise pattern in an interferometric phase image and thus cannot be quantified.

5.2 Monitoring of Alpine landforms along a profile

This part describes a method to monitor active rock glaciers using DInSAR technique with TSX data acquired in facing mode and with a time interval of 11 days during late summers from 2009 to 2011. Usually, the spatial distribution of a rock glacier's surface deformation derived from DInSAR data using conventional unwrapping processes fails due to the relatively small size and the complex movement of the rock glacier. Thus, a specific profile is here defined through the rock glacier and is used to analyze the DInSAR products along it. First, the methodology itself is presented. Then, the performance is discussed through some comparisons with DGPS data measured on three Alpine rock glaciers located in the Western Swiss Alps.

5.2.1 Method of Alpine rock glacier monitoring along a profile

5.2.1.1 Data selection

TSX data used for this study were acquired during the summers 2009 to 2011. In order to analyze fast moving landforms, DInSAR data in facing mode with the smallest time interval of 11 days are chosen to prevent, as much as possible, signal decorrelation in order to permit the quantification of the velocity rate. To obtain high quality interferometric pairs, the selection is based on well-known requirements: a small perpendicular component, no perennial snow patches, and no weather/atmospheric influences. SAR products phase and coherence are then extracted on the region of interest using standard DInSAR processes (coregistration, interferogram generation, flat Earth removal, baseline correction, topographic phase estimation using external DEM, subtraction of the estimated topographic phase).

5.2.1.2 *Profile definition*

The profile is defined through the rock glacier as a longitudinal path following the general flow of the landform (from orthoimages and/or field analysis). It could start and end outside the landform in stable terrain and has to follow as much as possible the highest coherence values on the best defined interferometric pair (small perpendicular component, without perennial snow patches, no weather/atmospheric influences, and with high coherence values or avoiding noisy pattern of interferometric phase). For landforms showing several lobes moving independently, several profiles should be defined (Figure 5.1).

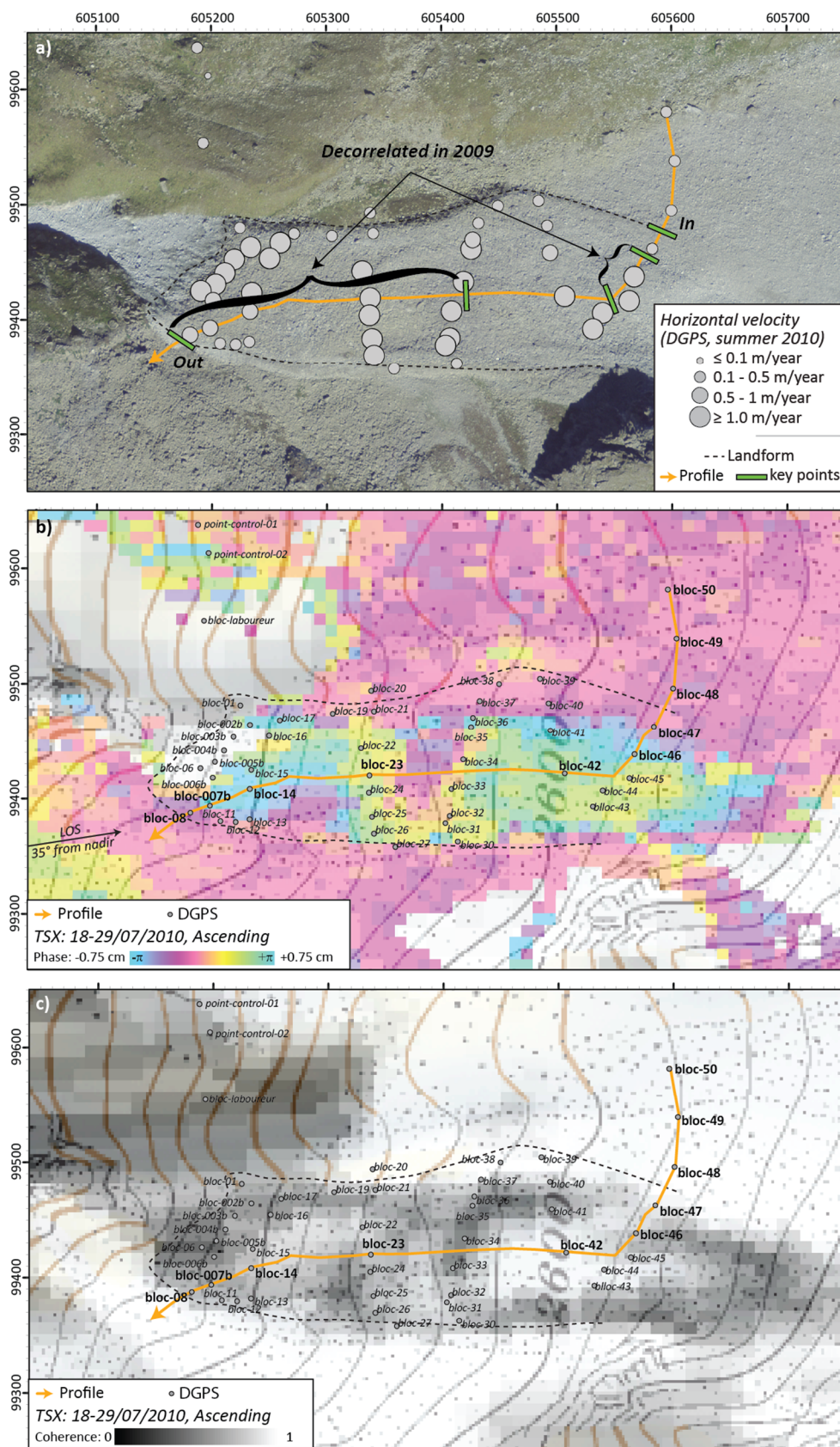


Figure 5.1: Example of profile definition on the Tsarmine rock glacier. a) Location and displacements observed thanks to DGPS (campaigns of summer 2011) superimposed on the swissimage ©Swisstopo 2010. b) Phase and c) coherence images of the best defined TSX interferometric pair.

5.2.1.3 Coherence trend

The interferometric coherence is analyzed along the profile for each selected interferometric pair. Values, drops and flat areas are interpreted thanks to a detailed analysis of combined topography, orthoimage and interferometric phase. The coherence trend is here estimated and key points along the profile like acceleration, entrance and exit of the landform or break slope, are defined (Figure 5.2).

Next, the profile is used to roughly evaluate the change in the activity rate of the landform by analyzing the coherence on different selected DInSAR pairs. This analysis may reveal some specific responses of the observed rock glacier depending on the period of TSX acquisitions. On the one hand, the analysis consists of the observation of inter-annual variations, which means to analyze coherence trends and key points along the profiles for different years. This study allows the general behavior of the landform from year to year to be indicated by comparing annual trends. On the other hand, intra-seasonal activity is examined by comparing coherence profiles of pairs from the same season. Here the specific behavior of the landform is studied pair by pair throughout the season.

In the example in Figure 5.2b, the coherence analysis suggests a signal decorrelation in 2009 not observed in 2010 and may reveal a potential deceleration of the landform between 2009 and 2010. In 2010, only two pairs are available and the coherence observed on these two profiles is quite similar, suggesting a constant behavior in between this two selected periods of TSX acquisitions, hereafter called snapshots.

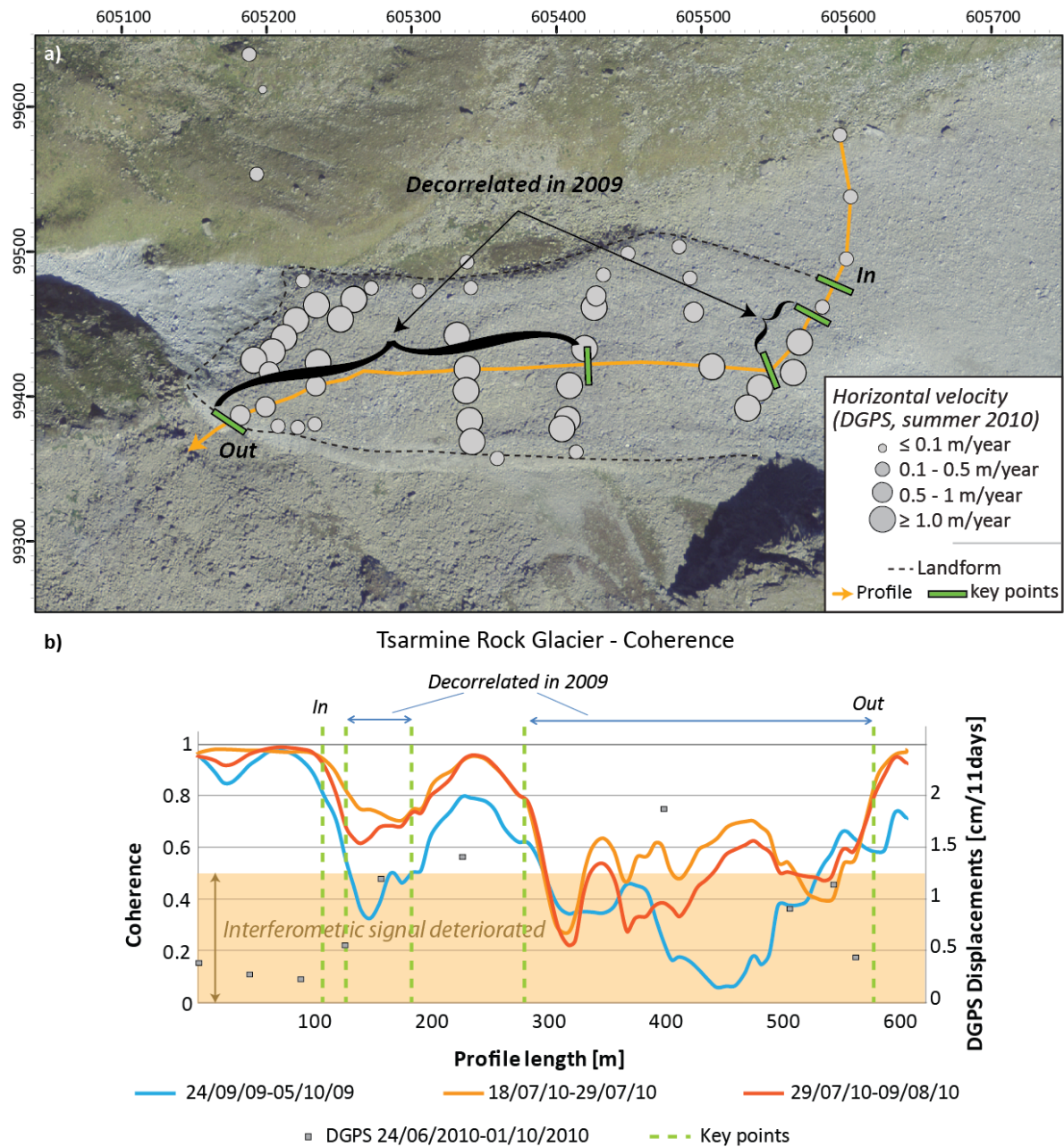


Figure 5.2: a) Location of key points and displacements observed thanks to DGPS (campaigns of summer 2011) superimposed on the swissimage ©Swisstopo 2010. b) Coherence analysis on Tsarmine rock glacier profile.

5.2.1.4 Deformation rate along the profile

A high quality interferometric pair is generally given by the high values of interferometric coherence (values typically higher than 0.5), and by a good stability of interferometric phase (not many phase drops due to wrapped values in between π and $-\pi$). When the quality of the pair is efficient, it is possible to estimate precisely the deformation rate in the radar LOS direction (Figure 5.3). In this step, the interferometric phase and deformation rate along the profile is manually derived. Prerequisites

imply that the displacements should be known at least at the start of the profile (it is suggested to start the profile in a stable area), should not have too many variations in the phase along the profile in order to reduce efforts for unwrapping phase, and should analyze phase drops according to the previous study of coherence trends and key points.

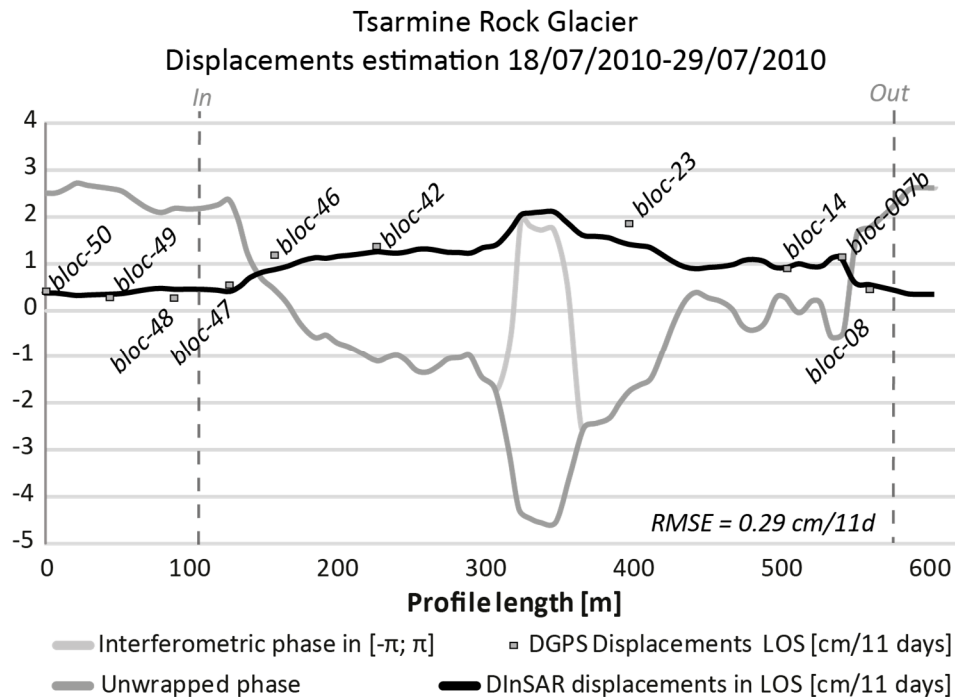


Figure 5.3: Displacement estimation along a profile from the selected DInSAR pair from the 18-29/07/2010.

5.2.2 Performance

The performance of this presented methodology to observe the behavior of a landform along a profile is evaluated by comparing the displacements derived from DInSAR analysis with displacements derived from DGPS measurements on three selected Alpine rock glaciers. To produce comparable observations, the DGPS displacements are chosen from the shortest measured campaigns surrounding DInSAR snapshots and are projected into the LOS direction. DGPS campaigns are performed seasonally on these three landforms allowing the comparison of summer displacements derived from DGPS with displacements derived from DInSAR data observed in 11 days. Comparisons are explained here after for each of the three selected rock glaciers. Finally, general performance is evaluated from summers 2010 to 2011.

5.2.2.1 Performance of DInSAR profile analysis over 3 Alpine rock glaciers

a. Tsarmine rock glacier

Tsarmine is a west oriented tongue-shaped rock glacier of 500 meters in length located in the Arolla Valley (Figure 5.2). This landform displays evidence of a recent acceleration. Annual horizontal velocity is about 1.5 m/year. DGPS measurements have been seasonally carried out since 2004. This

landform is particularly suitable for monitoring displacement using DInSAR as its flow is entirely directed toward the down slope direction, nearby the LOS direction and does not show abrupt acceleration. The mean displacement derived from DInSAR data acquired in ascending mode during summer 2010 (using 2 DInSAR pairs) is maximal at the central part of the rock glacier with a velocity up to 2.06 cm/11 days in the LOS (Figure 5.4). The comparison of the mean velocity values computed from the profiles of 2010 with the velocity values acquired by geodetic measurements in summer 2010 projected in the LOS direction gives a RMSE of 0.21 cm/11 days. In 2009, the coherence analysis suggests a signal decorrelation and it is not possible to estimate deformation rate which was, according to DGPS measurements, up to 2.75 cm/11 days in the LOS direction.

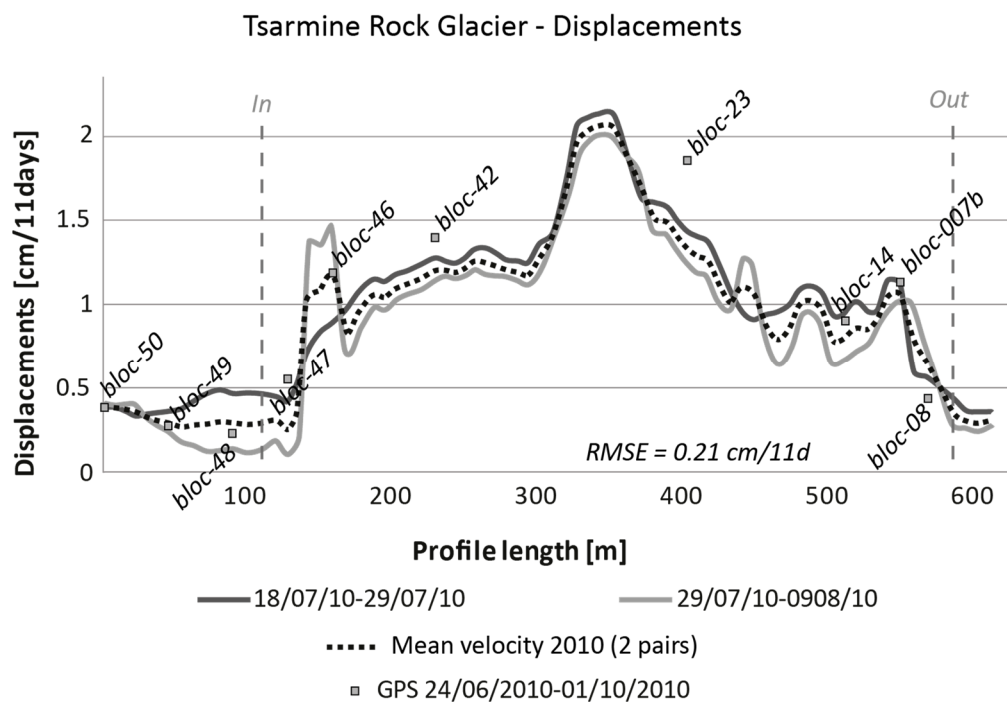


Figure 5.4: Displacement of Tsarmine rock glacier derived from DInSAR analysis (2 pairs from 2010).

b. Gänder rock glacier

Gänder is a north-west oriented rock glacier located in Zermatt Valley showing evidence of destabilization (Figure 5.5a). The very active frontal part (up to 4 cm/11 days in the LOS) could not be monitored on the profile (Figure 5.5b). The flow directed nearby the perpendicular of the LOS direction is highly compressed and takes positive and negative values when projected into the LOS direction. On the upper part, the movement is estimated from 6 DInSAR pairs acquired in ascending mode during summer 2011. By comparing displacements with DGPS displacements projected in the LOS, the RMSE ranges from 0.14 to 0.39 cm/11 days for the 6 selected interferometric pairs (Figure 5.55c). By estimating the mean displacements in summer 2011 (average of 6 pairs), the RMSE falls to 0.08 cm/11 days.

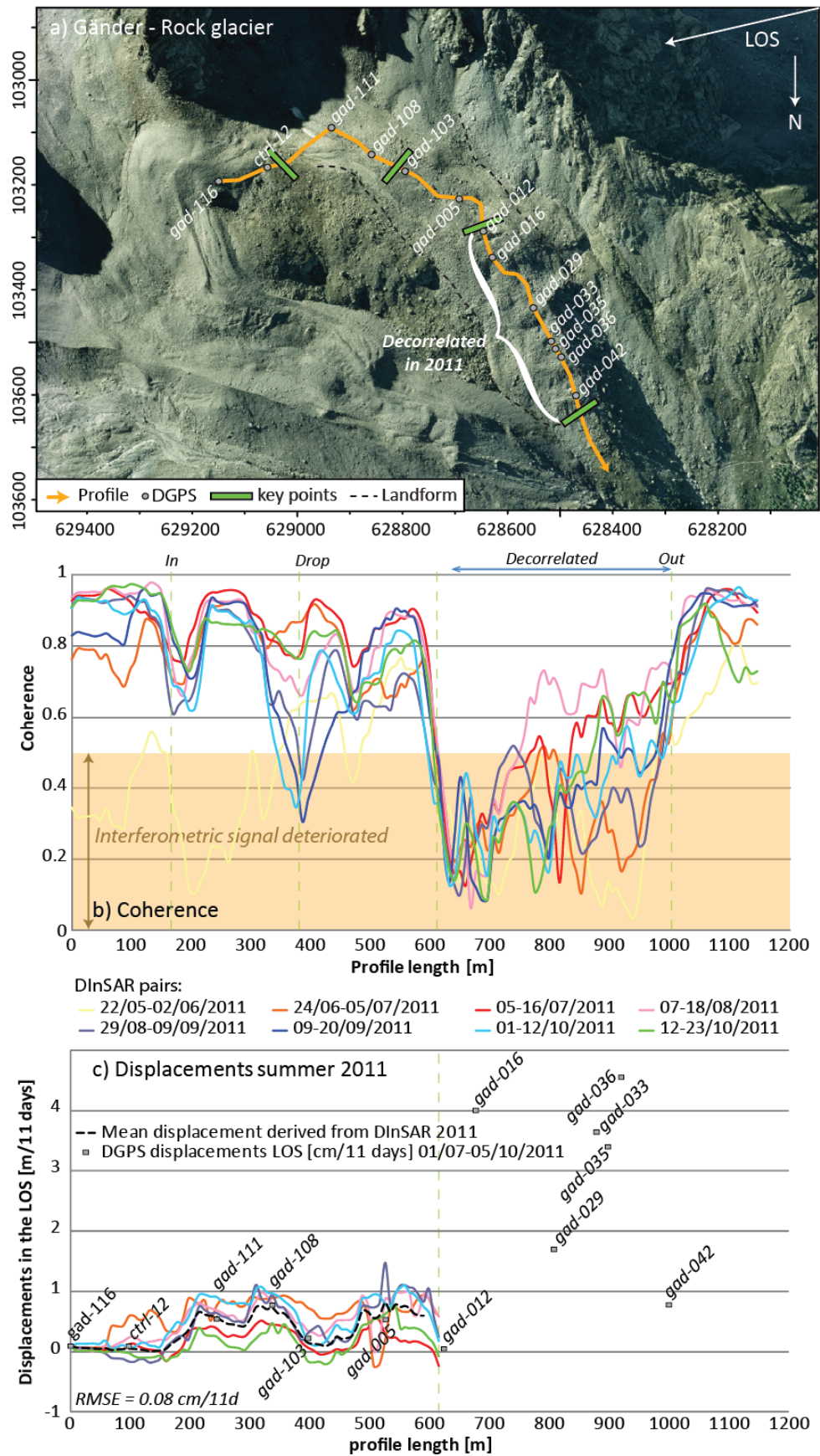


Figure 5.5: a) Gänder rock glacier. b) Coherence analysis on Gänder rock glacier profile. c) Displacements of Gänder rock glacier derived from DInSAR analysis along the profile (6 pairs from 2011).

c. Jegi rock glacier

Jegi is a west oriented rock glacier moving up to 3 m/year (Figure 5.6a). In facing mode, the velocity is well compressed in the LOS direction allowing the analysis and potential quantification of the displacements. The movement is estimated for 6 DInSAR pairs acquired in ascending mode during summer 2011. By comparing values with DGPS displacements measured in between the 27th of June and the 4th of October 2011, the RMSE ranges between 0.38 and 0.58 cm/11 days for the 6 selected interferometric pairs (Figure 5.6c). By estimating the mean displacements in summer 2011 (average of 6 pairs), the RMSE falls to 0.36 cm/11 days.

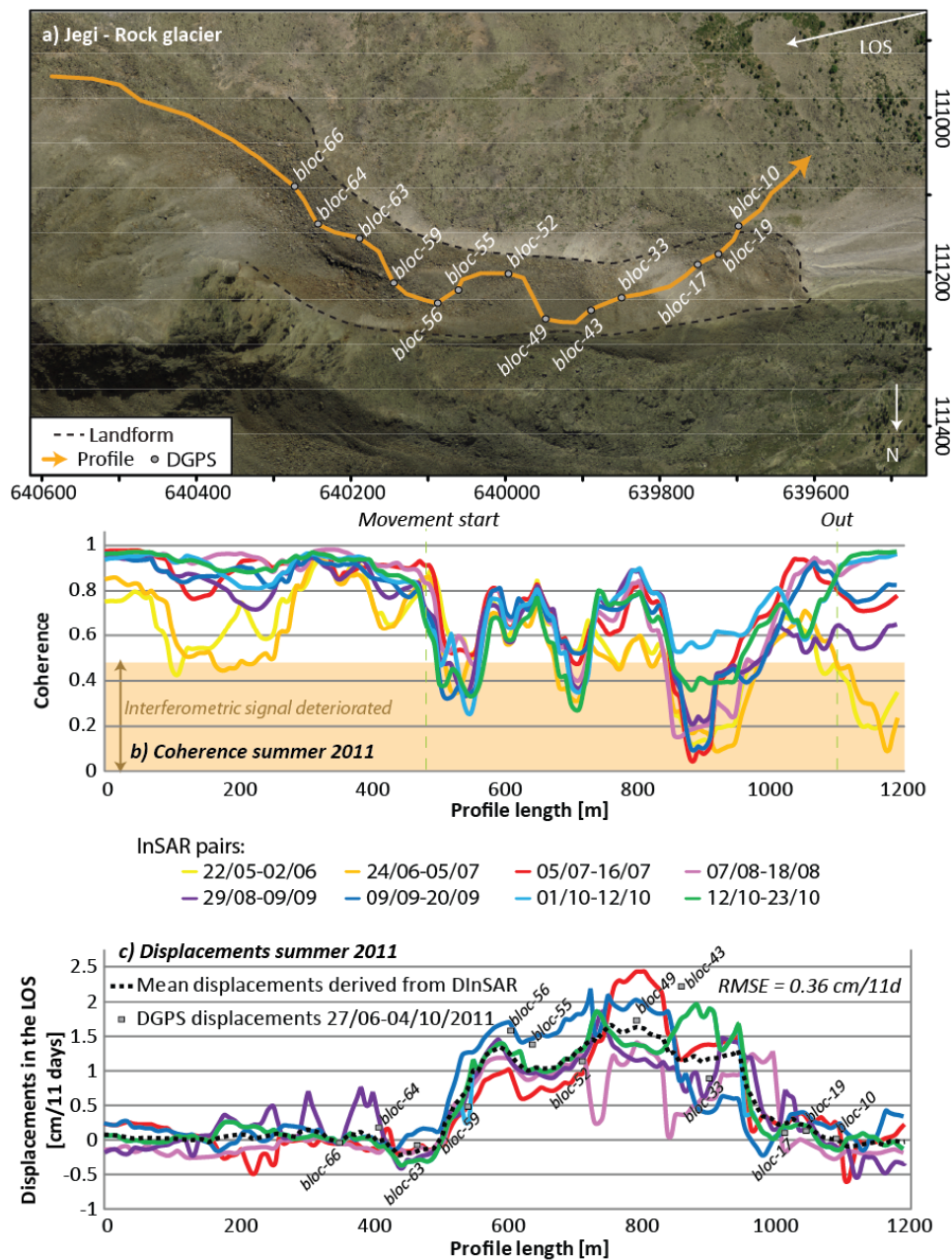


Figure 5.6: a) Jegi rock glacier. b) Coherence analysis on Jegi rock glacier profile. c) Displacements of Jegi rock glacier derived from DInSAR analysis (6 pairs from 2011)

5.2.2.2 General performance of DInSAR profile analysis

Displacements derived from DInSAR analysis along a profile are computed for the three landforms (Tsarmine, Gänder and Jegi rock glaciers) and for the eleven selected DInSAR pairs acquired during summer 2010 and 2011 in ascending modes (Table 5.1).

TSX DInSAR pairs, Ascending mode	Number of DGPS positions
18-29/07/2010	20 (Tsarmine)
29/07-09/08/2010	20 (Tsarmine)
20-31/08/2010	6 (Gänder)
31/08-11/09/2010	6 (Gänder)
24/06-05/07/2011	6 (Gänder)
05-16/07/2011	6 (Gänder), 13 (Jegi)
07-18/08/2011	6 (Gänder), 13 (Jegi)
29/08-09/09/2011	6 (Gänder), 13 (Jegi)
09-20/09/2011	6 (Gänder), 13 (Jegi)
01-12/10/2011	6 (Gänder), 13 (Jegi)
12-23/10/2011	6 (Gänder), 13 (Jegi)

Table 5.1: Table of selected DInSAR pairs for displacement estimation from a profile analysis. The number of DGPS positions from each rock glacier used for validation is indicated.

Eleven DInSAR pairs from summers 2010 and 2011 were used to derive displacements on the three selected landforms. A total of 39 DGPS positions were used as references for comparison. On the Jegi rock glacier comparisons were performed at thirteen DGPS positions using six DInSAR pairs from summer 2011. On the Tsarmine rock glacier comparisons were performed at twenty DGPS positions using two DInSAR pairs from summer 2010. And on the Gänder rock glacier comparisons were performed at six DGPS positions using nine DInSAR pairs from summers 2010 and 2011.

Finally, displacements derived from DInSAR data were compared with DGPS displacements projected into the LOS direction from different DGPS campaigns of measurements performed during summers 2010 and 2011 (Table 5.2).

Rock glaciers	DGPS campaigns
Tsarmine	24/06-22/09/2010
	24/06-10/10/2010
Jegi	27/06-04/10/2011
Gänder	01/07-07/10/2010
	01/07-05/10/2011

Table 5.2: DGPS campaigns used for comparison with displacements derived from DInSAR.

Figure 5.7 shows an acceptable agreement between the displacements estimated from DInSAR profile analysis and DGPS measurements. The mean of differences is 0.0468 cm/11 days and 95% of the differences lie within the limits of agreement -0.7033 to 0.7970 cm/11 days. The Figure 5.7 also shows the scatter of the differences that increases with the averaged displacements illustrating the

difficulty to estimate displacement when it is near the maximal detectable deformation rate (half a wavelength). The high accuracy illustrated by the mean of differences and low precision given by the large limits of agreement could be explained by the fact that we compare values derived from DInSAR pairs on a snapshot of 11 days with seasonal DGPS measurements derived from campaigns of about three months.

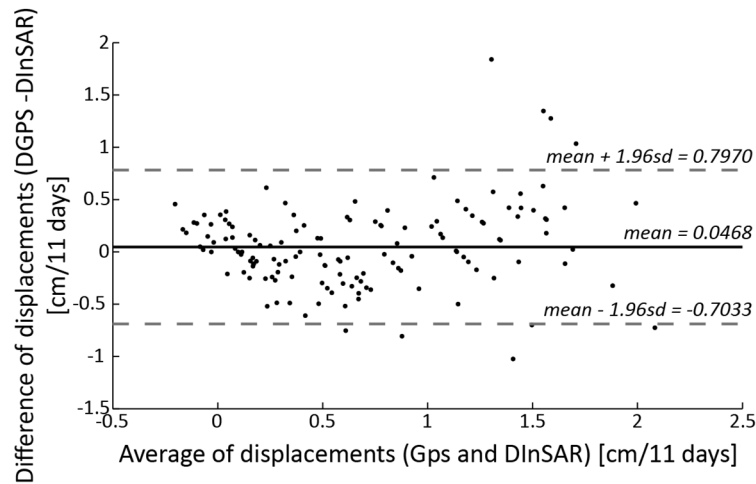


Figure 5.7: Bland-Altman plot for agreement assessment of velocity measurements from DGPS and DInSAR.

5.2.3 Discussion

5.2.3.1 Requirements

This study confirms the potential of DInSAR to monitor velocity with respect to different parameters:

- The size of the landform: the minimum width of the landform is experienced at 100m in facing mode;
- The orientation of the landform and of its flow direction: the cell resolution of the observed area on the ground and the projection of the observed deformation rate differ according to the location;
- The deformation rate of the landform: the deformation rate has to be lower than $\lambda/2$ in the LOS (that is 1.55 cm/11 days with 11-day TSX interferograms) to be quantified;
- The complexity of the landform's observed surface: several profiles can be defined over the landform;
- The noise due to weather such as snow or rain;
- The atmospheric artifacts: in the easiest case of homogeneous tropospheric delay affecting the image by creating a distinct color gradient visible from the bottom of the valley to the top, a linear trend can be applied to remove it;

- g) The quality of the interferometric phase: when many high drops affect the interferometric phase signal along the profile, it involves difficulty to unwrap it;
- h) The acquisition date: the observed DInSAR signal depends on the period of DInSAR acquisitions.

The ascending mode is chosen on the studied landforms due to the facing mode when observing these west oriented rock glaciers. This configuration allows a higher compression of the deformation rate when projected in the LOS direction and thus a better observation and estimation of the rate (observed as fringe pattern).

5.2.3.2 Subjectivity

The method is simple and efficient to evaluate the deformation of the landform along a profile. The profile can be drawn along the landform to roughly estimate the displacement rate along it. It has to be drawn in the direction of the flow and in the central part of the landform to respect its natural behavior. The position of this profile could change some meters according to the expert; however, the general behavior will be roughly the same whatever the position.

When using the profile for estimating displacements, and manually unwrapping the interferometric phase, the methodology is dependent on the knowledge of the expert. Moreover, the lower the quality of the phase (with several drops difficult to interpret), the more difficult the phase unwrapping and the displacement estimation are. Consequently, displacements derived from DInSAR may be different depending on the expert.

5.2.3.3 Detection of seasonal variations

For successful results, a large dataset of SAR scenes is recommended to considerably increase the relevance of DInSAR measurements for seasonal behavior analysis free from in-situ measurements. When the interferometric phase cannot be accurately explored, the analysis of only the coherence parameter offers all the same the possibilities to estimate qualitatively annual and/or intra-seasonal variations.

Moreover, the RMSE is evaluated by comparing the displacements derived from DInSAR and displacements observed from DGPS. For the three landforms investigated above, the RMSE computed for displacements derived from each DInSAR pair is larger than the RMSE computed for the mean displacement derived from all the DInSAR pairs of the summer. In other words, by averaging displacements derived from a set of repeated DInSAR pairs throughout the summer, the results are more accurate. This result can be explained by the fact that the comparison pair by pair is performed between displacements observed in snapshots of 11 days with DInSAR and a period of several months with DGPS. At a time interval of 11 days, it is potentially possible to detect seasonal variations.

To improve the relevance of this extremely short response analysis, a large set of data is needed. A complete set of repeated DInSAR pairs available for several repeated years could moreover show if this observed seasonal behavior exists every year.

5.2.3.4 *Sensors compatibility*

Other SAR sensors can successfully be used for this analysis. However, the comparison between coherence trends gathered from different sensors is not guaranteed as the coherence reflects the quality of the signal for a defined position depending mainly on the observed velocity, which is not the same according to the parameters of each sensor (wavelength, time interval, incidence angle involving compression of the observed velocity, etc.). Thus compatibility between sensors is not always possible and has to be taken into consideration.

5.2.4 Conclusion

The analysis of DInSAR data acquired in facing mode could allow the monitoring of active Alpine rock glaciers. The investigation of DInSAR profile analysis along a landform demonstrates the potential to monitor movements when the signal is not decorrelated; however, the experiments show a low precision for the quantification of deformation rate. When the unwrapping of the interferometric phase on the profile is not possible, the potential to detect annual and seasonal variations is shown by analyzing only the interferometric coherence. The latter method could also be promising for automated change state detection. The main limitation of this proposed technique of profile analysis is not taking advantage of DInSAR to provide a continuous map of surface deformation. Here the deformation is analyzed along the profile only.

5.3 Monitoring of rock glaciers using maps of DInSAR signal and maps of slope movements

This part describes two methods aiming to evaluate the behavior of Alpine rock glaciers using DInSAR signal and slope movement maps derived from DInSAR analysis (for details about mapping of DInSAR signal and slope movement maps please see Chapter 4).

5.3.1 Rock glacier behavior from automated mapping of DInSAR signal

Two methods are presented in this section. The first one uses slope movement maps derived from a large set of TSX DInSAR data having different time intervals in order to roughly estimate the deformation rate of a landform (see details for slope movement mapping in Part 4.3). The second one uses the classification of DInSAR signal on a complete set of repeated TSX data in summer in order to detect intra-seasonal variations of a landform (see details of DInSAR signal classification in Part 4.2).

5.3.1.1 Rough estimation of deformation rate

As seen in Chapter 4, the mapping of DInSAR signal allows the identification of areas with plain pattern, (partly) fringe pattern and noise pattern from a selected DInSAR pair. The slope movement map derived from a set of DInSAR signal maps with the same time interval permits the identification of related areas without deformation, with gentle deformation and with large deformation at this specific time interval. An extra class “NaN” is used in this mapping of slope movements when the algorithm is not able to determine the right class of deformation.

As seen in Chapter 3 (Part 3.2.4), the rate of terrain movement which can be detected depends among others on the time interval and on the wavelength (Figure 3.5). The interferometric SAR signal will decorrelate when the displacement gradient between adjacent pixels is higher than half the wavelength during the selected time interval (Massonnet and Feigl, 1998).

Consequently, it is possible to roughly evaluate the deformation rate on a spatially outlined area with an almost homogeneous deformation rate by analyzing the evolution according to time interval of each portion of slope movement given by the automated mapping. Two thresholds can be detected: 1) s_{stab} corresponding to the time interval until the proportion of plain pattern is higher than 50% and 2) s_{dec} corresponding to the time interval from when the proportion of noise pattern is higher than 50%. The period in between these two thresholds represents the time intervals where (partly) fringe pattern can be observed. From the correspondence given in Table 5.3, the deformation rate can finally be evaluated according to the 4 classes used in previous inventories of slope movements using DInSAR, namely the classes “cm/year”, “cm/month”, “dm/month” and “cm/day” (see Part 4.1.1).

		Time interval (day)															
		11d	22d	33d	44d	55d	66d	77d	88d	352	363	374	638	649	660	704	715
Classes of deformation rate	cm/day	n	n	n	n	n	n	n	n	n	n	n	n	n	n	n	n
	dm/month	f/n	n	n	n	n	n	n	n	n	n	n	n	n	n	n	n
	cm/month	f	f	f	f	f/n	f/n	f/n	f/n	n	n	n	n	n	n	n	n
	cm/year	p	p	p	p	p/f	p/f	p/f	p/f	f	f	f	f/n	f/n	f/n	f/n	f/n
p: plain pattern, f: (partly) fringe pattern, n: noise pattern																	

Table 5.3: Correspondence between class of deformation rate and time interval according to TSX DInSAR signal observed on the interferometric phase image.

As past inventoried DInSAR polygons from the 1990s describe the delimitation of areas with an almost homogeneous deformation rate (Part 4.1.1), they can be used to perform such of analysis. In Figure 5.8, an example of the evolution of slope movements is given for four of these DInSAR polygons inventoried in the region of the Jegi rock glacier in the 1990s. The slope movement maps

derived on the studied area using the large dataset of 140 TSX DInSAR data is also used here (see details about TSX data and the studied region of Jegi rock glacier in Subsection 4.1.2.3). The model II using the LDA statistical classifier and the grid resolution of 25 meters was used to compute these maps. The class of deformation rate of the four examples of DInSAR polygons is finally indicated in Figure 5.8. It has to be noted that in the case of superimposed movements, the pixels must be separated in order to avoid the DInSAR signal behavior from different deformation rates influencing each other.

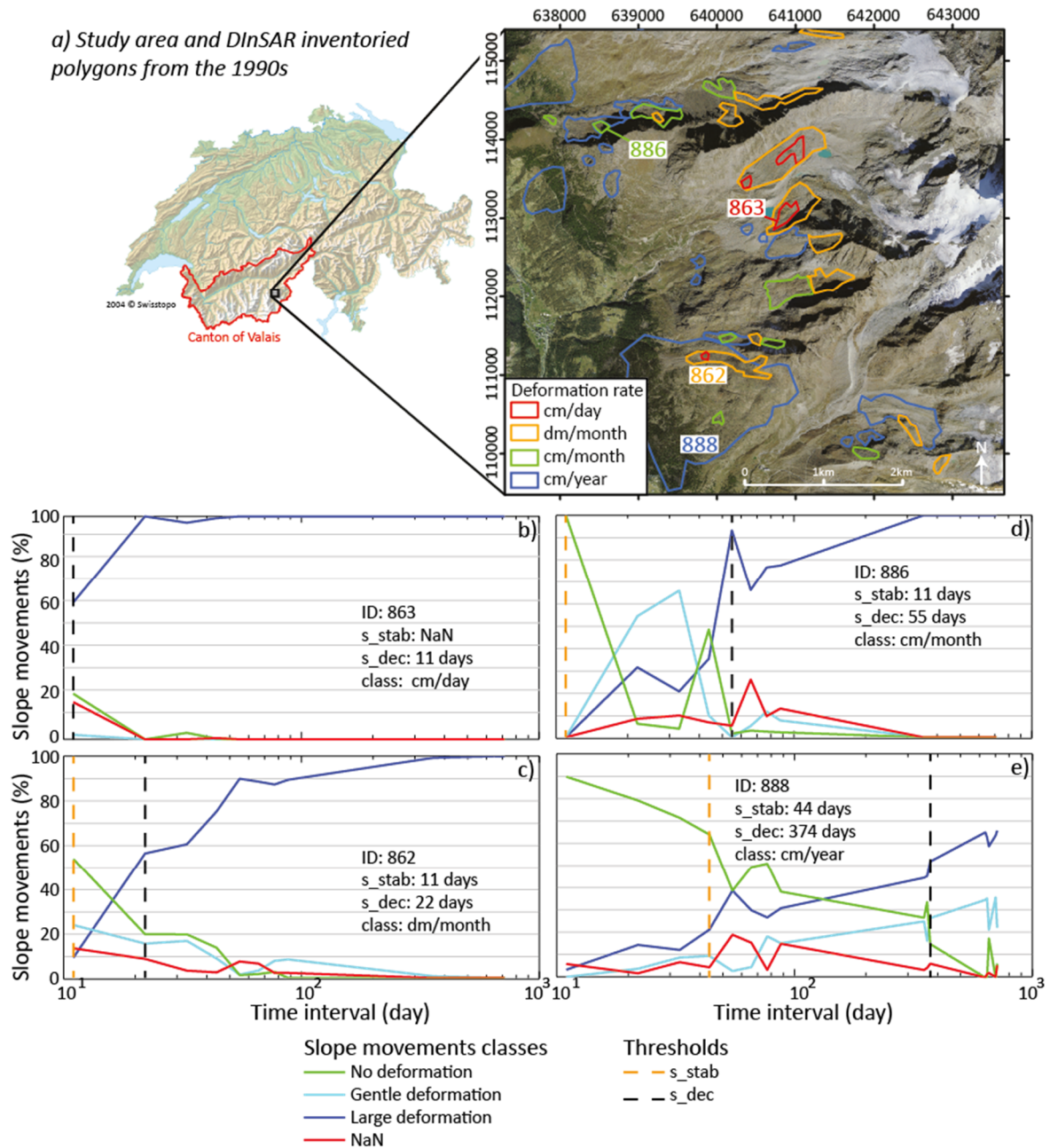


Figure 5.8: a) Location of the four selected DInSAR polygons. Proportions of slope movements for the four selected DInSAR polygons moving at the velocity rate of b) cm/day, c) dm/month, d) cm/month and e) cm/year.

5.3.1.2 *Change in the behavior of the observed landform*

In this subsection, the evolution of DInSAR signal is analyzed during the summer season on a series of selected interferograms having a time interval of 11 days. The mapping of DInSAR signal is used here in order to evaluate seasonal changes in the behavior of a studied landform. As seen in Chapter 4, using statistical classifiers applied on selected texture features extracted from the interferometric phase image, the DInSAR signal can be classified into three classes of pattern: 1) no change defined by a plain pattern; 2) smooth change characterized by a (partly) fringe pattern and 3) decorrelated signal expressed by a noise pattern. In this section we propose to classify the texture of each pixel describing the studied landform on the interferometric phase image using the LDA statistical model. The analysis is here restricted to the landform itself (outlined area drawn as dotted line in Figure 5.9). Then the proportion of each of the three DInSAR signal patterns observed in the delimited area of the landform is compared for each selected DInSAR pair in order to analyze the evolution of these patterns during the summer (Figure 5.9a).

In Figure 5.9a, the variation in time of each DInSAR signal pattern can indicate the increase or decrease in the activity rate of the landform. For instance, the single peak of noise pattern (and respective drop of (partly) fringe pattern) seen in the end of June can be related to the increase in the activity over the frontal part of the rock glacier that can also been observed on the interferometric phase image (Figure 5.9 e). To go further and interpret the specific processes involved in this landform, the weather conditions at or up to two days before each SAR image date based on available meteorological data has to be considered to evaluate whether the variation of the texture pattern is due to the behavior of the landform or to external artifacts (rain events, snow, etc.).

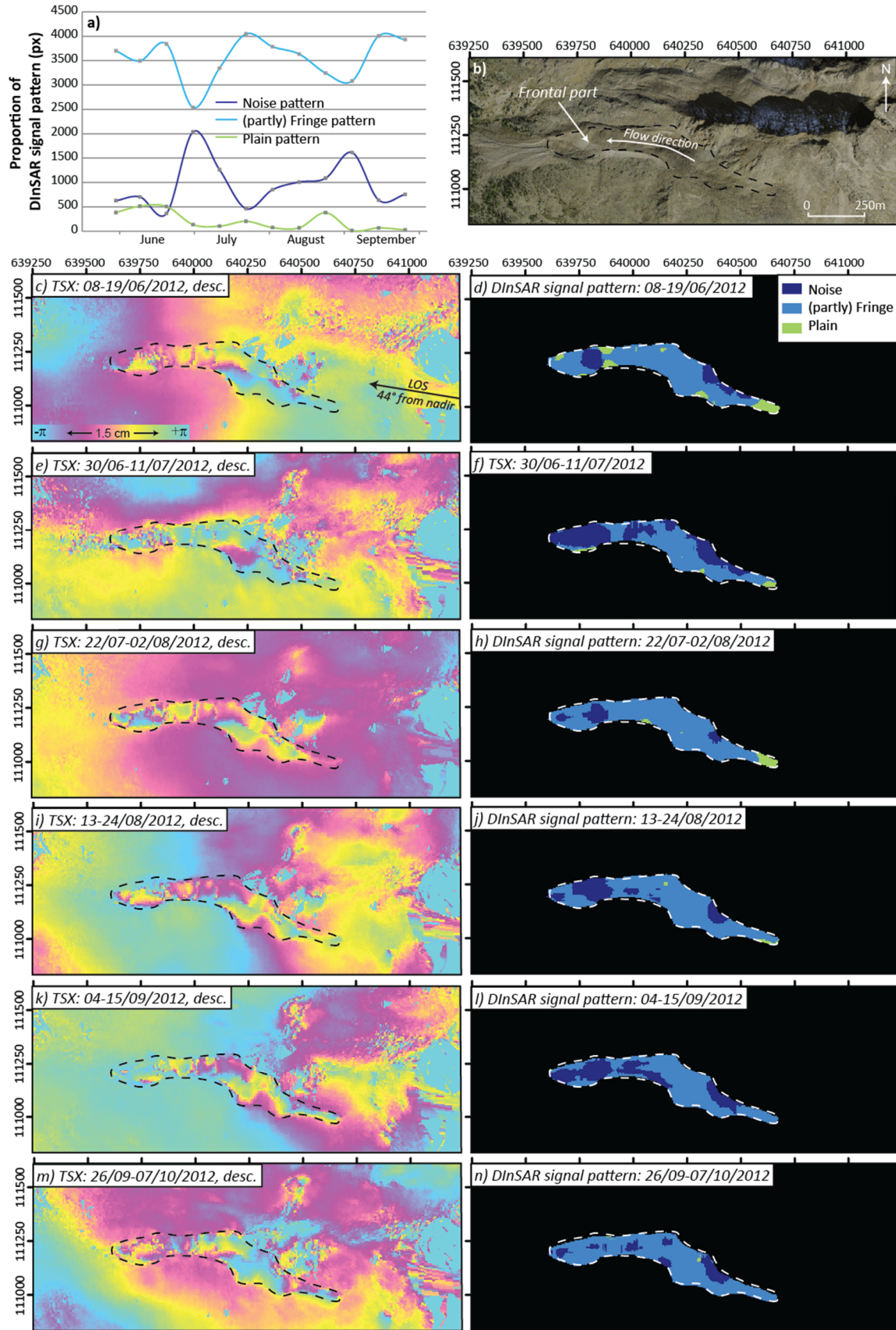


Figure 5.9: a) Seasonal behavior of the DInSAR signal patterns observed on Jegi rock glacier in 2012. b) Orthoimage of the Jegi rock glacier with the outline of the observed area drawn as dotted lines. c) to n) Interferometric phase image and corresponding automated DInSAR signal pattern classification.

5.3.2 Performance

5.3.2.1 *Evaluation of deformation rate estimation using DGPS*

The results of automated velocity rate estimation using slope movement maps are here compared with available DGPS measurements performed on surveyed landforms. Only two fast moving landforms (with velocities “cm/day” and “dm/month”) are observed with DGPS measurements in the region of interest: the Jegi and the Gruben rock glaciers. As their velocity rate is estimated from summer TSX interferograms with a short time interval acquired between 2008 and 2012, and in order to neglect inter-seasonal variation of the displacements, the comparison is performed using only summer displacements derived from available DGPS campaigns. Summer campaigns from 2009 to 2013 are used for the Jegi rock glacier, and summer campaigns from 2012 and 2013 are used for the Gruben rock glacier.

Five inventoried DInSAR polygons were detected on these two rock glaciers in the 1990s (Figure 5.10 a and d). Using slope movement maps automatically derived from TSX DInSAR data from 2009 to 2012 (Part 4.1.2.3), each of these five DInSAR polygons are classified into the same categories of deformation rate as 20 years before (Figure 5.10 b-c, e-g). When comparing the average 3D velocity rate measured from DGPS measurements over each of these polygons, it seems that these polygons were not always correctly classified. It appears that the two delineated polygons of the Jegi rock glacier are correctly classified (Figure 5.10 b, c): the polygon 812 is described by 9 DGPS points having an average 3D velocity of 0.7 cm/day in between 2009 and 2012 (class “cm/day”), and the polygon 862 is described by 47 points moving with a velocity rate of 6.8 cm/month (class “dm/month”). The polygon 864 of the Gruben rock glacier is also correctly classified: the average 3D velocity is about 6.7 cm/month in between 2012 and 2013, which corresponds to the class of velocity “dm/month” (Figure 5.10 g). However, the two fastest DInSAR polygons of the Gruben rock glacier are not correctly classified (Figure 5.10 e and f): the average velocity of 0.3 and 0.4 cm/day given by the DGPS measurements is too low compared to the class of deformation “cm/day” that was automatically estimated. The difference observed over the Gruben rock glacier can also be explained by the fact that DGPS measurements are not available during the same period of observation as the DInSAR data. The automated rate estimation is performed from TSX data acquired during 2008-2012 and is compared to DGPS measurement campaigns from 2012 and 2013 summers only. Thus, the validation of the presented methodology has to be carefully interpreted for this rock glacier.

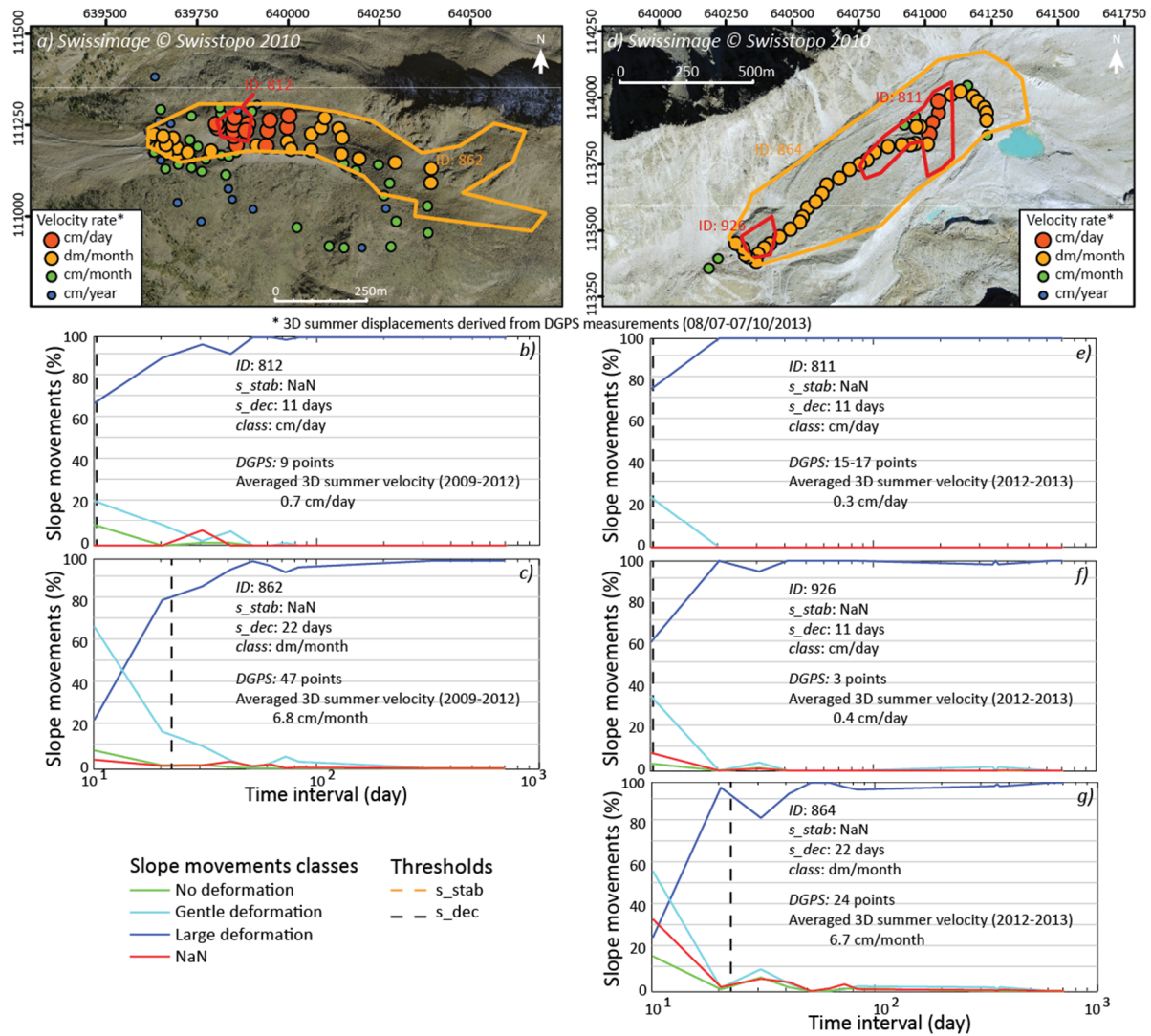


Figure 5.10: a) and b) Averaged 3D summer velocity rates derived from DGPS measurements over the Jegi and Gruben rock glaciers. b-g) Rough estimation of the velocity rates over five inventoried DInSAR polygons according to the four classes of velocity: cm/day, dm/month, cm/month and cm/year.

5.3.2.2 Evaluation of seasonal change in the behavior of the landform

Unfortunately, it is not possible to use available DGPS measurements in order to assess the intra-seasonal variation in the behavior of the Jegi rock glacier detected with the analysis of the DInSAR signal derived from a complete set of repeated TSX data (Figure 5.9). DGPS campaigns are generally performed during the end of June and the end October. Thus only the total displacements between these two dates are known and cannot be correlated to individual behaviors observed with DInSAR data in an 11 days snapshot. As seen in Figure 5.11, the horizontal velocity observed from seasonal DGPS measurements differs according to the season; summer displacements are higher than winter.

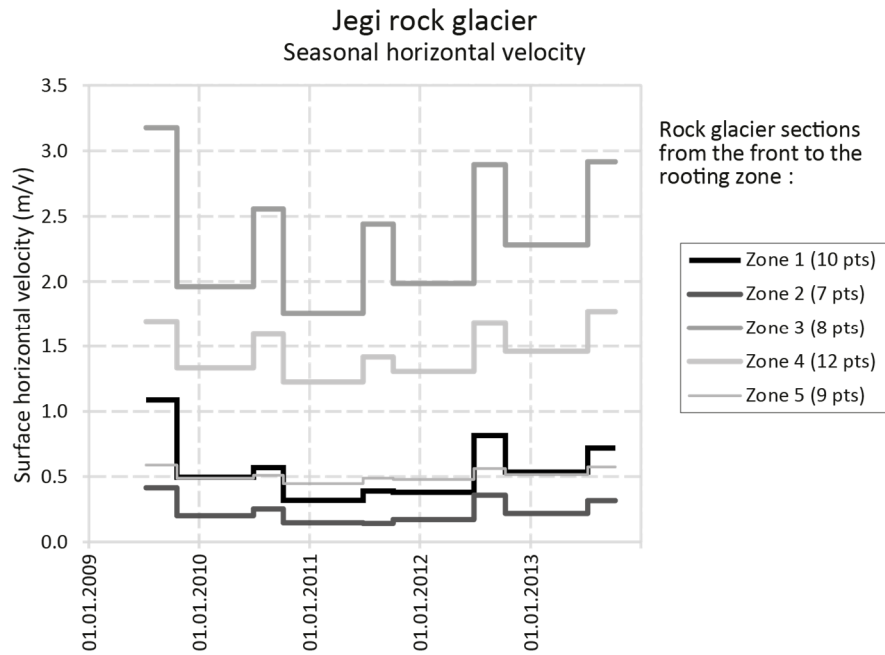


Figure 5.11: Seasonal horizontal velocity of Jegi rock glacier measured by DGPS.

However, potential intra-seasonal variations cannot be distinguished using these DGPS measurements. The best way to assess observed variations of deformation rate during the summer would be to use displacements measured from a continuous GPS at the same time as DInSAR data. Unfortunately, no data is available on this rock glacier for the summer 2012 (a DGPS station was installed on the Jegi rock glacier in August 2012 as part of the PERMOS network). These kinds of GPS stations allowing continuous measurements are either installed on very rapid rock glaciers where the deformation is too high to be monitored with DInSAR (noise pattern) or on rock glaciers where no complete series of repeated TSX data are available. Consequently, the presented methodology cannot be verified on these rock glaciers currently monitored by continuous GPS.

5.3.3 Discussion

5.3.3.1 Characteristics of deformation rate

As already seen previously in Section 3.2.4, the interferometric SAR signal will decorrelate when the deformation rate or displacement gradient between adjacent pixels is higher than half the wavelength during the selected time interval. Moreover, the nature of the change within a pixel can introduce noise in the measuring phase difference (Klees and Massonnet, 1999) and the information on the deformation is coherent only if the entire surface within the pixel deforms homogeneously. However there is no typical velocity rate that is known at which the DInSAR signal decorrelates on a rock glacier and this threshold therefore has to be deduced from experience (4.3.3.2 a). When observing results of Figure 5.9 a) and d), it seems that the DInSAR signal observed on the Gruben rock glacier decorrelates at a lower displacement rate than the Jegi rock glacier. This hypothesis was

already formulated in the previous chapter when assuming that the typical velocity rate at which the decorrelation is observed is 2λ for the Jegi rock glacier and λ for the Gruben rock glacier (4.3.3.2 a). Consequently, the relationship between observed DInSAR signal patterns and quantity of deformation observed in the area has to be taken carefully and the proposed method to evaluate the deformation rate from slope movement's maps is only performed roughly. It seems that the four different classes of deformation rate ("cm/day", "dm/month", "cm/month" and "cm/year") used for past inventoried DInSAR polygons are suitable for this kind of analysis. The categorization of the movement in more subtle categories of deformation rate, even using TSX data with a small wavelength and high temporal sampling, would be quite challenging.

5.3.3.2 *Delineation of moving zones*

The rough estimation of deformation rate using the analysis of slope movement maps (Section 5.3.1) has to be performed on a spatially outlined area with a nearly homogeneous deformation rate. Consequently, this method can easily be used more widely in order to estimate the velocity rate of a large set of DInSAR polygons. However, the problem now is to deal with the compatibility between different SAR sensors. As seen before (Section 4.4.5), the outline of the slope movement can basically differ due to different ground resolution, incidence angle or acquisition mode. In comparison to ERS or JERS used for the first inventory of DInSAR polygons, recent very high-resolution X-Band sensors such as TerraSAR-X (TSX) permit a more precise spatial detection and delimitation of moving slopes. Moreover, with a repeated cycle of 11-days, subtle changes in the deformation rate of moving slopes can be detected. Thus, a change in the outline of a homogeneous deformation rate using TSX data could explain the wrong classification of DInSAR polygons on the Gruben rock glacier. It must be noted that the velocity is observed in the LOS and the related topography has to be compared with the results in order to understand the spatial variation of the landform's movements.

Finally, the use of this methodology, in order to update the past inventoried DInSAR polygons in terms of deformation rate derived from the observation of ERS and JERS data from the 1990s with the new TSX DInSAR data from the 2010s, may be a difficult task and will have to be performed carefully.

5.3.3.3 *Understanding movement processes*

The last proposed method (Section 5.3.2) allows the detection of intra-seasonal variation in the DInSAR signal potentially related to the variation of the deformation rate. However, to validate these observations of short-term activity fluctuations, measurements with a high temporal resolution are required. Currently, there is no available data permitting the validation of these detected seasonal changes. The only way to assess the visualization of seasonal variations would be to explain them according to similar geomorphological processes observed on other rock glaciers. As this practice to

find hypotheses about potential movements governing the deformation rate of landforms is closer related to interpretation than validation, it will be developed in more detail in the Third part “Applications” and particularly in Chapter 8, “Examples of DInSAR contribution for site specific analysis”.

5.3.4 Conclusion

The two presented methods in Part 5.3 aim to evaluate the behavior of Alpine rock glaciers using DInSAR signal and slope movement maps derived from DInSAR analysis. The first one allows the rough estimation of deformation rate thanks to an analysis of evolution in time of the proportion of slope movements mapped from a large set of DInSAR data. The second one permits the potential detection of seasonal variation in the deformation rate of the landform thanks to the analysis of the evolution in time of the DInSAR signal patterns mapped from a complete repeated set of TSX data during the summer. The main limitation when applying each of these techniques comes from the availability and accessibility of large series of DInSAR data. It may be restricted by costs sometimes too high for scientific purposes and by availability. For example, TSX successive stripmaps are acquired in the same orbit, making the availability of two contiguous areas impossible for the same time period. If there is no order conflict, these data are available and could permit the monitoring of the kinematics of rock glaciers defined as the quantification of a landform’s movement and thus provide basic understanding of ongoing processes over time.

5.4 Overall conclusion

In this chapter, the challenge was to find methods to monitor annual and seasonal behavior of rapid rock glaciers (1.5-3 m/year) using the new high spatio-temporal resolution of TSX data.

The first presented method aims to quantify the deformation rate of a landform along a profile (Part 5.2). Whereas the mean deformation rate derived from a series of TSX DInSAR data was validated using DGPS measurements and show acceptable performance, the deformation rate measured on each DInSAR pair separately is really poor. Moreover, this proposed methodology is difficult to apply and is dependent on the experience of the analyst in DInSAR signal understanding. Thus we can make conclusions about the difficulty of using this method of analyzing interferometric phases along a profile to accurately quantify the deformation rate of rapid rock glaciers (1.5-3 m/year). However, when comparing the interferometric coherence signal along the profile, it seems that variations between selected snapshots of TSX pairs can be revealed and used to detect potential changes in the related deformation rate.

The second method (Section 5.3.1.1) shows that the mapping of slope movements proposed in Chapter 4 using a large set of DInSAR data with different time intervals can be used to roughly

estimate the deformation rate of a moving zone. Whereas the first presented method proposes the analysis only on a profile along the landform, the main advantage of the second method is to be performed on the whole landform's surface. It represents moreover an easy, fast and objective method to roughly evaluate the deformation rate of a landform.

The third method (Section 5.3.1.2) proposing the analysis of DInSAR signal maps developed in Chapter 4 on a complete set of repeated TSX acquisitions in summer allows the detection of seasonal variations of rock glaciers that cannot be detected with traditional DGPS campaigns performed in early and late summer.

Lastly, despite the huge quantity of DGPS measurements over the studied area, we noticed the difficulty in validating DInSAR observations with available DGPS data as they differ in time (date and period of acquisition). These different data sources should be used rather as complementing data to understand processes occurring during the season.

Chapter 8 will be dedicated to the use of these different methodologies to monitor Alpine moving landforms. Different specific sites will be studied in detail in order to suggest potential processes involved in the monitored landforms by combining the analysis of DInSAR signal from the up to date TSX dataset with other available data such as field surveys or archives of orthoimages.

3rd Part:

Applications using DInSAR technique for detecting, mapping and monitoring mass movements in the Western Swiss Alps

The 3rd part proposes different applications in order to show the potential of DInSAR technique for the study of slope movements in the specific Alpine environment of the Western Swiss Alps. This part is divided into three chapters. First, the suitability of DInSAR data is assessed for the research on mass wasting dynamics in the Western Swiss Alps. Then some pilot studies and promising applications are proposed for the detection and mapping of slope movements in the Western Swiss Alps. Finally, a few examples of DInSAR contributions are proposed for site specific analysis.

6 Suitability of DInSAR data for the research on mass wasting dynamics in the Western Swiss Alps

In this chapter, the suitability of DInSAR data is presented for the Western Swiss Alps (Valais). In the first part, the potential of ERS DInSAR data for the detection of slope movements in the Valais is presented in detail from past studies where more than 1500 landforms were mapped using a large DInSAR dataset (Part 6.1). Among all these DInSAR detected landforms, twenty-six are monitored by DGPS campaigns and are introduced in Part 6.2. Then the suitability of the new TSX DInSAR data will be studied in detail for the region of interest using the proposed proof-of-concept study presented in Chapter 3 (Part 3.3); the TSX DInSAR visibility is analyzed (Section 6.3.1), and the theoretical maximal measurable deformation rate is estimated for the twenty-six monitored landforms (Section 6.3.2). Finally, a conclusion sums up the main results (Part 6.4).

6.1 Potential of ERS DInSAR data for the detection of slope movements in the Western Swiss Alps

As already discussed in Chapter 4, since 2005 (Delaloye et al., 2007a, 2007b, 2008b, 2010b; Lambiel et al., 2008), several inventories of DInSAR detected slope instabilities have been compiled at a regional scale in the Western Swiss Alps using a large set of ERS data archive from 1991 to 2000 (Part 4.1.1). In the following sections, the detailed results will be presented in order to demonstrate the potential of ERS DInSAR data to detect Alpine periglacial landforms.

6.1.1 Detailed results observed in the Western Swiss Alps

The topography of the Western Swiss Alps, mainly consisting of north-south oriented valleys, was optimal for an application of the DInSAR technique (Figure 6.1). A total of 1791 DInSAR polygons related to about 1500 landforms were detected, with velocities ranging from about one centimeter to several meters per year (Table 6.1).

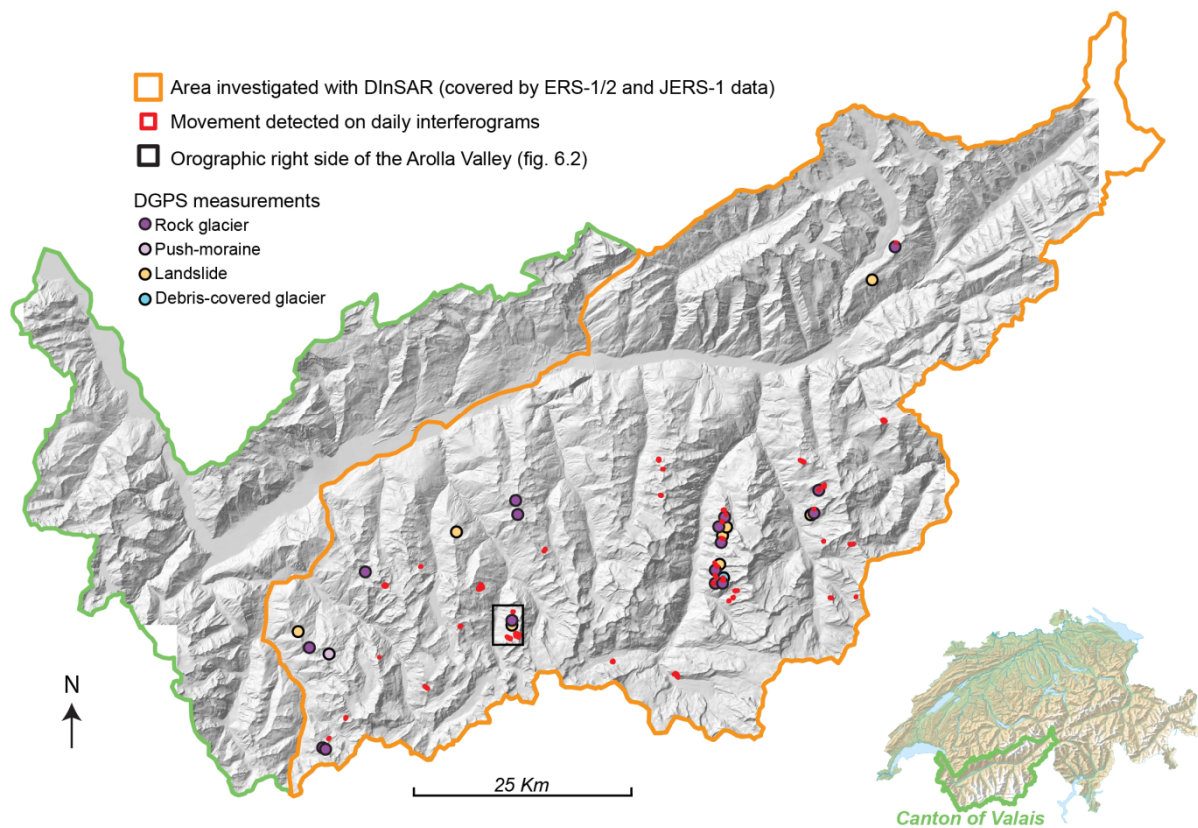


Figure 6.1: Area investigated by systematic mass wasting inventories based on ERS DInSAR data. Stars represent the twenty-six study sites where DGPS measurements have been performed since 2006 and are sources of validation. Red outlines correspond to forty-two DInSAR polygons detected on daily interferograms related to solifluction slopes, landslides, push-moraines as well as rock glaciers moving rapidly.

Velocity of DInSAR Polygons Typology of InSAR polygons	cm/day	dm/month	cm/month	cm/year	Total
Solifluction slope	2	62	103	303	470
Landslide	5	16	87	197	305
Push-moraine	9	47	28	24	108
Rock glacier	26	202	329	351	908
Total	42	327	547	875	1791

Table 6.1: Frequency of the inventoried DInSAR polygons related to mass wasting phenomena according to their typology and velocity. Debris-covered glaciers are not included. Some polygons can be related to the same landform.

The frequency of rapidly moving landforms was relatively high. Forty-two DInSAR polygons were detected on daily interferograms (Figure 6.1, Table 6.1), which corresponds to a velocity higher than 1-2 m/year. These detected moving slopes concern two solifluction slopes, five landslides, nine push-moraines and twenty-six rock glaciers. The inventory has especially contributed to the early detection of potentially hazardous active rock glaciers (Delaloye et al., 2010b). Most of the rock glaciers were then identified on monthly interferograms. 202 were not detected on 1-day interferograms but were decorrelated on 35-day interferograms (dm/month class), and 329 were detected on monthly interferograms and decorrelated for larger time intervals (cm/month class). These two velocity classes contain most of the detected push-moraines too. Active landslides are usually detected on

monthly interferograms (cm/month to dm/month classes), whereas the low activity (sub-stable) landslides, sometimes up to several squared kilometers wide, were evidenced only using annual time intervals (cm/year class). Several complex slope systems were also detected where landforms are juxtaposed, if not superimposed (Figure 6.2).

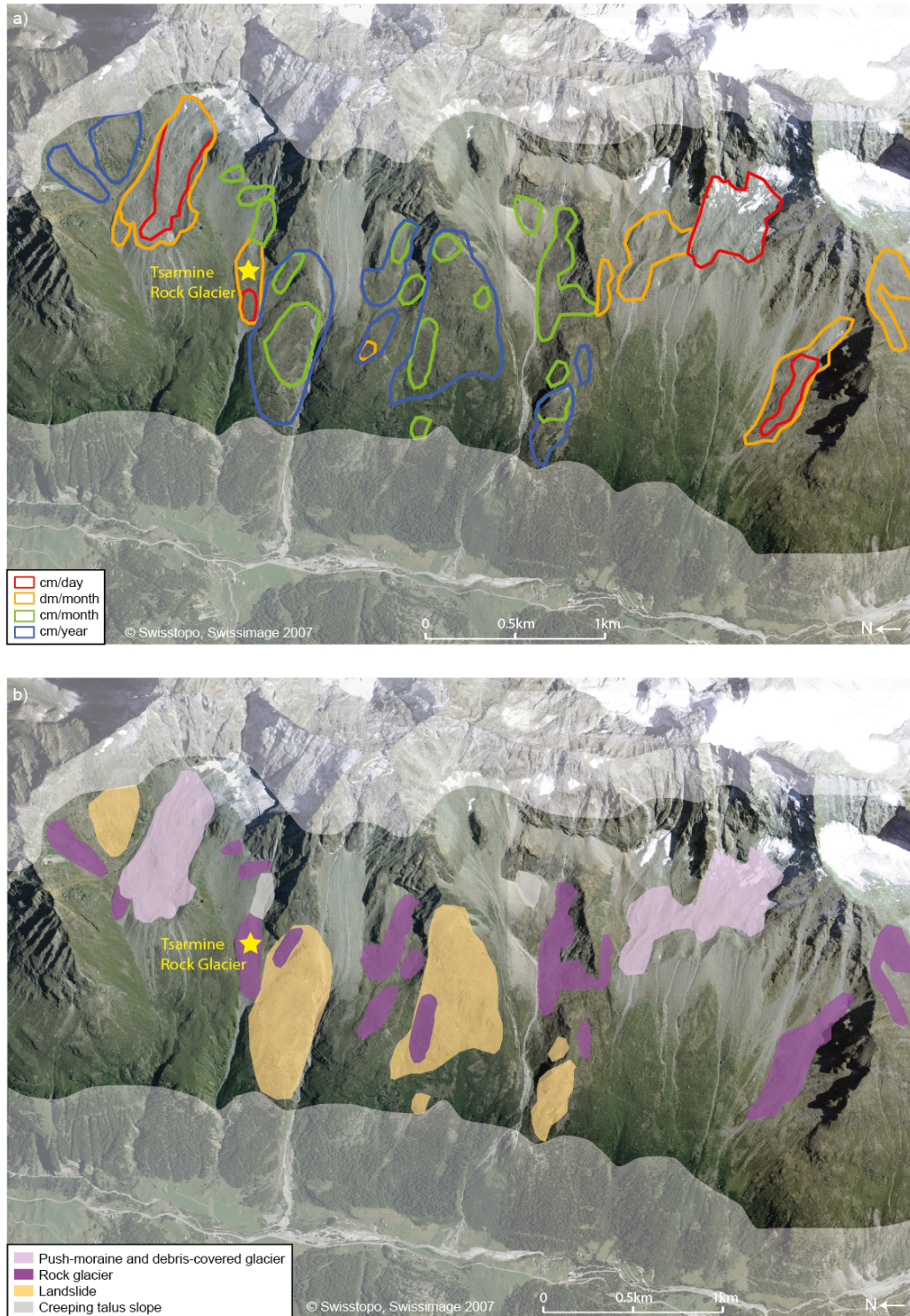


Figure 6.2: Moving landforms are often juxtaposed, when not superimposed, and compose a “complex slope system”, as illustrated by the orographic right side of the Arolla Valley. Here, moving features, including push-moraines, rock glaciers, landslides and saggings, are coalescent. a) DinSAR detected moving zones, b) Related landforms. The investigated area is limited due to layover, shadow and vegetation (transparent belt).

6.1.2 Examples of detected Alpine landforms with ERS DInSAR data

In the studied region, DInSAR detected landforms are mainly related to debris-covered glaciers, rock glaciers, push-moraine, solifluction slopes and landslides. Debris-free glaciers have not been inventoried in our study. However, coherent fringe patterns can easily be observed on 1-day interferograms from the tandem ERS-1/2 in the wintertime. As reported by Weydahl (2001), heavily crevassed zones moving fast have a considerably low coherence and always display noisy DInSAR signals. Debris-covered glaciers are sometimes observed on 1-day interferograms in the wintertime, displaying a coherent signal pattern. The outline of debris-covered glaciers or large dead ice bodies is, however, better delimited at a daily or monthly time interval in the summertime (Figure 6.3 a, b). A decorrelated signal is usually observed and is caused, in addition to the movement of the glacier, by the exposure of the melting ice itself (thin debris coverage) and/or by the rapid settlement and movement of the glacier surface.

The velocity range of active rock glaciers is large, from some centimeters to several meters per year (Delaloye et al., 2008b, 2010b; Lambiel et al., 2008). An obvious signal is detectable with the majority of the sensors for these active features (Figure 3.5). For the most active rock glaciers, a signal may already be detected at a 1-day interval of tandem ERS-1/2 (Delaloye et al., 2008b) (Figure 4.1 a, b) and decorrelation is widespread over the landform at a monthly interval on C-Band interferograms (Figure 4.1 e) and at all minimal time intervals on L- and X-Band interferograms. For the slowest rock glaciers, any signal can be difficult to be evidenced at a monthly time interval but becomes evident, and sometimes decorrelated, at a yearly interval whatever the sensor (see *Lambiel et al. 2008* for additional examples). However, as the signal noise increases significantly at the yearly time interval, low active, quasi-inactive rock glaciers may be difficult to detect.

Current push-moraines in the Alps are thick volumes of frozen debris that have been deformed by a glacier advance during the Little Ice Age. They could still contain superimposed debris-covered glacier ice internally. Push-moraines are frequently affected by the back-creeping of still frozen sediments toward the former glacier talweg and/or by surface subsidence due to melting of massive ice (Delaloye, 2004). These processes imply the possible decorrelation of the area at a daily time interval in summer, although rarely in winter, and a complete decorrelation on monthly interferograms (Figure 6.3 c, d).

On talus slopes or heavily weathered inclined regolith (here called debris mantle) solifluction processes may occur. They tend to form small lobes moving heterogeneously on the slope. The DInSAR signal tends to become progressively decorrelated especially on interferograms with a time interval larger than several months (Delaloye et al., 2007b). It is, however, possible to identify exceptional daily signals on such slopes, which may be explained by the water impregnation of the

ground surface rather than the terrain motion. In any case, the signal related to solifluction processes remains difficult to interpret and to distinguish from noise due to the small size of the single lobes and probably to the non-continuity of the movement during the summertime.

Finally, active deep-seated landslides of various sizes displaying deformation rates ranging from some millimeters to several decimeters per year have been detected. Whereas yearly intervals are the best suited to identify slowly moving landforms, rapid deformations can also be well detected on monthly interferograms (Figure 6.3 e, f). Some landslides are large (up to several km²) and may affect almost the whole of a mountain slope. Other active landforms like rock glaciers may be superimposed on the landslide area.

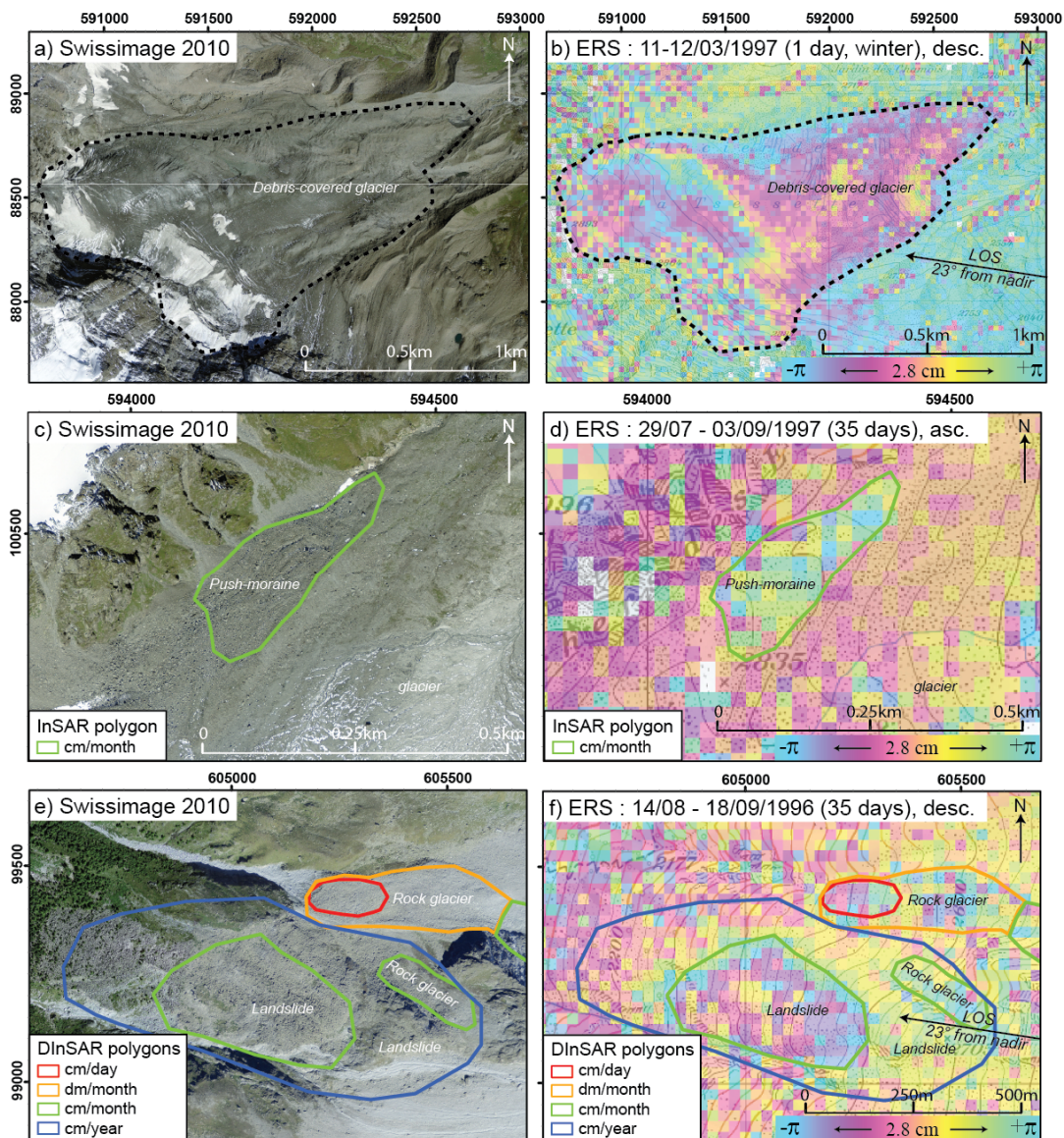


Figure 6.3: Orthoimages of a) the debris-covered glacier of La Tsessette, c) the push-moraine of Ecoulaies, and g) the landslide of Perroc and their respective DInSAR signal on a 1-day interferogram (b) or on monthly interferograms (d and f).

As debris-covered glaciers are not included in the inventory, no polygon is drawn in a) or b). InSAR polygons were determined using a larger series of interferograms than the ones illustrated here (d and f). In spite of all the DInSAR polygons drawn in c to f, the monthly interferograms allow only the detection of DInSAR polygons with dm/month (signal decorrelated) and cm/month ((partly)-fringe pattern).

6.1.3 Conclusion

From this past study, the potential of ERS DInSAR data was demonstrated to: 1) detect moving areas (DInSAR polygons) larger than 0.01 km^2 , occurring on several hundreds of active landforms and displacing faster than 0.01 m/year ; 2) delineate the outline of the polygons with an accuracy of $\pm 25 \text{ m}$; 3) characterize their deformation rate into four categories; and 4) assess for each polygon, sometimes juxtaposed and superimposed in composite slope systems, the related geomorphologic process causing their motion. The joint analysis of DInSAR data and orthoimages, and the verification of DInSAR-detected velocities with DGPS data, has attested to the reliability of ERS DInSAR for inventorying mass movements in remote areas. The construction of the inventory has permitted, in particular, to quantify for the first time the velocity of many landforms (rock glaciers, landslides) for which no data was available so far and to indicate potentially hazardous landforms like very rapid rock glaciers ($1\text{-}3.5 \text{ m/year}$) using the former ERS 1-day and 3-day interferograms. This is a revolutionary technique for short and long term studies of surface deformation in not only Alpine environments, but also in other mountainous regions.

6.2 Moving landforms monitored by DGPS in the Western Swiss Alps

6.2.1 Generalities

Among all of the detected active landforms in the region of interest, twenty-six are annually or seasonally surveyed by DGPS field measurements, the longest series having been monitored since 2001 (Figure 6.1, Table 6.2). Campaigns are generally performed annually or seasonally: either once a year generally in late June, or twice a year generally in late June and late October.

	<u>Site</u>	<u>Type</u>	<u>Years</u>	<u>DGPS campaigns</u>
Entremont	Petit-Vélan	Rock glacier	2005-...	annual + season.
	Aget (Rogneux)	Push moraine / rock glacier	2001-...	annual + season.
	Mille	Rock glacier	2003-...	multi-year
	Six Blanc	Landslide / solifluction	2007-...	multi-year
Mont-Gelé	Lapieres	Rock glacier	2008-...	annual + season.
Val d'Hérens	Vendes	Landslide	2007-...	multi-year
	Perroc	Landslide	2005-...	multi-year
	Tsarmine	Rock glacier	2005-...	annual + season.
Réchy/Moiry	Réchy (Becs-de-Bosson)	Rock glacier	2004-...	annual + season.
	Lona	Rock glacier	2004-...	multi-year
Anniviers	Bonnard (Péterey)	Rock glacier	2006-...	Annual
Mattertal	Grosse Grabe	Rock glacier	2007-...	annual + season.
	Breithorn	Landslide	2009-...	annual + season.
	Gugla	Rock glacier	2007-...	annual + season.
	Längenschnee	Landslide	2007-...	Annual
	Dirru	Rock glacier	2007-...	annual + season.
	Grabengufer	Rock glacier	2008-...	annual + season.
	Grabengufer	Landslide	2009-...	annual + season.
	Chessi	Rock glacier	2009-...	annual + season.
	Chessi	Debris-covered glacier	2009-...	annual + season.
	Gänder	Rock glacier	2009-...	annual + season.
Saastal	Jegi	Rock glacier	2009-...	annual + season.
	Gruben	Rock glacier	2012-..	annual + season.
Aletsch	Moosfluh	Landslide	2007-...	annual + season.
	Grosses Gufer	Rock glacier	2007-...	Annual

Table 6.2: List of Alpine landforms monitored by DGPS campaigns located in the Western Swiss Alps and covered by past ERS DInSAR campaigns.

6.2.2 Characteristics of landforms

The test sites consist of different landform types (sixteen rock glaciers, one push moraine, seven landslides and one debris-covered glacier). The characteristics of these twenty-six landforms are summarized in table 6.3. All of them are located in the Alpine periglacial belt, and specifically in between 2000 and 3000m (Figure 6.4). Most of them occur on moderately steep slopes (12° to 34°) and their surface areas vary from a few hectares to 178 hectares. The characteristics concerning the amplitude and direction of their mean annual displacements monitored by DGPS measurements are

given in Table 6.3. The mean annual velocity rate of these twenty-six landforms ranges from some centimeters to several meters per year.

<i>Site</i>	<i>Elevation (m)</i>	<i>Orientation</i>	<i>Surface (ha)</i>	<i>Slope (°)</i>	<i>Annual velocity (m/y)¹</i>
Petit-Vélan	2450-2800	NE	9.5	26	0.85-5.35
Aget	2825-2900	E	6.5	18	0.05-0.25
Mille	2330-2440	NE	3.0	22	0.02
Six Blanc	2200-2400	N	3.0	26	0.01-0.25
Lapires	2600-2700	NE	7.0	32	1.05
Vendes	2100-2300	NE	23.5	25	0.01-0.6
Perroc	2310-2660	W	12.0	33	0.02-0.08
Tsarmine	2460-2640	W	7.5	23	2.15
Réchy	2640-2830	NW	25.0	19	0.85-1.2
Lona	2640-2800	NE	7.5	17	0.05-0.25
Bonnard	2800-3200	SW	37.0	21	0.55-1.20
Grosse Grabe	2340-2700	W	15.5	33	0.25-3.25
Breithorn	2600-3178	W	49.0	29	0.15-0.55
Gugla	2620-2950	W	9.5	26	1.6-17.4
Längenschnee	2560-2640	W	3.0	33	0.2
Dirru	2380-3160	NW	25.0	27	0.9-7.3
Grabengufer RG	2350-2770	NW	10.0	34	10-115
Grabengufer L	2670-3000	NW	23.5	34	0.25-0.55
Chessi RG	2490-3050	NW	16.0	27	0.2-0.8
Chessi CG	2800-3000	NW	12.5	21	1.1
Gänder	2400-2900	NW	19.0	27	0.6-2.5
Jegi	2440-2740	W	10.0	24	0.25-2.45
Gruben	2760-2900	SW	35.5	12	0.3-1.15
Moosfluh	1750-2330	NW	178.0	26	0.08-0.45
Grosses Gufer	2350-2620	NW	19.5	23	1.85-2.4

¹The range of the annual horizontal velocity is indicated for the whole landform and derived from the last DGPS campaign in early 2014.

Table 6.3: Characteristics of the twenty-six landforms monitored by DGPS in the region of interest.

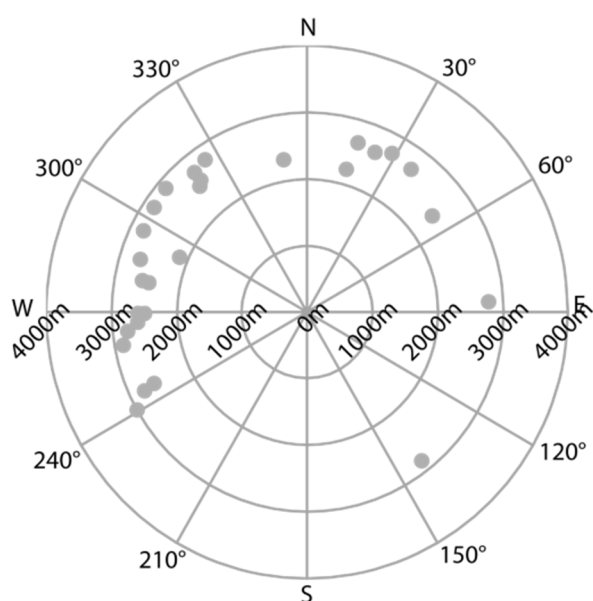


Figure 6.4: Elevation and orientation of the twenty-six monitored landforms.

6.2.3 Direction of a landform's displacement at each DGPS position

As discussed in Chapter 3 (Part 3.3), before proceeding to the proof-of-concept study to assess the potential of the new TSX DInSAR data to map and monitor slope movements in the region of interest and in order to estimate the maximal measurable deformation rate, it is required to verify the assumption that deformation is directed along the slope direction. To perform this verification, the direction of the landform's displacement is compared with the highest slope direction at each DGPS position for two resolution levels: 25 meters using DHM25 (©Swisstopo 2010) and 2 meters using SwissAlti3D (©Swisstopo 2013).

The direction of the displacement is characterized by two parameters: the vertical inclination of the displacement (difference in elevation) and the horizontal orientation of the displacement (regarding the north direction). These two parameters can be estimated from DGPS measurements using the following equations:

$$\text{Inclination } n = a \tan \left(\frac{\text{vertical disp.}}{\text{horizontal disp.}} \right)$$
$$\text{Orientation } n = a \tan \left(\frac{\text{disp. West} - \text{East}}{\text{disp. South} - \text{North}} \right)$$

The values of the horizontal orientation and the vertical inclination of the local slope are extracted for each DGPS position by calculating them from the adjacent cells of each DEM using bilinear interpolation. Then, the direction of the displacement given by DGPS measurements from seasonal, annual or multi-year campaigns is compared to these extracted values at each DGPS position. The smallest interval between DGPS measurements showing significant displacements (set to 10 cm/y) is chosen for the calculation of the displacement direction. Finally, the mean differences over each landform are given in Table 6.4.

The displacements of these observed landforms are more or less 10.0° directed towards the highest local slope orientation and are more or less 18.2° directed towards the highest local slope inclination regardless of the resolution of the DEM used to estimate the local slope direction.

<i>Site</i>	<i>Measures</i>	<i>≠ with SwissAlti3D</i>		<i>≠ with DHM25</i>	
		<i>Inclination (°)</i>	<i>Orientation (°)</i>	<i>Inclination (°)</i>	<i>Orientation (°)</i>
Petit-Vélan	annual + season.	7.3	12.8	5.9	12.8
Aget (Rogneux)	annual + season.	14.9	14.3	14.6	12.0
Mille	multi-year	16.1	13.5	15.9	10.2
Six Blanc	multi-year	2.1	8.1	5.6	14.0
Lapires	annual + season.	5.4	15.9	4.4	8.0
Vendes	multi-year	7.4	16.4	7.9	27.5
Perroc	multi-year	9.1	15.8	8.6	11.6
Tsarmine	annual + season.	5.7	10.4	5.1	13.2
Réchy (Becs-de-Bosson)	annual + season.	8.0	25.4	8.0	16.6
Lona	multi-year	30.5	21.0	31.1	30.9
Bonnard / Péterey	Annual	11.1	24.1	22.5	16.3
Grosse Grabe	annual + season.	8.1	15.3	7.7	19.2
Breithorn	annual + season.	10.7	25.0	8.6	22.0
Gugla	annual + season.	4.4	15.8	4.6	15.3
Längenschnee	Annual	6.2	7.2	6.5	7.3
Dirru	annual + season.	6.0	17.1	5.7	17.1
Grabengufer RG	annual + season.	9.4	9.9	7.7	9.9
Grabengufer L	annual + season.	9.7	33.2	8.3	33.2
Chessi RG	annual + season.	11.9	10.0	12.0	10.0
Chessi CG	annual + season.	18.4	9.7	18.8	17.1
Gänder	annual + season.	5.1	14.5	5.8	14.4
Jegi RG	annual + season.	5.2	22.6	5.5	13.1
Gruben	annual + season.	19.0	26.4	20.5	19.8
Moosfluh	annual + season.	12.6	58.1	13.2	25.0
Grosses Gufer	Annual	4.7	14.7	5.4	7.87
AVERAGE		10.0	18.2	10.4	16.2

Table 6.4: Differences between the displacements direction derived from DGPS measurements and the local slope direction derived from DEM in terms of orientation and inclination at two resolution levels: 25 meters using DHM25 and 2 meters using SwissAlti3D.

6.2.4 Conclusion

Twenty-six landforms are monitored with seasonal, annual or multi-year DGPS measurements in the region of interest. Their distribution seems to be representative of the region by their location, aspect, elevation and velocity. As seen in Chapter 3, before proceeding to the proof-of-concept study, it is useful to verify the assumption of deformation directed along the slope direction. According to Section 6.3.3, this assumption is verified at 10.0° for the slope inclination and 18.2° for the slope orientation for the twenty-six monitored Alpine landforms located in the region of interest and confirms the possibility to use the methodology of the proof-of-concept study presented in Chapter 3 (Part 3.3). In the next part, this proof-of-concept study is used to assess the suitability of the new TSX DInSAR data to map and monitor Alpine landforms located in this specific region of interest.

6.3 Suitability of TSX DInSAR data in the Valais

6.3.1 Visibility

Six different stripmaps of TSX SAR data are used to observe the region of interest: three in ascending mode and three in descending mode (Figure 6.5).

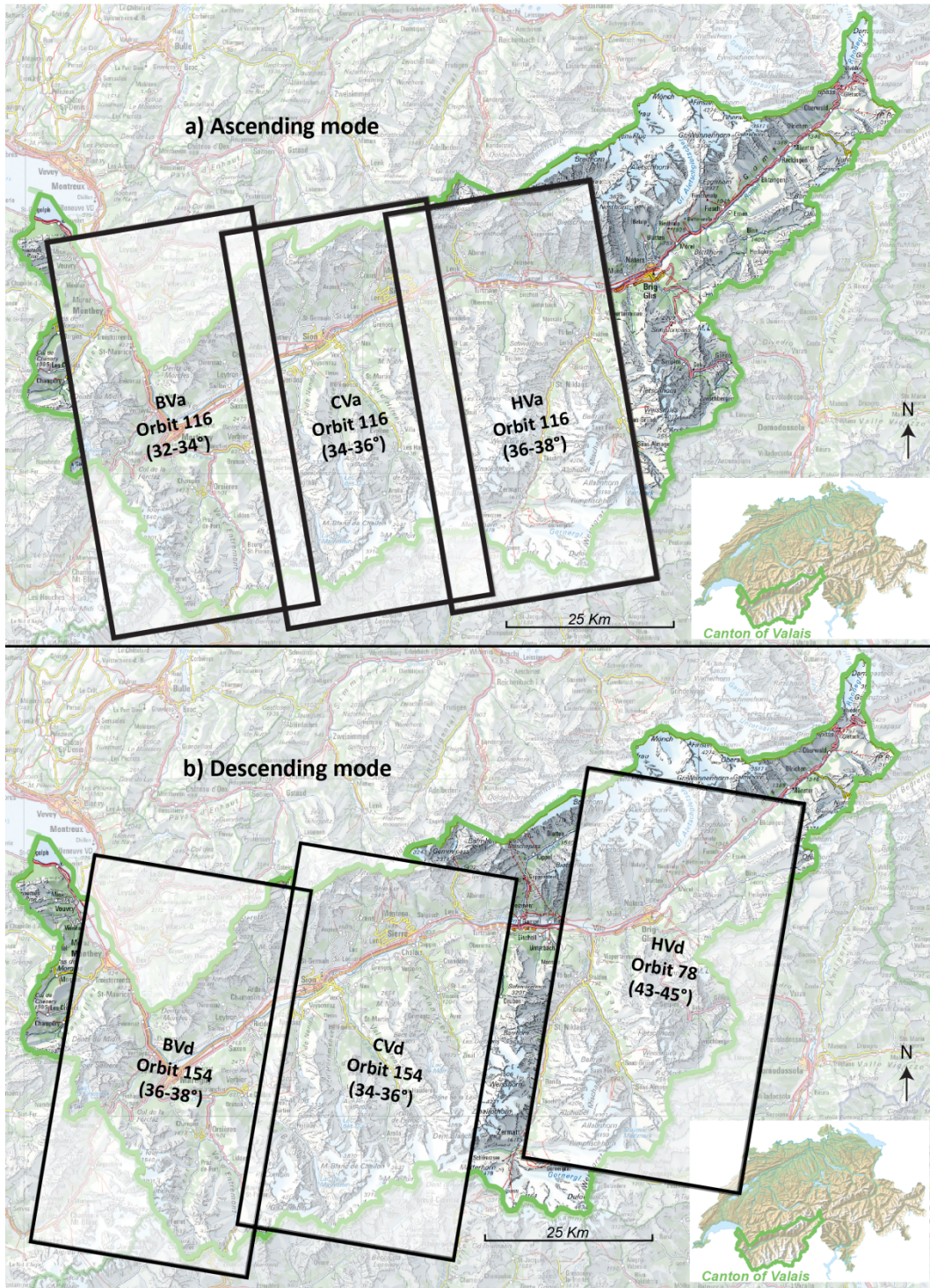


Figure 6.5: Stripmaps of TSX SAR data over the region of interest.

To estimate the visibility of TSX DInSAR data in the studied region, the mask of layover and shadow was computed using the Gamma function *gc_map*. The results are summarized in Table 6.5 and show that 85% of the Alpine periglacial belt in the Valais (digitized manually from the tree line to the bottom of the glaciated area) are visible by TSX DInSAR. Remaining areas are either masked by layover or shadow, or not covered by the selected stripmaps. Almost 50% of this belt is visible in both modes.

		VALAIS		VALAIS periglacial area		Movement Slopes (inventories from 1991-2000)	
		Surface (km ²)	Proportion (%)	Surface (km ²)	Proportion (%)	Surface (km ²)	Proportion (%)
Ascending	No cover	1760.5	33.72	1022.5	38.63	38.2	25.41
	Visible	3460.5	66.28	1624.4	61.37	112.2	74.59
Descending	No cover	1138.3	21.80	684.5	25.86	11.8	7.83
	Visible	4083.1	78.20	1962.5	74.14	138.6	92.17
Ascending OR descending	No cover	627.1	12.02	379.1	14.32	3.7	2.48
	Visible	4592.2	87.98	2267.7	85.68	146.7	97.52
Ascending AND Descending	No cover	2267.6	43.45	1318.9	49.83	46.3	30.77
	Visible	2951.8	56.55	1327.8	50.17	104.2	69.23
Total		5220 km²		2650 km² (50.8% of the Valais)		150 km² (2.9% of the Valais)	

Table 6.5: Proportion of the Western Swiss Alps that is covered by TSX DInSAR data. The periglacial area is digitized manually from the tree line to the bottom of the glaciated area.

The visibility is also estimated for each of the twenty-six observed landforms. Table 6.6 expresses the percentage of visibility for each observed landform using ascending and descending modes. These landforms are generally more visible using descending mode.

<i>Site</i>	<i>Ascending</i>	<i>Descending</i>	<i>DMax Asc. (m/y)</i>	<i>DMax Desc. (m/y)</i>	<i>Orientation (°)</i>
Petit-Vélan	100.0	96.7	0.82	2.22	24
Aget (Rogneux)	100.0	100.0	0.86	4.02	141
Mille	100.0	79.2	0.69	3.21	54
Six Blanc	90.5	100.0	1.12	1.21	352
Lapires	100.0	94.9	0.87	1.40	18
Vendes	100.0	100.0	1.01	1.91	16
Perroc	38.8	100.0	X	0.55	280
Tsarmine	95.2	100.0	2.77	0.62	280
Réchy (Becs-de-Bosson)	100.0	100.0	3.21	0.90	325
Lona	100.0	98.9	0.98	2.32	29
Bonnard /Péterey	46.7	99.9	2.37	0.72	240
Grosse Grabe	3.7	75.9	X	0.52	270
Breithorn	49.9	96.4	X	0.55	260
Gugla	70.2	99.9	2.88	0.56	264
Längenschnee	0.7	87.2	X	0.52	266
Dirru	94.8	100.0	3.61	0.59	303
Grabengufer RG	63.7	99.1	X	0.58	310
Grabengufer L	34.5	72.3	X	0.63	320
Chessi RG	92.5	98.3	3.75	0.57	296
Chessi	78.3	97.7	2.82	1.01	334
Gänder	98.0	100.0	2.30	0.73	320
Jegi RG	91.7	99.0	2.85	0.56	268
Jegi L	98.2	100.0	2.37	0.58	245
Gruben	99.5	99.8	2.01	0.62	240
Moosfluh	0.0	99.0	X	0.71	293
Grosses Gufer	0.0	100.0	X	0.73	319

Table 6.6: Percentage of visibility of the twenty-six landforms using TSX data. The maximum measurable deformation rate is expressed for ascending and descending mode. Orientation of the landform is also indicated.

6.3.2 Maximum measurable deformation rate

Theoretically, the maximum measurable deformation rate $DMax_{LOS}$ in the LOS direction is one fringe per pixel per time difference between the two acquisitions forming the interferogram. For instance, using TerraSAR-X data with a wavelength of 3.1 cm and the shortest time interval of 11 days, $DMax_{LOS}$ is equal to 0.51 m/year. If the deformation rate exceeds this threshold the signal will be decorrelated (see section 3.2.4). The maximum measurable deformation rate along the slope direction $DMax_{HS}$ can be computed using the following equation:

$$DMax_{HS} = \frac{DMax_{LOS}}{Md_{HS}}$$

Md_{HS} is the index defined as the dot product between the unit vector in the maximum slope direction e_{HS} and the unit vector in the LOS direction e_{LOS} . The maximal measurable deformation rate is computed for this study at 25 meters sampling for the whole landform. As explained in Subsection 3.3.2.2, the unit vector e_{HS} is calculated thanks to parameters given by the Gamma functions *gc_map* using the DHM25, and e_{LOS} thanks to parameters given by the Gamma function *look_vector*. Finally, $DMax_{HS}$ is deduced for the twenty-six landforms using the equation given above at 25 meters sampling.

The maximal measurable deformation rate is averaged over the whole landform for each mode and illustrated in Figure 6.7. Results show that the mode has a strong influence on the maximum value of $DMax_{HS}$ according to the orientation of the landform.

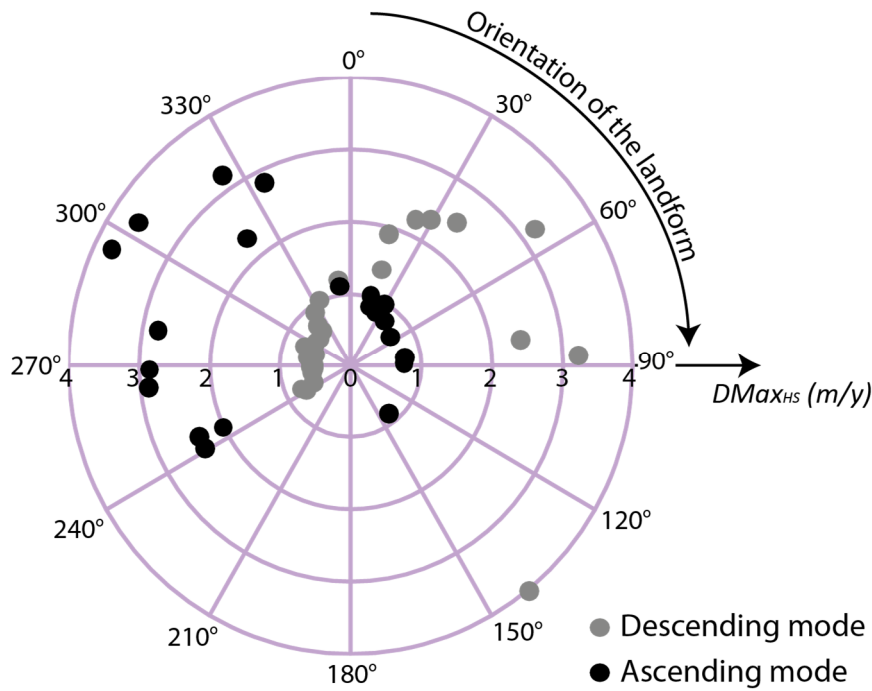


Figure 6.6: Maximum measurable deformation rate according to the orientation of the landform.

For most of the west-oriented landforms, results show that $DMax_{HS}$ can reach 1 m/y in descending mode, and 3.5 m/y in ascending mode; the reverse phenomenon appears for east-oriented landforms. $DMax_{HS}$ usually reaches about 1 m/y in both ascending and descending modes for north-oriented slopes.

The influence of the incidence angle of TSX (full capacity between 20° to 55°) is also investigated for each landform to see if it is suitable to survey them with different incidence angles using orbits other than the ones selected. An example of results for the west oriented Tsarmine rock glacier is shown in Figure 6.7. For most of the west-oriented landforms, the incidence angle has generally little influence on $DMax_{HS}$ in ascending mode, which can reach 7 to 8 m/y for some of these landforms. However, due to steep topography, large layover and distortions could occur on landforms for this mode and this kind of incidence angle. In the descending mode, the incidence angle usually has no influence on $DMax_{HS}$. The reverse phenomenon appears for east-oriented landforms.

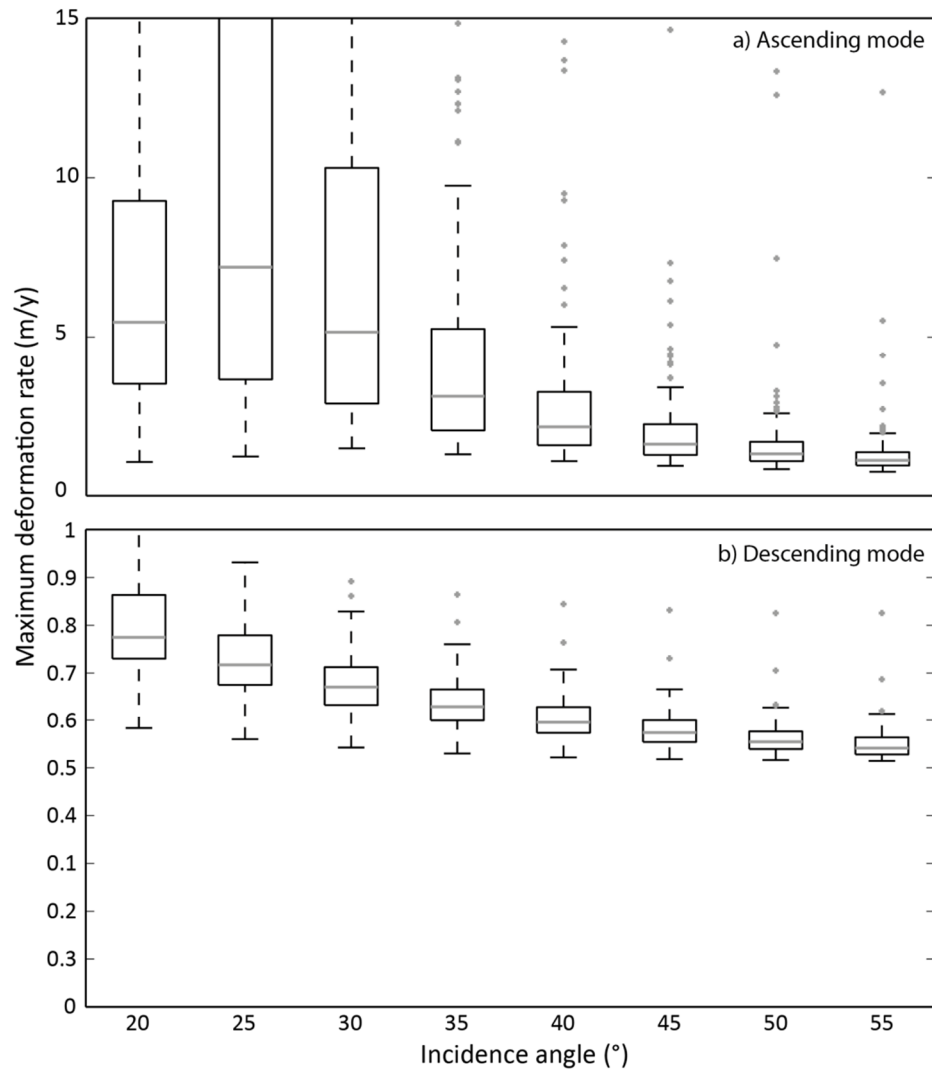


Figure 6.7: Example of maximum measurable deformation rate in the highest slope direction for the west oriented Tsarminé rock glacier according to incidence angle in a) ascending mode and b) descending mode. The bottom and top of the box, the gray line and gray crosses show respectively the upper and lower quartiles, the median value and outliers.

6.3.3 Discussion

As discussed in Chapter 3, Section 3.2.4, the rate of terrain movement which can be detected depends, among others, on the time interval and on the wavelength (Figure 3.5). The interferometric SAR signal will decorrelate when the deformation (displacement gradient between adjacent pixels) is higher than half the wavelength during the selected time interval (Massonnet and Feigl, 1998). This means that the decorrelation occurrence is favored by the roughness of the surface and the displacement rate. The time interval over which the displacement is measured must be matched to the observed surface deformation (Rosen et al., 2000). Moreover, the nature of the change within a pixel can introduce noise in the measuring phase difference (Klees and Massonnet, 1999).

Some comparisons are performed combining DInSAR observations and DGPS measurements. As a first approximation, the velocity of each surveyed DGPS position is compared to the theoretical

maximal deformation rate measurable at this position in the LOS direction. When the velocity given by DGPS measurement and projected in the LOS direction is lower than $DMax_{LOS}$, the DGPS position is classified as detectable. In the opposite situation, the DGPS position is classified as undetectable.

In most cases, the DGPS position classification corresponds to the DInSAR observation (in terms of correlated and decorrelated DInSAR signal). However, some cases reveal incorrect evaluations of the visibility mainly due to the fact that the maximal deformation rate is not directly related to the velocity (but rather its spatial derivative). Thus, it is sometimes possible to detect a higher velocity rate than indicated. Past studies using ERS technologies have shown that decorrelation occurs when the velocity rate is up to $\lambda/2$ for these kinds of slope instabilities where roughness is an important factor (Delaloye et al., 2007b). There seems to be a higher limit of rate for TSX.

As seen in Figure 6.8, the Tsarmine rock glacier reached a mean velocity of 1 m/y during summer 2010. Its frontal part was moving almost 1.5 m/y. As expected from previous results, this area was not decorrelated in ascending mode, and was decorrelated in descending mode. Consequently, the comparison of $DMax_{LOS}$ and the annual velocity known through DGPS campaigns shows that the landform could be correctly observed in ascending mode. The two red points classified as undetectable on Figure 6.8b are an illustration of the limitation explained before.

Lastly, as previously discussed in Subsection 3.3.5.1 and in order to be more accurate, it would be interesting to compute the maximum measurable deformation rate in the actual displacement direction of the observed landforms rather than in the highest slope direction. However, the proposed proof-of-concept study is only used here to assess the potential of TSX DInSAR data for the observation of Alpine slopes in the Western Swiss Alps, and to roughly estimate the maximum deformation rate that can be quantified in this specific region.

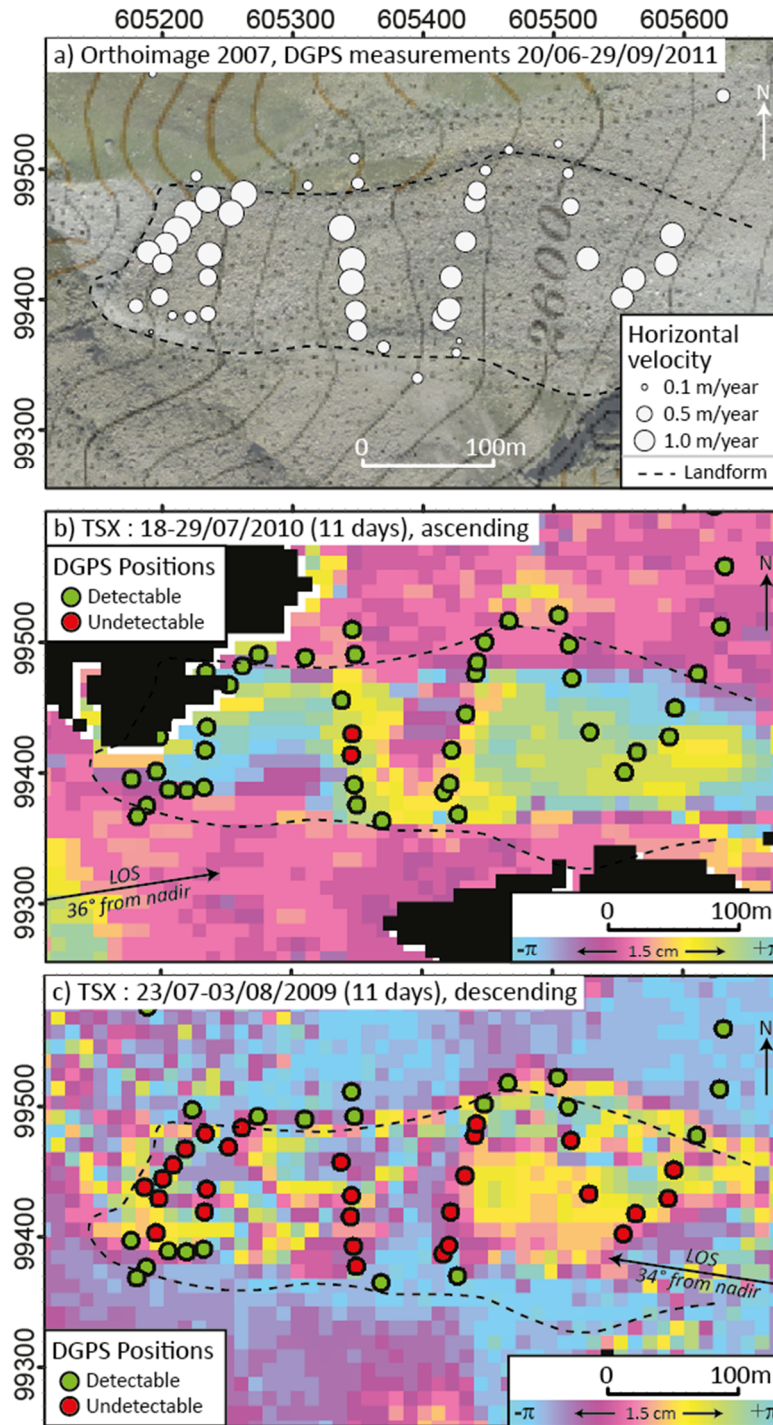


Figure 6.8: Example of a rapidly moving landform. a) Orthoimage of the Tsarmine rock glacier (2005). Location of DGPS positions detectable (green) and undetectable (red) by TSX DInSAR data using (b) ascending and (c) descending modes. Layover and shadow are masked in black.

6.3.4 Conclusion

According to the proof-of-concept study, TSX DInSAR data appears to be suitable for mapping slope movements in the Western Swiss Alps where more than 83% of the Alpine periglacial belt (digitized manually from the tree line to the bottom of the glaciated area) is visible with the selected stripmaps of TSX DInSAR data. Moreover, it is possible to monitor some very active rock glaciers (1-3.5 m/y),

when geometrical distortions do not hide them, with the shortest time interval of 11 days using the ascending mode. Lower deformation rates could be well monitored using longer time intervals and both modes. At higher deformation rates, decorrelation occurs in most cases using both modes and TSX appears to be unsuitable for a precise analysis of these very rapidly moving landforms.

6.4 Conclusion

DInSAR technique is particularly suitable to detect and monitor Alpine landforms, especially in the periglacial belt of the Western Swiss Alps with no densely vegetated areas. As seen in the previous chapter, the suitability of DInSAR technique for applications in an Alpine environment is discussed in many studies that have assessed the capability of DInSAR for analyzing slope movements and pay attention to the large number of requirements to select, analyze and interpret DInSAR correctly in this specific topographical context. In the Western Swiss Alps, past studies show the potential of ERS DInSAR data: for the detection of moving areas (DInSAR polygons) larger than 0.01 km², occurring on several hundreds of active landforms and displacing faster than 0.01 m/year; for the delineation of the outline of the polygons with an accuracy of +/-25 m; for the characterization of their deformation rate into four categories; and for the assessment of each polygon, sometimes juxtaposed and superimposed in composite slope systems, of the related geomorphologic process causing their motion. In the region of interest more than 1500 active landforms were detected thanks to this technique, and among them twenty-six are currently observed by DGPS measurements. The joint analysis of DInSAR data and orthophotos, and the verification of DInSAR-detected velocities with DGPS data, have attested to the reliability of ERS DInSAR for inventorying mass movements in remote areas.

One of the main objectives now would be to update (changes in activity rate) and upgrade (more accurate identification of active landforms and quantification of displacement rate) these inventoried creeping landforms, particularly the active rock glaciers in the region of interest using current TSX DInSAR data. According to the proof-of-concept study, the new TSX DInSAR data appears to be suitable for mapping slope movements in the Western Swiss Alps where more than 83% of the Alpine periglacial belt is visible. Moreover, it is theoretically possible to monitor rapidly moving landforms with a maximal measurable deformation rate of 3.5 m/y using facing mode. Thus, by combining TSX DInSAR analysis with field measurements, needed in most cases to validate and confirm observations at a local scale, the new TSX DInSAR data has a strong potential for surveying active rock glaciers and other kinds of rapidly moving Alpine landforms located in the periglacial belt of the Western Swiss Alps.

7 Mapping of slope movements in the Western Swiss Alps with DInSAR: pilot studies and promising applications

In this chapter, two applications for the mapping of Alpine slope movements are proposed to illustrate the potential of slope movement maps developed in Chapter 4. The first application proposes methods for the update and upgrade of past inventoried DInSAR polygons (Part 7.1). The second one aims to refine and assess glacier outlines over debris-covered glaciated areas (Part 7.2). Finally, a conclusion sums up the main results observed from these two applications (Part 7.3).

7.1 Update and upgrade of DInSAR polygon inventory

The main objective of this application is to – so far as possible – automatically update past inventoried DInSAR polygons by integrating the most recent data to detect potential changes in the activity rate of landforms, and upgrade them by giving a more accurate identification of active landforms and quantification of displacement rate. In order to obtain this up to date information, a large set of TSX DInSAR data (2008-2012) is used, analyzed and interpreted (Section 7.1.1). First, a procedure to visually update and upgrade DInSAR polygon inventories is given in Section 7.1.2. Then a procedure is presented using slope movement mapping derived from DInSAR signal analysis in order to update automatically the inventoried DInSAR polygons (Section 7.1.3). The performance of these two approaches is evaluated in Section 7.1.4. A discussion and a conclusion are finally proposed in Sections 7.1.5 and 7.1.6 respectively. This section is extracted and adapted from Barboux et al. (2013a).

7.1.1 Study site and data processing

7.1.1.1 *Jegi rock glacier area and TSX dataset*

In this section, the restricted Jegi rock glacier area already presented in part Subsection 4.1.2.3 (Figure 4.3) is chosen in order to show the potential use of slope movement maps for the automated update of past inventoried DInSAR polygons. The complete TSX dataset presented in Subsection 4.1.2.3 and processed using standard steps were used (Table 4.1).

7.1.1.2 *DInSAR signal and slope movement maps*

The use of model II with a grid resolution of 25 meters, showing good accuracy and precision for each type of slope movement, was chosen to compute the sixteen maps of slope movements (one for each time interval) according to the presented method in Chapter 4. The classification of the slope

movement map is defined in terms of the DInSAR signal and the related slope movements according to the 3 following classes: 1) plain pattern = no deformation rate, 2) (partly) fringe pattern = gentle deformation rate and 3) noise pattern = large deformation rate. The NaN class is used when the algorithm was not able to determine the right class (for details see Chapter 4).

7.1.2 Visual update and upgrade of past inventoried DInSAR polygons

7.1.2.1 Methodology

The methodology for the visual update and upgrade of slope movement inventories aims a) to identify the new moving landforms over the region, b) to spatially renew the outline of the past inventoried DInSAR polygons, c) to categorize (or update) the deformation rate of the detected DInSAR polygons and d) to eliminate possible errors (or no longer moving areas) of the past inventories.

As with the previous visual methodology presented in Section 4.1.1, the detection of movement is performed by looking for a fringe pattern and/or noise on an interferogram, which means looking at a single pixel according to its neighbors together. In this study, the slope movement maps are used as a useful tool for visual interpretation. As explained in Chapter 4, Part 4.3, the pixels of the slope movement maps are classified into the most represented class of DInSAR signal in the set of selected interferograms having the same time interval. The maps are used here to evaluate the similarity of the DInSAR signal over a large selected set of DInSAR pairs and to prevent from misinterpretation of single artifacts visible on few analyzed pairs.

The estimation of the deformation rate is then performed by assessing qualitatively the DInSAR signal and related deformation rate that can be observed on interferograms with different time intervals. The four defined categories of deformation rate defined for the previous inventory – namely the “cm/day”, “dm/month”, “cm/month” and “cm/year” – are kept for this analysis as they allow a good separation of the movement rates with the observed TSX DInSAR signal and are suitable to describe the geomorphic features observed in the Alpine periglacial belt of the Western Swiss Alps.

7.1.2.2 Results

Figure 7.1 shows the visual upgrade of the studied area. A lot of DInSAR polygons have been separated into different objects and numerous new moving objects are found. Few new moving landforms have been identified. The outlines of the past inventoried polygons have been renewed due to the new high spatio-temporal resolution of TSX data. Few polygons show changes in terms of velocity rate.

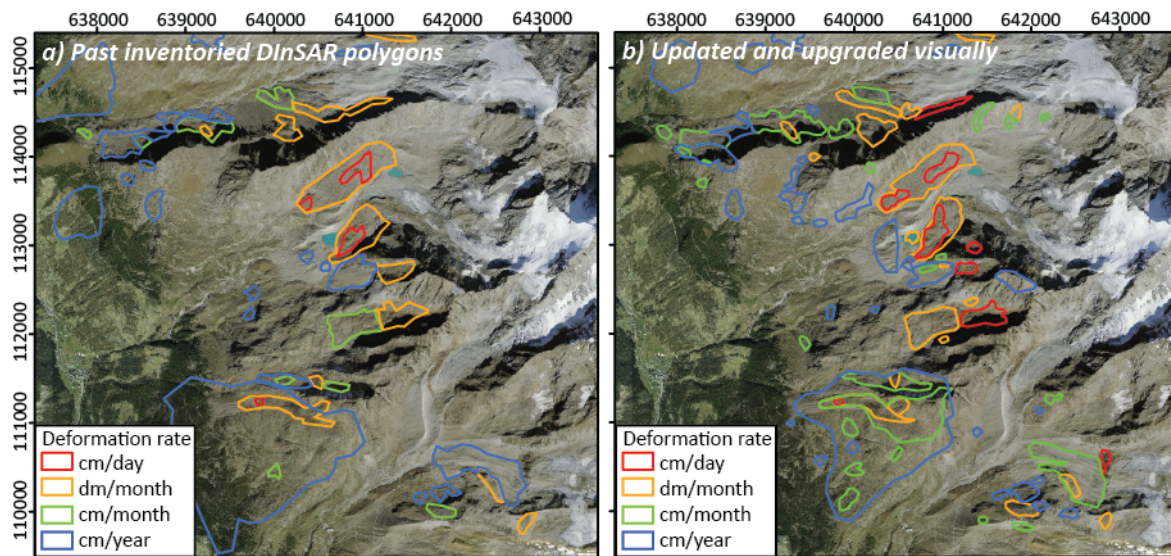


Figure 7.1: Manual update and upgrade of past inventoried DInSAR polygons in the Jegi rock glacier area.

7.1.3 Automatic update of DInSAR polygon inventory

7.1.3.1 Methodology

As discussed in Chapter 5 (Subsection 5.3.1.1), it is possible to roughly evaluate the deformation rate on a spatially outlined area with an almost homogeneous deformation rate by analyzing the evolution according to time of each portion of slope movement given by the automated mapping. From the sixteen maps of slope movements, two thresholds can be detected: 1) s_{stab} corresponding to the time interval until which the proportion of plain pattern (no deformation) is higher than 50% and 2) s_{dec} corresponding to the time interval from which the proportion of noise pattern (large deformation) is higher than 50%. The period in between these two thresholds represents the time intervals where (partly) fringe pattern can be observed (gentle deformation). Then, the deformation rate can be evaluated according to the 4 categories of deformation rate “cm/year”, “cm/month”, “dm/month” and “cm/day” (for details see Subsection 5.3.1.1). The corresponding DInSAR polygon is finally updated. It is thus possible to detect a potential change in the activity rate of landforms.

7.1.3.2 Results

Figure 7.2 shows the automated update of the deformation rate observed on past inventoried DInSAR polygons. Several polygons show changes in terms of velocity rate and will be compared with the visual update (Part 7.1.4) in order to see if these changes can be truly attributed to an acceleration or deceleration of the landform.

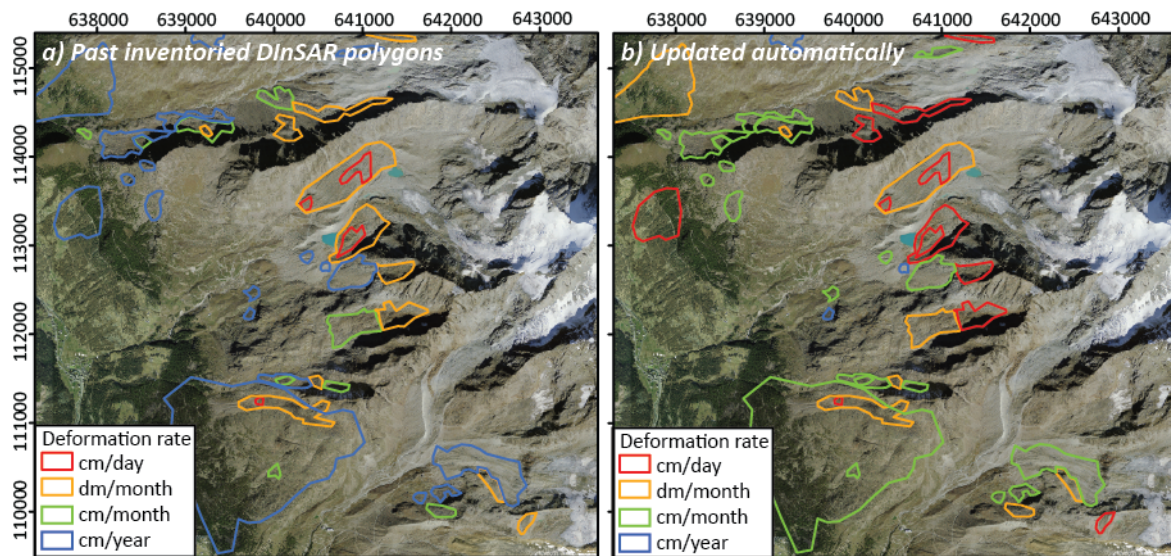


Figure 7.2. Result of semi-automated change in velocity rate detection of the past inventoried DInSAR polygons.

7.1.4 Performance

To evaluate the performance, the automated update of past inventoried DInSAR polygons is compared to the visual update and upgrade.

7.1.4.1 Deformation rate classification

The first observation looks at the correct deformation rate classification by comparing the classification of deformation rate given by the automated method with the classification given by the visual interpretation whatever the change of the outline of the considered DInSAR polygons. The confusion matrix related to the classification of deformation rate is computed and counts the number of past inventoried DInSAR polygons assigned to a class of deformation rate by the automated process against the reference class of deformation rate visually interpreted (Table 7.1). An additional class “-” is defined for past inventoried DInSAR polygons no longer detectable with the newer TSX DInSAR data.

		Automatically classified as				
		cm/d	dm/m	cm/m	cm/y	NaN
Visually classified as	cm/d	6	6	0	0	0
	dm/m	13	5	8	0	0
	cm/m	12	0	0	12	0
	cm/y	11	0	1	6	3
	NaN	2	1	0	1	0

Ao: 0.68 k: 0.58

Table 7.1: Confusion matrix of automatic and manual deformation rate classification of the past inventoried DInSAR polygons localized in the region of interest. Each column represents the occurrence in the predicted class (automated), while each row represents the visually observed occurrence in each class (reference).

The automatic update of DInSAR polygons deformation rate is acceptable with an average error of 0.68. The kappa index of 0.58 shows a moderate agreement.

It has to be noted that a change of thresholds used to identify s_{stab} and s_{dec} (for instance a proportion of respective patterns higher than 40% or 60%) does not imply a change in the automated velocity rate classification. Actually, the period in between s_{stab} and s_{dec} , representing the time intervals where (partly) fringe pattern can be observed (gentle deformation), is simply extended or reduced while staying centered on the same range of time intervals and thus the same final classification of velocity rate is identified.

Wrong velocity rate classifications are often associated with a misclassification to a faster class of velocity. These results mainly come from the fact that the DInSAR signal is detected and interpreted as noise pattern on a shorter time interval than it should be due to the presence of noise.

7.1.4.2 Change detection

The second comparison aims to evaluate the use of this automated update of past inventoried DInSAR polygons to detect potential changes in the deformation rate of the landforms. In this case the change detection is defined as a change detected in the class of deformation rate. This change is compared with a potential change in terms of deformation rate of the landforms given by the visual interpretation. The confusion matrix related to the change detection is computed and counts the number of past inventoried DInSAR polygons located in the studied area assigned to a change in the deformation rate detected automatically against the reference visually interpreted.

		Automatically classified as	
		change	No change
Visually classified as	Change	14	0
	No change	30	18
		Ao: 0.73	k: 0.49 Sensitivity: 1 Specificity: 0.60

Table 7.2: Comparative Classification Performance (Confusion matrix) of automatic and manual change in velocity detection on past inventoried DInSAR polygons. Each column represents the occurrence in the predicted class (automated), while each row represents the visually observed occurrence in each class (reference).

The automatic change detection of the past inventoried DInSAR polygons in terms of deformation rate is good with an average error of 0.78. The kappa index of 0.49 shows a moderate agreement. The sensitivity reaches 1 and shows the ability of the algorithm to detect a change in deformation rate. The lower specificity value of 0.6 indicates however that a lot of past inventoried DInSAR polygons are detected as having a change in deformation rate whereas in reality, they do not. Results are discussed in the following part (Section 7.1.5.1).

7.1.5 Discussion

7.1.5.1 *False change detection*

False change detection concerns a total of twelve DInSAR polygons: five DInSAR polygons with a deformation rate of “dm/month” that were automatically detected at “cm/day”; eight DInSAR polygons with a deformation rate of “cm/year”, with six incorrectly classified as “cm/m” and one misclassified as “dm/month”; and two polygons which are not visible anymore and were automatically classified with a deformation rate of “cm/d” or “cm/m” (cross comparison of Table 7.1 and Table 7.2). These false detections are mainly due to external factors such as vegetation, snow or atmosphere (where the signal is noisy), to border effects in neighboring areas, to large seasonal variations in deformation, as well as to a change in the outline of the landform. Some examples are illustrated in Figure 7.3. The two DInSAR polygons 870 and 872 are incorrectly classified with a deformation rate of “cm/day” instead of “dm/month”. By looking at the two DInSAR pairs of 11 days, some parts of these polygons are sometimes decorrelated due to seasonal variations or potentially due to the presence of snow in the upper part. The two polygons 868 and 869 are misclassified due to the new delimitation of the outline. These polygons require a redefinition and subdivision of the outline into more precise polygons discernible thanks to the new high spatio-temporal resolution of TSX data.

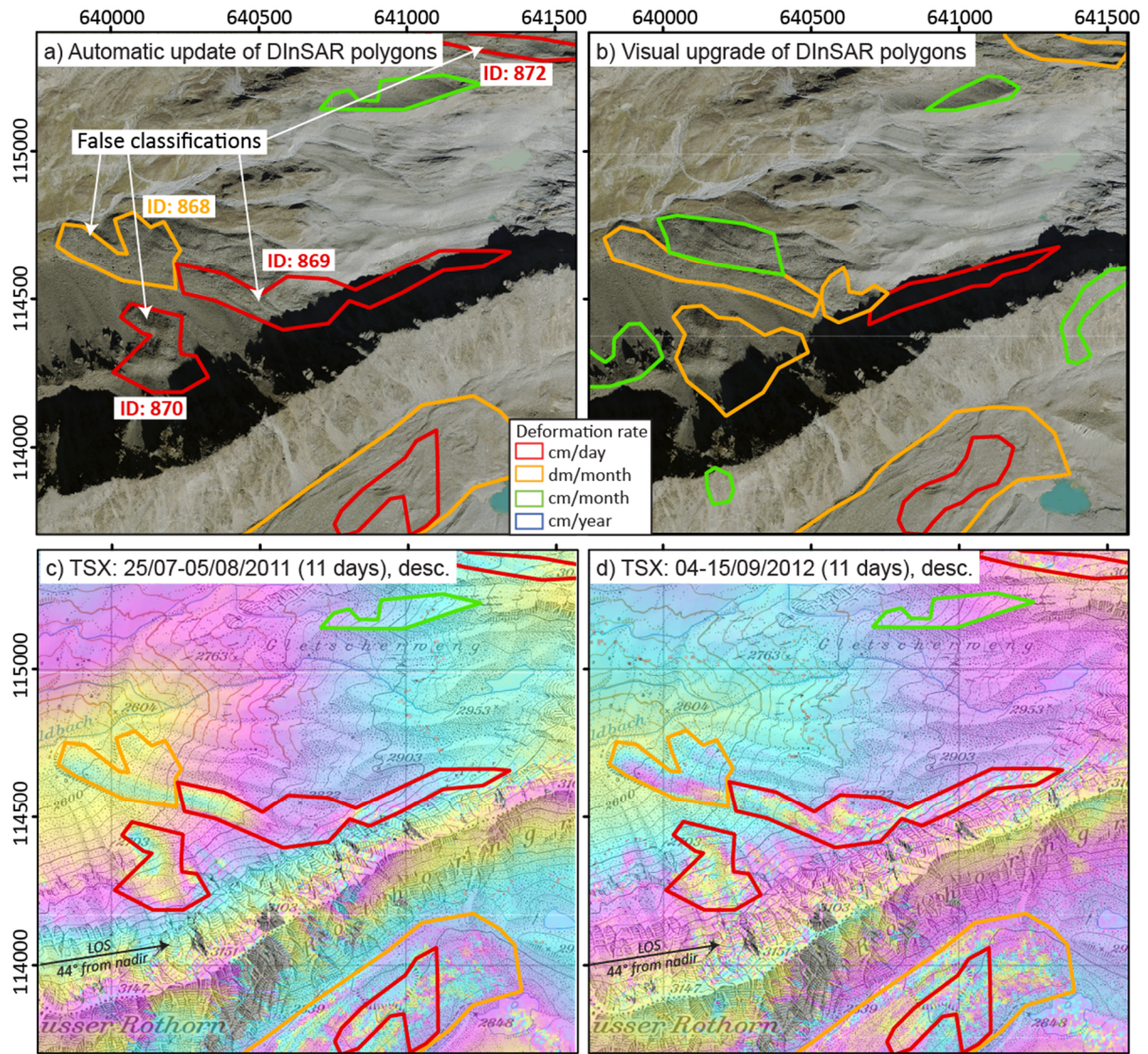


Figure 7.3: Example of false classification in terms of deformation rate of some past inventoried DInSAR polygons using the presented automated algorithm. Misclassified polygons are identified according to their ID code in figure a). a) DInSAR polygons automatically updated. B) DInSAR polygons visually updated and upgraded. c) and d) Examples of DInSAR signal observed on TSX interferograms with a time interval of 11 days.

7.1.5.2 New high spatio-temporal resolution of TSX

The new high-resolution of X-Band TSX provides better information about the landform outline and the landform displacement rate. Specifically, its short X-Band wavelength combined with a short repeated cycle would allow parsing the structure of four categories of velocity rate into more precise subcategories. In other words, new sensors permit the update of inventories (in terms of current deformation rate quantification) but also their upgrade (in terms of identification of the landform outline and finer quantification of landform displacement rate). However, when performing such inventories, the compatibility between different sensors has to be considered in order to allow future updates. Thus the same categories of deformation rate are kept in this study.

7.1.5.3 *Need of manual verification*

The presented method allows for easy identification of past inventoried DInSAR polygons having a change in velocity and is thus a powerful tool to update past inventories. However, to perform the upgrade of the inventory, each of these changing DInSAR polygons has to be manually checked in order to verify if the change is really due to a change in velocity rate and/or if the outline has to be modified. At a regional scale, first observations show that a large number of polygons are changing. Some landforms show current reactivation while others are slowing down. A lot of DInSAR polygon outlines have to be redefined or divided into different objects and numerous new moving objects are visually discovered due to the better definition of TSX data. Finally, the major conclusion from this study is that it is not advisable to automatically detect polygons having a change in velocity from the new TSX data if they were previously derived from another sensor, as here, which were derived from ERS and JERS data. A visual upgrade with the help of slope movement mapping as a useful tool for interpretation of a large DInSAR dataset is probably the best solution to perform an accurate up-to-date inventory.

7.1.6 Conclusion

The slope movement maps developed in Chapter 4 are used here to update and upgrade past inventoried DInSAR polygons in a defined area. Two approaches are proposed:

- a) A visual update and upgrade of DInSAR polygon inventories using slope movement maps to evaluate the similarity of the DInSAR signal over a large selected set of DInSAR pairs and to prevent from misinterpretation of single artifacts visible on only a few analyzed pairs (Section 7.1.2).
- b) An automated update of DInSAR polygon inventories using slope movement maps to roughly estimate the current deformation rate of each polygon (Section 7.1.3).

The two proposed applications were tested and compared in order to evaluate their potential. The method used to automatically detect changes in the deformation rate of DInSAR polygons works reliably. False change detection is mainly due to external factors such as vegetation, snow or atmosphere (where the signal is noisy), due to the border effect in layover and shadow areas, as well as due to a change in the outline of the landform. The method is thus powerful for updating inventories. However, to upgrade them, each of the detected changing DInSAR polygons has to be manually checked, and many new moving zones are not automatically detected. Hence, an automated assessment of Alpine periglacial landform changes based on the existing DInSAR polygon inventory is hardly possible as they differ regarding source of data, format and resolution. For these reasons, any derived changes detected in landform deformation rate using an automated process might be more artificial than real.

Moreover, as shown with the visual update and upgrade of the DInSAR polygon inventory, the simple use of the map of slope movements derived from DInSAR signal analysis can help experts in the detection of new moving areas, as well as in assisting in the development of accurate inventories when using a large set of DInSAR data. Moreover, the manual delineation of the landforms themselves (and not only the DInSAR polygons defined as the parts moving with a homogeneous deformation rate) could allow for the derivation of a change of landform in terms of spatial evolution and change in velocity. However, this requires hard work from analysts specialized in the geomorphology field.

Finally, it is suggested to use an automated update of DInSAR polygons only when the data source is not changing. To reduce working efforts when compiling visual updates of DInSAR polygons over a wide study area, the main recommendation is to reduce the investigated area by giving priority to specific watersheds (Kummert et al. 2014).

7.2 Refining and assessing glacier outlines over debris-covered areas: A pilot study in the Upper Valais

7.2.1 Introduction

The extent of glaciers in the European Alps has been mapped and inventoried consistently. Most of them have been outlined using semi-automated remote-sensing techniques. A major problem when deriving glacier outlines from satellite imagery is detecting debris-covered ice. Promising results using a semi-automatic method combining satellite multispectral images and a digital elevation model have been obtained in the Swiss Alps (Paul et al., 2011). However, even if manual delineation is very time-consuming and work-intensive for a large number of glaciers, it remains the best way to produce an accurate inventory of glacier ice bodies in the Alps, where outstanding data sources are available. For the Swiss Alps, the latest glacier inventory (SGI2010) was derived by manual digitization from high-resolution (25 cm) aerial orthoimages covering the entire Swiss Alps acquired between 2008–2011 (Fischer et al., 2014). In contrast to the known shortcomings of approaches based on satellite remote-sensing, the margins of very small glaciers are (with a few exceptions) clearly distinguishable on these images, even in shaded, snow- or debris-covered areas. The accuracy of this inventory was assessed by comparing the extents of clean, snow- and/or debris-covered glaciers derived from multiple digitizations by several experts.

A pilot study was conducted in the reduced region of interest of the Mischabel massif to refine and assess the accuracy of inventoried glacier outlines over debris-covered areas using DInSAR combined with airborne photography interpretation. First, the concept of the detection of debris-covered ice using DInSAR technique and airborne photography derived from literature is introduced in the next Section 7.2.2. Then the studied area of the Mischabel massif and TSX DInSAR data processing are detailed in Section 7.2.3. Section 7.2.4 presents the methodology for reassessing outlines from DInSAR data. The results for the reduced region of interest are described in Section 7.2.5. A discussion and conclusion are finally proposed in Section 7.2.6 and 7.2.7 respectively. This study is extracted and adapted from published papers Barboux et al. (2013b) and Fischer et al. (2014) .

7.2.2 Detection of debris-covered glaciers using DInSAR and airborne photography

Despite the high quality, resolution and level of detail visible on the Swissimage orthoimages, correct mapping of debris-covered glaciers or boundary areas has been most problematic. This has been confirmed in a number of previous studies, applying both automatic and manual glacier mapping techniques (e.g. Diolaiuti et al., 2012; Falaschi et al., 2013; Knoll and Kerschner, 2009). Frey et al. (2012) showed that debris-covered glaciers could be delimited using the coherence of interferograms

from radar images. Therefore, we investigated the potential of combining DInSAR with airborne photography data for more accurate mapping of debris-covered glaciers.

DInSAR is known as a well-established technique for mapping surface displacements at high spatio-temporal resolution over Alpine areas, where dense vegetation is no longer present (e.g. Massonnet and Feigl, 1998). The nature of the reflected microwave signal response depends on sensor parameters (wavelength, polarization, system noise etc.), on the imaging geometry (interferometric baseline, local incidence angle), and on target parameters (composition and surface roughness of the ground). The former two can mostly be identified as such during interferometric processing (Atwood et al., 2010; Strozzi et al., 2010b). If backscatter properties change between two consecutive image acquisitions, there is a loss of coherence between the SAR scenes used for interferometry (Klees and Massonnet, 1999). This phenomenon of decorrelation is expressed as a noise with contrasted colors of neighboring pixels on the interferogram and can be measured by means of local correlation. During wintertime, dry snow preserves stable scattering geometries, allowing high degrees of coherence and uniform colors on DInSAR interferograms. On the other hand, melting snow or wet ice causes changes of the scattering geometries and thus results in strong decorrelation and noise (Strozzi et al., 1999). A significant glacier motion (decimeters to meters per day) implies a strong glacier surface deformation and low coherence (Weydahl, 2001b). For debris-covered glaciers, a decorrelated signal is either caused by glacier motion, by exposure of the melting ice itself (thinner debris-coverage) and/or by the rapid settlement of the glacier surface (Delaloye et al., 2007b).

7.2.3 TSX DInSAR data processing and region study

For a representative subsample of 48 glaciers of all size classes and surface types in the Mischabel area (Figure 7.4), we compared the SGI2010 outlines from manual digitization with coherence images from ten selected TSX DInSAR pairs (five in descending and five in ascending mode) with a time interval of eleven days from the summers 2008 to 2012 (Table 7.3). DInSAR interferograms were processed with the commercial software GAMMA in the two-pass approach using the two meters resolution swissALTI3D DEM resampled to five meters pixel spacing. The interferometric phase and coherence images were derived for this selected dataset with a final pixel spacing of 5 meters.

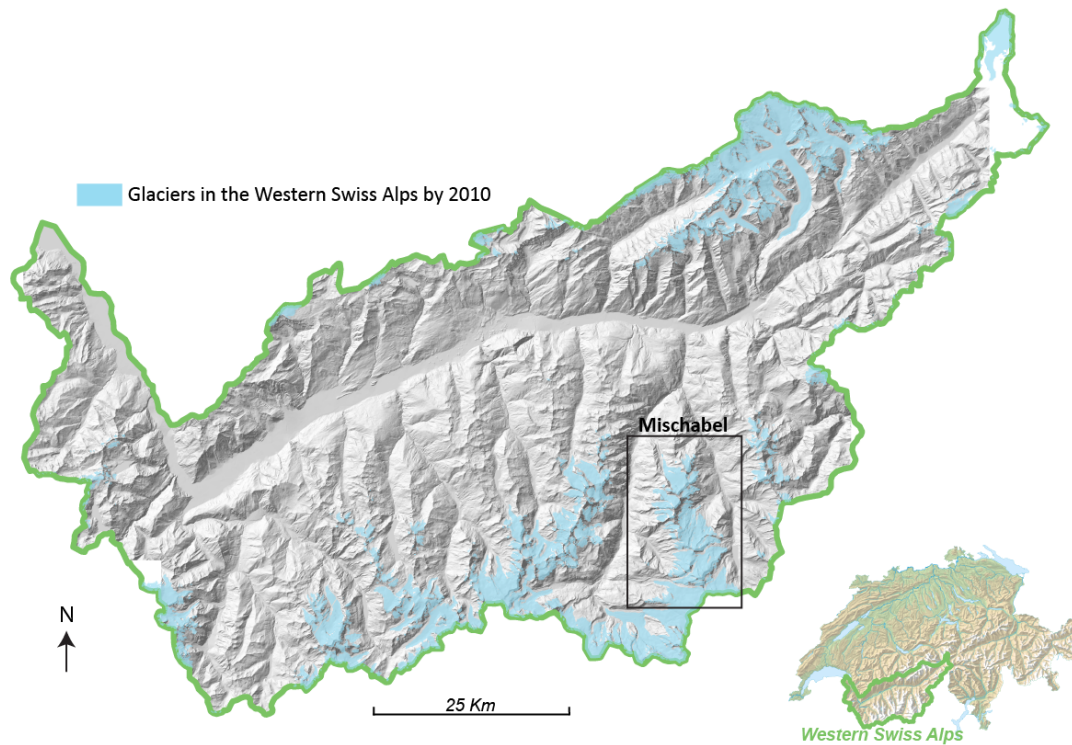


Figure 7.4: Glaciers in the Swiss Alps in 2010. The rectangle shows the subsample of glaciers within the Mischabel area used to test the potential refinement of glacier outlines with TSX DInSAR data.

Date	Mode	Spatial baseline (m)
22/08-02/09/2009	Ascending	-39.2
05-16/07/2011	Ascending	57.6
07-18/08/2011	Ascending	22.0
09-20/09/2011	Ascending	74.4
17-28/09/2012	Ascending	-51.3
29/08-09/09/2010	Descending	-97.7
09-20/09/2010	Descending	-76.0
25/07-05/08/2011	Descending	90.9
22/07-02/08/2012	Descending	-84.7
02-13/08/2012	Descending	-32.6

Table 7.3: TSX DInSAR data selected for the region of interest with a time interval of eleven days.

7.2.4 Methodology for reassessing outlines from DInSAR data

Two maps of DInSAR signals were derived from the ten selected DInSAR pairs: one in ascending mode and the second in descending mode. The methodology for mapping the slope movements from DInSAR signal analysis presented in Chapter 4 was adapted for this specific application. Here, only two classes of slope movements were selected: the noise pattern related to areas with a large deformation rate and the no-noise pattern (fringe or plain pattern) related to areas with a limited deformation rate. A pixel was classified as a noise pattern by thresholding each interferometric coherence image with a value of 0.8; higher values were classified as noise pattern and lower values as no-noise pattern. Finally, the maps of slope movements were computed for each mode by

combining this DInSAR signal classification from each selected DInSAR pair: the resulting pixels were classified by the most represented DInSAR signal pattern of the 5 selected pairs (Figure 7.5).

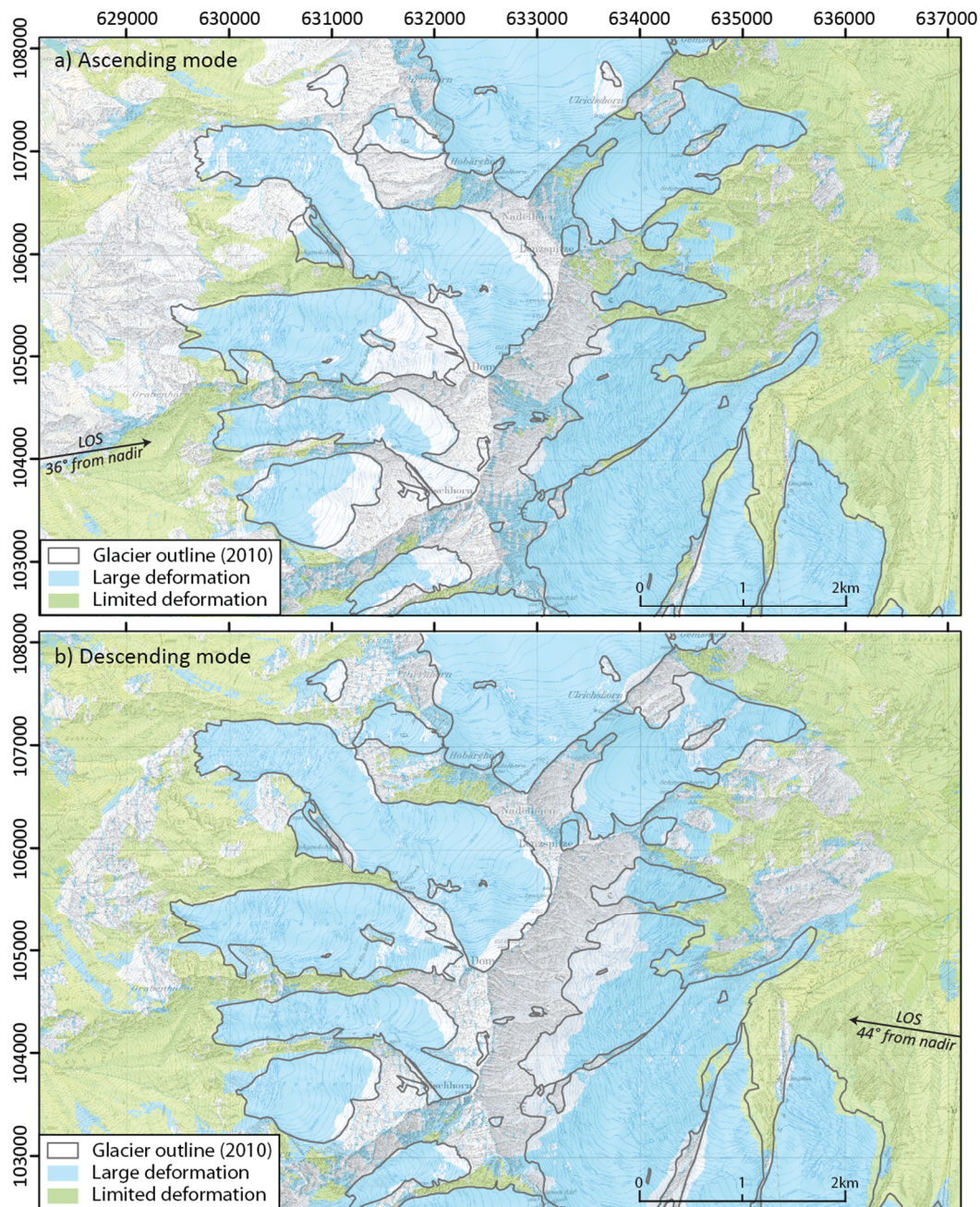


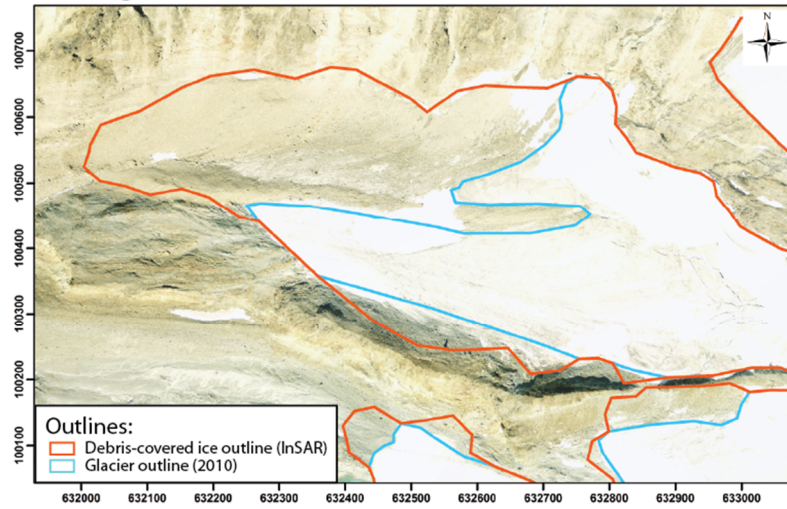
Figure 7.5: Maps of slope movements derived from the selected TSX DInSAR data in a) ascending and b) descending modes.

Different kinds of debris covered ice bodies can be detected with DInSAR. The noise pattern and related large deformation rate detected on DInSAR data can be related to debris-covered ice connected to a glacier (Figure 7.8), to dead ice no longer connected to any glacier source or no longer fed by the glacier (Figure 7.7) or not related to a debris-covered ice body (Figure 7.8). In any case, the combined analysis of this DInSAR signal analysis with orthophotos is required in order to discriminate between these typical landforms and to validate a new glacier contour.

Debris-covered ice connected to glacier

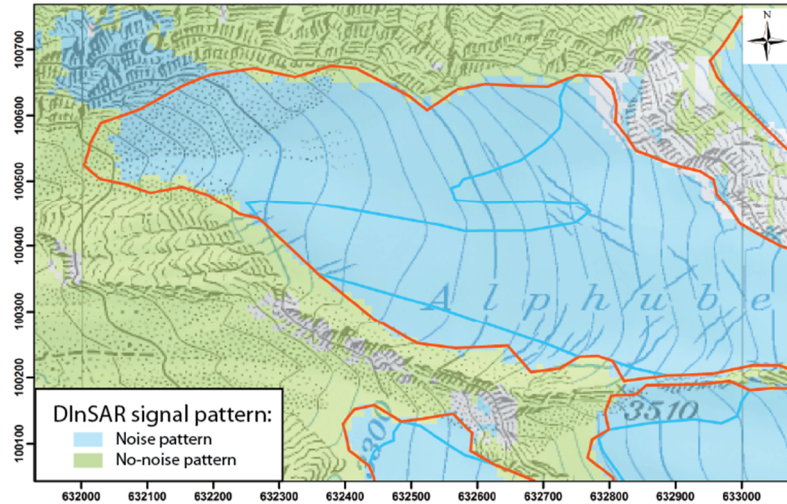
Alphubelgletscher (B55/16)

Orthoimage



Alphubelgletscher (B55/16)

Noise Detection (Descending)



Alphubelgletscher (B55/16)

TSX Descending: 25/07-05/08/2011 (11 days)

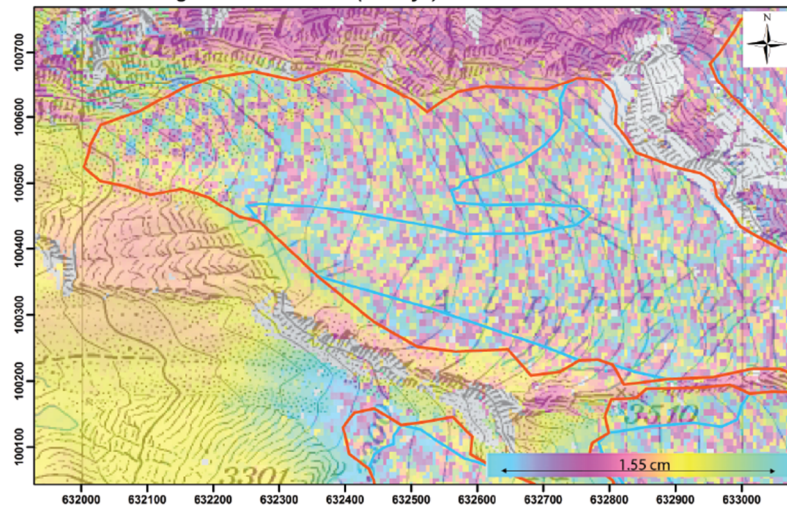
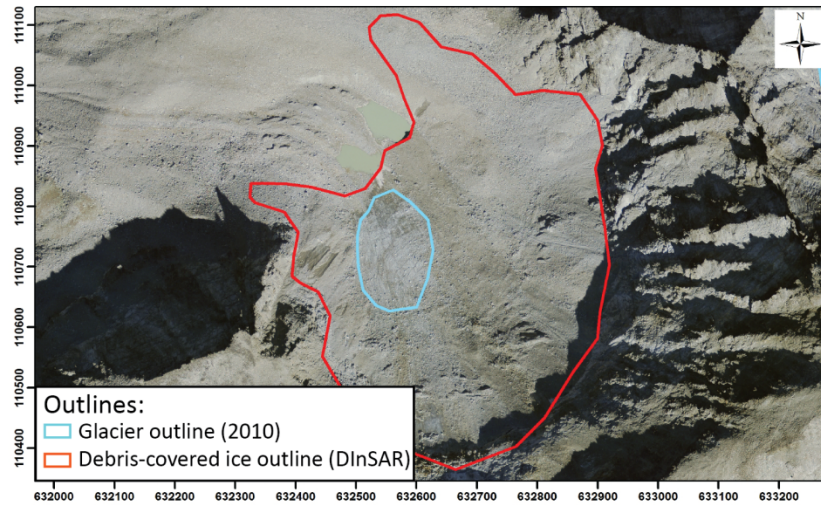


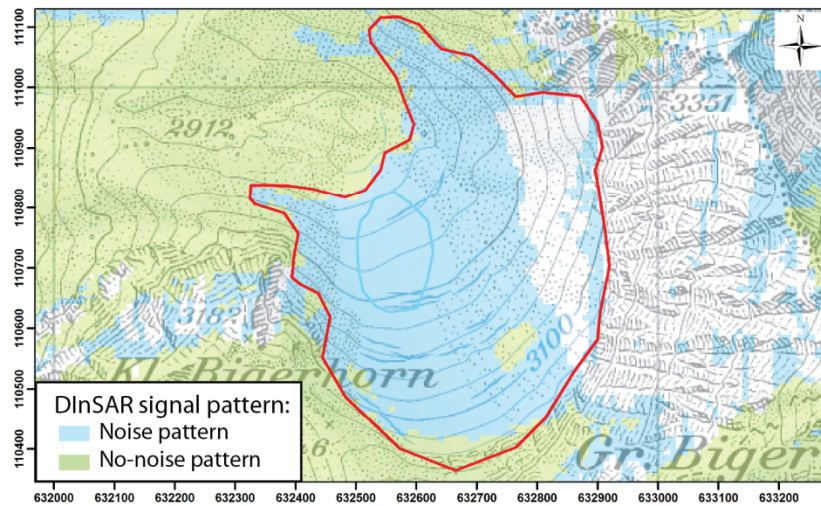
Figure 7.6: Debris-covered ice connected to a glacier detected with DInSAR.

Dead ice no longer fed by the glacier

Kleines Bigerhorn-E* (B54/01)
Orthoimage



Kleines Bigerhorn-E* (B54/01)
Noise detection (ascending and descending)



Kleines Bigerhorn-E* (B54/01)
TSX Descending: 02-13/08/2012 (11 days)

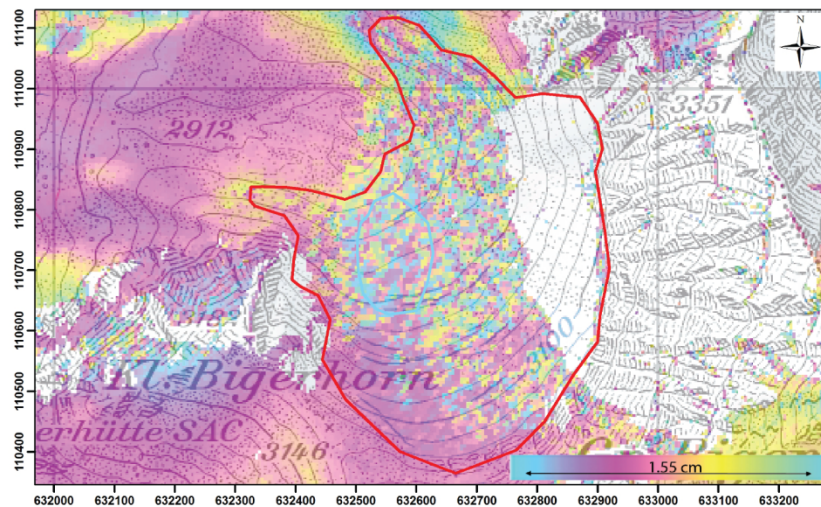
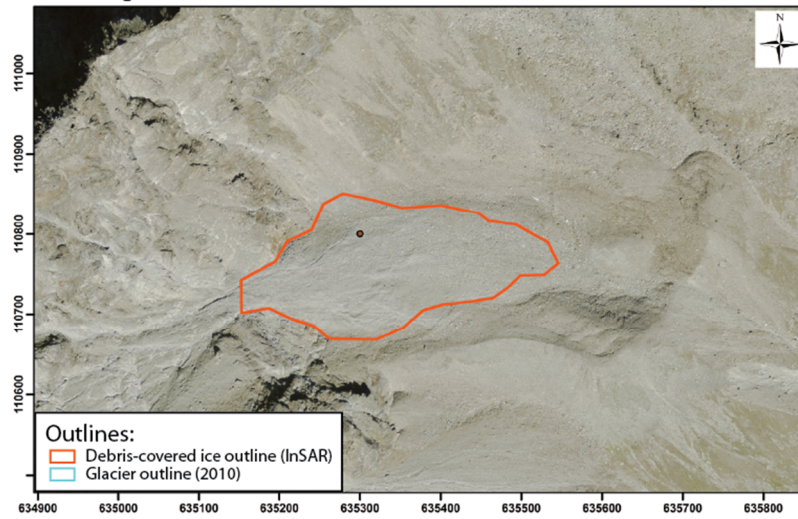


Figure 7.7: Dead ice no longer fed by the glacier detected with DInSAR.

Not related to debris-covered ice body

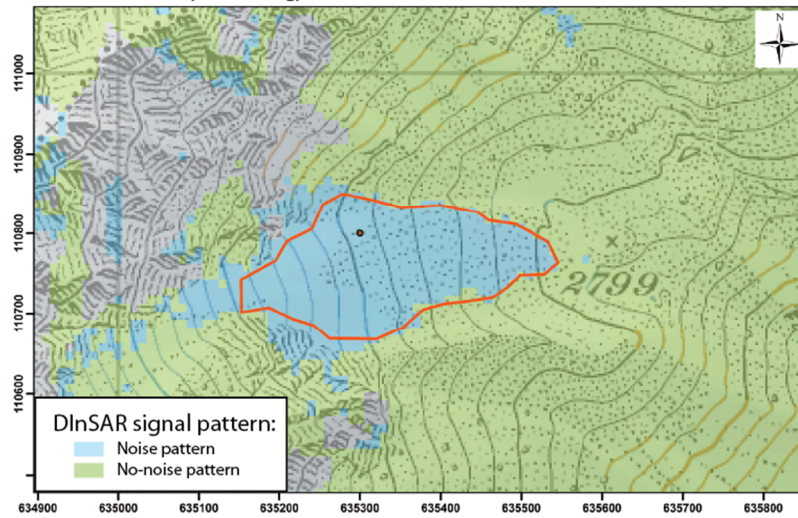
Nadelgrat-E-III* (B53/09)

Orthoimage



Nadelgrat-E-III* (B53/09)

Noise Detection (Ascending)



Nadelgrat-E-III* (B53/09)

TSX Ascending: 07-18/08/2011 (11 days)

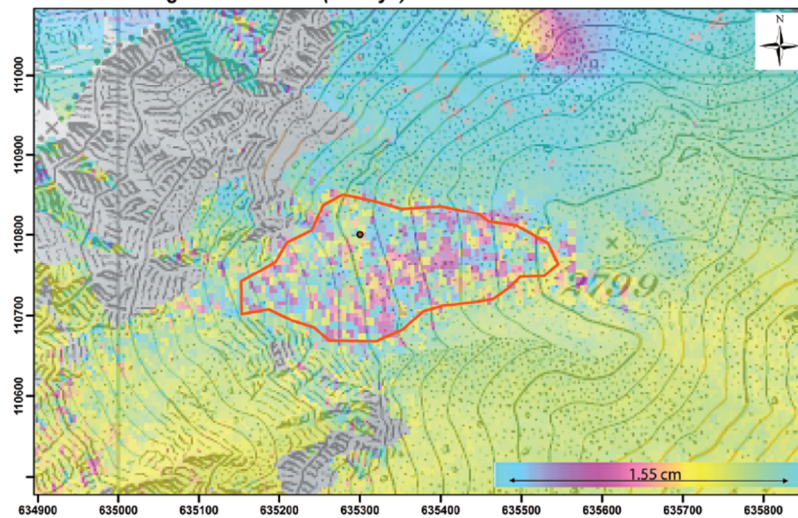


Figure 7.8: DInSAR signal over a landform not related to a debris-covered ice body.

Finally, each SGI2010 outline, and especially the outline of glaciers ending in a region of permafrost, is refined using a combined analysis of slope movement maps and orthophotos in order to discriminate between periglacial creeping landforms and debris-covered glacier tongues.

7.2.5 Results observed in the Mischabel massif

7.2.5.1 *Example of glacier outline refinement*

The terminus of Weingartengletscher-S-II in the Mischabel test area (0.78 km^2 in 1973, 0.42 km^2 in 2010) is heavily debris-covered (Figure 7.9a) and is a good example of a glacier for which the manual delineation on the basis of visible interpretation of only the aerial orthoimagery is particularly difficult. The potential to more accurately map partially or entirely debris-covered glaciers using DInSAR interferograms becomes obvious in Figure 7.9b. Areas of distinct regular noise can be distinguished as a result of strongly decorrelated radar signals in the interferogram. These were either caused by 1) the exposure of the melting ice itself (in the case of thin debris-coverage), by 2) the rapid settlement of the glacier surface and/or by 3) a significant glacier motion (Delaloye et al., 2007b). The latter two are probably the cause of the noise in the orographic upper-left part of the glacier which is still visible in the selected interferograms. For the lower-lying and sharply confined pattern that is still within the former 1973 glacier outline, 1) and 3) could largely explain the noise. From this we infer that Weingartengletscher-S-II, a rather large and highly debris-covered part of the current glacier tongue, was misclassified as no longer belonging to the glacier based on the initial digitization approach (Figure 7.9). The smallest outline delimited with DInSAR located in the orographic left side of the Weingartengletscher, was attributed to dead ice no longer fed by the glacier and was not included in the final glacier outline.

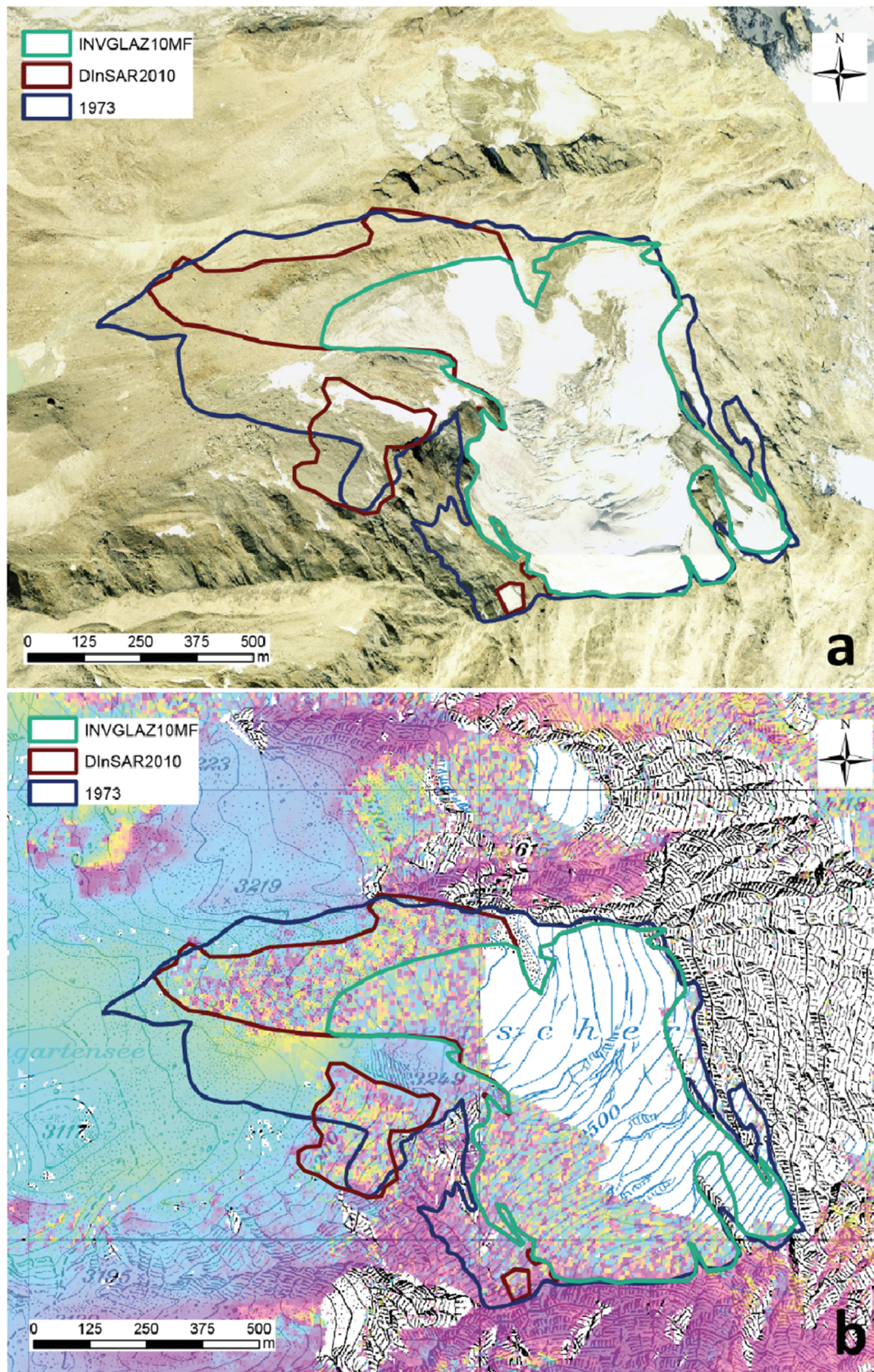


Figure 7.9: 1973 (blue), 2010 reassessed with DInSAR (red) and original 2010 (green) outlines of Weingartengletscher-S-II. Underlain are a) the SWISSIMAGE Level 2 orthoimage acquired in autumn 2010 and b) the 11 days TSX DInSAR pair from 09-20 September 2010 in combination with the topographical pixel map. Adapted from Fischer et al. (2014).

7.2.5.2 General results

The comparison of the SGI2010 outlines was performed with the outlines reassessed according to the respective slope movement maps derived from DInSAR signal analysis for a subsample of 48 glaciers in the Mischabel area (Figure 7.4) containing all size classes and surface types present in the Swiss Alps. The results showed that the example of Weingartengletscher-S-II (Figure 7.9) was rather at the upper end of possible misclassifications of debris-covered glacier ice (Figure 7.10). The cumulative total area of the 48 glaciers mapped based on the aerial orthophotos was 78.8 km², whereas the refinement of glacier outlines using DInSAR technique resulted in 81.8 km² (+3.8 km² or +3.8%). Reassessing the SGI2010 outlines for the Mischabel test area with DInSAR interferograms always resulted in an increase of the mapped glacier surface. Thus, there was a systematic bias in the SGI2010 for debris-covered glaciers. Furthermore, a trend of increasing scatter of the specific difference with decreasing glacier size could be observed (Figure 7.10). Very small glaciers tended to be either almost entirely debris-covered or made up of almost only bare ice.

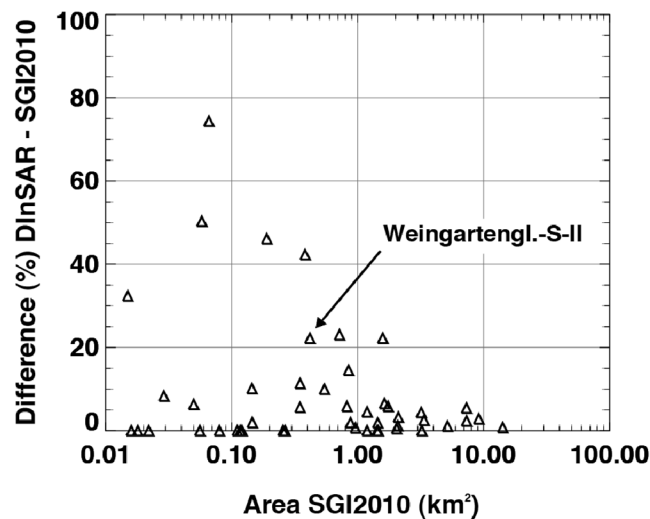


Figure 7.10: Relative difference between glacier outlines derived from a combination of DInSAR interferograms and aerial orthoimages minus glacier outlines derived solely from aerial orthoimages versus glacier area in 2010 for 48 individual glaciers in the Mischabel test region (fig. 7.5). From Fischer et al. (2014).

7.2.6 Discussion

7.2.6.1 Accuracy assessment using TSX DInSAR data

From the combination of aerial orthoimagery data with TSX DInSAR scenes of the shortest time interval, the outlines of debris-covered glaciers within the Mischabel test region can be reassessed. This always resulted in an increase in mapped glacier surface area. Thus, considering the delineation of glacier outlines from a combination of aerial orthoimages and DInSAR technique to be more accurate than the previous methodological approach chosen to create the SGI2010 for the entire Swiss Alps, the error of mapping debris-covered glaciers is a systematic one and increases steadily

towards the smallest glaciers. From the representative subsample of the Mischabel test area this error was quantified to +3.8% of the mapped area. This indicates that the total glacierized area in the Swiss Alps might be slightly underestimated by the SGI2010. The same probably also applies to the former 1973 inventory but does not affect our change assessment as errors cancel each other out.

7.2.6.2 Discrimination between glacial and periglacial landforms

When glaciers terminate in a region with permafrost, it is visually difficult to discriminate between forms of creeping scree and debris-covered glacier tongues as they exhibit similar surface structures. These features are a mix of glacial and periglacial landforms and simple differentiations between debris-covered glacier and rock glacier are not possible. The analysis should consider the high spatio-temporal resolution of DInSAR images with different time intervals in order to discriminate debris-covered glaciers from rock glaciers and from other creeping landforms. This extensive analysis could allow for the detection and discrimination between the different kinds of glacial and periglacial features.

In this study, the high spatio-temporal resolution of TSX DInSAR data allows for the better discrimination between debris covered glaciers and other periglacial landforms. For instance, only fast moving rock glaciers with a velocity higher than 2m/year express a noise pattern on DInSAR images. Using a time interval of eleven days, the surface of slower rock glaciers generally shows fringe pattern on the interferometric phase images. The distinction between fast moving rock glaciers encountered in the Swiss Alpine periglacial belt and debris-covered glaciers is relatively easy to identify on high resolution orthoimages, as the typical structures of these landforms show visible signs of destabilizations (cracks, activity at their steep front, breaking zones, etc.). Moreover, the presence and location of rock glaciers in the region of Mischabel is already well known thanks to the past inventory of Alpine moving landforms carried out in the entire Swiss Alps on the basis of ERS and JERS DInSAR data and orthoimages. This past inventory was also used to discriminate between glacial and periglacial landforms (Figure 7.11).

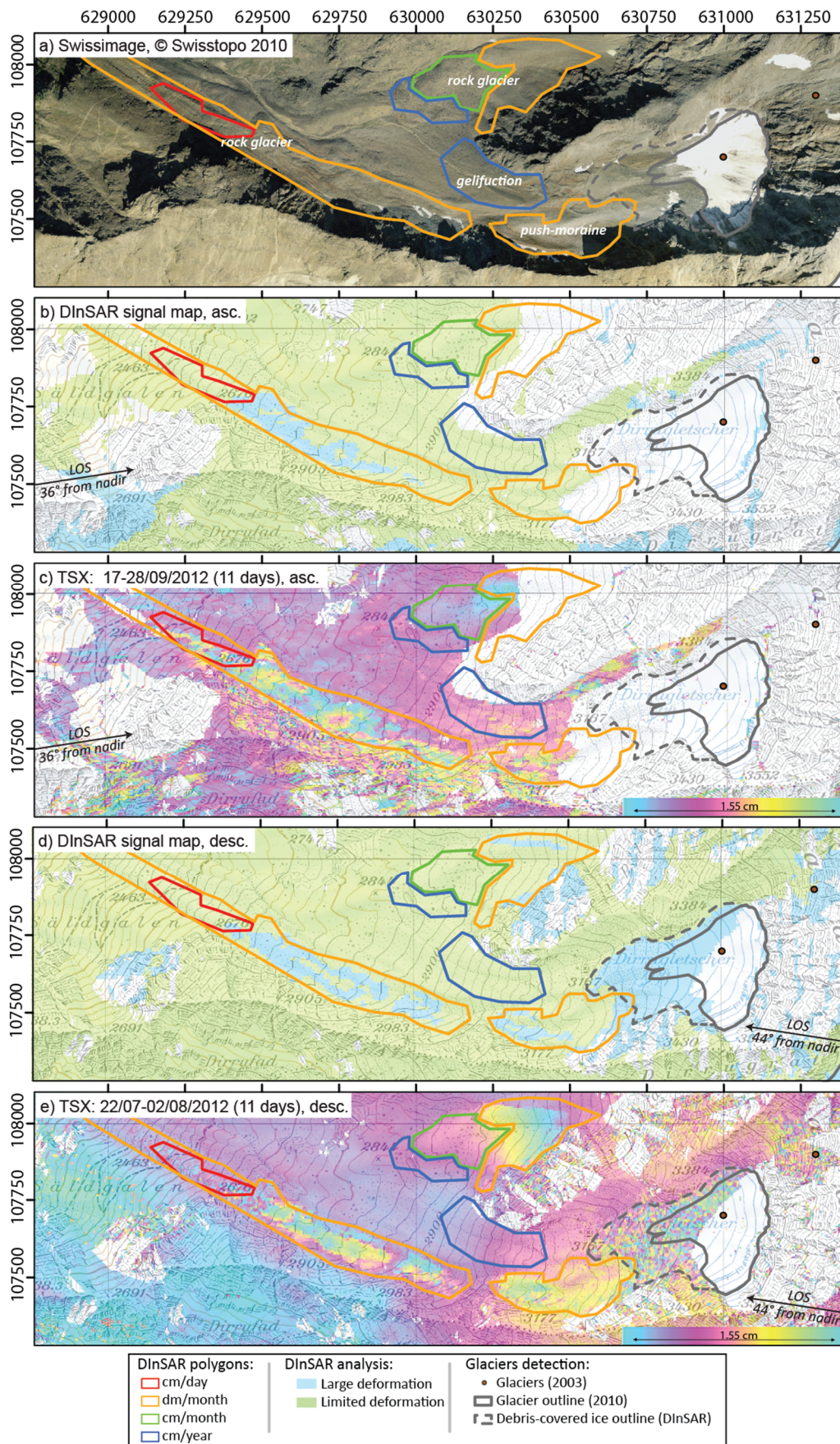


Figure 7.11: Example of glacier outline refinement using DInSAR signal maps, interferometric phase images and past inventoried DInSAR polygons.

7.2.7 Conclusion

The combination of aerial orthoimages with Differential SAR Interferometry techniques is promising to map debris-covered glaciers more precisely. Using coherence images from selected TSX DInSAR pairs, the glacier outlines in the Mischabel test area were reassessed where visual interpretation based only on the high-resolution orthoimages was difficult. The proposed method allows for the delimitation of the maximal extent of the glacier tongues ending in a region with permafrost by distinguishing them from rock glaciers and potential non-moving dead ice. From comparison of these refined outlines to those of the SGI2010, we could quantify the error of debris-covered glaciers as +3.8%.

This method allows for the refining of outlines of debris-covered glaciers where visual interpretation is difficult. Moreover, it allows the detection of debris-covered glacier ice bodies no longer connected to any glacier source or no longer fed by the glacier flow (dead ice). Current glacier inventories do not consider every type of debris-covered glacier ice as they are mainly used for climatic interpretation. However, the question remains whether it is necessary to take into account these (dead) ice bodies in glacier inventories if they are to be used to study runoff contribution, sediment transfer, slope dynamics, or natural hazards.

7.3 Conclusion

Slope movement maps, defined as the combination of DInSAR signal analyses at a specific time interval, are a useful tool for helping visual interpretation and mapping of Alpine moving landforms. These maps provide a general trend of DInSAR signal at a specific time interval deduced from an entire DInSAR dataset. The analysis of individual DInSAR images separately is nevertheless required as it highlights single patterns in the general trend of DInSAR signal displayed by the slope movement map and highlights patterns potentially related to specific behaviors, such as the seasonal variation of deformation rate for a specific landform.

In this chapter, the presented methodologies allow for the mapping of different kinds of Alpine landforms related to glacial and periglacial features encountered in the Alpine periglacial belt of the Western Swiss Alps using the map of these slope movements. The combination of DInSAR signal analysis with external data, like high resolution orthoimages, seems to be the best compromise to outline these different Alpine landforms with high precision and accuracy. In any case, these inventories are long and cumbersome and require a high competence in geomorphology. Generating DInSAR signal maps from interferometric coherence and phase images also requires specific software skills. However, the results of rigorous mapping of Alpine landforms could largely compensate working efforts.

8 Example of DInSAR contribution for site specific analysis

In this chapter, two applications for the monitoring of Alpine slope movements are proposed to illustrate the potential of TSX DInSAR data for site specific analysis. The first study proposes to analyze the pluri-decennial development of a rock glacier crisis using DInSAR data combined with terrestrial and airborne optical data (Part 8.1). The second one aims to show the potential of DInSAR data for the detection of intra-seasonal variation and geomorphological processes occurring on Alpine rock glaciers (Part 8.2). A discussion about main results for the monitoring of Alpine moving landforms using DInSAR observed from applications is given in Part 8.3. Finally, a conclusion offers a synthesis of DInSAR data contribution for the monitoring of these Alpine slope movements (Part 8.4).

8.1 Analyzing the pluri-decennial development of a rock glacier crisis using repeated DInSAR, terrestrial and airborne optical data

8.1.1 Introduction

Recent work based on the analysis of satellite Differential Synthetic Aperture Radar Interferometry (DInSAR) data have evidenced that 15 to 20 rock glaciers were affected by very rapid movements in the Swiss Alps between 1995 and 1999 (Delaloye et al., 2010b). Most of these rock glaciers, moving 2-5 m/year or more, exhibit transversal scarps and/or crevasses revealing some degree of destabilization (Lambiel et al., 2008; Roer et al., 2008). Nevertheless, the chronological and morphological development of the destabilization phase, indicated by changes in the kinematics, geometry and modified topography and which may differ from case to case, are actually not known for most of these rock glaciers. The aim of this study is to go back to the beginning of the destabilization phase to look for different factors involved in this process.

In this context, the development of the Grabengufer rock glacier (Zermatt valley, Valais, Swiss Alps) has been investigated. This landform has recently encountered a complete destabilization and has shown exceptionally high displacement rates. The maximal activity was recorded between July 2009 (start of the in-situ monitoring) and February 2010, with surface velocities ranging between about 10 and 40 cm/day. In order to understand the way in which the activity of this landform has changed throughout the past, a backward analysis was conducted on both the morphology and kinematics of the rock glacier based on repeated DInSAR data from 1991 to 2009, airborne optical data from 1930

to 2005 and terrestrial surveys. This study is extracted and adapted from (Barboux and Delaloye, 2010a, 2010b; Delaloye et al., 2013).

8.1.2 The Grabengufer

The Grabengufer rock glacier is about 600 m long and 100 m wide. It is located in a steep cirque dominated by highly fractured rocky slopes mainly taking part in a huge active deep-seated landslide. The rock glacier tongue terminates about 2400 m a.s.l. on a very steep slope where it dominates the Grabengufer gully, a large couloir collecting most of the material produced by the rapid erosion of the rock glacier front. The Grabengufer gully reaches the Dorfbach torrent at around 1800 m a.s.l.

This rock glacier has encountered recently a complete destabilization and exceptionally high displacement rates. The maximal activity was recorded between July 2009 (start of the in-situ monitoring) and February 2010 with surface velocities ranging between about 10 to 40 cm/day. After the paroxysmal phase and disregarding the seasonal fluctuations that regularly occur, the flow rate of the Grabengufer rock glacier has decreased gradually (Delaloye et al., 2013). Quasi continuous rock fall activity and debris flow events are triggered from the rock glacier snout (Bühler and Graf, 2013; Graf et al., 2013).

8.1.3 Reconstruction of the destabilization

Historical knowledge from local inhabitants, aerial photographs and more recent DInSAR have permitted the partial reconstruction of the timing and causes of the current destabilization phase, which can be summarized as follows:

1) On an oblique photo in 1930, the Grabengufer rock glacier cirque looks like an undefined accumulation of blocky material and no active front is clearly identifiable (Figure 8.1).



Figure 8.1 : The Grabengufer rock glacier observed from the opposite side of the valley in 1930 (oblique photograph number 380, data courtesy of the Federal Office for the Environment).

2) A first destabilization occurred around 1940. On a vertical aerial photo in 1941, where unfortunately only the front of the rock glacier is visible, active debris-flow channels are clearly perceptible from the rock glacier toward the Grüngarten area, south of the Grabengufer gully. At this time, several dams were built at the rock glacier front and downwards with the principal aim to conduct the debris flows back into the Dorfbach torrent (Figure 8.2).

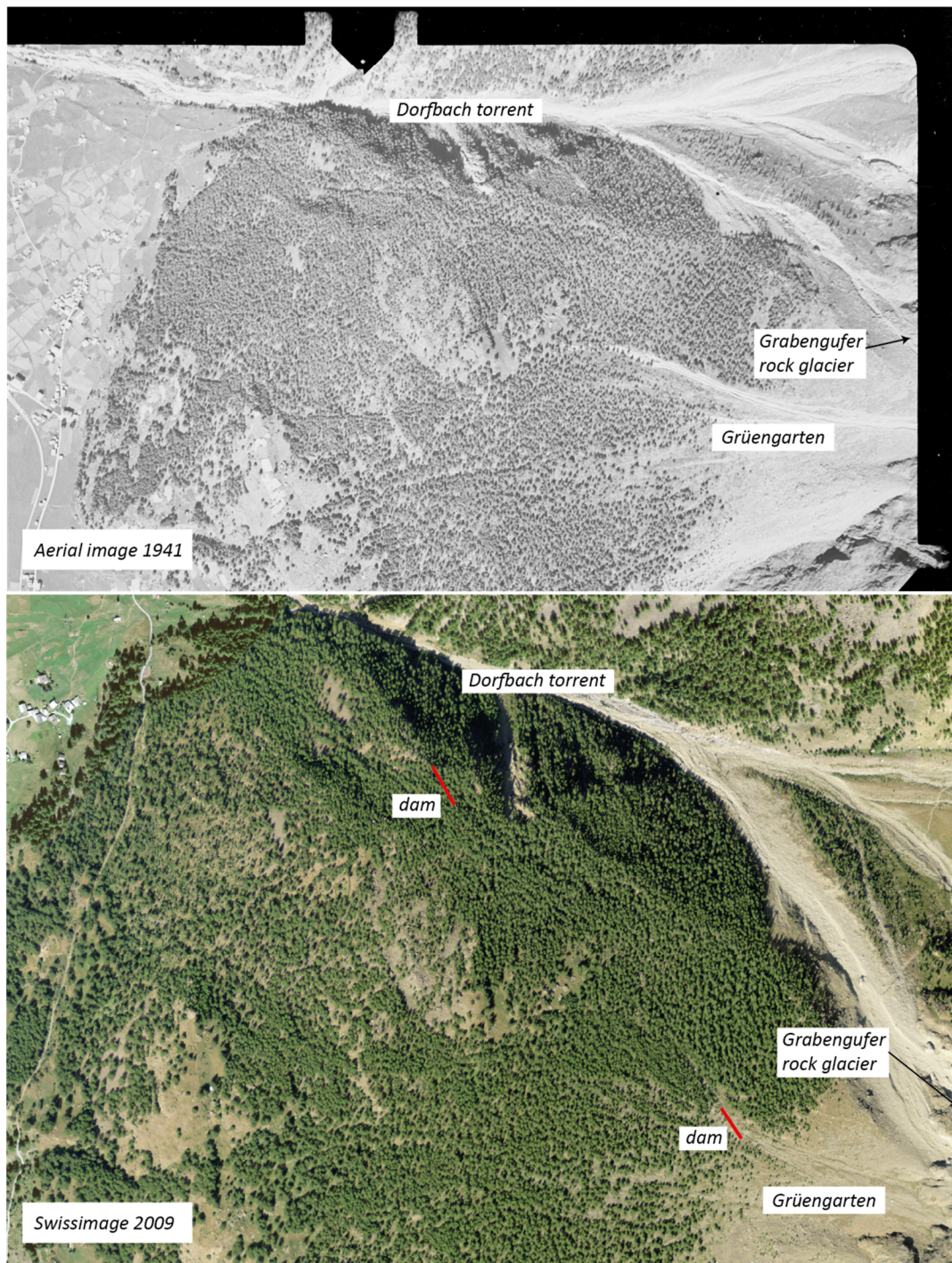


Figure 8.2: Vertical aerial photo in 1941 and 2009. In 1941, active debris-flow channels were clearly perceptible from the rock glacier toward the Grüngarten area, south of the Grabengufer gully. Two dams have been built during the 1940s in order to redirect debris flow back to the Dorfbach, visible in the Swissimage from 2009.

3) Between 1950 and 1980, the rock glacier appears to have returned to normal activity. In 1969, a large transversal crevasse is visible at the surface of the rock glacier as a morphological reminiscence of the previous destabilization phase. This feature was still visible on 1977 and 1982 aerial photographs (Figure 8.3).

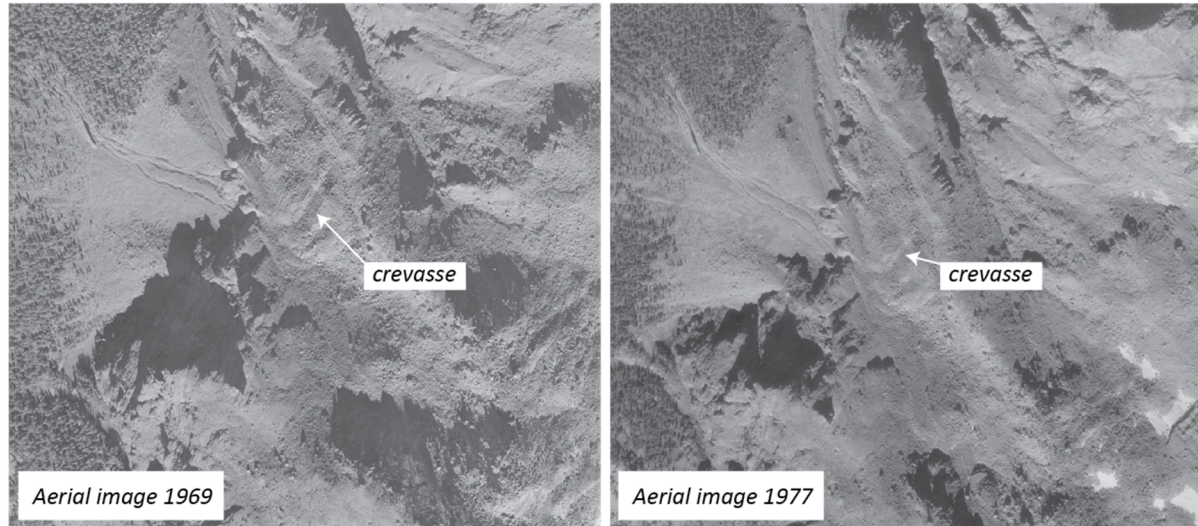


Figure 8.3: Large transversal crevasse is visible at the surface of the Grabengufer rock glacier.

4) According to the analysis of aerial photographs and DInSAR data archives, the current crisis started between 1982 and 1988 with the following simplified development (Figure 8.4) : A) progressive overloading of the rooting zone of the rock glacier due to landslide and rock fall activity from the head areas; B) buildup of a compressive wave starting from the rooting zone of the rock glacier; C) between 1995 and 2001 propagation of the compressive wave to the median part of the rock glacier, which began to strongly deform (development of new ridges and scarps); D) progressive acceleration of the frontal part up to 5 m/year between 2001 and 2005; E) increased destabilization of the frontal part due to its location on a steep convex slope and destabilization of the entire of the landform (situation in 2009), partly pulled down by the rapid advance of the rock glacier tongue; and F) after this paroxysmal phase, the flow rate of the Grabengufer rock glacier decreased gradually but nevertheless remains exceptionally high.

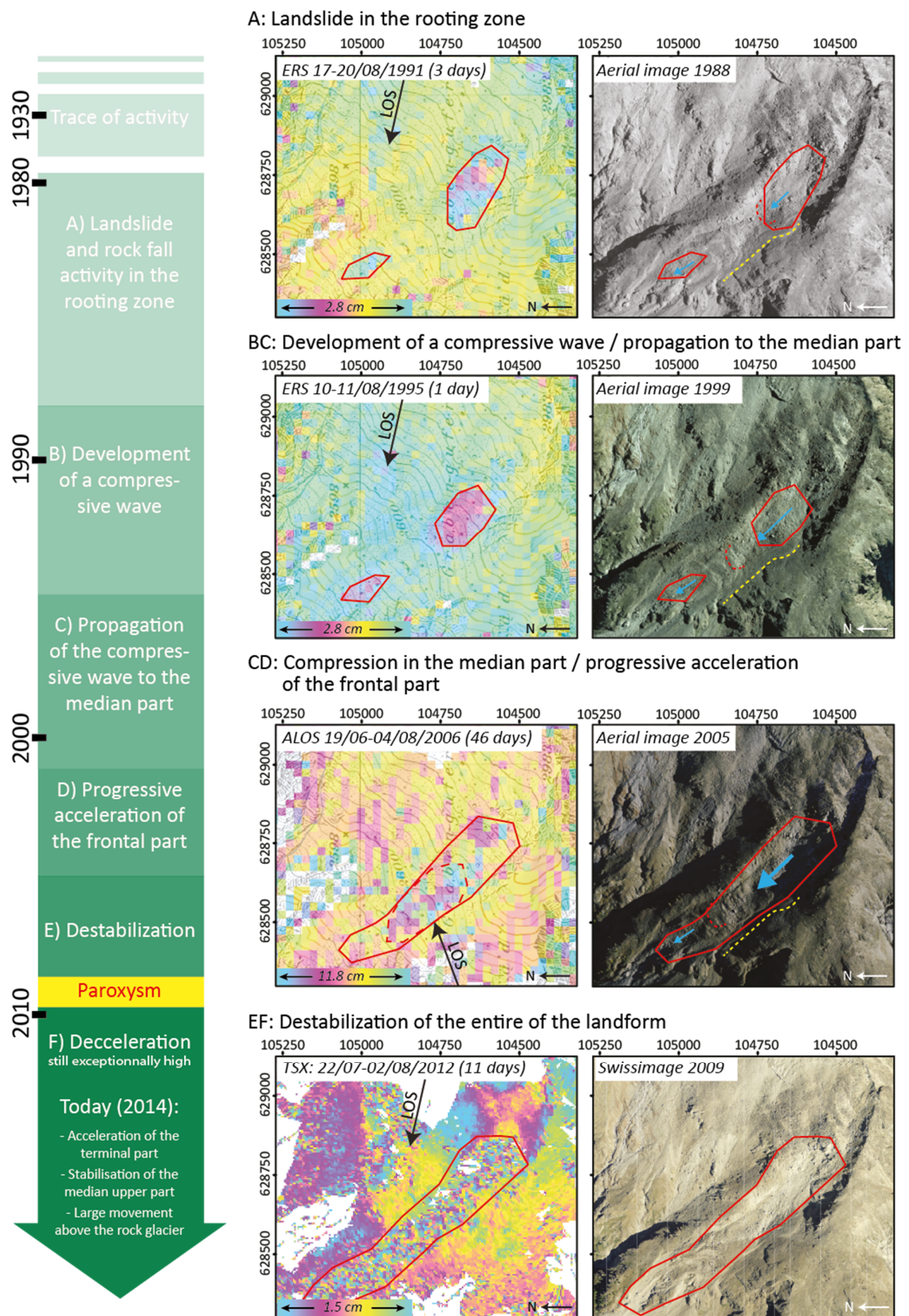


Figure 8.4: The onset of the destabilization of the Grabengufer rock glacier described by aerial images and DInSAR data in the period 1930-2010.

Figure 8.4 illustrates the situation in the early 1990's as observed using the DInSAR archive. On a 3-day interferogram in summer 1991, a rapidly moving mass wasting (permafrost creep or landslide?) was obviously visible in the rooting zone of the rock glacier. The displacement rate could be visually estimated as about 1 cm in 3 days in the LOS (1.2 m/year). In 1995, the displacement rate in this upper zone accelerated to about 1 cm per day in the LOS (3.5 m/year). According to orthophoto analysis (Barboux and Delaloye, 2010a), the displacements in the rooting zone reached about 1.7 m/y in between 1988 and 1999. After this time, only the location of fast deformation rates of this rock glacier could be outlined, which were estimated from orthophotos as up to 11 m/y in between 1999 and 2001 and even higher after 2001; however, the current SAR sensors are no longer suitable to monitor the Grabengufer rock glacier. Figure 8.5 shows the current annual velocity observed over the median part of the rock glacier determined from DGPS measurements.

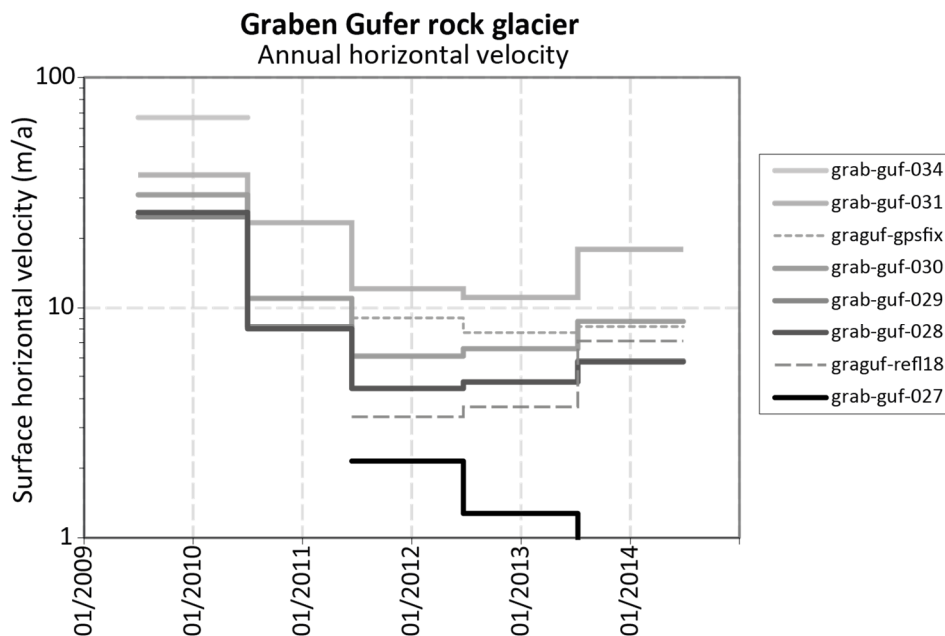


Figure 8.5: Annual velocity measured by DGPS over the median part of the rock glacier.

8.1.4 Conclusion

The development of the current crisis of the Grabengufer rock glacier appears to be the result of a succession of dynamic reactions over 25 years and can be qualified as a mechanical surge process starting from the rooting zone of the rock glacier. This development, and its chain reaction initially caused by the pulse in the rooting zone, differs dramatically from other destabilized rock glaciers that have been analyzed so far (Roer et al., 2008). This shows that the factors contributing to the destabilization of a rock glacier could be numerous. Nevertheless, looking at the strong increase in air temperature that has been occurring since the 1980's, these results do not challenge the potential origin of the destabilization in rheological properties of warming ice, which could happen in this specific case in the rooting zone of the rock glacier.

DInSAR scenes have built up a significant archive of data since 1991. In addition to surveying current phenomena, analyzing DInSAR data may also help for reconstructing the development and evolution of a landform. Unfortunately, due to the fast velocity of the Grabengufer rock glacier, the current high spatio-temporal TSX DInSAR data is not suitable to quantify the actual deformation rate of this rock glacier anymore.

8.2 Detection of intra-seasonal variation and geomorphological processes

This part aims to show the potential of DInSAR data for the detection of intra-seasonal variation and geomorphological processes occurring on Alpine rock glaciers. Two case studies are presented here and concern two active rock glaciers currently destabilized.

8.2.1 Gänder rock glacier

8.2.1.1 *Main geomorphological features*

Gänder is a north-west oriented rock glacier located in Zermatt Valley in between 2435 and 2800 meters a.s.l. showing evidences of destabilization (Figure 8.6a). It measures 850 meters long and 60 to 200 meters wide. It consists of a rooting zone where some snow patches often remain, an average wide body (zone 1), a southern side tongue (Gänder II) and an approximately 350 m long steep forehead tongue (zone 2). The inclination of the slope is about 15° in the rooting zone and body and reaches 32° in the frontal part. Only a portion of the tongue is destabilized and supplies sediments above the deep side channel of the Wildibach. Otherwise, the rock glacier tongue moves parallel to the channel and currently delivers no sediment down the valley (Delaloye et al., 2014). The velocity measured by DGPS increases from a few centimeters per year in the rooting zone to 3-7 m/year in the frontal part.

8.2.1.2 *Observations using DInSAR data*

Different zones can be distinguished on the Gänder rock glacier using the up-to-date TSX DInSAR data combined with orthoimagery. As seen in Figure 8.6 b to d, the two main moving zones observed on interferometric phase images concern the destabilized tongue showing noise pattern (zone 1) and the part including the rooting zone and the body of the rock glacier showing partly fringe pattern (zone 2).

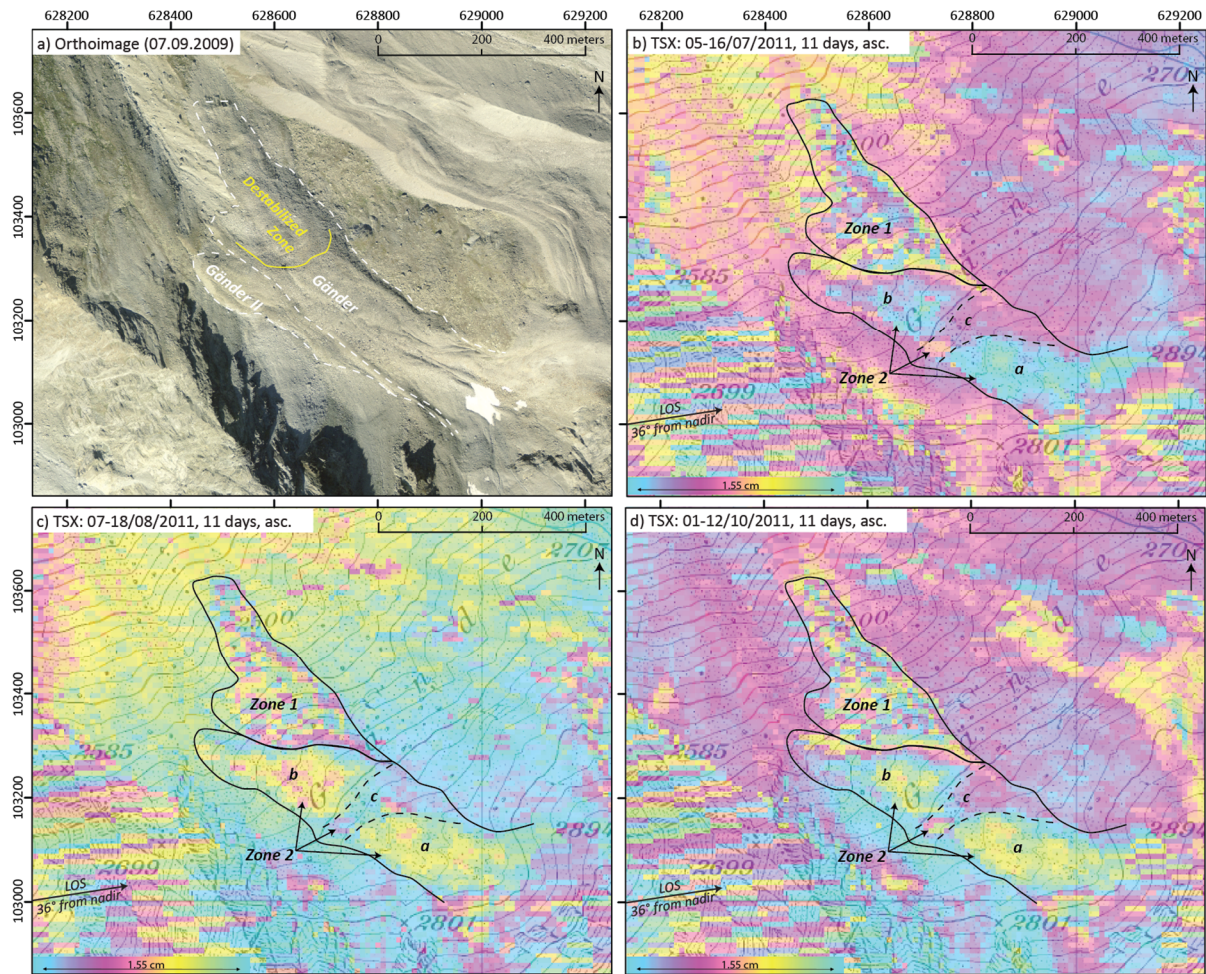


Figure 8.6: Gänder rock glacier. a) Orthoimage from 2009 ©Swisstopo. b-d) Spatial extent of the different moving zones over the rock glacier detected by DInSAR observations at different time periods.

As previously seen in sub-section 5.2.2.1 b, the very active frontal part cannot be monitored using the shortest time interval of TSX DInSAR data as it always appears decorrelated (Figure 8.6b-d). Consequently, TSX DInSAR data could not provide more information about this part, except the spatial extent delimited by the noise pattern observed on interferometric phase images.

Zone 2 can be observed using TSX DInSAR data. As seen in Subsection 5.2.2.1 b, the flow directed nearly perpendicular to the LOS direction is highly compressed and takes on positive and negative values when projected into the LOS direction. Consequently, it is very difficult to derive surface deformation along a profile from TSX DInSAR data. The analysis of the coherence trend can however point out specific behaviors that can be observed along the landform. As shown in Figure 8.7, the analysis of the coherence along the profile defined on the Gänder rock glacier reveals a specific region with a decrease of the coherence values during summer 2012, potentially related to intra-seasonal processes.

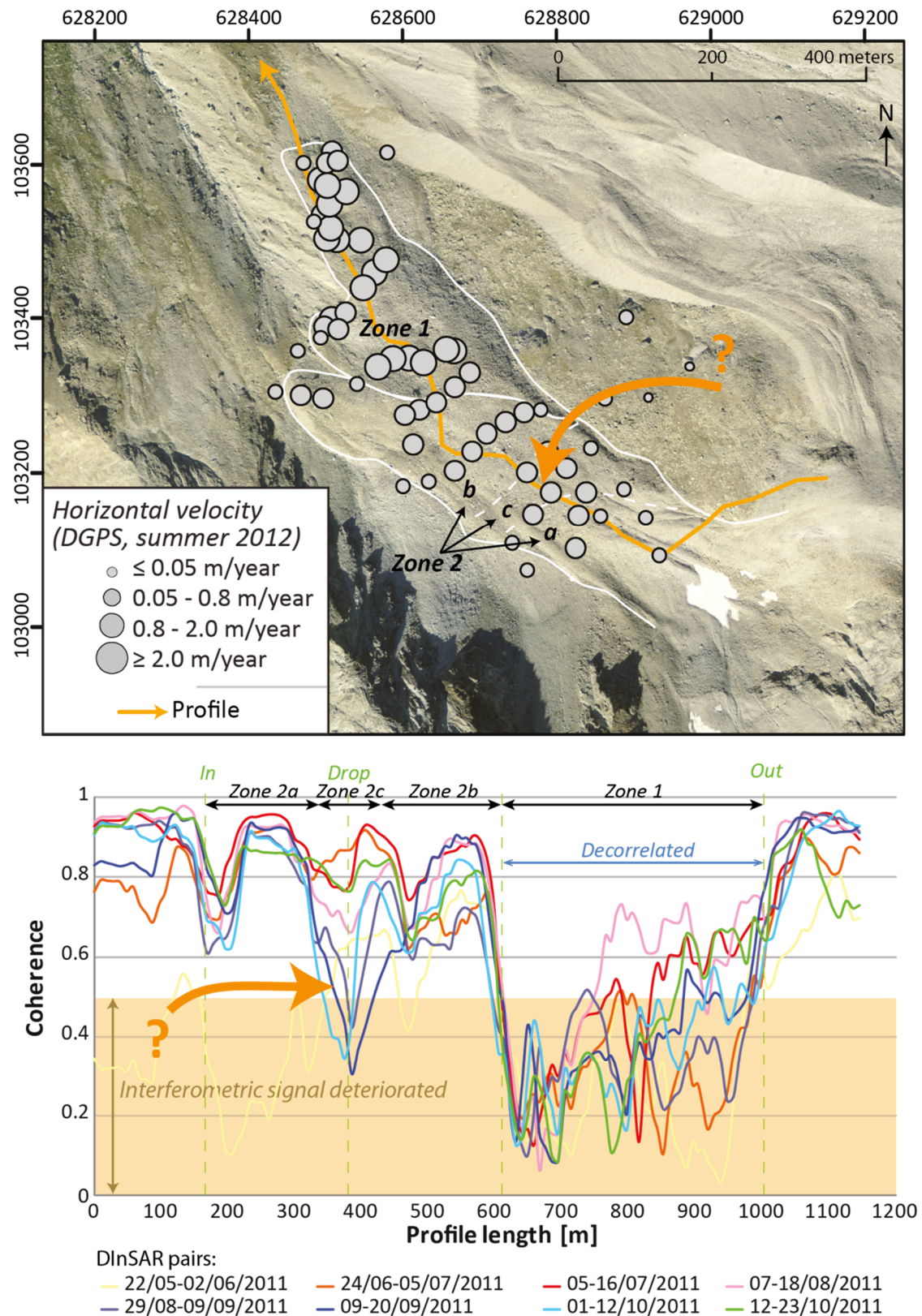


Figure 8.7: DInSAR coherence analysis along a profile.

When observing the interferometric phase images throughout the summer, it seems that two distinct homogeneously moving areas can be defined in zone 2 (Figure 8.6 b-d): the rooting zone (zone 2a) and the body of the rock glacier (zone 2b). In between, a transition zone (zone 2c) is observed corresponding to the part identified along the profile as having a loss of coherence during the summer. According to DGPS measurements, zone 2b accelerates progressively compared to zone 2a (Figure 8.8). The transition zone 2c corresponds to the change of slope in between zone 2a and 2b, and seems to be affected by a potential extension. It has to be noted that zone 2c is steeper than the two zones 2a and 2b. The DInSAR signal is thus highly compressed in facing mode at this zone. This can explain why the visual interpretation of the deformation rate would indicate a rate lower than the two other zones, which is not the case when looking at DGPS measurements.

According to field measurements, the rooting zone and the body of the rock glacier (zone 2) are frozen. Ice patches originating from a glacier are locally present below the first surface sediment layer (Delaloye et al., 2014). The DGPS measurements show a spatial increase in the velocity when going down the rock glacier (Figure 8.8a). Actually, the zone 2a located in the upper part moves slower than the zone 2b located in the lower part. The zone 2c located in between seems to be affected by an extension of the displacements. The DGPS measurements also show an acceleration of the displacements of zones b and c occurring in summer (and especially in the second part of the summer as shown in 2012 where three campaigns were performed during summer, Figure 8.8a). Moreover, the inclination of the displacements seems to be more significant in summer for these two zones than in winter, and particularly in the transition zone c which shows larger seasonal variations (Figure 8.8b). The observed process can thus be explained by the melt affecting the ice located under the sediments in this zone. The significant increase of inclination of the displacement in summer observed in zone c is probably caused by the thinner layer of sediments due to the extension of the surface layer.

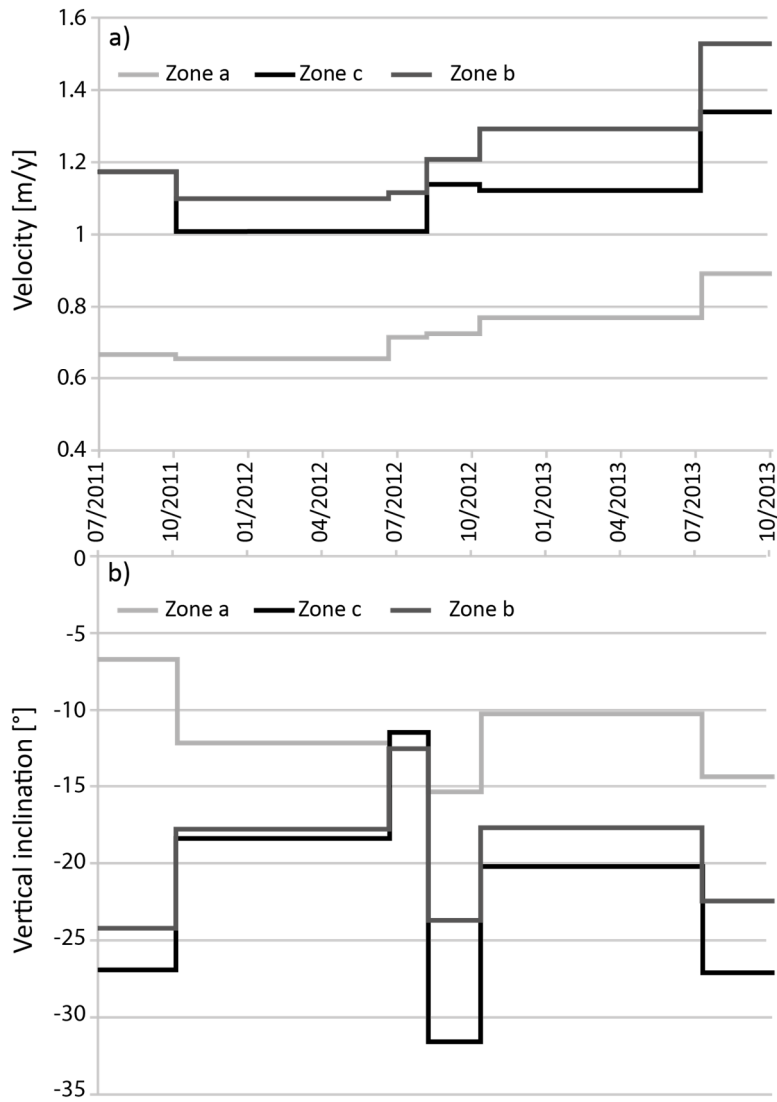


Figure 8.8: DGPS measurements over the zone 2a, 2b and 2c of the Gänder rock glacier: a) horizontal velocity and b) vertical inclination.

8.2.1.3 Conclusion

The use of up-to-date TSX DInSAR data combined with orthoimagery and terrestrial surveys allows the understanding of specific processes involved in the Gänder rock glacier. Specifically, the TSX DInSAR data helps to determine the location of these phenomena and precise terrestrial surveys may help to focus and individualize the analysis of these distinct processes. Nevertheless, due to the actual fast velocity of the rock glacier's tongue, the current high spatio-temporal TSX DInSAR data is not suitable for monitoring this region of interest.

8.2.2 Jegi rock glacier

8.2.2.1 *Main geomorphological features*

Jegi is a west oriented rock glacier located in the Saas Valley in between 2400 and 2700 meters a.s.l. (Figure 8.9a). It measures 720 meters long and 100 to 150 meters wide. It consists of a rooting zone and an average wide body down to the first front (zone 1), and an approximately 150 m long second tongue located below the first one (zone 2). The inclination of the slope is about 20° in the rooting zone, 15° in the zone of the body and reaches 30° in the frontal parts. The velocity measured by DGPS increases from a few decimeters per year in the rooting zone to 2-2.5 m/y in the first frontal part. The second front is only moving 0.2-0.5 m/y.

8.2.2.2 *Observation using DInSAR data*

Different zones can be distinguished on the Jegi rock glacier using the up-to-date TSX DInSAR data combined with orthoimagery. As seen in Figure 8.9 b to d, the two main moving zones observed on interferometric phase images concern the part including the rooting zone and the body of the rock glacier to the first front, showing a signal from (partly) fringe pattern to noise pattern (zone 1), and the second tongue showing only fringe pattern (zone 2).

By analyzing DInSAR signal, the landform can be separated into more precise zones corresponding to different deformation rates (Figure 8.9b, c). The zone 1 can be divided in three main areas: the rooting zone (zone a) showing small (partly) fringe pattern that can be estimated as a deformation rate of 0.5 m/year in June 2011 and 2012, the main body (zone b) showing closer fringe patterns that can be related to a deformation rate up to 1.5 m/year in June 2011 and 2012, and the first front (zone c) that is observed through a noise pattern and probably moving higher than 1.5 m/year in June 2011 and 2012. The zone 2 can also be divided in two parts; the eastern part (zone d) with a deformation rate quantified at 0.25 m/year in June 2011 and 2012, seems to be moving slower than the frontal part (zone e), where a concentric fringe is observed that can be quantified at 0.5 m/year in June 2011 and 0.75 m/year in June 2012. These deformation rates are roughly estimated visually by quantifying the change in color on the interferometric phase image. The estimation of deformation rate can be verified by comparing with DGPS measurements (Figure 5.11). Furthermore, the change in deformation rate observed between June 2011 and June 2012 is visible.

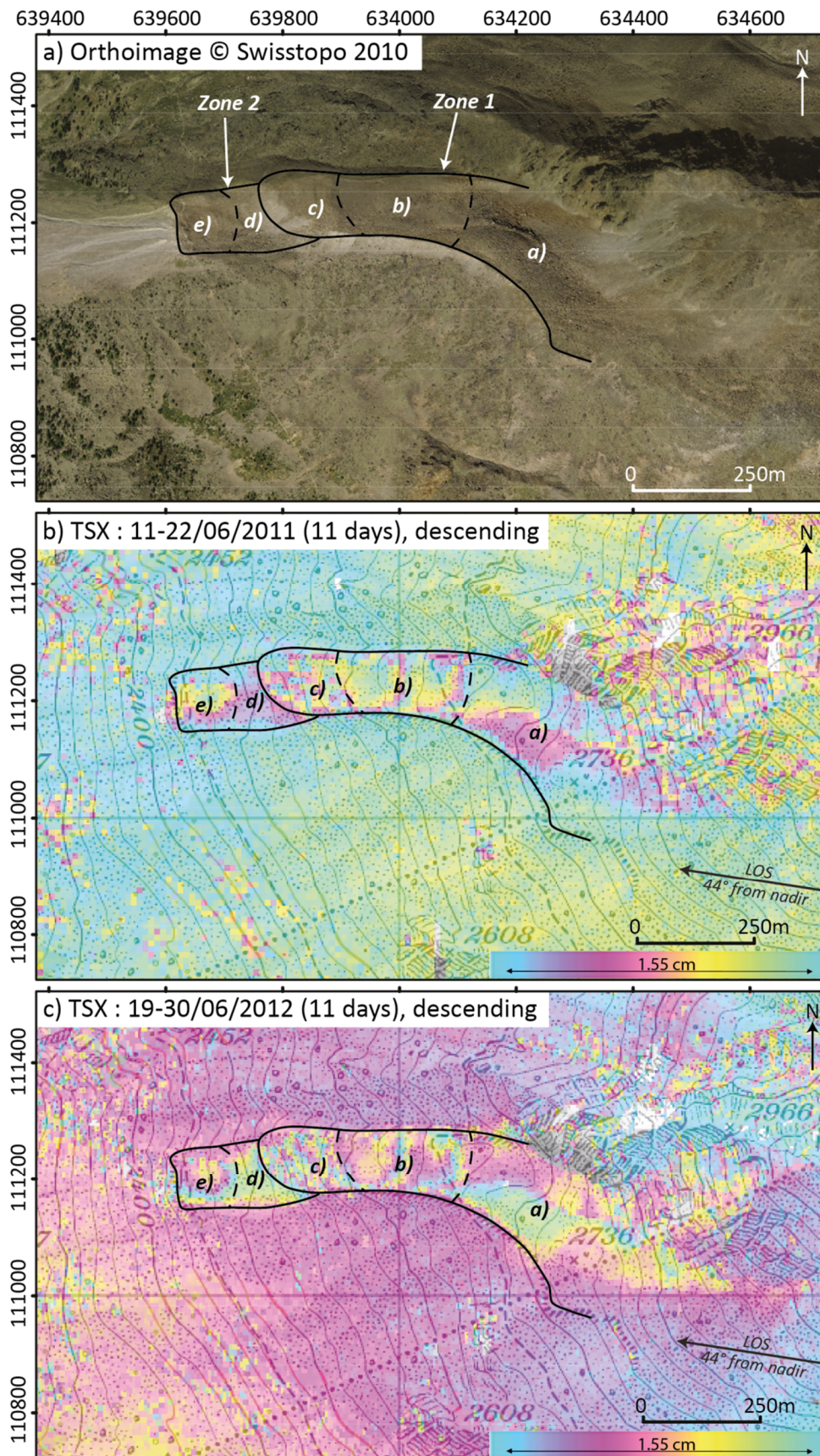


Figure 8.9: Zoning of the Jegi rock glacier using DInSAR signal interpretation. a) Orthoimage from 2010 ©Swisstopo. b) and c) Spatial extent of the different moving zones over the rock glacier detected by DInSAR observations.

In Chapter 5 (Subsection 5.3.1.2), the evolution of the DInSAR signal was analyzed during the summer of 2012 on a complete set of available DInSAR pairs acquired in descending mode with a time interval of eleven days. The mapping of DInSAR signal was used here in order to evaluate seasonal changes in the behavior of the Jegi rock glacier. The variation in time of the DInSAR signal pattern is observed during summer 2012 (Figure 8.10). A first single peak of noise pattern (and respective drop of (partly) fringe pattern) is observed at the end of June; then an increase of the noise pattern (and respective decrease of the fringe pattern) is gradually observed during the summer until September, when finally the proportion of noise pattern is low and the fringe pattern is high again in September-October. A second analysis is performed this time using a set of DInSAR data acquired in descending mode during summer 2011. However, this incomplete set of data does not allow the detection of the first single peak of noise pattern in June. The decrease of the noise and respective increase of the fringe pattern observed in the beginning of autumn seems to also appear in 2011. A third analysis is performed on a set of DInSAR data acquired in ascending mode during summer 2011. This data suggests the presence of a first single peak of noise pattern in the beginning of July. However, the temporal discontinuity between DInSAR pairs does not allow the possibility to evaluate the evolution of the DInSAR signal during the summer.

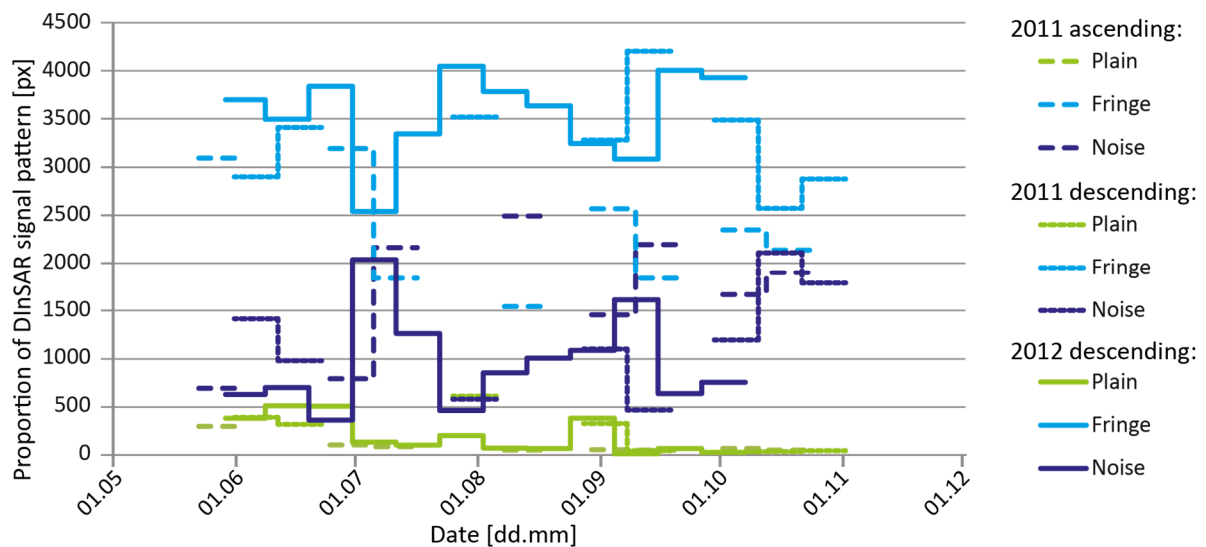


Figure 8.10: Evolution in time of the DInSAR signal pattern on the Jegi rock glacier.

Some data derived from continuous GPS measurements recently acquired on the Jegi rock glacier show intra seasonal variation (Figure 8.11). The maximum velocity seems to be reached in late autumn and an additional short peak in velocity occurs during May.

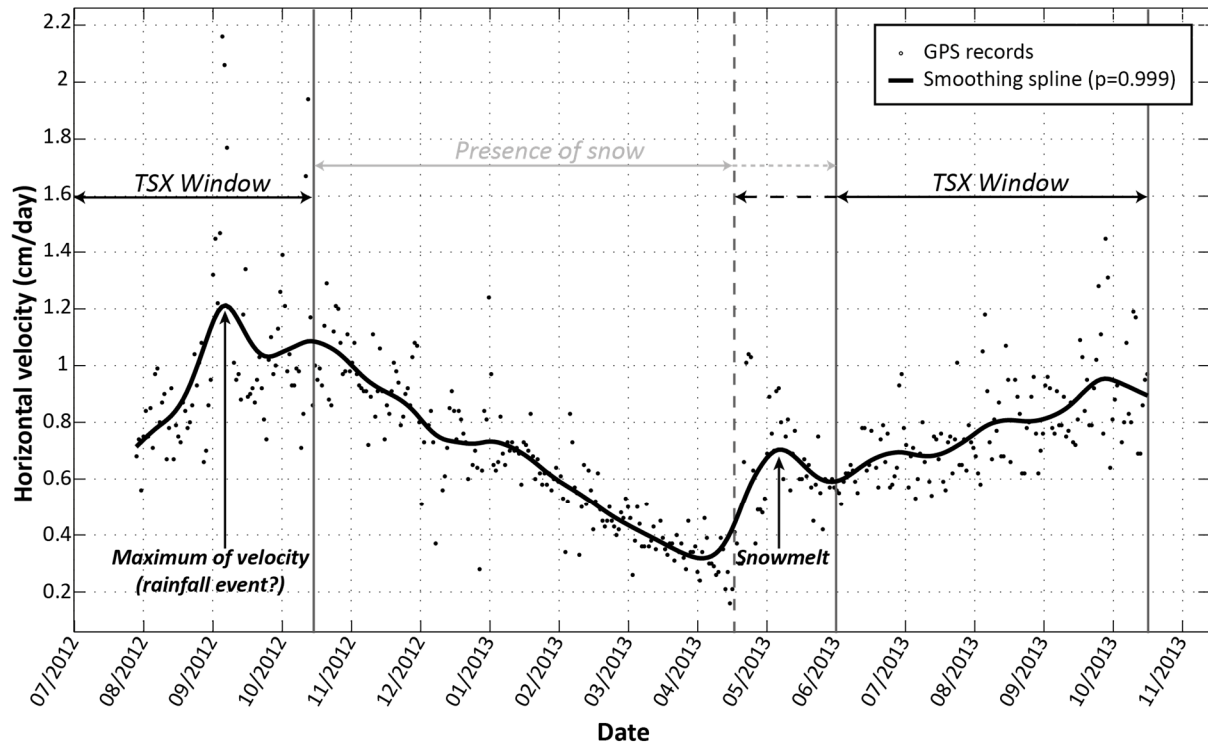


Figure 8.11: Horizontal velocity (cm/day) measured from a fixed GPS. Data courtesy of ETHZ.

Rock glaciers generally display strong inter-annual and seasonal velocity variations, with maximal values often reached in late summer or autumn (e.g. Delaloye et al., 2010a; Noetzli, 2013; Perruchoud and Delaloye, 2007; Wirz et al., 2014). The observed DInSAR signal variation over the Jegi rock glacier can be explained with the study of Wirz et al. (2014) where the same kind of intra-annual pattern of movement using continuous GPS measurements was observed: the maxima in velocity is reached in late autumn and an additional short peak in velocity occurs during the snowmelt period in the end of spring or early summer, which can be explained by the additional amount of water in the system. This kind of regime of velocity is generally observed on rock glaciers having high velocities ($\geq 2\text{m/year}$) with visible signs of destabilizations. However, this phenomenon could also be explained by heavy rain events that can also produce exceptional variations in the velocity of rock glaciers during a short period. These kinds of exceptional variations have been observed on the Gugla rock glacier (Mattertal) on 7-8.07.2014 where the velocity was multiplied by 25 during only a few hours after a heavy rain event. Thus, a combined analysis with available meteorological data would be a good solution to correctly interpret the velocity variations of each landform.

8.2.2.3 Conclusion

The use of up-to-date TSX DInSAR data combined with orthoimagery and terrestrial surveys allow the specific zoning of the Jegi rock glacier into different parts moving with a homogeneous deformation

rate. The analysis of a set of DInSAR data suggests the understanding of seasonal variations of the deformation rate of the landform. However, these kinds of interpretation have to be done very carefully and require a complete set of TSX DInSAR data.

8.3 Discussion

8.3.1 DInSAR dataset

DInSAR scenes have built up a significant archive of data since 1991. The analysis of DInSAR data may help in reconstructing the development and evolution of a landform. As seen in Part 8.1, DInSAR archive data have permitted the partial reconstruction of the timing and causes of the current destabilization phase of the Grabengufer rock glacier. In addition, the use of current DInSAR data may allow the surveillance of current phenomena. As seen in Part 8.2, a large dataset of TSX DInSAR scenes allows the detection of seasonal processes and suggests the understanding of seasonal variation of the deformation rate of some fast moving landforms encountered in the Western Swiss Alps. However, the DInSAR dataset has to be as complete as possible during the summer in order to increase considerably the relevance of DInSAR measurements for seasonal behavior analysis free from in-situ measurements.

8.3.2 Spatio-temporal resolution of DInSAR data

When looking at ERS data acquired in the 1990s, the advantage of DInSAR for detecting very small movements is apparent. The very high temporal resolution of 1 day using tandem ERS-1/2 was moreover very interesting to detect and roughly quantify the deformation rate of fast moving landforms moving faster than 1 m/year (up to 3-5 m/year). However, the low resolution of 25 cm does not allow the precise identification of the deformation field.

The current high spatio-temporal TSX DInSAR data has proven to be useful to delineate a rock glacier and precisely identify the different moving zones of the landform having a homogeneous behavior. However, due to the fast velocity of destabilized rock glaciers encountered in the Swiss Alps, the current TSX DInSAR data seems to be not suitable to quantify the deformation rate of these very active landforms. As seen in Chapter 6, the theoretical maximum measurable deformation rate in the highest slope direction could reach 3.5 m/y in facing mode using the shortest time interval of TSX. However, this measurable deformation rate seems to be lower in practice and depends on the displacement rate and on the nature of the displacement favored by the roughness and the complexity of the landform structure. In most of the cases, decorrelation is observed on these fast moving parts and no quantification of the deformation rate is possible yet. This performance could certainly be approached with CSK using a short term planning of one day; however, this has not been investigated in this thesis.

In any case, by improving the spatio-temporal resolution of detection, the spatio-temporal variability of the DInSAR detected moving area geometry increases too. Thus, evaluating the temporal changes in the behavior of active landforms on the basis of data inventoried from different sensor technologies may be a difficult task and will have to be performed carefully.

8.3.3 Surveying Alpine landforms from DInSAR data

As seen through these different applications, the use of DInSAR data allows the detection and delineation of parts of active rock glaciers moving homogeneously. The deformation rate derived from DInSAR data can be then evaluated visually on these homogeneously moving areas. For further interpretations, it would be interesting to compare deformation rate results with the related topography in order to observe and understand the spatial variation of the landform movements.

The DInSAR data seems to be powerful for a rough visual estimation of the deformation rate. The order of magnitude for the creep velocity compares well with photogrammetry, even if DInSAR reveals slightly higher speeds. The differences can be attributed to the fact that the photogrammetric analysis delivers an average of velocity over several years whereas DInSAR measurements represent snapshots over some days or weeks. Rock glaciers generally display strong inter-annual and seasonal velocity variations, with maximal values often reached in late summer or autumn (e.g. Delaloye et al., 2010a; Noetzli, 2013; Perruchoud and Delaloye, 2007; Wirz et al., 2014). Consequently, depending on what time an interferogram is available, the DInSAR-detected displacement rate may slightly differ from the average velocity. Hence, the short repeat cycles and repeated acquisitions of current TSX acquisitions have proven to be useful to observe this seasonal kinematical behavior.

In the case of precise analysis of deformation fields, the estimation of the deformation rate from DInSAR signal seems to be limited due to the micro-topography and the complex deformation of the observed landforms. It has to be noted that a rough estimation of deformation rate is expressed in the LOS and the 3D projection cannot be realized without a priori on the direction of the process observed. Thus, for the objective to determine the process involved in this particular landform, DInSAR appears to be unsuitable. Actually, through these different applications, it seems very tricky to precisely evaluate the deformation rate of an Alpine landform using DInSAR data. The major conclusion from these studies is that it is probably not advisable to use DInSAR data independently of field measurements in order to understand processes involved in Alpine landforms. DInSAR data can however point out specific phenomena which can then be analyzed in detail using external data such as aerial images, DGPS measurements as well as weather conditions.

Finally, the analysis of the evolution in time of the DInSAR signal using automated mapping of DInSAR signal over the delimited area of the moving landform (as seen for the Jegi rock glacier in Section 8.2.2) seems to be useful to roughly evaluate changes in the behavior of the landform. The analysis

of the coherence trend along a profile can also offer the possibility to detect change in time (see Chapter 5); however, the main advantage of DInSAR signal mapping is to provide information on the entire surface of the landform. Perspectives for surveying Alpine landforms are thus foreseen: by defining the boundary of several observed landforms, the presented methodology of automated mapping of DInSAR signal and analysis of its evolution in time can be widespread for large scale surveys.

8.4 Conclusion

In this chapter, the potential and contribution of the method for determining the past and current behavior of Alpine landforms located in the Western Swiss Alps are presented through different applications. However, these applications are not meant to be exhaustive and are given in order to demonstrate to geomorphologists the use of DInSAR technique in the Alpine environment and other mountainous environments.

The experience shows that the combination of DInSAR signal analysis with external data, like high resolution orthoimages or in-situ measurements, seems to be the best compromise to determine the behavior of Alpine landforms with high precision and accuracy. In any case, these kinds of interpretations are realized by combining high competences in geomorphology and specific software skills in order to provide suitable DInSAR data.

In the typical case of monitoring, the results are however not convincing for the specific case of fast moving rock glaciers (1-3.5 m/year) encountered in the Western Swiss Alps. In fact, the analysis provides a general overview of the mechanisms involved in these specific landforms and cannot be used to specifically understand the processes governing them. The main reason comes from the fact that the DInSAR signal is often disturbed due to the complexity of the velocity field and the proximity to maximal observable deformation rate (near decorrelation). Moreover, even if a complete TSX DInSAR dataset is available to observe seasonal behavior, the deformation rate is known only in the LOS direction regardless of how it is derived. Consequently, only a second acquisition acquired in the opposite mode and at exactly the same time could provide 3D information about an instantaneous deformation.

Consequently, the use of DInSAR data cannot compete with techniques currently used in the Alpine geomorphology field in order to understand dynamics of Alpine landforms. The use of DInSAR signal mapping and the analysis of the evolution in time of this signal over a landform suggest, however, a potential way to survey several Alpine landforms at a regional scale.

4th Part:

Synthesis and Conclusion

The last 4th Part provides a general discussion on the achievements of the thesis and the perspectives for future research.

9 Conclusion and perspectives

9.1 General results and main contributions

The research presented in this thesis consists in a multidisciplinary work involving signal and image processing, statistical classifiers, experimental protocols, data analysis, and finally Alpine geomorphology skills. Taking a methodological approach, this project focused on the potential of analysis of Alpine moving landforms offered by the relatively new technology of DInSAR technique. Challenges and solutions to detect, map and monitor Alpine moving landforms using DInSAR technique have been shown in this dissertation and specific contributions can be summarized as follows:

- A standard protocol for the suitability assessment of DInSAR technique for the detection, mapping and monitoring of Alpine moving landforms in a delimited area of interest has been proposed (Part 3.3).
- The suitability of TSX DInSAR data for the observation of Alpine landforms in the Western Swiss Alps has been assessed (Part 6.3).
- An automated procedure for the mapping of the slope movements derived from DInSAR data has been developed (Parts 4.2 and 4.3).
- The proposed automated mapping of the slope movements derived from DInSAR data has been tested for the update and upgrade (Part 7.1) of past inventoried DInSAR detected moving zones as well as for the refinement and the assessment of debris-covered glaciers (Part 7.2).
- The past development of the pluri-decennial development of a rock glacier crisis has been reconstructed using the combination of DInSAR, aerial and terrestrial data (Part 8.1).
- TSX DInSAR data has been used for the detection of seasonal and geomorphological processes governing the activity of rock glaciers (Part 8.2).

Through this whole study, the following main results can be observed according to the three main selected topics:

- 1) *Suitability of DInSAR data for the detection, mapping and monitoring of Alpine slope movements:*
 - The performance of DInSAR data for the purpose of Alpine research in a defined region of interest can be and should be evaluated before acquiring data thanks to a systematic procedure (Parts 3.3 and 6.3).

2) *Detection and mapping of Alpine slope movements using DInSAR technique:*

- The use of DInSAR data seems to be the current best method for a large-scale detection of slope instabilities. Using a large set of DInSAR data with various time intervals, this technique provides a regional overview of surface displacements at mm to cm resolution over Alpine areas (with sparse vegetation and during the snow-free period) (Subsection 4.1.1.4).
- The DInSAR signal pattern gives information about a detected area moving homogeneously which is dependent on the sensor characteristics. The margin of the moving zone depends mainly on the spatial resolution of the sensor, the time interval and the wavelength of the sensor, and the deformation rate of the moving zone (Section 3.2.4). Using a set of DInSAR data from the same sensor, it is possible to detect a change in deformation rate by observing the change of DInSAR signal pattern (Part 7.1). The evolution in time of the moving zones detected with different SAR sensors has to be performed carefully (Section 7.1.5).
- The automated mapping of DInSAR signal is possible by using image processing and statistical classifiers applied to the interferometric phase image. The related map of slope movements can then be compiled using a set of DInSAR data with the same time interval and provides a general overview of the stability of the terrain during this specific time interval (Part 4.4). This resulting map can be used as a useful tool for helping the visual interpretation and reducing the subjectivity (Part 7.1).
- The visual update and upgrade of past DInSAR polygons, passing through the past ERS technology to the current TSX technology, seems to be the most accurate solution to a problem of sensor compatibility. The margins of detected moving zones and the correspondence between DInSAR signal patterns and deformation rates differ according to the SAR sensor, creating difficulties for an automated approach (Section 7.1.5).
- The shortest time interval of eleven days of TSX DInSAR data can be used to refine the glacier outlines over debris-covered parts. The map of slope movements derived from TSX DInSAR data for the time interval of eleven days can be useful to detect and delimitate the debris-covered ice outlines (Part 7.2).

3) *Monitoring of Alpine slope movements using DInSAR technique:*

- DInSAR data, and especially archive data, when combined with external data such as aerial images, terrestrial data, etc. can be used to reconstruct the past evolution of an Alpine landform (Part 8.1).
- The new high spatio-temporal resolution of TSX DInSAR data does not allow the quantification of surging rock glacier deformation (velocity ≥ 2 m/year). Some cases of very active Alpine movement slopes (1-3.5 m/y) can be partly correctly monitored. However,

noise generally affects DInSAR signal over (some parts of) these landforms and inhibits the possibility to estimate precisely the deformation rate (Subsection 5.2.2.1; Part 8.2).

- The new high spatio-temporal resolution of TSX DInSAR data allows the change detection of rock glacier deformation during the summer. The use of a complete set of TSX DInSAR data during summer with a time interval of eleven days allows the qualitative estimation of seasonal variation of the landform deformation rate (Subsections 5.2.3.3 and 5.3.1.2; Part 8.2).
- The new high spatio-temporal resolution of TSX DInSAR data can be used to detect and indicate specific processes governing the Alpine landforms. However, to understand and interpret the processes governing the landform, DInSAR observations have to be combined with external data (Parts 8.1 and 8.2).

9.2 Further improvements and future research

The potential limitations and possible improvements of each method presented in this dissertation have been discussed in their respective chapters. Nevertheless, some general recommendations for further improvements or future research are formulated hereafter.

9.2.1 Suitability protocol

As already noted in the discussion part of Chapter 3 (Section 3.3.5), it would be really useful to develop an algorithm to help users perform a pre-survey analysis prior to the costly investment of a radar survey. The proposed proof-of-concept and similar approaches seen in the literature detailed the specific protocol to perform in order to determine the suitability of DInSAR data for surveying mountain slopes in a specific region of interest. Nevertheless, the current version of Gamma software needs at least one SLC parameter file to perform this analysis. It would be really useful to compute directly from this software a rough estimation of layover and shadow, as well as to determine the local looking vector knowing only the basic flight direction parameters (namely the LOS direction) in order to determine the suitability of the SAR sensors over a future region of interest.

9.2.2 Algorithm for slope movement mapping

One of the critical points which was identified as having a direct impact on the performance of the slope movement mapping and its use in deriving detection, mapping, and change detection of Alpine landforms deformation rate, is the compatibility between different sensors. Since the qualitative slope movement is directly derived from the analysis of DInSAR signal, it is dependent on the sensor's characteristics and has to be properly analyzed when combining analyses from DInSAR data derived from different sensors. Solutions could come from a calibration of the model using a kind of lookup

table that indexes the computation and allows the computational results to fit together whatever the sensor.

Another important issue comes from the fact that the proposed procedure is currently coded in Matlab language which makes this algorithm an experimental protocol. Due to computational timing restrictions, it does not allow for working with large sized images and needs to focus the analysis on a reduced area. This problem can be solved by coding the proposed algorithm in another more efficient language.

9.2.3 Requirements for the update and upgrade of past inventoried DInSAR polygons

In Chapter 4, a standard procedure was recommended to accurately map slope movements. This kind of slope movement map may support experts in the development of accurate slope movement inventories free from the subjectivity of the operator by using it as a useful tool for visually interpreting DInSAR data, especially when using a large SAR dataset. These maps have also been used to automatically update past inventoried DInSAR polygons in a reduced test area. However, results show that an automated detection of Alpine landform changes using current TSX data based on the existing DInSAR polygon inventory derived from ERS data is hardly possible due to the different sources of data. Specifically, the delimited moving zones cannot be compared if sensor technology differs. A visual upgrade with the help of slope movement mapping as a useful tool for interpretation of a large DInSAR dataset is probably the best solution to perform an accurate up-to-date inventory. However, is it really useful to update and upgrade the inventoried slope movements in the entire Western Swiss Alps? Representing probably a long and tedious task and which is perhaps not justified? In order to reduce the working efforts, a solution would consist in a prioritization of the landforms or regions to update. One can imagine focusing the update on only the Alpine landforms related to rock glaciers, or on only the watersheds containing Alpine moving landforms connected to a channel system with a high potential of torrential hazard. The choice has to be determined in advance in order to clearly delimitate the areas for action.

9.2.4 Early warning system using continuous up-to-date DInSAR data

The present methodological thesis mainly focused on the use of DInSAR data for the detection, mapping and monitoring of Alpine moving landforms. An extension of the present methods used as an early warning system allowing the automated detection of change in the surveyed Alpine landforms can be developed. Through the different methods presented and tested in this work, the solution would consist in analyzing the evolution in time of the DInSAR signal patterns over the delimited landform. As shown along the different works proposed in this dissertation, the DInSAR

signal is related to the deformation rate of the observed landform. Any change in the deformation rate is detected by a change in the DInSAR signal. Consequently, the monitoring of the evolution of the DInSAR signal over the delimited landform allows the qualitative detection of a change in the activity rate of the landform.

The change can be observed for active moving landforms using TSX DInSAR and its continuous revisiting time of eleven days. To perform such monitoring, a specific outline has first to be defined around each Alpine landform to survey. Then the general DInSAR signal behavior should be defined for each outlined landform. This general DInSAR signal behavior is given by the proportion of DInSAR signal patterns for the reference state of the landform and for the specific sensor characteristics. When a new SAR acquisition is performed, DInSAR data has to be computed and the current proportion of DInSAR signal patterns has to be compared with the reference state in order to determine potential changes in landform activity. Further investigations have to be performed in order to determine and validate specific thresholds indicating the change of landform activity when exceeded. Threshold can be adjusted as needed to detect an increase of activity, a decrease of activity, a change in the seasonal behavior, in the annual behavior, etc. In any case, the general behavior of DInSAR signal has to be defined for the landform and for each specific sensor in order to enhance the compatibility between sensors.

9.3 Perspective in Alpine geomorphology

9.3.1 Extension to other alpine regions

DInSAR technique is probably the best way to determine the distribution of moving slopes on an unknown region of interest and can certainly be applied in different mountain environments, such as the Andes or the Himalayas. The suitability of DInSAR data for the purpose of alpine research in a defined region of interest should however be evaluated before acquiring data, and could be performed by the proposed systematic procedure in order to determine precisely the area of possible observation and the most suitable data. The automatic data storing and systematic acquisition of SAR data are ensured worldwide for most of the sensors – for very high resolution SAR satellites the data acquisition is performed only upon request, consequently only few areas are available with large archives – and allow the application of the methodology to other parts of the globe from data archives. However, current data accessibility is not always possible. It may be restricted by costs sometimes too high for scientific purposes and by availability. For instance, TSX successive stripmaps are acquired in the same orbit, making the availability of the two contiguous areas impossible at the same time. Moreover, high quality DEM are not always available and the

topography of the region could be unsuitable for the application of DInSAR. This problem would be perhaps solved with the upcoming global DEM from the Tandem-X mission.

9.3.2 Processes understanding

The potential of DInSAR data for Alpine moving landform monitoring was presented through different applications aiming to determine the past and current behavior of these landforms. The combination of DInSAR signal analysis with external data, like high resolution orthoimages or in-situ measurements, seems to be the best compromise to determine the behavior of Alpine landforms with high precision and accuracy. In any case, these kinds of interpretations have to be performed by combining high competences in geomorphology and specific software skills in order to provide suitable DInSAR data.

Industry and manufacturing progress might continue increasing the spatial and temporal resolution of sensors in the upcoming years, thus leading to precise sensors for monitoring purposes. This would open the doors to the monitoring of fast moving Alpine slopes, the precise mapping of velocity rates and the possibility to observe particular changes in the behavior of Alpine landforms.

9.4 Conclusion

Finally, this thesis has shown that DInSAR technique is really suitable to detect and map Alpine moving landforms in a mountainous region. DInSAR is a good alternative and a powerful technique to give a general overview of the distribution of moving objects in an entire studied region, especially in mountainous areas often difficult to access. This kind of analysis, automatic or not, provides a meticulous starting point allowing the detection and selection of landforms that have to be monitored more precisely. This work has also demonstrated that precise techniques commonly used in the Alpine environment to analyze landform kinematics are probably more suitable than DInSAR technique to monitor rapidly moving Alpine landforms (≥ 1.5 m/year) and have to be used jointly to precisely understand the processes governing them.

Bibliography

- Abermann J, Fischer A, Lambrecht A, Geist T. 2010. On the potential of very high-resolution repeat DEMs in glacial and periglacial environments. *The Cryosphere* **4** : 53–65. DOI: 10.5194/tc-4-53-2010.
- Askne J, Hagberg JO. 1993. Potential of interferometric SAR for classification of land surfaces. *Geoscience and Remote Sensing Symposium, 1993. IGARSS '93.* **3** : 985–987.
- Atwood DK, Meyer F, Arendt A. 2010. Using L-Band SAR coherence to delineate glacier extent. *Canadian Journal of Remote Sensing* **36** : 186–195.
- Baldi P, Cenni N, Fabris M, Zanutta A. 2008. Kinematics of a landslide derived from archival photogrammetry and GPS data. *Geomorphology* **102** : 435–444. DOI: 10.1016/j.geomorph.2008.04.027
- Balzter H. 2001. Forest mapping and monitoring with interferometric synthetic aperture radar (InSAR). *Progress in Physical Geography* **25** : 159–177. DOI: 10.1177/030913330102500201.
- Bamler R, Hartl P. 1998. Synthetic aperture radar interferometry. *Inverse Problems* **14** : R1–R54.
- Barboux C, Delaloye R. 2010a. Aerial images analysis - Graben Gufer. Rapport pour l'Office Fédérale de l'Environnement. Département des Géosciences, Géographie, Université de Fribourg, non publié, 24p.
- Barboux C, Delaloye R. 2010b. Analysing the pluri-decennial development of a slimping rock glacier using airborne optical data, satellite and terrestrial SAR interferometry, and geodetic survey. *Swiss Geoscience Meeting, 19-20 November 2010, Fribourg (Poster)*.
- Barboux C, Delaloye R, Strozzi T, Collet C, Raetzo H. 2011. TSX InSAR assessment for slope instabilities monitoring in alpine periglacial environment (Western Swiss Alps, Switzerland). *Proceedings of the FRINGE 2011 workshop, 19-23 September (ESA SP-697, January 2012)*.
- Barboux C, Delaloye R, Strozzi T, Lambiel C, Collet C, Raetzo H. 2012. Monitoring active rock glaciers in the Western Swiss Alps: Challenges of Differential SAR Interferometry and solution to estimate annual and seasonal displacement rates. *Proceeding of IGARSS 2012, 22 - 27 July 2012*.
- Barboux C, Delaloye R, Strozzi T, Lambiel C, Collet C. 2013a. TSX DInSAR data for detecting and monitoring slope motion phenomena in an Alpine periglacial environment at different resolution scales (Western Swiss Alps, Switzerland). *TerraSAR-X Science Team Meeting, 10 - 12 June 2013, DLR Oberpfaffenhofen*.
- Barboux C, Fischer M, Delaloye D, Huss M. 2013b. Mapping of debris-covered ice using DInSAR and airborne photography : A pilot study in the Upper Valais (Swiss Alps). *Swiss Geoscience Meeting, 15-16 November 2013, Lausanne (Poster)*.
- Barboux C, Reynald D, Christophe L, Tazio S, Hugo R, Claude C. 2013c. Semi-automated detection of terrain activity in the Swiss Alpine periglacial environment from DInSAR scenes. *Living Planet Symposium. Edimburgh (Scotland)*.

Barboux C, Delaloye R, Lambiel C. 2014. Inventorying of slope movement in Alpine environment using DInSAR. *Earth Surface Processes and Landforms* (In Press) DOI: 10.1002/esp.3603.

Barrett BW, Dwyer E, Whelan P. 2009. Soil Moisture Retrieval from Active Spaceborne Microwave Observations: An Evaluation of Current Techniques. *Remote Sensing* **1** : 210–242. DOI: 10.3390/rs1030210.

Barsch D. 1992. Permafrost creep and rock glaciers. *Permafrost and Periglacial Processes* **3** : 175–188.

Barsch D, Caine N. 1984. The Nature of Mountain Geomorphology. *Mountain Research and Development* **4** (4): 287–298.

Bauder A, Rüegg R (eds). 2009. The Swiss Glaciers. 2003/04 and 2004/05. *Glaciological Report (Glacier) No. 125/126*. 111p.

Berger J, Krainer K, Mostler W. 2004. Dynamics of an active rock glacier (Ötztal Alps, Austria). *Quaternary Research* **62** : 233–242. DOI: 10.1016/j.yqres.2004.07.002.

Bishop CM. 2006. *Pattern recognition and machine learning* . Springer Science+Business Media, LLC.

Bosson J-B, Lambiel C. 2014. The current evolution of complex high mountain debris-covered glacier systems and its relation with ground ice nature and distribution : the case of Rognes and Pierre Ronde area (Mont-Blanc range , France). *Geophysical Research Abstracts* **16** : EGU2014–3652.

Bühler Y, Graf C. 2013. Sediment transfer mapping in a high-alpine catchment using airborne LiDAR. Graf, C. (Red.) *Mattertal – ein Tal in Bewegung*. Publikation zur Jahrestagung der Schweizerischen Geomorphologischen Gesellschaft 29. Juni – 1. Juli 2011, St. Niklaus. Birmensdorf, Eidg. Forschungsanstalt WSL. : 113–124.

Cohen J. 1960. A coefficient of agreement for nominal scales. *Educ. Psychol. Meas.* **20** : 37–46.

Congalton RG. 1991. A Review of Assessing the Accuracy of Classifications of Remotely Sensed Data. *Remote Sensing of Environment* **46** : 35–46.

Congalton RG, Green K. 1998. *Assessing the Accuracy of Remotely Sensed Data: Principles and Practices* . CRC Press.

Crozier MJ. 2004. Slope stability. In *Encyclopedia of Geomorphology*. Volume 2 , Goudie A (ed). Routedledge; 969–970.

Dammert PBG, Askne JIH, Sharon K. 1999. Unsupervised Segmentation of Multitemporal Interferometric SAR Images. *IEEE Transaction on Geoscience and Remote Sensing* **37** : 2259–2271.

Delacourt C, Allemand P, Casson B, Vadon H. 2004a. Velocity field of the “La Clapière” landslide measured by the correlation of aerial and QuickBird satellite images. *Geophysical Research Letters* **31** : 1–5. DOI: 10.1029/2004GL020193.

Delacourt C, Allemand P, Squarzoni C, Picard F, Raucoules D, Carnec C. 2004b. Potential and limitation of ERS-Differential SAR Interferometry for landslide studies in the French Alps and Pyrenees. *Proceeding of the FRINGE 2003 workshop*, 1-5 December 2003 (ESA SP-550, June 2004).

Delacourt C, Allemand P, Berthier E, Raucoules D, Casson B, Grandjean P, Pambrun C, Varel E. 2007. Remote-sensing techniques for analysing landslide kinematics: a review. *Bulletin de la Société Géologique de France* **178** : 89–100.

Delaloye R. 2004. Contribution à l'étude du pergélisol de montagne en zone marginale. PhD Thesis. Departement of Geosciences, Geography, University of Fribourg.

Delaloye R, Morand S. 1997. Du Val Ferret au Grand-Combin (Alpes Valaisannes): Inventaire des glaciers rocheux et analyse spatiale du pergélisol à l'aide d'un système d'information géographique (IDRISI). Master Project. University of Fribourg, Switzerland.

Delaloye R, Lambiel C, Lugon R. 2005. InSAR Bas-Valais. Validation of InSAR data in permafrost zone. ESA SLAM project, phase 2, Bas-Valais. Final report for the Federal Office of Water and Geology (unpublished).

Delaloye R, Lambiel C, Lugon R, Raetzo H, Strozzi T. 2007a. ERS InSAR for Detecting Slope Movement in a Periglacial Mountain Environment (Western Valais Alps, Switzerland). *Proceeding of HMRSC-IX, Grazer Schriften der Geographie und Raumforschung* **43** : 113–120.

Delaloye R, Lambiel C, Lugon R, Raetzo H, Strozzi T. 2007b. Typical ERS InSAR signature of slope movement in a periglacial mountain environment (Swiss Alps). *Proceeding of ENVISAT Symposium 2007 (ESA SP-636, July 2007)*.

Delaloye R, Perruchoud E, Lambiel C, Lugon R. 2008a. InSAR Haut-Valais: inventaire des mouvements de terrain par analyse de signaux d'interférométrie radar satellitaire (période 1993-2000). (non publié).

Delaloye R, Strozzi T, Lambiel C, Perruchoud E, Raetzo H. 2008b. Landslide-like development of rockglaciers detected with ERS 1-2 SAR interferometry. *Processing of FRINGE 2007 Workshop, 26-30 November (ESA SP-649, February 2008)*.

Delaloye R, Lambiel C, Gärtner-roer I. 2010a. Overview of rock glacier kinematics research in the Swiss Alps. Seasonal rhythm, interannual variations and trends over several decades. *Geographica Helvetica* **65** : 135–145.

Delaloye R, Strozzi T, Lambiel C, Barboux C, Mari S, Stocker A, Techel F, Raetzo H. 2010b. The contribution of InSAR data to the early detection of hazardous active rock glaciers in mountain areas. *Proceedings ESA Living Planet Symposium 2010, (ESA SP-686, December 2010)*.

Delaloye R, Morard S, Barboux C, Abbet D, Gruber V, Riedo M, Gachet S. 2013. Rapidly moving rock glaciers in Mättertal. Graf C (ed). *Mättertal - ein Tal in Bewegung*. Publikation zur Jahrestagung der Schweizerischen Geomorphologischen Gesellschaft 29. Juni - 1. Juli 2011, St. Niklaus, Birmensdorf, Eidg. Forschungsanstalt WSL. 164 S. : 21–31.

Delaloye R, Abbet D, Barboux C, Braillard L, Kummert M, Morard S. 2014. Blockgletscher und Hangrutschungen in Permafrostgebieten Departement für Geowissenschaften. Blockgletscher und Hangrutschungen in Permafrostgebieten, Projekt "Mättertal" (2009-2013), Gemeinde St.-Niklaus und Randa, Abschlussbericht 2013. Département des Géosciences, Géographie, université de Fribourg, non publié, 121p.

- Diolaiuti G a., Bocchiola D, Vagliasindi M, D'Agata C, Smiraglia C. 2012. The 1975-2005 glacier changes in Aosta Valley (Italy) and the relations with climate evolution. *Progress in Physical Geography* **36** : 764–785. DOI: 10.1177/0309133312456413.
- Duro J, Albiol D, Mora O, Payas B. 2013. Application of advanced InSAR techniques for the measurement of vertical and horizontal ground motion in longwall minings. 13th Coal Operators' Conference, University of Wollongong, The Australasian Institute of Mining and Metallurgy & Mine Managers Association of Australia : 99–106.
- Eberhardt E, Stead D, Coggan JS. 2004. Numerical analysis of initiation and progressive failure in natural rock slopes—the 1991 Randa rockslide. *International Journal of Rock Mechanics and Mining Sciences* **41** : 69–87. DOI: 10.1016/S1365-1609(03)00076-5.
- Echelard T, Schoeneich P, Gay M. 2013. Rockglacier movement detection by D-InSAR in French Alps using TerraSAR-X data: Inventory (large scale) and case study (local scale). TerraSAR-X Science Team Meeting, 10 - 12 June 2013, DLR Oberpfaffenhofen.
- Engdahl ME, Hyyppä JM. 2003. Land-Cover Classification Using Multitemporal ERS-1/2 InSAR Data. *IEEE Transaction on Geoscience and Remote Sensing* **41** : 1620–1628.
- Falaschi D, Bravo C, Masiokas M, Villalba R, Rivera A. 2013. First glacier inventory and recent changes in glacier area in the Monte San Lorenzo Region (47°S), Southern Patagonian Andes , South America. *Arctic, Antarctic and Alpine Research* **45** : 19–28.
- Ferretti A, Monti-guarnieri A, Prati C, Rocca F, Massonnet D. 2007. Part A: Interferometric SAR image processing and interpretation. In *InSAR Principles: Guidelines for SAR Interferometry Processing and Interpretation* , Fletcher K (ed). ESA Publications.
- Fischer M, Huss M, Barboux C, Hoelzle M. 2014. The new Swiss Glacier Inventory SGI2010 : Relevance of using high- resolution source data in areas dominated by very small glaciers. *Arctic, Antarctic, and Alpine Research* (In Press).
- Frey H, Paul F, Strozzi T. 2012. Compilation of a glacier inventory for the western Himalayas from satellite data: methods, challenges, and results. *Remote Sensing of Environment* **124** : 832–843. DOI: 10.1016/j.rse.2012.06.020.
- Gabriel AK, Goldstein RM, Zebker HA. 1989. Mapping Small Elevation Changes Over Large Areas: Differential radar interferometry. *Journal of Geophysical Research* **94** : 9183–9191.
- Giardino JR, Shroder J., Vitek J. (eds). 1987. *Rock glaciers* . Boston, Lo. Allen & Unwin.
- Goldstein R, Werner CL. 1998. Radar interferogram filtering for geophysical applications. *Geophysical Research Letters* **25** : 4035–4038.
- Graf C, Deubelbeiss Y, Bühler Y, Meier L, McArdeall BW, Christen M, Bartelt P. 2013. Gefahrenkartierung Mattertal: Grundlagenbeschaffung und numerische Modellierung von Murgängen. Graf, C. (Red.) Mattertal – ein Tal in Bewegung. Publikation zur Jahrestagung der Schweizerischen Geomorphologischen Gesellschaft 29. Juni – 1. Juli 2011, St. Niklaus. Birmensdorf, Eidg. Forschungsanstalt WSL. : 85–112.
- Haeberli W. 1979. Holocene push-moraines in Alpine permafrost. *Geografiska Annaler* **61A** : 43–48.

Hanssen RF. 2005. Satellite radar interferometry for deformation monitoring: a priori assessment of feasibility and accuracy. *International Journal of Applied Earth Observation and Geoinformation* **6** : 253–260. DOI: 10.1016/j.jag.2004.10.004.

Haralick RM. 1979. Statistical and Structural Approaches to Texture. *Proceedings of the IEEE* **67** : 786–804.

Haralick RM, Shanmugam K, Dinstein I. 1973. Textural features for image classification. *IEEE Transactions on Systems, Man and Cybernetics* **SMC-3** : 610–621.

Harris C. 2007. Periglacial landforms/Slope deposits and forms. In *Encyclopedia of Quaternary science*. Volume 3 , Elias SA (ed). Elsevier; 2207–2217.

Jain AK, Dubes RC. 1988. Algorithms for clustering data . Prentice Hall Advanced Reference Series.

Jones H., Vaughan RA. 2010. Remote sensing of vegetation: Principles, Techniques, and Applications . Oxford, N.

Kääb A. 2007. Periglacial landforms, rock forms/Rock glaciers and protalus forms. In *Encyclopedia of Quaternary science*. Volume 3 , Elias SA (ed). Elsevier; 2236–2242.

Kääb A. 2008. Remote Sensing of Permafrost-related Problems and Hazards. *Permafrost and Periglacial Processes* **19** : 107–136. DOI: 10.1002/ppp.619.

Kääb A, Haeberli W, Gudmundsson GH. 1997a. Analysing the Creep of Mountain Permafrost using High Precision Aerial Photogrammetry : 25 Years of Monitoring Gruben Rock Glacier , Swiss Alps. *Permafrost and Periglacial Processes* **8** : 409–426.

Kääb A, Haeberli W, Gudmundsson GH. 1997b. Analysing the creep of mountain permafrost using high precision aerial photogrammetry: 25 years of monitoring Gruben rock glacier, Swiss Alps. *Permafrost and Periglacial Processes* **8** : 409–426. DOI: 10.1002/(SICI)1099-1530(199710/12)8:4<409::AID-PPP267>3.0.CO;2-C.

Kääb A, Gudmundsson GH, Hoelzle M. 1998. Surface deformation of creeping mountain permafrost. Photogrammetric investigation on rock glacier Murtel, Swiss Alps. *Proceedings the 7th International Conference on Permafrost*, 531–537.

Kääb A, Kaufmann V, Ladstädter R, Eiken T. 2003. Rock glacier dynamics : implications from high-resolution measurements of surface velocity fields. *Proceedings of the 8th International Conference on Permafrost*, **1**: 501–506.

Kääb, A., Huggel, C., Fischer, L., Guex, S., Paul, F., Roer, I., Salzmann, N., Schläefli, S., Schmutz, K., Schneider, D., Strozzi, T., and Weidmann, Y. 2005. Remote sensing of glacier- and permafrost-related hazards in high mountains: an overview. *Natural Hazards and Earth System Science* **5** : 527–554. DOI: 10.5194/nhess-5-527-2005.

Kaufmann V. 1998. Deformation analysis of the doesen rock glacier (Austria). *Proceedings the 7th International Conference on Permafrost*, 551–556.

- Kaufmann V, Ladstädter R, Kienast G. 2007. 10 years of monitoring of the Doesen rock glacier (Ankogel Group, Austria) - A review of the research activities for the time period 1995-2005. 5th ICA Mountain Cartography Workshop: 129–144.
- Kenyi LW, Kaufmann V. 2000. Detection and quantification of rock glacier deformation using ERS D-InSAR data. Proceedings of the ERS-Envisat Symposium 16-20 October 2000.
- Kenyi LW, Kaufmann V. 2001. Estimation of alpine permafrost surface deformation using InSAR data. Proceedings of IGARSS 2001, 9-3 July (Cat. No.01CH37217) : 1107–1109.
- Kenyi LW, Kaufmann V. 2003. Estimation of rock glacier surface deformation using sar interferometry data. IEEE Transaction on Geoscience and Remote Sensing **41** : 1512–1515.
- Klees R, Massonnet D. 1999. Deformation measurements using SAR interferometry : potential and limitations. *Geologie en Mijnbouw* **77** : 161–176.
- Klein A. 2004. remote sensing in geomorphology. In *Encyclopedia of Geomorphology*. Volume 2 , Goudie AS (ed). Routledge; 844–846.
- Knoll C, Kerschner H. 2009. A glacier inventory for South Tyrol , Italy , based on airborne laser-scanner data. *Annals of Glaciology* **50** : 46–52.
- Krainer K, Mostler W. 2006. Flow velocities of active rock glaciers in the Austrian Alps. *Geografiska Annaler* **88A** : 267–280.
- Kummert M, Barboux C, Delaloye R. 2014. Classifying torrential catchments according to the contribution of slope movements in the sediment supply to the channel: a pilot study in the lower Valais (Swiss Alps). SGM2014, Fribourg. (Poster).
- Lambiel C, Reynard E. 2003. Cartographie de la distribution du pergélisol et datation des glaciers rocheux dans la région du Mont Gelé (Valais). In Maisch M, Vonder M.D. et Monbaron M., *Entwicklungstendenzen end Zukunftsperspektiven in der Geomorphologie*. Zürich: Universität Züürich, Geographisches Institut, Physische Geographie : 91–103.
- Lambiel C, Delaloye R. 2004. Contribution of real-time kinematic GPS in the study of creeping mountain permafrost: examples from the Western Swiss Alps. *Permafrost and Periglacial Processes* **15** : 229–241. DOI: 10.1002/ppp.496.
- Lambiel C, Delaloye R, Strozzi T, Lugon R, Raetzo H. 2008. ERS InSAR for assessing rock glacier activity. 9th Int. Conference on Permafrost, 29 June - 03 July 2008 : 1019–1025.
- Lateltin O, Haemmig C, Raetzo H, Bonnard C. 2005. Landslide risk management in Switzerland. *Landslides* **2** : 313–320. DOI: 10.1007/s10346-005-0018-8.
- Lilleøren KS, Etzel Müller B, Gärtner-Roer I, Käb A, Westermann S, Guðmundsson Á. 2013. The Distribution, Thermal Characteristics and Dynamics of Permafrost in Tröllaskagi, Northern Iceland, as Inferred from the Distribution of Rock Glaciers and Ice-Cored Moraines. *Permafrost and Periglacial Processes* **24** : 322–335. DOI: 10.1002/ppp.1792.
- Lillesand TM, Kieffer RW. 1994. *Remote Sensing and Image Interpretation* . 3rd ed. New York, Chichester, Brisbane, Toronto, Singapore: John Wiley & Sons.

- Liu L, Millar CI, Westfall RD, Zebker H a. 2013. Surface motion of active rock glaciers in the Sierra Nevada, California, USA: inventory and a case study using InSAR. *The Cryosphere Discussions* **7** : 343–371. DOI: 10.5194/tcd-7-343-2013.
- Lugon R, Delaloye R, Serrano E, Reynard E, Lambiel C, González-Trueba JJ. 2004. Permafrost and Little Ice Age glacier relationships, Posets Massif, Central Pyrenees, Spain. *Permafrost and Periglacial Processes* **15** : 207–220. DOI: 10.1002/ppp.494
- Malet J, Maquaire O, Calais E. 2002. The use of Global Positioning System techniques for the continuous monitoring of landslides : application to the Super-Sauze earthf low (Alpes-de-Haute-Provence, France). *Geomorphology* **43** : 33–54.
- Mantovani F, Soeters R, van Westen C. 1996. Remote sensing techniques for landslide studies and hazard zonation in Europe. *Geomorphology* **15** : 213–225.
- Massonnet D, Rabaute T. 1993. Radar interferometry: limits and potential. *IEEE Transactions on Geoscience and Remote Sensing* **31** : 455–464.
- Massonnet D, Feigl KL. 1998. Radar interferometry and its application to changes in the Earth's surface. *Reviews of Geophysics* **36** : 441–500.
- Matsuoka N. 2004. Solifluction. In *Encyclopedia of Geomorphology*. **2**: 984–987.
- Metternicht G, Hurni L, Gogu R. 2005. Remote sensing of landslides: An analysis of the potential contribution to geo-spatial systems for hazard assessment in mountainous environments. *Remote Sensing of Environment* **98** : 284–303. DOI: 10.1016/j.rse.2005.08.004.
- Nagler T, Mayer C, Rott H. 2001. Feasibility of DInSAR for mapping complex motion fields of alpine ice- and rock- glaciers. *Proceedings of the Third International Symposium on Retrieval of Bio- and Geophysical Parameters from SAR Data for Land Applications, 11-14 September 2001 (ESA SP-475, 2002)* : 377–382.
- Nagler T, Rott H, Kamelger A. 2002. Analysis of Landslides in Alpine Areas by Means of SAR Interferometry. *Proc. of IGARSS 2002, June 24-28* : 198–200.
- Noetzli J (ed). 2013. PERMOS 2013. Permafrost in Switzerland 2008/2009 and 2009/2010. *Glaciological Report Permafrost No. 10/11 of the Cryospheric Commission of the Swiss Academy of Sciences*, 80p.
- Nolan M, Fatland DR. 2003. Penetration depth as a DInSAR observable and proxy for soil moisture. *IEEE Transactions on Geoscience and Remote Sensing* **41** : 532–537. DOI: 10.1109/TGRS.2003.809931
- Nolan M, Fatland DR, Hinzman L. 2003. Dinsar measurement of soil moisture. *IEEE Transactions on Geoscience and Remote Sensing* **41** : 2802–2813. DOI: 10.1109/TGRS.2003.817211.
- Papke J, Strozzi T, Wiesmann A, Wegmueller U, Tate NJ. 2012. Rock glacier monitoring with spaceborn SAR in Graechen, Valais, Switzerland. *Proceedings of IGARSS 2012*: 3911–3914.
- Paul F, Frey H, Le Bris R. 2011. A new glacier inventory for the European Alps from Landsat TM scenes of 2003: challenges and results. *Annals of Glaciology* **52** : 144–152. DOI: 10.3189/172756411799096295.

Perruchoud E. 2007. Suivi par GPS des déformations de glaciers rocheux et moraines de poussée dans les Alpes valaisannes. Travail de Master. University of Fribourg (Switzerland).

Perruchoud E, Delaloye R. 2007. Short-Term Changes in Surface Velocities on the Becs-de-Bosson Rock Glacier (Western Swiss Alps). Proceedings of the 9th International Symposium on High Mountain Remote Sensing and Cartography, 2007, 248 S **2004** : 131 – 136.

Philippe L, Grimm D. 2009. Rock glacier monitoring with low-cost GPS receivers. Abstract Volume 7th Swiss Geoscience Meeting, November 2009, Neuchatel, Switzerland. : 247–248.

Plank S, Singer J, Minet C, Thuro K. 2012. Pre-survey suitability evaluation of the differential synthetic aperture radar interferometry method for landslide monitoring. International Journal of Remote Sensing **33** : 6623–6637. DOI: 10.1080/01431161.2012.693646.

Preiss M, Stacy NJS. 2006. Coherent Change Detection : Theoretical Description and Experimental Results.

Ravanel L, Allignol F, Deline P, Gruber S, Ravello M. 2010. Rock falls in the Mont Blanc Massif in 2007 and 2008. Landslides **7** : 493–501. DOI: 10.1007/s10346-010-0206-z.

Reynard E, Lambiel C, Delaloye R, Devaud G, Baron L, Chapellier D, Marescot L, Monnet R. 2003. Glacier/permafrost relationships in forefields of small glaciers (Swiss Alps). 8th International Permafrost Conference, Zurich, Switzerland : 947–952.

Richards JA. 2009. Scattering from Earth surface features. In Remote Sensing with Imaging Radar. Springer-Verlag Berlin Heidelberg; 135–186.

Rignot E, Hallet B, Fountain A. 2002. Rock glacier surface motion in Beacon Valley, Antarctica, from synthetic-aperture radar interferometry. Geophysical Research Letters **29** : 1–10.

Roer I, Kääb A, Dikau R. 2005. Rockglacier acceleration in the Turtmann valley (Swiss Alps): Probable controls. Norsk Geografisk Tidsskrift **59** : 157–163.

Roer I, Haeberli W, Avian M, Kaufmann V, Delaloye R, Lambiel C, Kääb A. 2008. Observations and Considerations on Destabilizing Active Rock Glaciers in the European Alps. 9th International conference on Permafrost: 1505–1510.

Rosen P a., Hensley S, Joughin IR, Li FK, Madsen SN, Rodriguez E, Goldstein RM. 2000. Synthetic aperture radar interferometry. Proceedings of the IEEE **88** : 333–382.

Rosenfeld CL. 2004. Geomorphological Hazard. In Encyclopedia of Geomorphology. Volume 1 , Goudie AS (ed). Routledge; 424–427.

Rott H, Scheuchl B, Siegel A, Grasemann B. 1999a. Monitoring very slope movements by means of SAR interferometry: A case study from a mass waste above a reservoir in the Ötztal Alps, Austria. Geophysical Research Letters **26** : 1629–1632.

Rott H, Siegel A, Grasemann B. 1999b. Analysis of Mass Movements in Alpine Terrain by Means of SAR Interferometry. Proceedings of IGARSS 99 : 1933–1936.

Rott H, Nagler T. 2003. InSAR techniques and applications for monitoring landslides and subsidence. Geoinformation for European-wide Integration. In Geoinformation for European-wide Integration, MillPress, Rotterdam, Eds. Benes: 25–32.

Singhroy V, Molch K. 2004. Characterizing and monitoring rockslides from SAR techniques. *Advances in Space Research* **33** : 290–295. DOI: 10.1016/S0273-1177(03)00470-8.

Smith LC. 2002. Emerging Applications of Interferometric Synthetic Aperture Radar (InSAR) in Geomorphology and Hydrology. *Annals of the Association of American Geographers* **92** : 385–398.

Strozzi T, Wegmuller U, Matzler C. 1999. Mapping wet snow covers with SAR interferometry. *International Journal of Remote Sensing* **20** : 2397–2403.

Strozzi T, Wegmüller U, Tosl L, Bitelli G, Spreckels V. 2001. Land Subsidence Monitoring with Differential SAR Interferometry. *Photogrammetric Engineering & Remote Sensing* **67** : 1261–1270.

Strozzi T, Wegmuller U, Werner C, Wiesmann A. 2002. Alpine landslide periodical survey. *Proceeding of IGARSS 2002* **6** : 3629–3631. DOI: 10.1109/IGARSS.2002.1027272.

Strozzi T, Kääb A, Frauenfelder R, Wegmüller U. 2003. Detection and Monitoring of Unstable High-Mountain Slopes with L-Band SAR Interferometry. *Proceeding of IGARSS 2003* : 1852–1854.

Strozzi T, Kääb A, Frauenfelder R. 2004. Detecting and quantifying mountain permafrost creep from in situ inventory, space-borne radar interferometry and airborne digital photogrammetry. *International Journal of Remote Sensing* **25** : 2919–2931.

Strozzi T, Farina P, Corsini A, Ambrosi C, Thüring M, Zilger J, Wiesmann A, Wegmüller U, Werner C. 2005. Survey and monitoring of landslide displacements by means of L-band satellite SAR interferometry. *Landslides* **2** : 193–201.

Strozzi T, Wegmüller U, Perruchoud E, Delaloye R, Kääb A, Ambrosi C. 2007. Evolution of a deep-seated rock mass movement observed with satellite SAR interferometry. *Proceeding of the FRINGE 2007 workshop*, 26-30 November, Frascati, Italy (ESA SP-649, February 2008).

Strozzi T, Wegmüller U, Werner C, Wiesmann A, Santoro M, Delaloye R, Raetzo H, Ambrosi C. 2008. Survey of landslide activity in the swiss alps with alos palsar. *Proceedings of the 2008 Joint PI Symposium of the ALOS Data Nodes*, 3-7 November 2008 (ESA SP-664, January 2009).

Strozzi T, Delaloye R, Raetzo H, Wegmüller U. 2009a. Radar interferometric observations of destabilized rockglaciers. *Proceeding of the FRINGE 2009 workshop*, 30 November - 4 December, Frascati, Italy.

Strozzi T, Wegmüller U, Werner C, Wiesmann A. 2009b. Survey of landslide activity and rockglaciers movement in the Swiss Alps with Terrasar-X. *Proceeding of IGARSS 2009* : 53–56.

Strozzi T, Delaloye R, Kääb A, Ambrosi C, Perruchoud E, Wegmüller U. 2010a. Combined observations of rock mass movements using satellite SAR interferometry, differential GPS, airborne digital photogrammetry, and airborne photography interpretation. *Journal of Geophysical Research* **115** : 1–11. DOI: 10.1029/2009JF001311.

Strozzi T, Paul F, Käab A. 2010b. Glacier mapping with ALOS PALSAR within the GlobGlacier project. Proceedings of the ESA Living Planet Symposium 2010, 28 June - 02 July 2010, Bergen, Norway 2010.

Strozzi T, Delaloye R, Poffet D, Hansmann J, Loew S. 2011. Surface subsidence and uplift above a headrace tunnel in metamorphic basement rocks of the Swiss Alps as detected by satellite SAR interferometry. *Remote Sensing of Environment* **115** : 1353–1360. DOI: 10.1016/j.rse.2011.02.001.

Strozzi T, Wegmüller U, Werner C, Kos A. 2012. Terrasar-X Interferometry for surface deformation monitoring on periglacial area. *Proceeding of IGARSS 2012* : 5214–5217.

Tarayre H, Massonnet D. 1994. Effect of a refractive atmosphere on interferometric processing. *Proceedings of IGARSS '94*, 8-12 August 1994, Pasadena, California : 717–719.

Tarayre H, Massonnet D. 1996. Atmospheric propagation heterogeneities revealed by ERS-1 interferometry. *Geophysical Research Letters* **23** : 989–992.

Tuceryan M, Jain AK. 1998. Texture Analysis. In *Handbook of Pattern Recognition and Computer Vision* (2nd Edition) , C. H. Chen, L. F. Pau PSPW (ed). World Scientific Publishing Co.; 207–248.

Ulaby FT, Dobson MC, Bradley G a. 1981. Radar reflectivity of bare and vegetation-covered soil. *Advances in Space Research* **1** : 91–104. DOI: 10.1016/0273-1177(81)90384-7.

Walter D, Busch W. 2012. Influence of DEM quality parameters on the topographic phase correction in DInSAR. *Proc. of IGARSS 2012* : 3927–3930.

Wegmüller U, Strozzi T. 1998. Characterization of Differential Interferometry Approaches. *Proc. of EUSAR '98*, 25-27 May 1998.

Wegmüller U, Strozzi T, Delaloye R, Raetzo H. 2012. Landslide mapping in Switzerland with ENVISAT ASAR. *Proceedings of IGARSS 2012*: 1829–1832.

Wegmuller U, Werner CL. 1995. SAR interferometric signatures of forest. *IEEE Transactions on Geoscience and Remote Sensing* **33** : 1153–1161. DOI: 10.1109/36.469479.

Werner CL, Strozzi T, Wiesmann A, Wegmüller U, Kos A, Delaloye R, Raetzo H. 2010. Motion measurement of destabilized slopes in Switzerland with the GPRI-I ground-based real-aperture radar (Invited). *American Geophysical Union, Fall Meeting 2010*, abstract #G21A-0790.

Weydahl DJ. 2001a. Analysis of ERS SAR coherence images acquired over vegetated areas and urban features. *International Journal of Remote Sensing* **22** : 2811–2830.

Weydahl DJ. 2001b. Analysis of ERS Tandem SAR coherence from glaciers, valleys, and fjord ice on Svalbard. *IEEE Transactions on Geoscience and Remote Sensing* **39** : 2029–2039. DOI: 10.1109/36.951093.

Wiesmann A, Wegmuller U, Honikel M, Strozzi T, Werner CL. 2001. Potential and methodology of satellite based SAR for hazard mapping. *Proceedings of IGARSS 2001*: 3262–3264.

Williams S, Bock Y, Fang P. 1998. Integrated satellite interferometry: Tropospheric noise, GPS estimates and implications for interferometric synthetic aperture radar products. *Journal of Geophysical Research* **103** : 27051–27067.

Wirz V, Geertsema M, Gruber S, Purves RS. 2014. Temporal variability of diverse mountain permafrost slope movements derived from multi-year daily GPS data, Mattertal, Switzerland. Landslides (In press). DOI: 10.1007/s10346-014-0544-3.

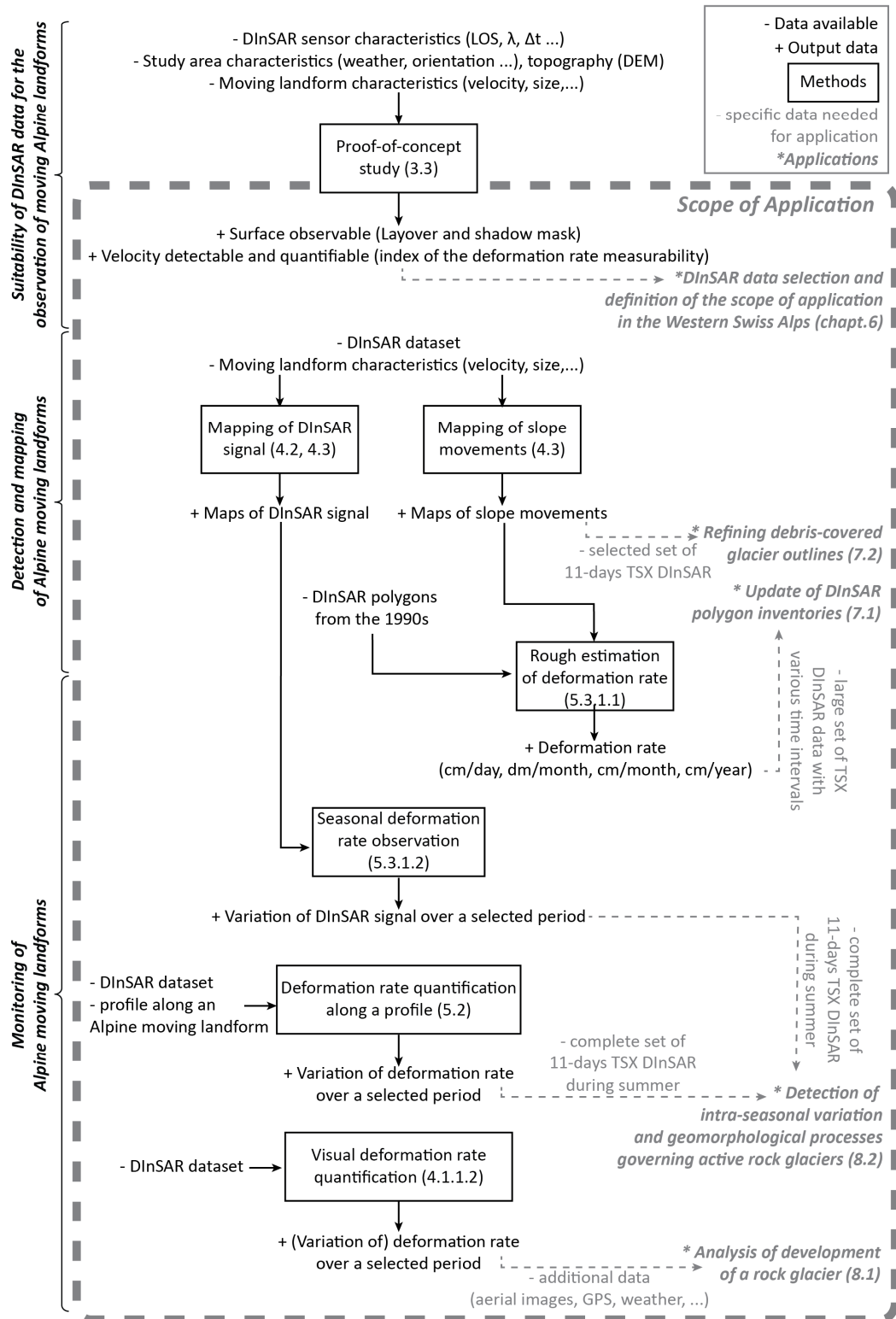
Zangerl C, Eberhardt E, Evans KF, Loew S. 2008. Consolidation settlements above deep tunnels in fractured crystalline rock: Part 2—Numerical analysis of the Gotthard highway tunnel case study. International Journal of Rock Mechanics and Mining Sciences **45** : 1211–1225. DOI: 10.1016/j.ijrmms.2008.02.005.

Zebker A, Rosen PA, Hensley S. 1997. Atmospheric effects in interferometric synthetic aperture radar surface deformation and topographic maps. Journal of Geophysical Research **102** : 7547–7563.

Zhang T, Zeng Q, Li Y, Xiang Y. 2008. Study on the relation between InSAR Coherence and Soil Moisture. The International Archives of the Photogrammetry, Remote Sensing and Spatial Information Sciences. **37** : 131–134.

Appendix 1

Organization of the research describing the general approach, the developed methods and protocol, the tests and application as well as the required input data and produced output data.



Curriculum Vitae

Barboux Chloé

Born the 20th of October 1984, Annecy (F)

Education

- Nov. 2014 **Doctor Rerum Naturalium (PhD)**, University of Fribourg, Geosciences department, Geography (CH) : « Detection, mapping and monitoring of slope movements in the Alpine environment using DInSAR » (Dir. : C. Collet et R. Delaloye).
- Oct. 2008 **Master of Science in Electronics, Telecommunication and Computer Sciences (ESCPE Lyon, F).**
2004/2006 *1st and 2nd years in ESCPE Lyon* (F): Department of Electronics, Telecommunications and Computer Sciences.
2006/2007 *Erasmus student at the EPFL* (Lausanne, CH): Department of Communication Systems.
- 2002 - 2004 **Preparatory classes:** MPSI and MP* (Annecy, F)
- 2002 **Scientific baccalaureate**, mathematics specialization (F).

Professional experiences

- Jan. 2010 **PhD candidate - University of Fribourg, Geography** (Fribourg, CH).
– Dec. 2014 Development of automated methods for the detection, the mapping and the monitoring of slope movements in an Alpine terrain using satellite Differential SAR Interferometry (DInSAR). Comparison with aerial images and GPS data.
Competences: Arcgis, Python, C/C++, Matlab, radar interferometry, photogrammetry, signal and image processing, Alpine geomorphology.
- Teaching:
– TPs Cartographie/Cartomatique
– TPs Méthodes quantitatives I
– Géodonnées physiques
Competences: Arcgis, Adobe Illustrator/Photoshop, Surfer, MapViewer, R, data processing and visualization.
- Creation of the Geomorphology website of the Geography Unit.
Competences: HTML, CSS, PHP, MySQL.
- Dec. 2008 **Researcher engineer CNRS Gipsa-Lab/INPG** (St Martin d'Hères, F), 6 months.
– May 2009 « Permafrost surface deformation and related hazards detection using InSAR technique in the Southern French Alps ». European project PermaNET/Alpine Space. *Competences: C/C++, IDL, Envi, radar interferometry, image processing.*

- Nov. 2007 – May 2008 **C++ and User Interface Developer intern PETZL** (Crolles 38 - F), 7 months.
« Optoelectronic tests optimization » Software design for luminous intensity profiles of headlamp's beam analysis and flux measurements automation.
Competences: C/C++, Qt, LabView, optics, instrumentation and metrology.
- Dec. 2006 – July 2007 **Researcher assistant EPFL/ITS** (Lausanne, CH), 8 months.
- « Silhouette detection from surveillance video stream » in collaboration with General Electric. Algorithms design for skin and gait recognition from video stream. *Competences: Matlab, C/C++, image processing.*
- « Automatic extraction of level 1, 2 and 3 features for fingerprint comparison. » Development of educational software.
Competences: Matlab, C/C++, image processing.

Main publications

Barboux, C., Delaloye, Lambiel, C. (2014). Inventorying slope movements in Alpine environment using DInSAR. *Earth Surface Processes and Landforms*. DOI: 10.1002/esp.3603 (In press).

Fischer, M., Huss, M., **Barboux, C.** and Hoelzle, M. (2014). The new Swiss Glacier Inventory SGI2010: Relevance of using high-resolution source data in areas dominated by very small glaciers. *Arctic, Antarctic, and Alpine Research*, 46(4) (In press).

Other publications

Barboux, C., Delaloye, R., Strozzi, T., Lambiel, C., Raetzo, H. and Collet, C. (2013). Semi-automated detection of terrain stability in the Swiss Alpine periglacial environment using segmentation and classification of DInSAR scenes: a useful tool to update past inventories of moving areas. *Living Planet Symposium. 09-13 september 2013 Edimburg, Scotland.*

Barboux, C., Delaloye, R., Strozzi, T., Lambiel, C., Collet, C., Raetzo, H. (2012). Monitoring active rock glaciers in the western Swiss Alps: challenges of Differential SAR Interferometry and solutions to estimate annual and seasonal displacement rates. *IEEE International Geoscience and Remote Sensing Symposium (IGARSS), 22-27 July 2012, Munich, Germany.*

Barboux, C., Delaloye, R., Strozzi, T., Collet, C. and Raetzo, H. (2012). Surveying the activity of landslides and rock glaciers above the tree line with InSAR. *Mattertal – ein Tal in Bewegung. Graf C. (Ed.) 2013. Publikation zur Jahrestagung der Schweizerischen Geomorphologischen Gesellschaft 29. Juni – 1. Juli 2011, St. Niklaus. Eidg. Forschungsanstalt WSL. P 7-19.*

Delaloye, R., Morard, S., **Barboux, C.**, Abbet, D., Gruber, V., Riedo, M. and Gachet, S. (2012). Rapidly moving rock glaciers in Mattertal. *Mattertal – ein Tal in Bewegung. Graf C. (Ed.) 2013. Publikation zur Jahrestagung der Schweizerischen Geomorphologischen Gesellschaft 29. Juni – 1. Juli 2011, St. Niklaus. Eidg. Forschungsanstalt WSL. P 21-31.*

Barboux, C., Delaloye, R., Strozzi, T., Collet, C., Raetzo, H. (2011). TSX InSAR Assessment for slope instabilities monitoring in alpine periglacial environment (western Swiss Alps). *Proceedings of FRINGE 2011 Workshop, 19–23 September 2011, Frascati, Italy (ESA SP-697, January 2012).*

Delaloye, R., Strozzi, T., Lambiel, C., **Barboux, C.**, Mari, S., Stocker, A., Techel, F. et Raetzo, H. (2010). The contribution of InSAR data to the early detection of potentially hazardous active rock glaciers in mountain areas. *Proceedings ESA Living Planet Symposium 2010, Bergen, Norway (ESA SP-686)*.

Conference abstracts

Barboux, C., Fischer, M., Delaloye, R., Huss, M. and Collet C. (2013). Observations of debris covered ice using DInSAR and airborne photography interpretation. A pilot study in the Upper Valais (Swiss Alps). *11th Swiss Geoscience Meeting, Lausanne 2013 (Poster)*.

Barboux, C., Delaloye, R., Strozzi, T., Lambiel, C. and Raetzo, H. (2013). Differential SAR Interferometry in alpine geomorphology: Potential of this high precision technology for detecting and surveying landforms in mountain environment. *8th IAG International Conference on Geomorphology - August 27th to 31st, 2013. Paris, France (Oral presentation)*.

Barboux, C., Delaloye, R., Strozzi, T., Lambiel, C. and Collet, C. (2013). TSX DInSAR data for detecting and monitoring slope motion phenomena in an Alpine periglacial environment at different resolution scales (Western Swiss Alps, Switzerland) - LAN 1145. *TerraSAR-X / TanDEM-X science team meeting, 10-14 June 2013, DLR Oberpfaffenhofen, Germany (Oral presentation)*.

Barboux, C., Delaloye, R., Strozzi, T., Lambiel, C., Raetzo, H. and Collet, C. (2012). Monitoring of Active Rock Glaciers with X-Band Differential SAR interferometry: Case-studies in Western Swiss Alps. *Tenth international conference on permafrost. 25-29 June, Salekhard, Russia (Poster)*.

Barboux, C., Delaloye, R., Strozzi, T., Lambiel, C., Raetzo, H. and Collet, C. (2011). InSAR Terrasar-X visibility assessment of moving landform monitoring in alpine periglacial environment: 30 case studies in the Valais Alps (CH). *9th Swiss Geoscience Meeting, Zurich 2011 (Poster)*.

Barboux, C., Delaloye, R., Collet, C., Strozzi, T. and Raetzo, H. (2011). Slope instabilities monitoring in mountain periglacial environment using DInSAR - Application to the Valais Alps. *Geophysical Research Abstracts Vol. 13, EGU2011-8325-1. European Geosciences Union, General Assembly 03-08 April 2011, Vienna, Austria (Oral presentation)*.

Barboux, C. and Delaloye, R. (2010). Analyzing the pluri-decennial development of a rock glacier crisis using repeated SAR interferometry, terrestrial and airborne optical data. *8th Swiss Geoscience Meeting, Fribourg 2010 (Poster)*.